

## **Themenschwerpunkt**

Proceedings of the  
"5<sup>th</sup> CCM international conference on  
pressure and vacuum metrology"  
and the  
"4<sup>th</sup> international conference  
IMEKO TC16"  
Berlin, May 2-5, 2011



Fachorgan für Wirtschaft und Wissenschaft

Amts- und Mitteilungsblatt der  
Physikalisch-Technischen Bundesanstalt  
Braunschweig und Berlin

121. Jahrgang, Heft 3, November 2011

## Inhalt

---

### Themenschwerpunkt

Proceedings of the „5<sup>th</sup> CCM international conference on pressure and vacuum metrology“ and the „4<sup>th</sup> international conference IME-KO TC16“ • Berlin, May 2-5, 2011

- eigenes Inhaltsverzeichnis 235

---

### Recht und Technik

- *Roman Schwartz*: Neues aus der OIML  
Bericht über die 46. Sitzung des Internationalen Komitees für gesetzliches Messwesen (CIML)

323

---

### Amtliche Bekanntmachungen

(eigenes Inhaltsverzeichnis)

326

---

## Impressum

Die **PTB-Mitteilungen** sind metrologisches Fachjournal und amtliches Mitteilungsblatt der Physikalisch-Technischen Bundesanstalt, Braunschweig und Berlin. Als Fachjournal veröffentlichen die PTB-Mitteilungen wissenschaftliche Fachaufsätze zu metrologischen Themen aus den Arbeitsgebieten der PTB. Als amtliches Mitteilungsblatt steht die Zeitschrift in einer langen Tradition, die bis zu den Anfängen der Physikalisch-Technischen Reichsanstalt (gegründet 1887) zurückreicht. Die PTB-Mitteilungen veröffentlichen in ihrer Rubrik „Amtliche Bekanntmachungen“ unter anderem die aktuellen Geräte-Prüfungen und -Zulassungen aus den Gebieten des Eich-, Prüfstellen- und Gesundheitswesens, des Strahlenschutzes und der Sicherheitstechnik.

### Verlag

Wirtschaftsverlag NW  
Verlag für neue Wissenschaft GmbH  
Bürgermeister-Smidt-Str. 74–76,  
27568 Bremerhaven  
Postfach 10 11 10, 27511 Bremerhaven  
Internet: [www.nw-verlag.de](http://www.nw-verlag.de)  
E-Mail: [info@nw-verlag.de](mailto:info@nw-verlag.de)

### Herausgeber

Physikalisch-Technische Bundesanstalt (PTB),  
Braunschweig und Berlin  
Postanschrift:  
Postfach 33 45, 38023 Braunschweig  
Lieferanschrift:  
Bundesallee 100, 38116 Braunschweig

### Redaktion/Layout

Presse- und Öffentlichkeitsarbeit, PTB  
Dr. Dr. Jens Simon (verantwortlich)  
Bernd Warnke (herstellerische Betreuung)  
Dr. Karl Jousten (wissenschaftliche Redaktion)  
Gisela Link  
Telefon: (05 31) 592-82 02  
Telefax: (05 31) 592-30 08  
E-Mail: [gisela.link@ptb.de](mailto:gisela.link@ptb.de)

### Leser- und Abonnement-Service

Marina Kornahrens  
Telefon: (04 71) 9 45 44-61  
Telefax: (04 71) 9 45 44-88  
E-Mail: [vertrieb@nw-verlag.de](mailto:vertrieb@nw-verlag.de)

### Anzeigenservice

Karin Drewes  
Telefon: (04 71) 9 45 44-21  
Telefax: (04 71) 9 45 44-77  
E-Mail: [info@nw-verlag.de](mailto:info@nw-verlag.de)

### Erscheinungsweise und Bezugspreise

Die PTB-Mitteilungen erscheinen viermal jährlich. Das Jahresabonnement kostet 55 Euro, das Einzelheft 16 Euro, jeweils zzgl. Versandkosten. Bezug über den Buchhandel oder den Verlag. Abbestellungen müssen spätestens drei Monate vor Ende eines Kalenderjahres schriftlich beim Verlag erfolgen.

© Wirtschaftsverlag NW, Verlag für neue Wissenschaft GmbH, Bremerhaven, 2011

Alle Rechte vorbehalten. Kein Teil dieser Zeitschrift darf ohne schriftliche Genehmigung des Verlages vervielfältigt oder verbreitet werden. Unter dieses Verbot fällt insbesondere die gewerbliche Vervielfältigung per Kopie, die Aufnahme in elektronische Datenbanken und die Vervielfältigung auf CD-ROM und in allen anderen elektronischen Datenträgern.

## Inhalt

- *Karl Jousten*  
Vorwort • Preface 237
- *Gianfranco Molinar Min Beciet*  
Historical perspectives of high pressure metrology using  
pressure balances 239
- *W. Sabuga*  
Pressure measurements in gas media up to 7.5 MPa for the  
Boltzmann constant redetermination 247
- *Wladimir Sabuga, Tasanee Priruenrom, Rob Haines, Michael Bair*  
Design and Evaluation of Pressure Balances with  $1 \cdot 10^{-6}$   
Uncertainty for the Boltzmann Constant Project 256
- *W. Sabuga, F. Sharipov, T. Priruenrom*  
Determination of the Effective Area of Piston-Cylinder Assemblies  
Using a Rarefied Gas Flow Model 260
- *Mark Fitzgerald, Chris Sutton, Darrin Jack*  
New MSL twin pressure balance facility 263
- *Yuanchao Yang, Jin Yue*  
Calculation of Effective Area for the NIM Primary Pressure  
Standards 266
- *P. Wongthep, T. Rabault, C. Sarraf, R. Noguera*  
New Model Of Fluid Flow To Determine Pressure Balance  
Characteristics 270
- *Tokihiko Kobata*  
Multiple cross-float system for calibrating pressure balances 274
- *Hiroaki Kajikawa, Kazunori Ide, Tokihiko Kobata*  
Stability of pressure generated by controlled-clearance pressure  
balance up to 1 GPa 278
- *Neville Owen*  
Linking Hydraulic and Pneumatic Pressure Scales Using a  
Common Piston Gauge 281
- *Sari Saxholm, Björn Hemming, Martti Heinonen, Pierre Otal,  
Markku Rantanen, Veli-Pekka Esala, Antti Lassila*  
Traceability of the pressure balance effective area at MIKES 284
- *Alaaeldin A. Eltawil, Shaker A. Gelany, Ali H. Magrabi*  
Traceability of NIS Piston-Cylinder Assemblies up to 500 MPa 287

- 
- *I. Kocas, W. Sabuga, M. Bergoglio, A. E. Eltawil, C. Korasie, P. Farar, J. Setina, B. Waller*  
EURAMET Key Comparison for 500 MPa Range of Hydraulic Gauge Pressure (EURAMET.M.P-K13) 291
  - *P. Otal, I. Morgado, D. Steindl, N. Medina Martín, A. Lefkopoulos, A. Altintas, L. Grgec Bermanec, S. Bursic, J. Setina, M. Bergoglio, I. Spohr, C. Wüthrich, M. Rantanen, C. Vámosy, W. Sabuga, I. Koças*  
Evaluation of cross-float measurements with pressure balances – Results of EURAMET project 1125 294
  - *Salustiano Ruiz, Nieves Medina*  
Comparison between GUM and Monte Carlo uncertainty frameworks in pressure field 298
  - *Irina Sadkovskaya, Aleksey Eichwald*  
The laser interferometric oil manometer with floats 301
  - *J. Könemann, S. Ehlers, M. Jescheck, W. Sabuga*  
The Mercury Micromanometer at PTB 303
  - *D. Herranz, N. Medina, S. Ruiz, J. Torres-Guzmán*  
Static Expansion System Validation at CEM 307
  - *A. Navarro-Nateras, J. C. Torres-Guzman*  
Characterization of the medium and high vacuum primary standard at CENAM, Mexico 310
  - *Frédéric Boineau*  
Characterization of the LNE constant pressure flowmeter for the leak flow rates measurements with reference to vacuum and atmospheric pressure 313
  - *K. Jousten*  
International standardization for vacuum metrology and technology in recent years 317
  - *C. Korasie, A. Eltawil*  
Traceability and accreditation process for vacuum and pressure laboratories in AFRIMETS 321

Alle auf den Seiten 239 bis 322 veröffentlichten Berichte wurden von jeweils 2 Experten begutachtet. Von 26 eingereichten Beiträgen wurden 4 abgelehnt.

All articles published on pages 239 to 322 were peer-reviewed by two experts. Out of 26 submitted papers 4 were rejected.

---

# Vorwort • Preface

Karl Jousten<sup>1</sup>

Die PTB richtete vom 1. bis zum 5. Mai 2011 die "5. CCM International Conference on Pressure and Vacuum Metrology" aus. Es ist die weltweit maßgebende Konferenz auf dem Gebiet der Druck- und Vakuummetrologie und wird alle 6 Jahre von den Arbeitsgruppen für Druck und Vakuum im CCM (Comité consultatif pour la masse et grandeurs apparentées) des CIPM organisiert. Sie wurde 2011 verbunden mit der 4. Konferenz des Technischen Komitees 16 „Druck und Vakuum“ der IMEKO.

Dieser Band veröffentlicht überwiegend die auf der Konferenz vorgestellten Beiträge, die eine enge Verbindung zu Primärnormalen haben. Die übrigen Beiträge werden in der Zeitschrift «Measurement» erscheinen.

Die Darstellung der Druckskaale umfasst insgesamt 18 Dekaden, von  $10^{-9}$  Pa bis  $10^9$  Pa. So reichen die Anwendungen der Druckmesstechnik in viele verschiedene Bereiche: Die kleinsten Drücke werden in Forschungsanlagen wie Hochenergiebeschleuniger oder Röntgenlaser benötigt, Hochvakuum in der

The PTB organised the 5<sup>th</sup> CCM International Conference on Pressure and Vacuum Metrology being held from May 1 to 5, 2011. It is the world's leading conference on measurement related issues in the pressure and vacuum field and is arranged by the Working Groups for pressure and vacuum within the CCM (Comité consultatif pour la masse et grandeurs apparentées) of the CIPM every 6 years. This time in 2011 this conference was held in conjunction with the 4<sup>th</sup> conference of the Technical Committee 16 "Pressure and Vacuum" of the IMEKO.

This volume publishes mainly those contributions presented at the conference that have a close relation to primary standards. Other reports will be published in the journal "Measurement".

The realized pressure scale encompasses 18 decades, from  $10^{-9}$  Pa to  $10^9$  Pa. That way the applications of pressure measurement technology reach into many fields: The smallest pressures are needed in large research facilities as high-energy accelerators or X-ray lasers, high vacuum



---

<sup>1</sup> Karl Jousten,  
Co-Chair of 5<sup>th</sup> CCM  
International Conference on Pressure and  
Vacuum Metrology and 4<sup>th</sup> Conference of  
IMEKO TC-16,  
Section Vacuum Metrology of PTB,  
Abbestr. 2-12,  
10587 Berlin  
karl.jousten@ptb.de

---

Mikroelektronik und Beschichtungstechnik (CD/DVD, Magnetspeicher, Brillen, Linsen, Architekturglas, Hartschichten auf Werkzeugen, Folienmetallisierung etc.), Fein- und Grobvakuum in der Metallurgie und der Lebensmittelindustrie. Druckmessung um den atmosphärischen Druck wird vor allem in der Meteorologie, der Luftfahrt und der Raumklimatisierung benötigt, Drücke im MPa Bereich bei der Energieversorgung, der Hydraulik und in der chemischen Industrie, die höchsten Drücke bei der Motorenentwicklung und Diamantsynthese.

120 Teilnehmer aus 32 Ländern aus allen Kontinenten kamen nach Berlin in das Konferenzhotel Relexa „Stuttgarter Hof“ in der Nähe des Potsdamer Platzes. 7 Redner wurden eingeladen, 11 Aussteller zeigten auf Ständen ihre einschlägigen Produkte. Am letzten Tag der Konferenz bekamen die Teilnehmer die Gelegenheit, die Laboratorien der PTB für Vakuum und Synchrotronstrahlung in Berlin oder für Druck, Kraft und Drehmoment in Braunschweig zu besichtigen.

in the microelectronic and coating industry, magnetic storage discs, glasses, lenses, architecture glass, hard coatings of tools, foil metallization etc.), medium and rough vacuum in metallurgy and food industry. Pressure measurement around atmospheric pressure is mainly needed in meteorology, air transportation and air conditioning, pressures in the MPa regime for energy supply, hydraulic and the chemical industry, the highest pressures for the development of engines and the synthesis of diamonds.

120 participants from 32 countries of all mainlands came to Berlin to the conference venue Hotel Relexa „Stuttgarter Hof“ near the Potsdamer Platz. 7 speakers were invited, 11 exhibitors showed their pertinent products in their booths. On the last day of the conference the attendees had the possibility to either visit the laboratories of PTB for vacuum and synchrotron radiation in Berlin or the laboratories for pressure, force and torque in Braunschweig.

# Historical perspectives of high pressure metrology using pressure balances

Gianfranco Molinar Min Beciet<sup>1</sup>

## Abstract

Development of pressure balances dates back to the beginning of the nineteenth century and was stimulated by the growth of industrial applications of steam engines and by the need of measuring accurately thermodynamic properties of gases and liquids at different pressures and temperatures. An historical review illustrating the fundamental steps in the development of pressure balances in gas and liquid media up to a maximum pressure close to 1 GPa is given.

## 1. Historical review related to pressure balances

References [1, 2] already provided a historical approach for pressure balances in liquid and gas. The development of liquid column manometers [3] began with the famous experiment of Torricelli in 1644 and from later studies (Pascal, 1648; Boyle, 1662; Guericke, 1672) of gas properties. Development of pressure balances dates back only to the beginning of the nineteenth century; it was stimulated by the growth of industrial applications of steam engines. Studies on steam engines of Huygens and Papin (1690), Newcomen (1700), Watt (1769 and 1780), and the associated studies of Lavoisier, Dalton, Gay-Lussac and Carnot, who established the principles of classical thermodynamics, are also of great importance for the development of pressure balances. In 1832, Parrot [4] published studies carried out on different materials subjected to compression at pressures up to 10 MPa; for pressure measurement he used a steel piston-cylinder unit loaded with weights connected to one arm of an analytical balance. The pressure balance is directly measuring the pressure as it is developed inside the steam chamber as can be seen in Figure 1.

In 1846, Galy-Cazalat [5] described an apparatus combining a mercury column and a hydraulic piston multiplier; the high pressure acted on a small piston, the low pressure was applied to a larger piston and was measured with a mercury manometer. Seyss, in 1869, [6] made an automatically loaded pressure balance. Amagat, in

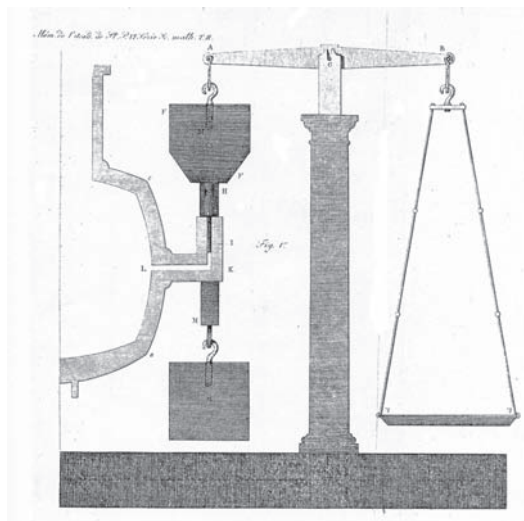


Figure 1. – Pressure balance of Parrot, 1832, taken from [4].

1893, designed and built the first pressure balance having a rotating piston to avoid friction against the cylinder wall. The pressure balance manufactured in 1883 [7] by Ruchholz had all the features of a modern pressure balance. A 50 MPa pressure balance equipped with a lever system for force application on the piston was made in 1897 by Stückrath at PTR in Berlin; its accuracy was estimated to be  $\pm 0.04\%$  at 25 MPa. The need to extend measurements to higher pressures soon led to remarkable progress and to new ideas in the construction of pressure balances of different types. Examples are the re-entrant piston-cylinder unit of Bridgman [8] and the controlled-clearance type of Bridgman [9] and Newhall [10], with which it was possible to make accurate pressure measurements to about 1.4 GPa in liquid media.

A significant growth, pushed by studies of different metrological institutes and top-level companies, started in 1950 and it is still going on. In Table 1 some of the most significant pressure balances are reported in order to give an idea of the different studies and of the available standards.

Current pressure balances have been substantially improved particularly as regards piston-cylinder materials, geometry and accuracy of the associated measurements (temperature, piston position, piston fall rates, piston rotation, etc.).

<sup>1</sup> Gianfranco Molinar Min Beciet  
Istituto Nazionale di Ricerca Metrologica (I.N.Ri.M.), Torino (Italy)  
Email : g.molinar@inrim.it



Table 1 . Significant pressure balances up to 2.6 GPa (FD = free deformation or simple, RE = re-entrant, CC = controlled clearance, NFD = negative free deformation, MX = mixed type, FPG= force-balanced and non-rotating piston gauge).

Laboratory	Main typical aspects or study	Main pressure balance configurations	Max pressure / GPa	References
NIST, USA	Pressure balance design, elastic distortions, Hg melting line, 2.6 GPa CC unique pressure balance	FD, RE, CC Large diameters piston units for gas media	1.4 (2.6 in the past)	[2, 10, 11, B3, 12]
NPL, UK	Similarity method, pressure balance design, elastic distortions	FD, RE, Grooved pistons	0.8	[13, B1, B2]
VNIIFTRI, Russia	Pressure balance design, Phase transitions	FD, CC	2.6	[14, 15]
PTB, Germany	Pressure balance design, elastic distortions, Hg melting line	FD, CC	1.0	[16, 17, 18, 57, 58, 62, 63]
LNE, France	Pressure balance design, elastic distortions, unique 0.2 and 1 GPa pressure balances	FD, CC, FPG	1.0	[19, B4, 20, 21, 38]
INRiM, Italy	Pressure balance design, elastic distortions, Hg melting line	FD, CC	1.0	[12, B5, 22, 23, 34, 35, B6]
WUT, Poland	Pressure balance design, elastic distortions	FD, MX	1.0	[24, 25]
NMIJ, Japan	Pressure balance design, elastic distortions	FD, CC, FPG	2.0	[26, 27, 28, 36]
SIMT, China	Pressure balance design, elastic distortions, phase transitions, unique 2.5 GPa CC pressure balance	RE, CC	2.5	Internal reports, Molinar visits 1983
DH-Budenberg (now WIKA), UK-France	Unique double-acting pressure balance, Design of multiplier up to 1 GPa, Design of pressure balances and highly automated pressure standards	FD, RE, CC, large diameters piston units	1.0	[19, 29, 30]
GE, Ruska (now Fluke), USA	Design of pressure balances and highly automated pressure standards	FD, RE	0.5	[31]
Harwood, USA	Design of pressure balances, mainly for very high pressures	FD, CC	1.4	[10]
DH Instruments (now Fluke), USA	Design of pressure balance and highly automated pressure standards	FD, CC, NFD, FPG	0.5	[32, 33, 34, 35, 37]

## 2. Peculiar aspects of some pressure balances

### 2.1 General

The main requirement for an “ideal” pressure balance is first of all the use of an “ideal” piston-cylinder having at least the following requirements:

- piston-cylinder unit made of hard materials, particularly able to withstand high compressive strength under elastic conditions;
- piston and cylinder machining and lapping made at the sub micrometer level with typical radial clearances smaller than  $0.5\ \mu\text{m}$  to  $1\ \mu\text{m}$ ;
- effective area at atmospheric pressure must be constant along the entire engagement length of piston and cylinder and the typical radial clearance  $h$  is normally below  $1\text{--}1.5\ \mu\text{m}$ , see for example [23];
- piston fall rate versus the applied pressure is an important reference measurement to be made. Values of piston fall rate depend on type of piston-cylinder and media, generally for free deformation units their values are lower than few  $\mu\text{m/s}$ .

### 2.2 Pressure balances in gas for very low-pressure range and for large piston-cylinder effective area

#### 2.2 a) Non-rotating pressure balances (force-balanced pressure balances)

An original device is the non-rotational pressure balance for gas operation developed at the NMIJ [39]. The piston-cylinder clearance is purposely irregular, weight suspension is obtained by means of a special mechanism, and piston inclination is detected by a monitoring technique. This pressure balance was used up to  $0.4\ \text{MPa}$  with stability better than  $1\ \text{ppm}$ . The same authors from NMIJ [36, 40] developed further this idea. They use an intentionally double-tapered cylinder in order to operate without piston rotation. The piston-cylinder, nominal effective area of  $2\ \text{cm}^2$ , is stabilised by a  $7\ \text{kPa}$  pressure inlet in the central part where clearance is larger. The second feature is the compensation of the piston weight by the measurement of this force by an electronic balance. The force-balanced principle allows pressure measurements from  $1\ \text{Pa}$  to  $10\ \text{kPa}$  with a sensitivity of  $5\ \text{mPa}$  and an estimated uncertainty of about  $15\ \text{mPa}$  or  $0.01\ \%$ .

DH Instruments [37, 41] further developed the idea of force balance pressure balances (FPG) in order to cover the gauge and absolute pressure range from  $1\ \text{Pa}$  to  $15\ \text{kPa}$ . The non-rotational piston-cylinder is schematically illustrated in Figure 2.

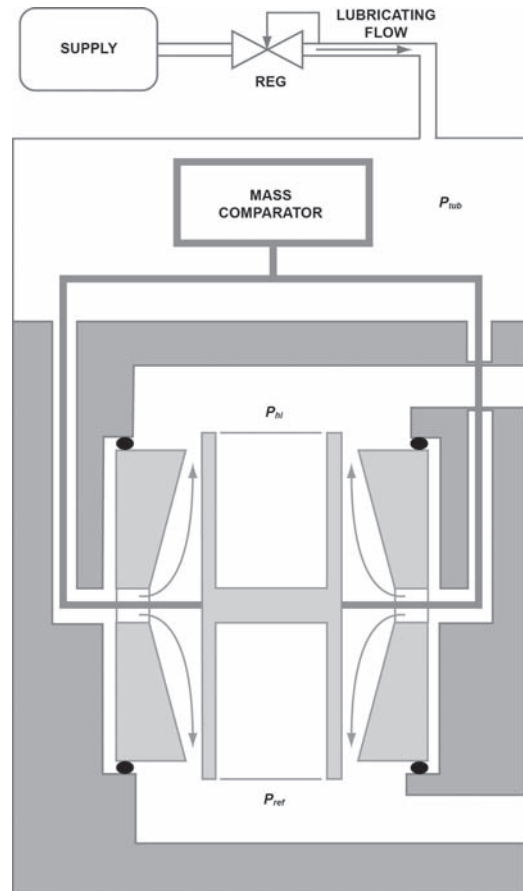


Figure 2. Non-rotational piston unit FPG as reported in a DH Instruments paper [37].

The piston-cylinder is made in tungsten carbide, the nominal effective area is  $9.8\ \text{cm}^2$ . The piston is straight while the cylinder is symmetrically tapered with a typical radial clearance of  $1\ \mu\text{m}$  (upper and lower part of the cylinder) and about  $4\ \mu\text{m}$  in the cylinder central part. An independent lubricating pressure ( $40\ \text{kPa}$  absolute for absolute mode or  $40\ \text{kPa}$  above atmospheric pressure for gauge mode) causes gas to flow through the piston-cylinder gap from the middle of the cylinder. A mass comparator measures the force on the piston and an automated pressure controller is used to adjust the flow across the different restrictions and to set and control pressure stability. With this system it is possible to have a pressure resolution of  $1\ \text{mPa}$  and an absolute measurement uncertainty of  $5\ \text{mPa} + 3 \cdot 10^{-5}p$  (with  $p$  expressed in Pa). These non-rotating piston devices are now very diffused in national metrology laboratories and different studies have been made. At LNE [38] they made a direct comparison of their FPG with a  $20\ \text{cm}^2$  pressure balance in gauge and in absolute mode. The relative difference of effective area was only  $1.2\ \text{ppm}$  and no significant effect of non-linearity was found between  $5\ \text{kPa}$  to  $15\ \text{kPa}$ . Other studies have been made at NIST [42, 43]. Four different FPG were compared (absolute mode from  $5\ \text{Pa}$  to  $15\ \text{kPa}$ ) with the ultrasonic NIST manometer (UIM). Good agreement within the uncertainty of  $(8\ \text{mPa} + 30 \cdot 10^{-6} \cdot p)$  was found. For comparison

an isolating capacitance diaphragm gauge was used to prevent humidified gas coming from FPG entering the UIM. This is a recommended good practice for applications of FPG and vacuum standards.

At Furness Controls [44] another interesting system was developed. The elimination of friction between piston and cylinder is achieved by a parallelogram suspension system. The piston has an effective area of 100 cm<sup>2</sup>, the gap between piston and cylinder is about 30 μm. There is a flow controller that supplies pressure and controls the flow, which is laminar through the engagement length of the piston-cylinder unit. The piston-cylinder is rigidly mounted on an electronic balance mechanism held at zero when only the piston is balanced. The declared uncertainty is 0.002 Pa + 0.003 % of the reading from zero to 1 kPa and 0.01 Pa + 0.003 % of the reading from 1 kPa to 3.2 kPa.

### 2.2 b) Large diameter pressure balances.

Particularly in gas pressure measurements around atmospheric pressure and up to few MPa, in absolute and in gauge mode, the use of large diameter piston-cylinder units of top-level geometry is now a reality. Rather normally piston-cylinder units of (2, 5, 10, 20, 50) cm<sup>2</sup> are used (some time even 100 cm<sup>2</sup>). The large area gives the possibility of reducing the pressure range, and if the geometry of the piston-cylinder is dimensionally regular it is also possible to reduce the pressure measurement uncertainty to below 10 ppm tending to approach few ppm. At LNE [45] an absolute pressure balance in the range from 150 kPa to 1 MPa was studied. The measuring systems are piston-cylinder units of nominal effective area of 10 cm<sup>2</sup> and 20 cm<sup>2</sup>. Such systems were later ameliorated [46] with automated masses loading on the floating elements,

using two 20-cm<sup>2</sup> and 10-cm<sup>2</sup> piston-cylinder units. The standard pressure uncertainty in the pressure range from 10 kPa to 1 MPa was 0.15 Pa + 3·10<sup>-6</sup>*p*, with *p* expressed in Pa.

DH Instruments [47] describe as well the early (1992-1995) NIST experience in using three 50 mm piston-cylinder units, in the absolute mode from 2.5 kPa to 175 kPa with a pressure uncertainty lower than 5·10<sup>-6</sup> and over a period of 20 months, a long term repeatability with a relative standard deviation of 2·10<sup>-6</sup> was obtained. Almost at the same time, investigations at NIST [48] presented piston-cylinder units of 50 mm in diameter reaching a relative expanded uncertainty of 5 ppm. Of course large diameter piston-cylinder unit can be used as well to measure pressure in liquid media [49]. Figure 3 shows the basic drawing of the tungsten carbide piston-cylinder of 50 mm (0.75 MPa maximum absolute and gauge pressure) that was used within EURAMET project 1039 for different numerical calculations.

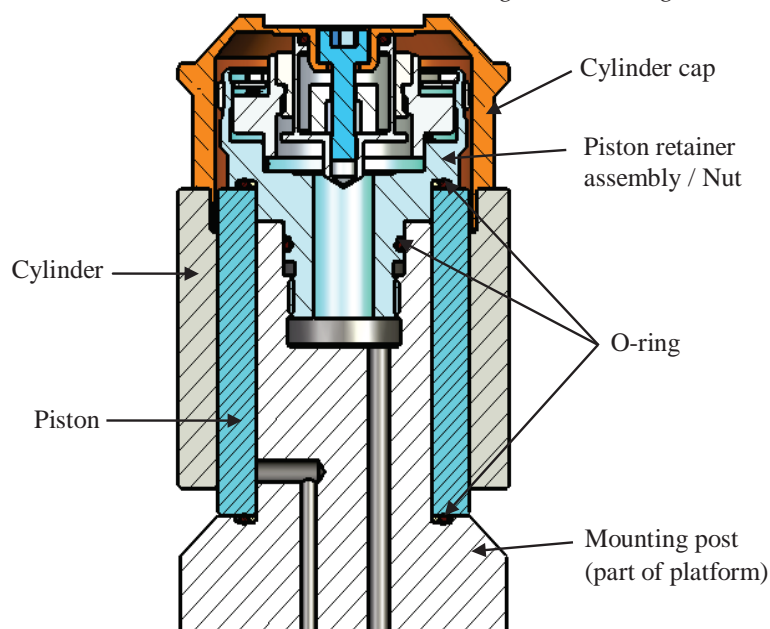
### 2.3 Pressure balances for very high range in liquids and mathematical modelling of pressure balances

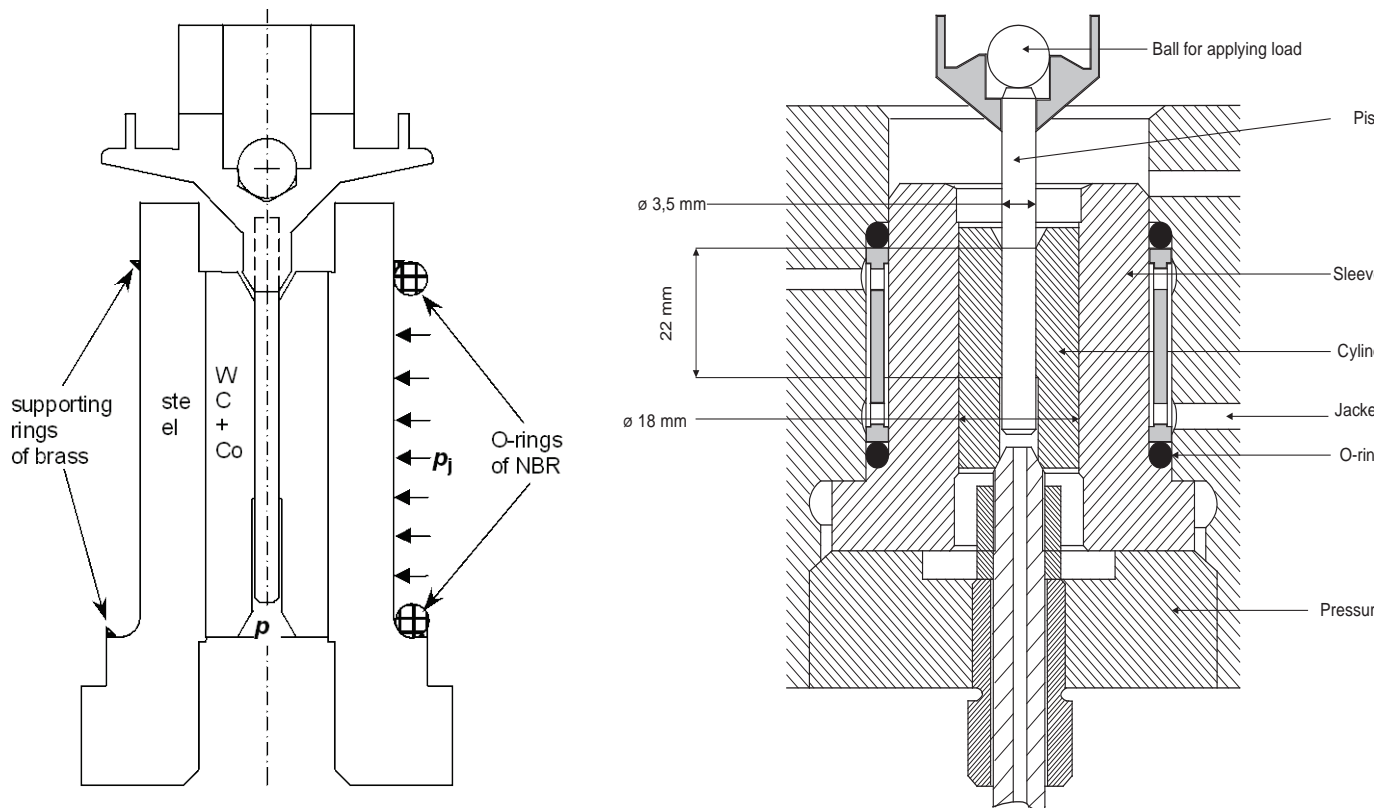
#### 2.3 a) Pressure balances for very high pressure range

Standard laboratories, frequently in cooperation with universities and top level industries in the pressure measurement field, have significantly contributed to the development of investigation methods and to basic research by developing, for example, the calculation of piston-cylinder elastic distortions, the measurement of physical properties of fluids and materials used in pressure metrology and the design of special pressure balances as well as the studies of different phase transitions.

Several companies have significantly contributed to the improvement of pressure balances both for industrial applications and for top-level metrological definitions of the pressure scale. For pressure measurements up to 100 MPa the different NMIs are generally equipped with free deformation piston-cylinder units. The present limits of free deforming units are from 500 MPa to 600 MPa, limits imposed by the high fall rates at high pressures that require the use of controlled clearance systems as being more reliable. A good example of modern pressure balances is given by DH Instruments and DH-Budenberg pressure balances [29, 30] operating in FD mode up to 500 MPa. Another example is DH Instruments pressure balance CC mode [32]. The development of CC systems has been extremely important because they are the only reliable systems that can be used for pressure measure-

Figure 3. PTB piston-cylinder assembly of 50 mm in diameter, 0.75 MPa full scale pressure, for absolute and gauge gas measurements, used in project EURAMET 1039. Extracted from EURAMET Project 1039 Reports.





ments above 0.6 GPa. Good examples of modern systems are the ones represented in Figure 4 of PTB and of LNE, [18, 21] both operative up to 1 GPa.

A significant example of cooperation between an NMI and a company is a unique controlled clearance system available at LNE, operating with different piston-cylinders units up to 200 MPa and 1 GPa. This installation is constituted by two fixed systems where different piston-cylinder can be mounted on 200 MPa or 1 GPa full scale set-up, allowing an important redundancy of systems [20, 21]. From 1 GPa to 3 GPa very few pressure balances are routinely in operation. Different attempts have been made in the past to extend safely the pressure range to 3 GPa. But this is not easy because fluids give serious problems of hydrostaticity and it is difficult to have intensifier routinely working up to 3 GPa. An interesting approach was made at NIST [11, B3] since 1967 and in China using a fully controlled clearance system with a final stage of high-pressure regulation. The controlled clearance pressure balance at NIST was used for the determination of the bismuth phase transition.

### 2.3 b) Mathematical modelling of pressure balances

In many NMIs it is almost routine to carry out finite-elements calculations to determine pressure distribution into the clearance and pressure distortion coefficient of a piston-cylinder unit

[13, 50, 51, 52, 53, 54 and B6] and these methods are important for the design of pressure balances.

The best example of top-level FEM calculation is represented by EURAMET Project 1039 (2008-2010), where 4 tungsten carbide piston-cylinder units are considered in gas for different modes of operation [55]. For all piston and cylinder units (10 cm<sup>2</sup> up to 1 MPa, 5 cm<sup>2</sup> up to 2 MPa, 20 cm<sup>2</sup> up to 0.75 MPa and 2 cm<sup>2</sup> up to 7.5 MPa) calculations are performed for nitrogen and helium in gauge and in absolute modes.

The task of this project was to minimize the uncertainty contribution produced by a pressure dependence of the effective area up to 7.5 MPa in order to verify that experimental pressure measurement uncertainty  $U(p)/p$  is close to 1 ppm, useful to Boltzmann constant experiment as in progress at PTB. Preliminary comparative results show that  $A_v, A_e = f(p)$  and  $\lambda$  are independent of the gas used within viscous flow model but there is fluid dependence for piston fall rates versus pressure; the larger contributions on  $\lambda$  uncertainty come from operation mode together with uncertainty on dimensional data and elastic constants; larger differences on  $\lambda$  are due to  $A_0$  discrepancies and the agreement in pressure is within 0.5 ppm up to 2 MPa. In the last years different attempts have been made to compare FEM calculated results between them; they are reported in [56, 57 and 58].

Although these methods have to be consi-

Fig 4 - Controlled clearance piston-cylinder units of PTB (left,  $A_0$  of 5 mm<sup>2</sup>, max load of 500 kg) and of LNE (right,  $A_0$  of 10 mm<sup>2</sup> and max load of 1000 kg), operative in liquids up to 1 GPa. Extracted from EURAMET Project 463 reports.

dered with precautions, they nevertheless represent a very useful attempt to increase confidence in calculation of pressure distortion coefficients. They prove the importance that dimensional measurements, pressure gradient distribution into the clearance, and elastic-constant determinations have in the uncertainty of calculated elastic distortion coefficients of pistons and cylinders.

#### 2.4 Special applications and highly automated pressure balances

Industrial developments have involved the production of extremely interesting and innovative pressure balances and devices allowing pressure multiplication up to 1 GPa as well as the use of twin pressure balances used to perform differential pressure measurements at high line pressure. It is worth to mention DH-Budenberg multiplier (ratio 1:10) where the low-pressure side uses a pressure balance having a 100 MPa full scale. Knowing the multiplier ratio (nominally 1:10), by measuring the low pressure and when the high side piston is in equilibrium, it is possible to calculate the high pressure on the specific side of the multiplier up to 1 GPa. This device was used as well as transfer standard for pressure comparisons up to 1 GPa [30]. An interesting evolution of a special pressure balance is DH Instruments (model 7202) aimed to operate also in gas up to 100 MPa in a negative free deformation (NFD) mode, assuring in this way an important link of the calibration chain between liquid and gas [59]. The modern pressure balances can be easily programmable to perform automatic calibration cycles where the pressure value is fully computed at the time of measurement.

#### 3. State of the art for pressure measurement uncertainty using pressure balances

Today pressure standard uncertainty, when using pressure balances, ranges from few ppm (10 kPa to some MPa) to a little less than 10 ppm

close to 100 MPa and from 80 ppm to 100 ppm at 1 GPa. This reflects as well the actual approved best CMC for calibration of pressure balances that range, on the average, from 10 ppm close to 0.1 MPa and up to some MPa, 40 ppm close to 100 MPa and 200 ppm close to 1 GPa.

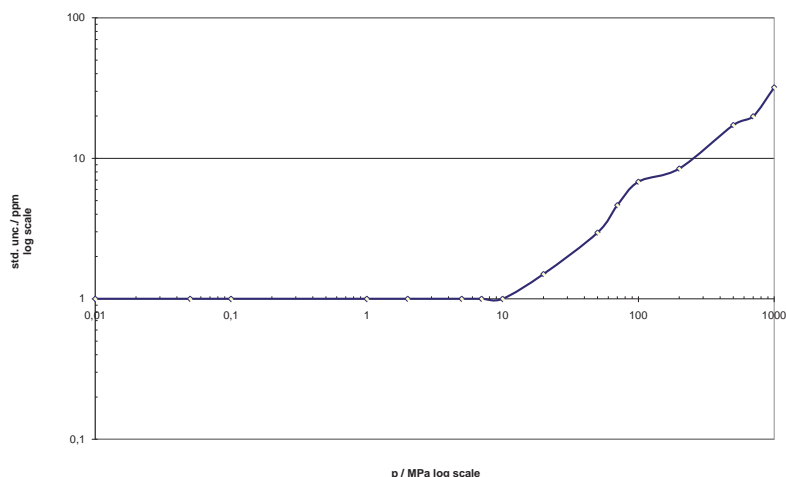
But there is a possibility today to reduce standard uncertainty in pressure measurements using improved pressure balances.

As an example of actual possibilities in Figure 5 are given possible standard uncertainties versus pressure in the range from 10 kPa to 1 GPa (logarithmic scales). As can be seen the uncertainty is 1 ppm from 10 kPa to 7 MPa as this is due to the main effort in some NMIs regarding the combined need of pressure measurements and the Boltzmann constant experiment. Starting from these results, a calculation was made considering the possibilities of deriving the effective area  $A_0$  by cross floating with sensitivities lower than 0.5 ppm and having elastic distortion coefficients derived from experimental verifications and FEA calculation with standard uncertainty of elastic distortion coefficients to less than 5%. Of course the graph in Figure 5 at actual stage is not fully achieved, it has to be demonstrated but at least can be considered a possibility for the future.

#### 4. Conclusions

- With some of the pressure balances available today, masses are automatically handled and loaded on pistons, all-important quantities significant for pressure calculations are automatically acquired and users can predetermine pressure steps procedures in order to run automatically pressure calibration cycles.
- One of the major efforts in pressure metrology is linked to Boltzmann constant determination. For a determination of Boltzmann constant, different approaches are on the way using different acoustic thermometry techniques [60, 61, 62, 63]. The dielectric-constant gas thermometer technique needs pressure standard measuring absolute pressure in helium up to 7 MPa with a relative standard uncertainty of 1 ppm. The success will not only constitute an important advance for temperature metrology, but it will also generate important advances for pressure metrology achieving a 1 ppm uncertainty for absolute gas pressure measurements up to 7 MPa with pressure balances. This will have an impact as well in reducing the estimated uncertainty in the highest-pressure range.

Fig. 5 Pressure measurement standard uncertainty (ppm) versus pressure (MPa) in logarithmic scales by pressure balances: are we ready to announce these achievements?



## References

- [1] Molinar G., *Metrologia*, (1993-1994), **30**, 615-623.
- [2] Ehrlich C., *Metrologia*, (1993-1994), **30**, 585-590.
- [3] Tilford C. R., Pressure and Vacuum Measurements, *Physical Methods of Chemistry*, Vol. 6, Chap. 2, New York, J. Wiley & Sons, 1992.
- [4] Parrot M., *Mem. St. Peter. Acad.*, 1832, **2**, 595-630.
- [5] Galy-Cazalat, *Bull. Soc. Eng. Industr. Nat. Paris*, 1846, 590-592.
- [6] Seyss L., *Dinglers Polytechnisches*, 1869, **191**, 352-354.
- [7] Rucholz E., *Dinglers Polytechnisches*, 1883, **247**, 21.
- [8] Bridgman P. W., *Proc. Am. Acad. Arts Sci.*, 1911, **47**, 321-343.
- [9] Bridgman P. W., *Proc. Am. Acad. Arts Sci.*, 1909, **44**, 201-217.
- [10] Johnson D. P., Newhall D. H., *Trans. ASME*, 1953, 301-310. See also Newhall D. H., US patent number **2796229**, 1957.
- [11] Johnson D.P. and Heydemann P.L.M., *Rev. Sci. Instrum.*, 1967, **38**, 1924.
- [12] Molinar G., Bean V.E., Houck J., Welch B., *Metrologia*, 1991, **28**, 353-354.
- [13] Samaan N.D., Mathematical modelling of instruments for pressure metrology, *Ph.D. Thesis*, City University, London, UK, 1990.
- [14] Zolotich E.V., *High Pressure research*, VNIIFTRI editor, Moscow (in Russian), 1987.
- [15] Sekoyan S.S., Strelchev G.K., Shmin Y.I., *Izmer. Tekh.*, 1989, **7**, 31-32.
- [16] Jäger J., Klingenberg G., Schoppa G., *PTB Mitteilungen*, 1982, **92**, 321-327.
- [17] Klingenberg G., *BIPM Monographie 89/1*, 1989, 1-11.
- [18] Jäger J. and Sabuga W., *Proc. of the Second International Pressure Metrology Workshop*, 26-30 November 2001, New Delhi, India, Editor Bandyopadhyay A. K. et al., NPL-India, 15-20, 2001.
- [19] Legras J.C., Huot A., Delajoud P., *Bulletin BNM*, 1982, **No. 48**, 9-33.
- [20] Legras J.C., *BIPM Monographie 89/1*, 1989, 41-52.
- [21] Legras J. C. , *Proc. of the Second International Pressure Metrology Workshop*, 26-30 November 2001, New Delhi, India, Editor Bandyopadhyay A. K. et al., NPL-India, 9-4, 2001.
- [22] Molinar G., Maghenzani R., Cresto P.C., Bianchi L., *Metrologia*, 1992, **29**, 425-440.
- [23] Molinar G., Bergoglio M., Sabuga W., Otal P., Ayyildiz G., Verbeek J., Farar P., *Metrologia*, 2005, **42**, 197-201.
- [24] Wisniewski R., Rostocki A.J., Rajski K., Bock W., *Wysokie Cisnienia*, Warsaw, Poland, Editor Wydawnictwa Naukovo-Techniczne (in polish), 1980.
- [25] Molinar G., Buonanno G., Dell'Isola M., Maghenzani R., Urbanski M., Wisniewski R. *Metrologia*, 1999, **36**, 585-590.
- [26] Yasunami K., *Metrologia*, 1968, **4**, 168-177.
- [27] Nishibata K., Yamamoto S., Kaneda R., *Jap. Journ. Appl. Phys.*, 1980, **19-11**, 2245-2256.
- [28] Yamamoto et al., *Bull. NRLM*, 1985, **34(3)**, 218-223.
- [29] Budenberg G. F., *Instrument Control System*, 1971, 120-121.
- [30] Delajoud P., *BIPM Monographie 89/1*, 1989, 114-124.
- [31] GE Sensing document, Ruska Hydraulic Piston Gauge mod. 2485, 2005, www.gesensing.com.
- [32] Delajoud P. and Girard M., *Proc. of the Second International Pressure Metrology Workshop*, 26-30 November 2001, New Delhi, India, Editor Bandyopadhyay A. K. et al., NPL-India, 2001, 33-37.
- [33] Delajoud P. and Girard M., *Proc. of the IMEKO TC 16 International Symposium on Pressure and Vacuum*, 22-24 September 2003, Beijing, China, Acta Metrologica Sinica Press, Beijing, 2003, 154-159.
- [34] Buonanno G., Molinar G., Giovinco G., Delajoud P., Haines R., *Metrologia*, 2005, **42**, 207-211.
- [35] Buonanno G., Giovinco G., Molinar G., Delajoud P., Haines R., *Proceedings of XVIII IMEKO WORLD CONGRESS Metrology for a Sustainable Development*, September, 17 - 22, Rio de Janeiro, Brazil, 2006.
- [36] Ooiwa A., *Metrologia*, (1993/94), **30**, 607-610.
- [37] Delajoud P. and Girard M., *Proceedings of the NCSLI Conference*, San Diego (CA, USA), 2002.
- [38] Otal, P., Legras, J.C., *Metrologia*, 2005, **42**, S216-S219.
- [39] Ooiwa, A., *BIPM Monographie 89/1*, 1989, 67-72.
- [40] Ooiwa, A., Ueki, M., *Vacuum*, 1993, **44**-5-7, 603-605.
- [41] Haines, R., Blair, M., *Presented at 2002 JAN Measurement Science Conference*, Anaheim, CA, USA, 2002.
- [42] Haines, R., Bair, M., *XIX IMEKO World Congress*, Lisboa, Portugal, 6-11 September 2009, Conference Proceedings, 2009, 2071-2076.
- [43] Hendricks, J.H., Olson, D.A., *XIX IMEKO World Congress*, Lisboa, Portugal, 6-11 September 2009, Conference Proceedings 2009, 2077-2083.
- [44] Rendle, C.G., *Metrologia*, (1993/94), **30(6)**, 611-613.
- [45] Legras, J.C., Le Guinio, J., *Proceedings of the 7<sup>th</sup> International Congress Metrologie*, France, 1995, 319-324.

- [46] Le Guinio, J., Legras, J.C., El-Tawil, A., *Metrologia*, 1999, **36**, 535-539.
- [47] Delajoud, P., Girard, M., Ehrlich, C., *Metrologia*, 1999, **36**, 521-524.
- [48] Schmidt, J.W., Cen, Y., Driver, R.G., Bowers, W.J., Houck, J.C., Tison, S.A., Ehrlich, C., *Metrologia*, 1999, **36**, 525-529.
- [49] Jäger, J., Sabuga, W., Wassmann, D., *Metrologia*, 1999, **36**, 541-544.
- [50] Wisniewski, R., Sendys, R., Wisniewski, D. and Rostocki, A.J., *BIPM Monographie 89/1*, 1989, 27-30.
- [51] Samaan, N.D. and Abdullah, F., *Metrologia*, (1993/94), **30**, 641-644.
- [52] Buonanno, G., Dell'Isola, M. and Maghenzani, R., *Metrologia*, 1999, **36**, 579-584.
- [53] Fitzgerald, M. P., Sutton, C.M. and Jack, D.G., *Metrologia*, 1999, **36**, 571-573.
- [54] Molinar, G., Buonanno, G., Giovinco, G., Delajoud, P. and Haines, R., *Metrologia*, 2005, **42**, S207-S211.
- [55] Sabuga, W., Priruenrom, T., Molinar, G., Buonanno, G., Raboult, T., Wongthep, P. and Prazak, D., *paper presented to the 5<sup>th</sup> CCM pressure and 4<sup>th</sup> IMEKO TC 16 Conference*, Berlin, DE, 2-5 May 2011, 2011.
- [56] Molinar, G., Sabuga, W., Robinson, G. and Legras, J.C., *Metrologia*, 1998, **35**, 739-759.
- [57] Sabuga, W., Molinar, G., Buonanno, G., Eward, T., Rabault, T. and Yagmur L., *Metrologia*, 2005, **42**, S202-S206.
- [58] Sabuga, W., Molinar, G., Buonanno, G., Eward, T., Legras, J.C. and Yagmur L., *Metrologia*, 2006, **43**, 311-325.
- [59] Buonanno, G., Giovinco, G., Molinar, Min Beciet, G., Delajoud, P. and Haines, R., XVIII IMEKO World Congress, Rio de Janeiro, Brazil, 17-22 September 2006, *available on CD Conference Proceedings (section TC 16)*, 2006.
- [60] Moldover, M. R., *13<sup>th</sup> Symposium on thermophysical properties*, NIST June 1997, 1997, 386.
- [61] Schmidt, J. W., Jain, K., Müller, A.P., Bowers, W.J. and Olson, D.A., *Metrologia*, 2006, **43**, 53-59.
- [62] Zandt, T., Gaiser, C. and Fellmuth, B., IV<sup>th</sup> International Workshop "Progress in determining the Boltzmann constant", 22-24 September 2009, INRiM, Torino, Italy, 2009.
- [63] Sabuga, W., *AdMET Conference, New Delhi-India*, Conference proceedings on CD, paper 58, 2006, 555-564.
- Books dealing with pressure balances**
- [B1] Dadson R. S., Lewis S., Peggs G. N., *The pressure balance. Theory and practice*, Teddington, UK, National Physical Laboratory, 1982.
- [B2] Lewis S., Peggs G. N., *The pressure balance. A practical guide to its use*, 2<sup>nd</sup> ed., Teddington, UK, National Physical Laboratory, 1992.
- [B3] Heydemann P. L. M., Welch B. E., In *Experimental Thermodynamics*, Vol. 2, Chap. 4, Part 3 (Edited by B. Le Neindre and B. Vodar), London, Butterworth, 1975.
- [B4] Legras J. C., *La mesure des pressions statiques*, Paris, Chiron Editeur, 1988.
- [B5] Pavese F., Molinar G., *Modern gas-based temperature and pressure measurements*, New York, Plenum PublishingCo., 1992. Second Edition, in progress.
- [B6] Buonanno G. and Molinar G. Editors, Ten years of experience in modelling pressure balances in liquid media up to few GPa, Università di Cassino, pp. 182, ISBN:978-88-8317-037-9, 2007. Free download at [http://casino.adacto.it/sba/modelling\\_pressure.cfm](http://casino.adacto.it/sba/modelling_pressure.cfm) .

# Pressure measurements in gas media up to 7.5 MPa for the Boltzmann constant redetermination

W. Sabuga<sup>1</sup>

## Abstract

For the redetermination of the Boltzmann constant using a dielectric-constant gas thermometer (DCGT), which requires absolute pressure measurements in helium up to about 7 MPa with a relative standard uncertainty ( $u$ ) as low as  $1 \cdot 10^{-6}$ , new special absolute pressure balances were developed and characterised. Traceability of pressure measurements up to 7.5 MPa to the SI base units on a low uncertainty level is achieved by improvements in the determination of the piston-cylinder units' (PCUs) effective area ( $A_0$ ) from dimensional measurements, quality of weights, knowledge of the local gravity acceleration and the cross-float performance of the pressure balances. With enhanced dimensional measurements and advanced models,  $A_0$  of primary 20 cm<sup>2</sup> PCUs was determined with  $u \leq 0.7 \cdot 10^{-6}$ . Pressures up to 7.5 MPa are measurable with three 2 cm<sup>2</sup> PCUs traceable to the three 20 cm<sup>2</sup> PCUs. Pressure distortion coefficients were determined by the finite element method using PCUs' dimensional and elastic constants, the latter measured by resonant ultrasound spectroscopy. Cross-float measurements were performed in absolute mode using differential pressure cells with  $u \leq 1 \cdot 10^{-6}$ . The present combined uncertainty of pressures (1–7) MPa is  $(1.8\text{--}2.1) \cdot 10^{-6}$ .

**Keywords:** Gas pressure balance, effective area, pressure distortion coefficient, finite element analysis, Boltzmann constant

## 1. Introduction

To prepare a new definition of the temperature unit kelvin – which is presently defined by the temperature of the triple point of water and thus linked to a material property – on the basis of the Boltzmann constant ( $k$ ), several projects have been started worldwide to independently measure its value [1]. The independent measurements should demonstrate their reliability by results consistent with each other and with the known value determined by the acoustic gas thermometry method [2] and recommended by CODATA for international use [3]. Among the potential methods there is dielectric-constant gas ther-

mometry (DCGT), which is used at PTB. In this method, the temperature ( $T$ ) and the pressure ( $p$ ) of a gas are measured simultaneously with the electrical capacitance ( $c$ ) of a capacitor immersed in the gas [1, 4, 5]. The Boltzmann constant can be determined by combining the equation of state with the Clausius-Mossotti equation to form the expression

$$\frac{p}{T} \frac{\alpha_0}{\varepsilon_0 k} \approx \chi \left[ 1 + \frac{B}{N_A \alpha_0 / \varepsilon_0} \chi + \frac{C}{(N_A \alpha_0 / \varepsilon_0)^2} \chi^2 + \dots \right], \quad (1)$$

with  $N_A$  and  $\varepsilon_0$  being the Avogadro and the electric constants,  $B$  and  $C$  the second and third density virial coefficients,  $\alpha_0$  the static electric dipole polarisability of the gas atom, and  $\chi$  the gas dielectric susceptibility. As a gas, helium is used because its  $\alpha_0$  can be calculated theoretically. The value of  $\chi$  is determined by capacitance measurements at vacuum and pressure conditions,  $\chi = c(p)/c(0) - 1$ . The optimal pressure range of the DCGT experiment is from 2 MPa to 7 MPa, which is defined by the uncertainty of  $\chi$  decreasing with pressure and the uncertainties of  $B$  and  $C$  increasing with it. In order to achieve the relative standard uncertainty of  $k$  of about  $2 \cdot 10^{-6}$ , as targeted in the present phase of the project, absolute pressure measurements should be performed with a relative standard uncertainty of about  $1 \cdot 10^{-6}$  (1 ppm); all uncertainties considered in this work are standard uncertainties. A feasibility analysis for such a small uncertainty of the absolute pressure measured with a pressure balance was performed in [6]. Following this, special pressure balances were developed and extensively studied, theoretically and experimentally, and are being applied in the DCGT measurements.

## 2. Pressure balances

A system of special pressure balances was developed and manufactured by DH Instruments, Fluke Corporation, USA [7]. The design supports the reduced uncertainty with focus on the areas of temperature stability, mass uncertainty, effective area, and pressure distortion coefficient. The system includes two pressure balance platforms, three 20 cm<sup>2</sup> piston-cylinder units (PCUs) identi-

<sup>1</sup> W. Sabuga, Physikalisch-Technische Bundesanstalt (PTB), Braunschweig, Germany, E-mail of author: wladimir.sabuga@ptb.de



fied by serial nos. 1159, 1162 and 1163, and three 2 cm<sup>2</sup> PCUs with serial nos. 1341, 1342 and 1343, the 20 cm<sup>2</sup> PCUs being of cylinder floating, and the 2 cm<sup>2</sup> PCUs being of piston floating configuration. The decision to cover the pressure range up to 7.5 MPa using PCUs of two different sizes was dictated by the limited accuracy of the dimensional measurements, which provide uncertainties in the zero pressure effective area ( $A_0$ ) below 1 ppm only for large PCUs, and was based on the expectation of linking the smaller PCUs to the large primary ones by cross-float measurements with experimental standard uncertainties essentially smaller than 1 ppm. Each platform is equipped with automated mass handlers and a mass set of 150 kg total, allowing cross-float and pressure measurements in gauge and absolute mode, operated manually or automatically by a computer.

To enable determination of the piston or cylinder load on the uncertainty level  $\ll 1$  ppm, the eleven 12.5 kg main masses in each pressure balance were designed in accordance with the requirements of recommendation OIML R 111-1 to masses of Class E1 concerning their material mechanical and magnetic properties, and were made of special austenitic stainless steel HE210 and had polarization (magnetization)  $\mu_0 M < 0.5 \mu\text{T}$ , magnetic susceptibility  $\chi_m < 0.004$  and surface roughness  $R_z < 0.15 \mu\text{m}$ . Their densities were determined by the hydrostatic weighing at the PTB mass laboratory with a standard uncertainty of 0.85 kg/m<sup>3</sup> and varied for the 22 weights between 8063.1 and 8064.7 kg/m<sup>3</sup>. Their masses were measured with a relative standard uncertainty of 0.05 ppm in 2008 and – after a one year operation of the pressure balances – in 2010. The relative change of the masses was between 0.08 and 0.024 ppm. Such a quality of the masses could be achieved as a result of their manufacture by a company specialising in the production of reference masses. In the first tests of the pressure balances in 2008, it turned out that, in spite of the excellent properties of the weights as reference masses, not all masses met the dimensional tolerance requirements of the pressure balances which then had to be re-machined. An additional set of 7 so-called binary masses of 0.1, 0.2, 0.4, ..., 6.4 kg was contained in each pressure balance. Their masses were determined with relative standard uncertainties from 0.5 to 1.5 ppm.

In order to perform automated cross-floats with the pressure balances in absolute mode – automatically and with a possibility of different gases in them – at a high level of cross-float sensitivity [8], and after testing different various pressure cells (DPCs) [6], an MKS Baratron type 698A11TRC at pressures up to 0.75 MPa and a Rosemount type 3051S1CD1A at pressures up to

7.5 MPa were chosen to indicate pressure equilibrium. Both DPCs were calibrated at atmospheric pressures using a digital pressure balance FRS-4 by Furness Control, UK, and, at high static pressures, using the two pressure balances by the technique described in [9, 10]. The uncertainty of their calibration was 0.1 Pa for the MKS Baratron and 0.25 Pa for the Rosemount. Later, the Rosemount DPC was also used to separate the DCGT capacitor, which was filled with helium of the highest purity, from the reference pressure balance.

Further details of the pressure balances' design and the results of their experimental evaluation are presented in [7].

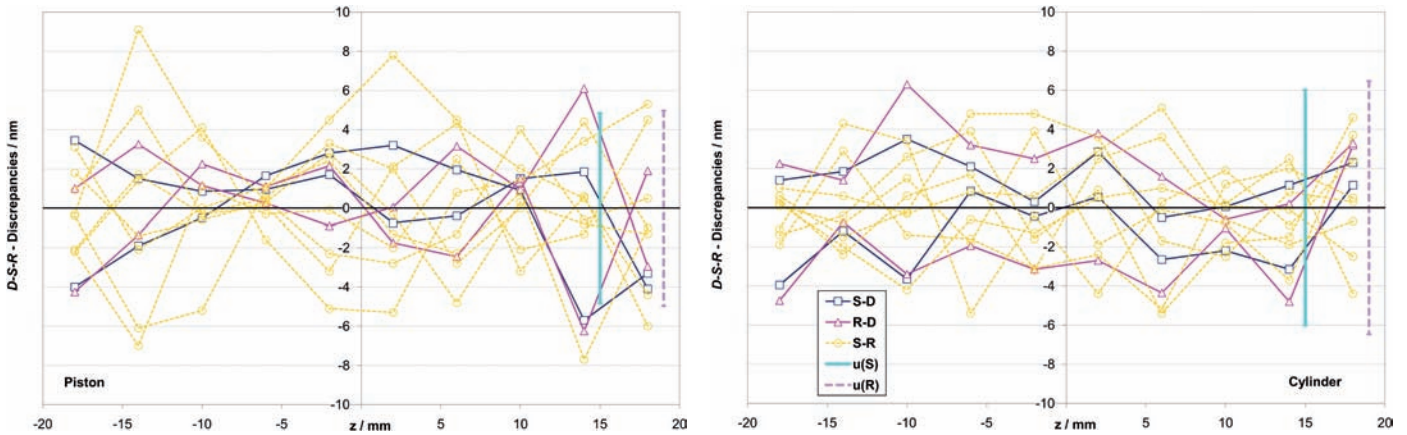
One of the 6 PCUs, PCU 1341, which had to be re-machined, has not been completely characterised yet and is not considered in the following. For another 2 cm<sup>2</sup> PCU, 1342, dimensional properties have not yet been finally stated and are not reported.

### 3. Dimensional measurements

Four different dimensional instruments were investigated to get best measurements of diameters ( $D$ ), straightness ( $S$ ) and roundness ( $R$ ) of the PCUs: the comparator KOMF specialising in  $D$  measurements [11], a modified RTH Talyrod 73 instrument providing lowest uncertainties for  $R$  [12], a universal modified MarForm instrument MFU8 capable of measuring all  $D$ ,  $S$  and  $R$  [13], and, finally, a new instrument MFU110WP that can measure  $D$ ,  $S$  and  $R$  with tactile and optical (contactless) probes and, additionally, can perform a high-density scan of a complete lateral surface of the piston and cylinder bore [14]. The lowest uncertainties in 3D data generated on the basis of  $D$ ,  $S$  and  $R$  data could be achieved with a combination of KOMF with MFU8 [15-17]. Optimal dimensional results could be achieved after numerous measurements carried out in the period from June 2008 to April 2011, in which measurements on the 20 cm<sup>2</sup> PCUs were repeated up to 5 times, and on the 2 cm<sup>2</sup> PCUs up to 2 times. As a criterion of the quality of the dimensional measurements the uncertainty of 3D data was considered, the data including piston and cylinder radii along the straightness and roundness traces,  $r_s$  and  $r_r$ . These radii were generated by a new approach [18] which links  $D$ -,  $S$ - and  $R$ -data using the weighted least squares method and leads to minimum discrepancies between the different types of data after the link. The uncertainties of the radial values  $u(r_s)$  and  $u(r_r)$  were then calculated by the relationships

$$u(r_r) = \left\{ \left[ u(D)/2 \right]^2 + \delta^2(r_{D-R}) + \delta^2(r_{R-S}) \right\}^{0.5}, \quad (2)$$

$$u(r_s) = \left\{ \left[ u(D)/2 \right]^2 + \delta^2(r_{D-S}) + \delta^2(r_{R-S}) \right\}^{0.5}, \quad (3)$$



where  $u(D)$  is the uncertainty of the diameter measurements, and  $\delta(r_{D-R})$ ,  $\delta(r_{D-S})$  and  $\delta(r_{R-S})$  are mean discrepancies between the  $D$  and  $R$ ,  $D$  and  $S$  as well as  $R$ - and  $S$ -based radii, respectively. Figure 1 shows  $\delta(r_{D-R})$ ,  $\delta(r_{D-S})$ ,  $\delta(r_{R-S})$ ,  $u(r_S)$  and  $u(r_R)$  for the piston and cylinder of PCU 1343.

The lowest uncertainty for  $D$ ,  $u(D) = 5$  nm for the piston and  $u(D) = 10$  nm for the cylinder, could be achieved with KOMF, which was applied to all 20 cm<sup>2</sup> PCUs. For the 2 cm<sup>2</sup> PCUs, a complete  $D$  measurement with KOMF was possible for several constraints only on PCU 1343 in 2011. The other  $D$  measurements were performed with MFU8 and are less reliable. Thus, the lowest uncertainties in the 3D data could be obtained for the three 20 cm<sup>2</sup> PCUs and PCU 1343 with the uncertainty components reported in table 1.

In the calculation of  $u_r(A_0)/A_0$ ,  $u(r)$  of the cylinder and piston were considered to be non-correlated because the systematic uncertainty contribution of the diameter measurements, 2.5 nm for piston and 5 nm for cylinder, is small compared with the contribution of the randomly distributed  $\delta(r_y)$  values.

#### 4. Zero pressure effective area

In the calculation of  $A_0$  from the dimensional data, the basic idea by Dadson et al. [19] was used to determine the three forces acting on the floating piston or cylinder – of the measurement and residual pressures on the piston/cylinder bases ( $F_0$ ), the net axial component of the pressure in the piston-cylinder gap ( $F_p$ ), and the drag force of the gas flowing through the gap ( $F_d$ ). However, further developments were made to address the axial non-symmetry of the real PCUs and the flow of the real gases through the gap.

Instead of using the one-dimensional flow model and calculating the mean effective area for all azimuthal directions with its standard deviation as uncertainty contribution, a two-dimensional model was applied, based on the following 2D continuity equation [20]:

$$\frac{\partial^2 p^2}{\partial y^2} + \frac{\partial^2 p^2}{\partial z^2} + \frac{3}{h} \frac{\partial h}{\partial y} \frac{\partial p^2}{\partial y} + \frac{3}{h} \frac{\partial h}{\partial z} \frac{\partial p^2}{\partial z} = 0, \quad (4)$$

where  $z$  and  $y$  are axial and tangential coordinates,  $0 \leq z \leq l$ ,  $l$  being the gap length;  $y = r\varphi$ ,  $r$  – radius and  $\varphi$  – angle,  $0 \leq \varphi \leq 2\pi$ ;  $p$  and  $h$  are local pressure and the gap width, respectively, being both functions of  $z$  and of  $y$ . Numerical integration of (4) furnished  $p(z, y)$  and allowed calculation of a single  $A_0$  value for the entire 2D PCU gap without any assumption of the axial symmetry and uncertainty associated with this assumption [21].

Potential dependence of  $A_0$  on the gas flow behaviour and, thus, on pressure, operating mode and gas type [22] was considered, and former theoretical [19, 23-25] and experimental [25-28] works analysed with the following summary:

- Force  $F_0$  is independent of gas flow;
- Pressure distribution along the piston-cylinder gap  $p(z)$  depends on the gas flow behaviour;
- The sum of the drag forces acting on piston and cylinder ( $F_{dp}$  and  $F_{dc}$ ) is defined by the fundamental relation

$$\frac{d(F_{dp} + F_{dc})}{dz} = -\frac{dp}{dz} h r, \quad (5)$$

valid for any flow regime, which means that  $F_{dp} + F_{dc}$  is unequivocally defined by the pressure distribution and, at a given  $p(z)$ , is independent of the gas flow behaviour.

Figure 1. Discrepancies between  $r_s$  and  $r_D$  (S-D),  $r_r$  and  $r_D$  (R-D),  $r_s$  and  $r_r$  (S-R) as well as radii uncertainties along the S and R traces ( $u(S)$  and  $u(R)$ ) for piston (a) and cylinder (b) of PCU 1343

Table 1. PCUs, their cylinders and pistons, discrepancies  $D$ ,  $R$  and  $S$  data ( $\delta_{D-R}$ ;  $\delta_{D-S}$ ;  $\delta_{R-S}$ ), uncertainty of radii along  $R$  and  $S$  traces ( $u(r_R)$ ;  $u(r_S)$ ), and resulting uncertainty contributions for  $R$ - and  $S$ -based effective areas ( $u_{r,R}(A_0)$ ;  $u_{r,S}(A_0)$ )

PCU	Cylinder		Piston		$u_{r,R}(A_0)/A_0$ ; $u_{r,S}(A_0)/A_0 \times 10^6$
	$\delta_{D-R}$ ; $\delta_{D-S}$ ; $\delta_{R-S}$ /nm	$u(r_R)$ ; $u(r_S)$ /nm	$\delta_{D-R}$ ; $\delta_{D-S}$ ; $\delta_{R-S}$ /nm	$u(r_R)$ ; $u(r_S)$ /nm	
1159	16; 11; 8	19; 14	6; 6; 5	8; 9	0.8; 0.7
1162	4; 6; 4	8; 9	7; 6; 4	9; 8	0.5; 0.5
1163	11; 7; 6	14; 11	5; 3; 8	9; 9	0.7; 0.6
1343	3; 2; 3	7; 6	3; 3; 3	5; 5	1.0; 1.0

Table 2. Dimensional effective areas and their relative uncertainties of 4 PCUs calculated with the viscous (Dadson) and rarefied gas flow (RGF) theory, in gauge (g) and absolute (a) mode for N<sub>2</sub> and <sup>4</sup>He

	1159	1162	1163	1343
Dadson, g	19.610122	19.610066	19.610447	1.9610934
RGF, g, N <sub>2</sub>	19.610119	19.610062	19.610443	1.9610925
RGF, g, <sup>4</sup> He	19.610116	19.610061	19.610441	1.9610921
RGF, a, N <sub>2</sub>	19.610114	19.610060	19.610441	1.9610919
RGF, a, <sup>4</sup> He	19.610112	19.610058	19.610439	1.9610910
$u(A_0)/A_0 \times 10^6$	0.7	0.5	0.6	1.0

For better understanding and estimation of the gas flow effect, consideration of the 4 following models is helpful.

- **Model 1:** Plane gap of constant width, which corresponds to a geometrically ideal PCU with  $h/r \rightarrow 0$ . Here,  $F_p = 0$ ,  $F_{dp} = F_{dc}$  and, therefore,  $A_0$  is independent of the gas flow.
- **Model 2:** Plane gap of variable width along  $z$ , which corresponds to a dimensionally real PCU with  $h/r \rightarrow 0$ . Here,  $F_{dp} = F_{dc}$ , but  $A_0$  depends on the gas flow because  $F_p$  depends on  $p(z)$ .
- **Model 3:** Annular gap of constant width, which corresponds to a geometrically ideal PCU whose relation of  $h$  to  $r$  is taken into account. In this case,  $F_p = 0$ , but  $F_{dp}$  and  $F_{dc}$  are generally not equal. The difference between them depends on the gas flow and becomes larger with increasing  $h/r$ . The effect of this difference on  $A_0$  when changing from viscous to molecular flow regime was considered in [19, 23, 24] with different approaches but qualitatively similar results: the change from the viscous to molecular flow regime produces a relative change in  $A_0$  of about  $0.6 \cdot (h/r)^{1.5}$ . For the present 20 cm<sup>2</sup> and 2 cm<sup>2</sup> PCUs with their mean  $h/r$  of  $1.2 \cdot 10^{-5}$  to  $2.9 \cdot 10^{-5}$  the relative effect of the gas flow on  $A_0$  due to the drag force is only  $2.6 \cdot 10^{-8}$  to  $1 \cdot 10^{-7}$  maximum.
- **Model 4:** Annular gap of variable width along  $z$ , which corresponds to a dimensionally real PCU whose relation of  $h$  to  $r$  is taken into account. For this most general model,  $F_{dp}$  and  $F_{dc}$  depend on  $h/r$  and gas flow as shown in model 3. For the particular 20 cm<sup>2</sup> and 2 cm<sup>2</sup> PCUs this produces a negligibly small effect as shown for model 3. However, the PCUs' not ideal geometry implies non-zero  $F_p$ , whose determination requires the calculation of  $p(z)$  being dependent on the gas flow behaviour.

In view of these theoretical conclusions, two general explanations for the experimentally ob-

Table 3. Pressure distortion coefficients ( $\lambda_1$  and  $\lambda_2$ ) and uncertainty of  $\lambda_1 + \lambda_2 p$  ( $u(\lambda)$ ) at maximum pressure of the PCUs calculated by RGF model in absolute mode

PCU	$\lambda_1 \times 10^6$ MPa	$\lambda_2 \times 10^6$ MPa <sup>2</sup>	$u(\lambda) \times 10^6$ MPa
1159	7.072	-2.728	0.10
1162	6.358	-2.511	0.08
1163	5.055	-1.697	0.10
1342	1.302	-0.008	0.034
1343	2.604	-0.103	0.029

served effects of gas and the operation mode on  $A_0$  in the past [25-28] can be suggested. The PCUs in those studies had a much larger ratio  $h/r$  than that of the

present PCUs and could be effected by the changing drag force. The second effect, which appears to be much stronger than the first one, could be produced by different pressure distributions with different gases and operating modes in combination with larger  $h/r$  and, thus, larger relative dimensional irregularities of the former PCUs.

For the high accuracy of the effective areas required in the Boltzmann constant project, accurate calculation of  $p(z)$  was performed by the methods of modern rarefied gas dynamics. Numerical solutions of gas flows based on the kinetic equation and valid over a wide range of the gas rarefaction were applied as presented with more detail in [29]. Results furnished by the Dadson and the new theory for the 4 PCUs are shown in table 2.

They were obtained by calculating pressure-dependent effective areas ( $A_p$ ) of the 20 cm<sup>2</sup> PCUs in the range 0.01 to 0.7 MPa and of the 2 cm<sup>2</sup> PCU in the range 0.1 to 7 MPa, and extrapolating them to  $p = 0$ . For the 20 cm<sup>2</sup> PCUs the effect of gas sort is < 0.1 ppm and of operation mode < 0.2 ppm. The use of viscous flow theory produces an error of up to 0.5 ppm. The final combined uncertainty of  $A_0$  is dominated by the uncertainty of the dimensional data.

## 5. Pressure distortion coefficient

The pressure distortion coefficients ( $\lambda$ ) of the PCUs for different operation modes, gases, and taking into account real dimensional properties of the PCUs were calculated by the finite element method (FEM), combined with the viscous flow [19] and the RGF model [29]. The methodology of calculating  $\lambda$  and its uncertainty for gas-operated PCUs by the FEM had been developed and analysed within research project EURAMET 1039 [30]. The Young modulus ( $E$ ) and the Poisson coefficient ( $\mu$ ) of the tungsten carbide (WC) hard alloy which the PCUs are made of were determined by resonant ultrasound spectroscopy [31] with uncertainties  $u(E) = 1.9$  GPa

and  $u(\mu) = 0.0013$ . As  $\lambda$  depended on pressure, it was expressed by equation  $\lambda = \lambda_1 + \lambda_2 p$ . The values of  $\lambda_1$  and  $\lambda_2$  determined for absolute mode and the uncertainty of  $\lambda$  are given in table 3.

The uncertainty budget for  $\lambda$  of PCU 1159 is presented in table 4 as an example. The main uncertainty sources are PCU's dimensional and material properties.

**6. Cross-float measurements and areas synchronisation**

By the cross-float measurements, the performance of the pressure balances (their sensitivity, repeatability and linearity with pressure) was defined, theoretical  $A_0$  and  $\lambda$  reported in tables 2 and 3 verified, unknown  $A_0$  determined and, finally, a consistent set of  $A_0$  and  $\lambda$  generated. The measurements were carried out with each of the 10 possible pairs combined from the 5 PCUs (PCU 1341 was excluded). The most cross-float comparisons contained 180 single measurements; the minimum was 72 and the maximum 327 points. In addition, cross-float measurements in gauge mode of selected PCUs were performed against PTB primary pressure balances of 10 cm<sup>2</sup> effective area, serial no. 288,  $p \leq 1$  MPa, and 5 cm<sup>2</sup> effective area, serial no. 6222,  $p \leq 2$  MPa, which had participated in key comparisons [32-34]. All cross-float measurements were carried out in absolute mode with nitrogen and some measurements additionally with helium. The pressure balances had a similar performance with both nitro-

X	$u_x$	$u_x(\lambda) \times 10^6$ MPa
FEM model		0.012
Young's modulus of cylinder	1.9 GPa	0.010
Poisson coefficient of cylinder	0.0013	0.001
Young's modulus of piston	1.9 GPa	0.004
Poisson coefficient of piston	0.0013	0.003
Gap width	10 nm	0.008
Gap conicity	0.6 nm/mm	0.099
$u(\lambda) \times 10^6$ MPa		<b>0.10</b>

Table 4. Uncertainty sources (X), their values ( $u_x$ ), contributions to  $\lambda$  ( $u_x(\lambda)$ ), and combined uncertainty ( $u(\lambda)$ ) of PCU 1159 calculated by RGF model in absolute mode

gen and helium. Results of the cross-float measurements are summarised in table 5.

Evaluation of the cross-float measurements between PCUs 1342 and 1343 with their  $\lambda$  as reported table 3 showed a pressure dependence of  $A_{0,i}/A_{0,j}$  and an increased standard deviation, which is a result of a contradiction in their  $\lambda$  of  $5.57 \cdot 10^{-7}$  MPa<sup>-1</sup>. For this reason, their  $\lambda$  were adjusted by a correction of  $5.57 \cdot 10^{-7}/2$  MPa<sup>-1</sup> applied to PCU 1342 and of  $5.57 \cdot 10^{-7}/2$  MPa<sup>-1</sup> applied to PCU 1343. The quadratic presentation of

PCU <sub>i</sub> /PCU <sub>j</sub>	$R_{ij}$	$u_{A,Rij} \times 10^6$	$u_{Rij} \times 10^6$
1159/1162	1.00000342	0.22	0.64
1162/1163	0.99998100	0.18	0.50
1163/1159	1.00001559	0.20	0.67
1159/1342	9.99929664	0.55	0.83
1343/1159	0.10000422	0.59	0.87
1342/1162	0.10000741	0.56	0.84
1162/1343	9.99953954	0.55	0.87
1163/1342	9.99944614	0.57	0.83
1343/1163	0.10000269	0.49	0.82
1342/1343	1.00002709	1.39; 0.63 <sup>*)</sup>	0.96 <sup>*)</sup>

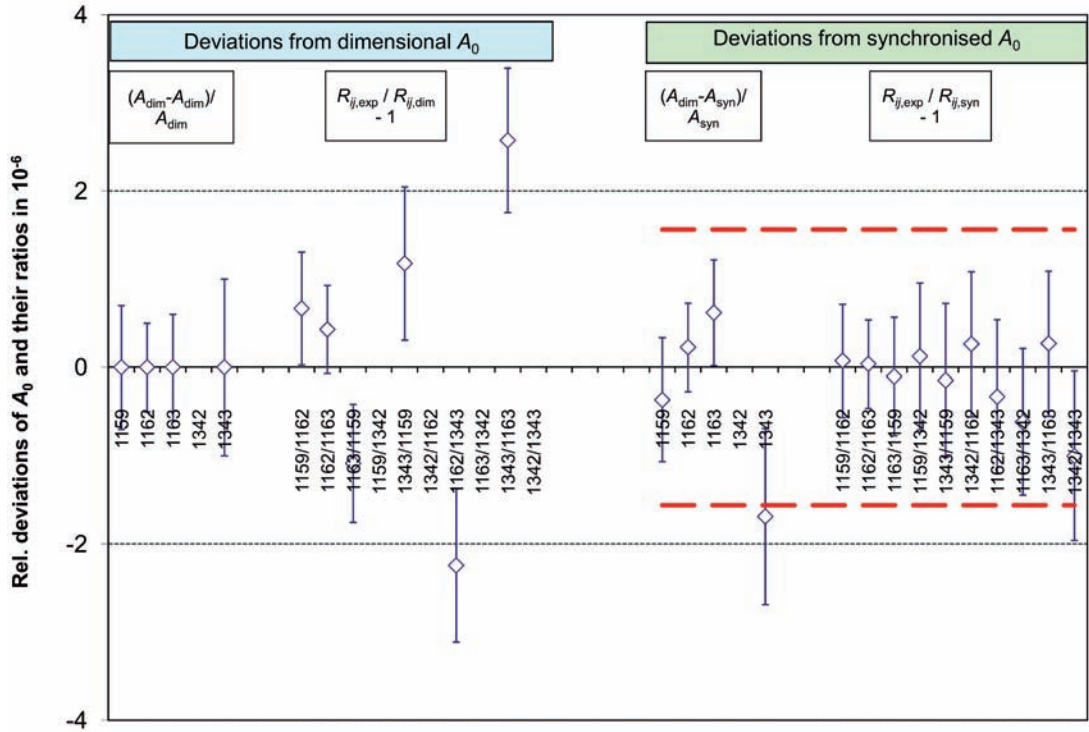
Table 5. Cross-float ratios of the effective areas ( $R_{ij} = A_{0,i}/A_{0,j}$ ), their relative type A ( $u_{A,Rij} = u_A(R_{ij})/R_{ij}$ ) and combined uncertainties ( $u_{Rij} = u(R_{ij})/R_{ij}$ ) obtained in absolute mode with N<sub>2</sub>

Quantity	Uncertainty	$u_B(A_{0,i}/A_{0,j}) \times 10^6$
Room temperature	4.0·10 <sup>-1</sup> °C	0.013
Gas density fluid for height difference	1.0·10 <sup>-3</sup> rel.	0.009
Residual pressure in Ref	2.0·10 <sup>-3</sup> Pa	0.004
Residual pressure in DUT	2.0·10 <sup>-3</sup> Pa	0.004
Height difference	2.8·10 <sup>-1</sup> mm	0.032
PRT calibration in Ref	6.0·10 <sup>-3</sup> °C	0.054
PRT calibration in DUT	6.0·10 <sup>-3</sup> °C	0.054
Temperature inhomogeneity in Ref	2.1·10 <sup>-2</sup> °C	0.075
Temperature inhomogeneity in DUT	4.1·10 <sup>-2</sup> °C	0.19
Calibration uncertainty of DPC	1.0·10 <sup>-1</sup> Pa	0.22
Standard deviation of DPC	3.5·10 <sup>-1</sup> Pa	0.078
Thermal expansion coefficient of Ref	2.2·10 <sup>-7</sup> K <sup>-1</sup>	0.021
Thermal expansion coefficient of DUT	2.2·10 <sup>-7</sup> K <sup>-1</sup>	0.031
Distortion coefficient of Ref	8.0·10 <sup>-8</sup> MPa <sup>-1</sup>	0.040
Distortion coefficient of DUT	1.6·10 <sup>-7</sup> MPa <sup>-1</sup>	0.080
Verticality of Ref	4.0·10 <sup>-1</sup> mm/m	0.080
Verticality of DUT	4.0·10 <sup>-1</sup> mm/m	0.080
Cylinder + weight carrier mass of Ref	5.5·10 <sup>-7</sup> kg	0.006
Cylinder + weight carrier mass of DUT	2.0·10 <sup>-7</sup> kg	0.022
Main ring weights of Ref	1.3·10 <sup>-5</sup> kg	0.088
Main ring weights of DUT	2.6·10 <sup>-6</sup> kg	0.52
Combined uncertainty		0.63

Table 6. Type B uncertainty budget for the effective areas ratios of PCUs 1162 – reference (Ref) and 1342 – device under test (DUT)

<sup>\*)</sup> Values obtained after synchronisation of  $\lambda$  of PCUs 1342 and 1343.

Figure 2. Differences between dimensional ( $A_{dim}$ ,  $R_{ij, dim}$ ) and cross-float ( $R_{ij, exp}$ ) results (left half), as well as between dimensional, cross-float and synchronised ( $A_{syn}$ ,  $R_{ij, syn}$ ) results (right half). The vertical bars are uncertainties of ( $A_{dim}$ ) and ( $R_{ij, exp}$ ). The dashed lines show maximum uncertainty limits of  $A_{syn}$ .



the pressuredependent effective area ( $A_p$ ) through  $\lambda_1$  and  $\lambda_2$  was replaced by a linear presentation through a single  $\lambda$  value with an additional uncertainty contribution due to the adjustment taken as  $5.57 \cdot 10^{-7}/2/\sqrt{3}$ . The  $\lambda$  values and their uncertainties obtained by this procedure are

$$\begin{aligned} \lambda_{1342} &= (1.534 \pm 0.16) \times 10^{-6} \text{ MPa}^{-1} \text{ and} \\ \lambda_{1343} &= (1.732 \pm 0.16) \times 10^{-6} \text{ MPa}^{-1}. \end{aligned} \quad (6)$$

The  $\gamma$ -marked uncertainty values in table 5 were obtained with these synchronised distortion coefficients.

The product of all 10 experimental ratios of the effective areas given in table 5 deviates from 1 by less than 1.5 ppm. The product of the three ratios for the 20 cm<sup>2</sup> PCUs deviates from 1 only by 0.01 ppm. Table 6 presents a type B uncertainty budget for the comparison 1162/1342 taken as example. Forty-one uncertainty contributions were analysed in total. The table lists only uncertainty sources with relative uncertainty contributions higher than  $10^{-9}$ .

Thus, the main sources of uncertainty in the cross-float  $A_0$ -ratios are temperature gradient, differential pressure measurement, main masses and repeatability.

Based on the dimensional effective areas ( $A_{di}$ ) with the associated relative uncertainties ( $u_{di} = u(A_0)/A_0$ ) from table 2 and the cross-float

effective area ratios ( $R_{ij}$ ) with their relative uncertainties ( $u_{Rij}$ ) from table 5, such so-called synchronized effective areas ( $A_i$ ) were determined that show the best agreement with both dimensional and cross-float data. As a criterion, the minimum sum of squared weighted deviations between  $A_i$  and  $A_{di}$  as well as between ratios  $A_i/A_j$  and  $R_{ij}$  was used:

$$S = \sum_{i=1}^n \left( \frac{A_{di} - A_i}{A_{di} u_{di}} \right)^2 + \sum_{i=1}^{n-1} \sum_{j=i+1}^n \left( \frac{R_{ij} - A_i / A_j}{R_{ij} u_{Rij}} \right)^2 \rightarrow \min \quad (7)$$

with  $i = 1, \dots, n, j = 1, \dots, n$  and  $n = 5$  being the number of PCUs. Minimisation of  $S$  gives  $A_i$ , their type A ( $u_{i,A}$ ), type B ( $u_{i,B}$ ) and combined ( $u_i$ ) relative uncertainties as

$$A_i = \left( \frac{A_{di}}{u_{di}^2} + \sum_{j=1}^n \frac{R_{ij} A_j}{u_{Rij}^2} \right) / \left( \frac{1}{u_{di}^2} + \sum_{j=1}^n \frac{1}{u_{Rij}^2} \right), \quad (8)$$

$$u_{i,A} = \left\{ \left[ \left( \frac{A_{di} - A_i}{A_{di} u_{di}} \right)^2 + \sum_{j=1}^n \left( \frac{R_{ij} - A_i / A_j}{R_{ij} u_{Rij}} \right)^2 \right] \left( \frac{n}{n-1} \right) / \left[ \frac{1}{u_{di}^2} + \sum_{j=1}^n \frac{1}{u_{Rij}^2} \right] \right\}^{1/2} \quad (9)$$

$$u_{i,B} = \left\{ \left[ \frac{1}{u_{di}^2} + \sum_{j=1}^n \frac{u_{j,B}^2}{u_{Rij}^2} \right]^2 + \sum_{j=1}^n \frac{1}{u_{Rij}^2} \right\}^{1/2} / \left[ \frac{1}{u_{di}^2} + \sum_{j=1}^n \frac{1}{u_{Rij}^2} \right] \quad (10)$$

$$u_i = \sqrt{u_{i,A}^2 + u_{i,B}^2}, \quad (11)$$

which were calculated iteratively. The results for the synchronized effective areas and their uncertainties are summa-

Table 7. Synchronised effective areas ( $A_i$ ), their type A ( $u_{i,A}$ ), type B ( $u_{i,B}$ ) and combined ( $u_i$ ) relative uncertainties

PCU	$A_i/\text{cm}^2$	$u_{i,A} \times 10^6$	$u_{i,B} \times 10^6$	$u_i \times 10^6$
1159	19.610121	0.2	1.2	1.2
1162	19.610056	0.2	1.1	1.1
1163	19.610429	0.4	1.1	1.2
1342	1.9611503	0.6	1.3	1.5
1343	1.9610952	0.9	1.3	1.6

rized in table 7.

The relation between the dimensional, cross-float and synchronised effective areas and their ratios is shown in figure 2.

The original dimensional and cross-float data have a maximum discrepancy of 1.1 ppm for the 20 cm<sup>2</sup> PCUs and 2.6 ppm for all 4 PCUs. The results pass the consistency check based on the chi-squared test. The synchronised effective areas agree with the original dimensional areas within 1.7 ppm and with the original cross-float data within 1.0 ppm.

## 7. Pressure measurement in DCGT experiment

In first DCGT experiments, PCU 1342 was used for the pressure measurement with its zero pressure effective area and distortion coefficient given in table 7 and equation (6), respectively. The distribution of the gravity acceleration ( $g$ ) in the DCGT room had been measured by the Federal Agency for Cartography and Geodesy, Frankfurt am Main, using an absolute and a relative movable gravimeter with a relative standard uncertainty of  $1.6 \cdot 10^{-8}$ . Without considering temporal changes of  $g$ , its constant measured value was used with a relative uncertainty of 0.2 ppm.

Therewith, the relative standard uncertainty of the absolute pressure measured at the reference level of the pressure balance is given by equation  $u(p)/p = [1.8^2 + (0.16 \cdot p/\text{MPa})^2]^{0.5} \times 10^{-6}$ . (12)

The pressure at the middle of the capacitor in the DCGT ( $p_{\text{DCGT}}$ ) was calculated by applying head corrections to the pressure of the pressure balance ( $p_{\text{PrBal}}$ ) due to height differences ( $\Delta h_i$ ) along the pressure line connecting the pressure balance with the DCGT chamber:

$$p_{\text{DCGT}} = p_{\text{PrBal}} + g \cdot \sum [\rho_{\text{He}}(t_i) \cdot \Delta h_i], \quad (13)$$

where  $\rho_{\text{He}}(p_i, t_i)$  is the helium density at pressure  $p_i$  and temperature  $t_i$ ,  $t_i$  having been measured along each vertical section  $i$  of the pressure line. Finally, the relative standard uncertainty of the absolute pressure in the DCGT chamber was estimated by

$$u(p_{\text{DCGT}})/p_{\text{DCGT}} = [2.0^2 + (0.16 \cdot p/\text{MPa})^2]^{0.5} \times 10^{-6}. \quad (14)$$

## 8. Conclusions and outlook

The new pressure balances were developed, characterised and applied to measure the absolute helium pressure in the DCGT experiment on the redetermination of the Boltzmann constant. Five of their 6 PCUs were compared by cross-float measurements and 4 of them were characterised dimensionally, both types of measurements having approximately the same uncertainty of 0.5 to 1 ppm. The uncertainty of the synchronised  $A_0$  lies between 1.1 and 1.6 ppm, and of pressures (1-7) MPa between 1.8 and 2.1 ppm. These results document the present status of the

PTB Boltzmann constant project in its intermediate stage.

The next steps intended to reduce uncertainty while keeping in mind the target value of 1 ppm are: involving the 6<sup>th</sup> 2 cm<sup>2</sup> PCU 1341; finishing dimensional characterisation of all 6 PCUs; improvement of temperature homogeneity inside the pressure balances; better calibration of the differential pressure cells; taking into account correlation due to the same two mass sets used in numerous cross-float measurements; reduction of discrepancies between theoretical and cross-float pressure  $\lambda$ ; simultaneous synchronisation of  $A_0$  and  $\lambda$  of all 6 PCUs.

## 9. Acknowledgments

I very much appreciate the essential contribution to this project by Ms. T. Priruenrom, PTB guest researcher from NIMT (Thailand), who evaluated dimensional and cross-data results, calculated effective areas and pressure distortion coefficients and performed cross-float measurements with different gases; by Mr. T. Konczak, Mr. S. Scheppner and Ms. H. Ahrendt of the PTB Pressure Working Group, who took care of the technical part of the project, installed and operated the pressure balances, carried out numerous cross-float and related measurements, and developed software. I thank Dr. O. Jusko and Mr. H. Reimann of the PTB Geometrical Standards Working Group for the dimensional characterisation of the piston-cylinder assemblies. Important progress in the effective area calculation with rarefied gas flow models has been done with a valuable contribution by Prof. F. Sharipov of Paraná University, Curitiba, Brazil. And finally, I am indebted to Mr. R. Haines and Mr. P. Delajoud as well as the team from DH Instruments for their ideas, technical innovations and active cooperation in the project, and the development and preliminary characterisation of the new pressure balances. This research was stimulated by and performed in numerous discussions with Dr. B. Fellmuth, Dr. J. Fischer, Dr. C. Gaiser and Dr. T. Zandt, who are carrying out the Boltzmann constant project at PTB. This research was supported as a part of the EURAMET joint research project receiving funding from the European Community's Seventh Framework Programme, iMERAPlus, under Grant Agreement No. 217257, which is gratefully acknowledged.

## References

- [1] *Fellmuth B., Gaiser Ch., Fischer J.*: Determination of the Boltzmann constant – status and prospects, *Meas. Sci. Technol.*, **17** (2006), 145-159
- [2] *Moldover M.R., Trusler J.P.M., Edwards T.J., Mehl J.B., Davis R.S.*: Measurement of the universal gas constant  $R$  using a spherical acoustic resonator, *J. Res. Natl. Bur. Stand.*, **93** (1988), 85-144
- [3] *Mohr P.J., Taylor B.N.*: CODATA recommended values of the fundamental physical constants: 1998, *Rev. Mod. Phys.*, **72** (1998), 351-495
- [4] *Gugan D., Michel G.W.*: Dielectric constant gas thermometry from 4.2 to 27.1 K, *Metrologia*, **16** (1980), 149-167
- [5] *Luther H., Grohmann K., Fellmuth B.*: Determination of thermodynamic temperature and  $^4\text{He}$  virial coefficients between 4.2 K and 27.0 K by dielectric constant gas thermometry, *Metrologia*, **33** (1996), 341-352
- [6] *Sabuga W.*: Towards 7 MPa pressure standards with  $1 \cdot 10^6$  uncertainty, *MAPAN – J. Metrology Soc. India*, **22** (2007), 3-11
- [7] *Sabuga W., Priruenrom T., Haines R., Bair M.*: Design and evaluation of pressure balances with  $1 \cdot 10^{-6}$  uncertainty for the Boltzmann constant project. Proc. of 5<sup>th</sup> CCM Pressure Metrology & 4<sup>th</sup> IMEKO TC16 Int. Conf., Berlin, May 2–5, 2011, *PTB-Mitteilungen*, vol. 4/2011, ???
- [8] *Simpson D.I.*: Computerized techniques for calibrating pressure balances, *Metrologia*, **30** (1993/94), 655-658
- [9] *Kojima M., Kobata T., Saitou K., Hirata M.*: Development of small differential pressure standard using double pressure balances, *Metrologia*, **42** (2005), 227-230
- [10] *Kobata T., Kojima M., Saitou K., Fitzgerald M., Jack D., Sutton C.*: Final report on key comparison APMP.M.P-K5 in differential pressure from 1 Pa to 5000 Pa, *Metrologia*, **44** (2007), Tech. Suppl., 07001
- [11] *Neugebauer M., Lüdicke F., Bastam D., Bosse H., Reimann H., Topperwien C.*: A new comparator for measurement of diameter and form of cylinders, spheres and cubes under clean-room conditions, *Meas. Sci. Technol.*, **8** (1997), 849-856
- [12] *Neugebauer M.*: Uncertainty analysis for roundness measurements by the example of measurements on a glass hemisphere, *Meas. Sci. Technol.*, **12** (2001), 68–76
- [13] *Lüdicke F., Jusko O., Reimann H.*: Form and length measurements by use of a modified commercial form measurement instrument, *ASPE Annual Meeting 2000*, Scottsdale, AZ, USA
- [14] *Jusko O., Neugebauer M., Reimann H., Drabarek P., Fleischer M., Gnausch T.*: Form measurements by optical and tactile scanning, Proc. of 5<sup>th</sup> Int. Symp. on Instrumentation Science and Technology, ISIST, Shenyang, China, 15-18, Sept., 2008
- [15] *Jusko O., Neugebauer M., Reimann H., Sabuga W., Priruenrom T.*: Dimensional calibration techniques for pressure for pressure balances to be used in the new determination of the Boltzmann constant, *Congresso Internacional de Metrologia Mecanica: Anais, I-CIMMEC, 1<sup>st</sup> Int. Congr. on Mechanical Metrology*, Rio de Janeiro, 8-10 October, 2008
- [16] *Jusko O., Bastam D., Reimann H.*: Tactile and optical cylinder calibration with nanometre uncertainties, Proc. ASPE Spring Topical Meeting “Mechanical Metrology and Measurement Uncertainty”, Albuquerque, NM, USA, 2009, 11-14
- [17] *Jusko O., Bastam D., Neugebauer M., Reimann H., Sabuga W., Priruenrom T.*: Final results of the geometrical calibration of the pressure balances to be used for the new determination of the Boltzmann constant, *Key Engineering Materials*, **437** (2010), 150154
- [18] *Sabuga W., Priruenrom T.*: An approach to the evaluation of dimensional measurements on pressure-measuring piston-cylinder assemblies, *IMEKO 20<sup>th</sup> TC3, 3<sup>rd</sup> TC16 and 1<sup>st</sup> TC22 Int. Conf. “Cultivating metrological knowledge”*, Merida, Mexico, 27<sup>th</sup> to 30<sup>th</sup> November, 2007, <http://www.imeko.org/publications/tc16-2007/IMEKO-TC16-2007-074u.pdf>
- [19] *Dadson R.S., Lewis S.L., Peggs G.N.*: The Pressure Balance – Theory and Practice, London, HMSO, 1982
- [20] *Caubergh M., Draisma J., Franx G.J., Hek G., Prokert G., Rienstra S., Verhoeven A.*: Measure under pressure, calibration of pressure measurement, in “Mathematics in Industry”, Scientific proc. of 55<sup>th</sup> Europ. Study Group with Industry, January 30 to February 3, 2006, Eindhoven, Ed. by E.R. Fledderus et al., December 8, 2006 <http://www.wiskgenoot.nl/swi/Proceedings/Eindhoven2006/SWI2006-scientific.pdf>
- [21] *Sabuga W., Priruenrom T.*: Two-dimensional flow model for calculation of the effective area of axially non-symmetric piston-cylinder units, 5<sup>th</sup> APMP Pressure and Vacuum Symp., 11-13 November 2010, NIMT, Prathumthani, Thailand
- [22] *Ehrlich C.*: A review of gas-operated piston gauges, *Metrologia*, **30** (1993/94), 585-590
- [23] *Sutton C.M.*: The effective area of a pressure balance at low pressures, *J. Phys. E: Sci. Instrum.*, **13** (1980), 857-859

- [24] Sutton C.M.: The pressure balance as an absolute pressure standard, *Metrologia*, **30** (1993/94), 591-594
- [25] Schmidt J.W., Tison S.A., Ehrlich C.D.: Model for drag forces in the crevice of piston gauges in the viscous-flow and molecular-flow regimes, *Metrologia*, **36** (1999), 565-570
- [26] Schmidt J.W., Welch B.E., Ehrlich C.D.: Gas and mode, vertical and rotational effects with a three piston gauge apparatus, *Metrologia*, **30** (1993/94), 599-602
- [27] Welch B.E., Edsinger R.E., Bean V.E., Ehrlich C.D.: *BIPM Monography* 89/1 (1989) 81
- [28] Meyer C.W., Reilly M.L.: Measurements of the gas dependence of the effective area of a piston gauge using H<sub>2</sub>, <sup>3</sup>He, <sup>4</sup>He, N<sub>2</sub>, CO<sub>2</sub> and SF<sub>6</sub>, *Metrologia*, **30** (1993/94), 595-597
- [29] Sabuga W., Sharipov F., Priruenrom T.: Determination of the effective area of piston-cylinder assemblies using a rarefied gas flow model, Proc. of 5<sup>th</sup> CCM Pressure Metrology & 4<sup>th</sup> IMEKO TC16 Int. Conf., Berlin, May 2–5, 2011, PTB-Mitteilungen, vol. 4/2011, ???
- [30] Sabuga W., Priruenrom T., Molinar G., Buonanno G., Rabault T., Wongthep P., Pražák D.: FEA calculation of pressure distortion coefficients of gas-operated pressure balances – EURAMET project 1039, Proc. of 5<sup>th</sup> CCM Pressure Metrology & 4<sup>th</sup> IMEKO TC16 Int. Conf., Berlin, May 2–5, 2011, Measurement, 2011, ???
- [31] Sabuga W., Ullbig P., Salama D.: Elastic constants of pressure balances' piston-cylinder assemblies measured with the resonant ultrasound spectroscopy, Proc. of Int. Metrology Conf., Cairo, Egypt, April 18-23, 2010
- [32] Legras J.C., Sabuga W., Molinar G.F., Schmidt J.W.: CCM key comparison in the pressure range 50 kPa to 1000 kPa (gas medium, gauge mode). Phase A2: Pressure measurements, *Metrologia*, **36** (1999), 663-668
- [33] Molinar G., Legras J.C., Jäger J., Ooiwa A., Schmidt J.: Results of the CCM pressure key comparison (Phase B) in gas media and gauge mode from 80 kPa to 7 MPa, Final report, CCM key comparison 7 MPa, Phase B (CCM.P-K1.c), IMGC-CNR Technical Report 42, October 2000 [http://kcdb.bipm.org/appendixB/appbresults/ccm.p-k1.c/ccm.p-k1.c\\_final\\_report.pdf](http://kcdb.bipm.org/appendixB/appbresults/ccm.p-k1.c/ccm.p-k1.c_final_report.pdf)
- [34] Kiselev Yu., Sabuga W., Dapkeviciene K., Farar P., Saczuk K., Sandu I.: Final report on key comparison COOMET.M.P-K1 in the range 0.05 MPa to 0.5 MPa of pneumatic gauge pressure, April 2007, [http://kcdb.bipm.org/appendixB/appbresults/ccm.p-k1.b/coomet.m.p-k1\\_final\\_report.pdf](http://kcdb.bipm.org/appendixB/appbresults/ccm.p-k1.b/coomet.m.p-k1_final_report.pdf)



# Design and Evaluation of Pressure Balances with $1 \cdot 10^{-6}$ Uncertainty for the Boltzmann Constant Project

Wladimir Sabuga<sup>1</sup>, Tasanee Priruenrom<sup>2</sup>, Rob Haines<sup>3</sup>, Michael Bair<sup>3</sup>

## Abstract

In support of the project for determination of the Boltzmann constant by dielectric constant gas thermometry, a system of pressure balances has been designed and constructed with the goal of defining pressures in helium in gauge and absolute measurement modes up to 7 MPa with a relative standard uncertainty of  $1 \cdot 10^{-6}$ . The design addresses temperature stability, mass uncertainty, effective area and pressure distortion coefficient in particular. The system includes two pressure balance platforms, three 20 cm<sup>2</sup> and three 2 cm<sup>2</sup> piston-cylinder assemblies (PCAs), two 150 kg mass sets and automated mass handlers. The design of the PCAs was optimized to reduce pressure distortion coefficients and mounting induced deformations. In order to perform automated cross-floats with the pressure balances in gauge or absolute mode differential pressure cells (DPCs) were applied to indicate pressure equilibrium. The effective area ratios obtained from cross-floats for all possible combinations of PCAs are consistent within  $0.96 \cdot 10^{-6}$ . Using dimensional measurements, the effective areas of the 20 cm<sup>2</sup> and 2 cm<sup>2</sup> PCAs were determined with relative standard uncertainties of  $0.7 \cdot 10^{-6}$  and  $1 \cdot 10^{-6}$ , respectively. Based on the currently available dimensional and cross-float data the relative standard uncertainty of the absolute pressure of 7 MPa is equal to  $2.1 \cdot 10^{-6}$ .

**Keywords:** Pressure balance, Boltzmann constant, 1 ppm, cross-float, effective area, piston-cylinder assembly

## 1 Introduction

For the last several years PTB has been pursuing a project aimed at re-determining the Boltzmann constant ( $k$ ) [1, 2]. To achieve the aims of the project it is necessary to perform absolute pressure measurements with a relative standard uncertainty of  $1 \cdot 10^{-6}$  in the range of 2 to 7 MPa in helium [3].

In order to achieve the desired uncertainty a system of pressure balances was designed and constructed with features supporting reduced uncertainty in key areas. Three 20 cm<sup>2</sup> nominal

area PCAs were created with the intention of determining effective area ( $A_0$ ) by dimensional measurements and to inter-compare with each other and with other pressure standards in the pressure range up to 750 kPa. Three 2 cm<sup>2</sup> nominal area PCAs were created to inter-compare and to extend the pressure range to 7 MPa.

## 2 Design

The design of the 7 MPa pressure balances incorporated as many standard production elements as possible to maximize use of proven tooling and processes and to minimize risk. Several new designs and design modifications were created in order to achieve the required level of performance. Particular attention was given to design areas affecting temperature stability, mass uncertainty, effective area and distortion coefficient.

### 2.1 Temperature

To minimize potential thermal gradients within the pressure balances, all active electrical components are placed in a remote electronics module. The large thermal mass of the piston-cylinder mounting post provides a good base both for thermal stability as well as for piston-cylinder temperature measurement. To further improve thermal performance the contact area between the 2 cm<sup>2</sup> cylinder and the mounting post is maximized, improving thermal coupling (see Figure 1).

In addition to improving the thermal stability of the piston-cylinder assemblies, a second platinum resistance thermometer (PRT) is installed in each mounting post. The two temperature readings may be averaged for calculation of thermal expansion and the values may be compared to indicate temperature homogeneity.

### 2.2 Mass uncertainty

The mass load consists of the floating piston or cylinder, mass carrying bell, annular main masses and tubular binary masses. Automated mass handlers improve mass uncertainty by minimizing wear from manual mass loading.

The eleven 12.5 kg main masses in each mass set are made from austenitic stainless steel alloy

<sup>1</sup> Wladimir Sabuga, Physikalisch-Technische Bundesanstalt (PTB), Braunschweig, Germany

<sup>2</sup> Tasanee Priruenrom, National Institute of Metrology (Thailand) (NIMT), Pathumthani, Thailand, guest researcher at PTB

<sup>3</sup> Rob Haines, Michael Bair, Fluke Calibration, Phoenix, AZ, USA, Email of corresponding author: rob.haines@fluke.com

HE210, noted for long term stability and for having no residual magnetism. They were designed and manufactured in accordance with recommendation OIML R 111-1, class E1, concerning material mechanical and magnetic properties [4]. The seven tubular binary masses in each mass set are made from 304L stainless steel and range from 0.1 to 6.4 kg. After demagnetisation the binary masses correspond to class F1 to F2 of OIML R 111-1.

### 2.3 Effective area and distortion coefficient

The effective areas of the six PCAs are determined by dimensional measurements and by cross-float [3, 5, 6]. To reduce uncertainty in effective area and distortion coefficient several measures were taken, see Figure 1.

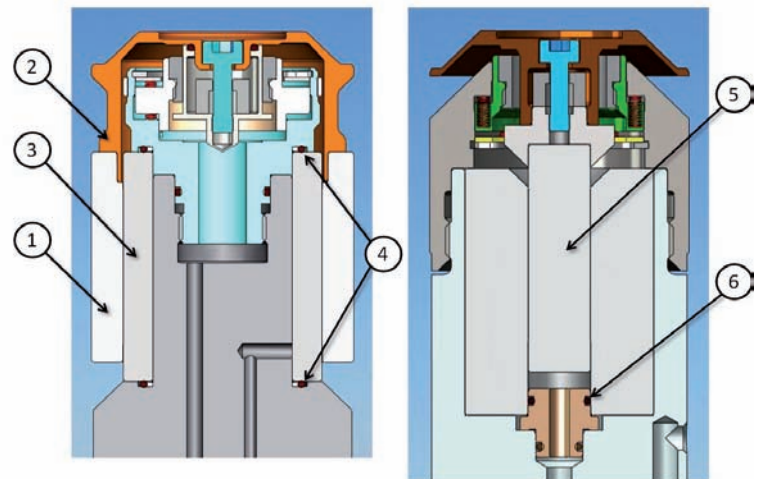
In the 20 cm<sup>2</sup> PCA, the wall thickness of cylinder (1) is doubled from the previous production design from 4 to 8 mm. Although this increases the minimum mass and the minimum achievable pressure, the thicker cylinder reduces the deformation coefficient by approximately 30%. In addition the thicker cylinder is less prone to distortion when assembled to cylinder cap (2), significantly improving roundness. Mounting of the 20 cm<sup>2</sup> PCA piston (3) is improved by moving o-ring seals (4) from the inner diameter to the top and bottom surfaces eliminating small discontinuities in radial stress and reducing variations associated with assembly.

The 2 cm<sup>2</sup> PCA was redesigned from the standard hollow piston configuration operating in negative free deformation. The piston (5) is solid to reduce deformation coefficient and the PCA is operated in positive free deformation. The test pressure seal (6) is on the inner diameter of the cylinder rather than on the bottom surface to eliminate end loading of the cylinder.

### 2.4 Automated cross-float

In order to accomplish comparisons at the highest level in both gauge and absolute modes, automated cross-float techniques are used [7]. The Compass® for Pressure Cross Float Extension allows for automated or semi-automated operation of cross-floats for PCAs using a low range DPC to indicate small differences between the two pressure balances. Test sequences control the pressure generation, valve actuation and DPC zeroing (at each pressure) for 1:1 as well as for non-equal area comparisons.

Additions to the Cross Float Extension were created for this project, including support of all new hardware, logging of all discrete parameters, and independent measurements of residual vacuum. In addition a new stability (*Ready*) criterion was added to existing pressure balance *Ready* criteria, permitting data collection only



when the DPC stability causes changes in the calculated effective area of the device under test (DUT) to be less than or equal to  $2 \cdot 10^{-6}$  (adjustable).

### 2.5 Piston-cylinder gap

The gap between piston and cylinder is critical for pressure balance design and operation. The ideal piston-cylinder gap size is a balance between fall rate, sensitivity, robustness and uncertainty in effective area. Smaller gaps produce lower fall rates and lower uncertainty of effective area, however smaller gaps can result in PCAs that have decreased sensitivity or that are difficult to clean and maintain, particularly for automated operation. For this program the piston-cylinder gaps were made as small as possible while maintaining desirable performance characteristics.

## 3 Results and discussion

Temperature stability and homogeneity is quantified by comparison of the PRTs in the mounting posts during operation. The temperature increase during a 4.5 hour cross-float is typically 0.1 °C with the difference between PRTs in a given pressure balance less than or equal to 0.03 °C.

The 12.5 kg main mass values were measured with a relative standard uncertainty of  $0.05 \cdot 10^{-6}$  in 2008 and in 2010, after a year of operation. The relative change of the main masses is between  $-0.080 \cdot 10^{-6}$  and  $0.024 \cdot 10^{-6}$ . The binary mass values were determined with relative standard uncertainties from  $0.5 \cdot 10^{-6}$  to  $1.5 \cdot 10^{-6}$ .

In 2009 detailed dimensional measurements of the 20 cm<sup>2</sup> piston-cylinders were performed on pistons and cylinders with estimated uncertainties of 8 nm on pistons and 16 nm on cylinders. A repeat measurement of PCA 1159 in 2010 provides an indication of dimensional stability. Differences in radius of the piston from 2009 to 2010 are within  $\pm 19$  nm, a relative difference of  $\pm 0.8 \cdot 10^{-6}$ . Differences in radius of the cylinder are

Figure 1 – 20 cm<sup>2</sup> and 2 cm<sup>2</sup> piston-cylinder assemblies. 1) 20 cm<sup>2</sup> cylinder, 2) cylinder cap, 3) 20 cm<sup>2</sup> piston, 4) piston o-rings, 5) 2 cm<sup>2</sup> piston, 6) cylinder o-ring

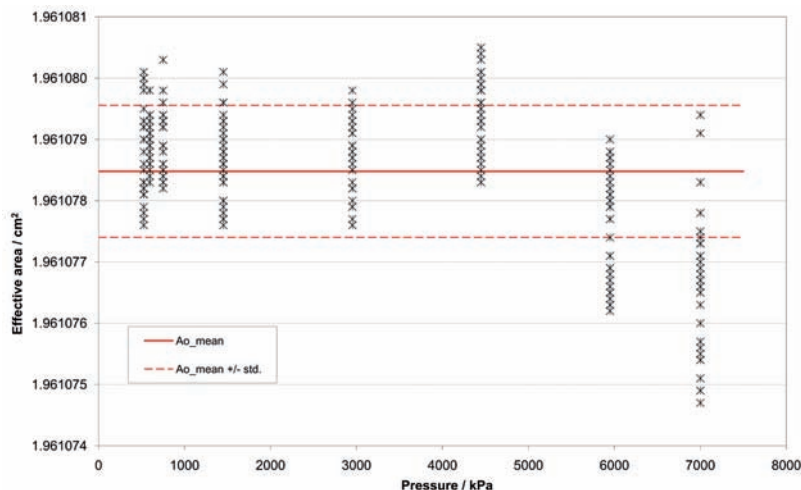


Figure 2 – Cross-float of two 2 cm<sup>2</sup> PCAs, 1342(Ref) and 1343(DUT) in N<sub>2</sub>

between -9 and 27 nm, a relative difference of  $(-0.4 \text{ to } 1.1) \cdot 10^{-6}$ .

The gap initially manufactured for PCA 1341 allowed normal operation at the manufacturer, however proved difficult to maintain during inter-comparisons in the project. It was decided to remove a small amount of material from the piston to increase the gap. As measured by drop test at the manufacturer the gap was increased by approximately 20%, a value to be confirmed with dimensional measurements. The PCA is now able to perform as required for the project and will return to service once dimensional re-determination is complete.

The effective areas determined for the three 20 cm<sup>2</sup> piston cylinders by dimensional measurements for PCA 1159, 1162 and 1163 respectively are 19.610114, 19.610060 and 19.610441 cm<sup>2</sup>. Their standard uncertainties range from  $0.5 \cdot 10^{-6}$  to  $0.7 \cdot 10^{-6}$ . From the dimensionally determined effective areas the areas of the 2 cm<sup>2</sup> PCAs are determined by automated cross-float in absolute

	A <sub>0</sub> -ratio	u(A <sub>0</sub> -ratio) · 10 <sup>6</sup>
1159/1162	1.00000342	0.64
1162/1163	0.99998100	0.50
1163/1159	1.00001559	0.67
1159/1342	9.99929664	0.83
1343/1159	0.10000422	0.87
1342/1162	0.10000741	0.84
1162/1343	9.99953954	0.87
1163/1342	9.99944614	0.83
1343/1163	0.10000269	0.82
1342/1343	1.00002709	0.96

Table 1 – Cross-float area ratios and their standard uncertainties (k=1)

mode. Every PCA is compared to each of the others to validate the cross-float performance and to determine the uncertainty of the ratios. Figure 2 shows the result of a cross-float between 2 cm<sup>2</sup> PCAs as an example. Each cross-float consists of five to six cycles up and down.

Pressure balance performance is demonstrated, in part, by cross-float performance. Table 1 shows the effective area ratios and uncertainties of all ten combinations of the three 20 cm<sup>2</sup> PCAs and 2 cm<sup>2</sup> PCAs 1342 and 1343.

## 4 Conclusion

The evaluation of the pressure balances for the Boltzmann constant project indicates that the pressure balances should be capable of generating pressure in the range of 2 to 7 MPa with the required uncertainties. Minimizing sources of variation as well as minimizing the values of quantities such as deformation coefficient contributes to these results. Automated cross-float, particularly in absolute mode, is important for this effort.

The cross-float area ratios of the three 20 cm<sup>2</sup> PCAs are consistent within  $0.01 \cdot 10^{-6}$ . All ten cross-float area ratios of the PCAs were determined over their full operational pressure ranges and are consistent within  $1.5 \cdot 10^{-6}$ . The pressure balances demonstrate the performance required for the Boltzmann constant project and, at present, allow pressure measurement up to 7 MPa with a relative combined standard uncertainty below  $2.1 \cdot 10^{-6}$ . Future work includes continued inter-comparison involving PCA 1341 and other standards as well as further evaluation of dimensional and mass stability.

## Acknowledgements

The authors acknowledge the contributions of Thomas Konczak and Steffen Scheppler (both of PTB) for their contributions to the installation, operation and evaluation of the pressure balances. The authors give special acknowledgment to Pierre Delajoud (DHI retired) for extensive design, communications and consultation throughout the project. Support of this research by the International Graduate School of Metrology (IGSM) Braunschweig is acknowledged.

## References

- [1] Fellmuth B., Fischer J., Gaiser C., Priruenrom T., Sabuga W., Ulbig P., The international Boltzmann project – the contribution of the PTB, *C. R. Physique*, 2009, **10**, 828-834
- [2] Sabuga W., Towards 7 MPa pressure standards with  $1 \cdot 10^6$  uncertainty, *MAPAN – J. Metrology Soc. India*, 2007, **22**, 311
- [3] Sabuga W., Pressure measurements in gas media up to 7.5 MPa for the Boltzmann constant redetermination, Proc. of 5<sup>th</sup> CCM int. conf. on pressure metrology, Berlin, May 2–5, 2011, to be published in *PTB Mitteilungen*, 2011, no. 4,
- [4] OIML R 111-1, Weights of classes E1, E2, F1, F2, M1, M1–2, M2, M2–3 and M3 Part 1: Metrological and technical requirements (2004), OIML
- [5] Sabuga W., Priruenrom T., An approach to the evaluation of dimensional measurements on pressure-measuring piston-cylinder assemblies, IMEKO 20<sup>th</sup> TC3, 3<sup>rd</sup> TC16 and 1<sup>st</sup> TC22 Int. Conf. “Cultivating metrological knowledge”, 27<sup>th</sup> to 30<sup>th</sup> November, 2007
- [6] Jusko O., Bastam D., Neugebauer M., Reimann H., Sabuga W., Priruenrom T., Final results of the geometrical calibration of the pressure balances to be used for the new determination of the Boltzmann constant, *Key Engineering Materials*, 2010, **437**, 150
- [7] Bair, M. and Delajoud, P., The Design and Implementation of a Fully Automated Crossfloat System for the Comparison of Piston Gauges in Both Gauge and Absolute Measurement Modes, 2007, Presented at IMEKO 2007, Merida, Mexico.

# Determination of the Effective Area of Piston-Cylinder Assemblies Using a Rarefied Gas Flow Model

W. Sabuga<sup>1</sup>, F. Sharipov<sup>2</sup>, T. Priruenrom<sup>3</sup>

## ABSTRACT

Numerical solutions of gas flows between parallel plates and in an annular gap based on the kinetic equation and valid over a wide range of the gas rarefaction are applied to calculate the pressure distribution in the gap between a piston and cylinder, the viscous force acting on the piston and, finally, the effective area of real 10 cm<sup>2</sup> and 20 cm<sup>2</sup> piston-cylinder assemblies (PCAs) which were accurately characterised by dimensional measurements and are used as primary gas pressure standards at PTB. The calculations are performed for the gauge and absolute mode as well as for different gases. The calculated effective areas are compared with those obtained by the Dadson theory and with the effective areas' ratios determined experimentally by the cross float method using nitrogen, helium and sulphur hexafluoride. The results confirm that even in the case of PCAs of a large effective area ( $\geq 10$  cm<sup>2</sup>), the effect of the flow regime and of the gas type should be taken into account, if a relative uncertainty in pressure measurements of the order of 10<sup>-6</sup> is envisaged and, in particular, when the pressure balances are operated in absolute mode.

**Keywords:** Effective area, piston-cylinder assembly, Knudsen number, Poiseuille coefficient, rarefaction parameter

## 1. Introduction

The effective area of PCAs used in primary pressure balances is usually determined from dimensional properties of the piston and cylinder by applying the Dadson theory, in which the gas flow in the piston-cylinder gap is treated as viscous [1]. In fact, the gas flow along the gap can partially be realised in the molecular flow regime. Especially in the absolute operation mode with a sufficiently low residual pressure, the gas flow varies from the viscous at the entrance, over the transition in the middle, to the molecular regime at the exit from the piston-cylinder gap, so that the Dadson equation validity is limited.

In the present work, the values of reduced flow rate ( $G_p$ ), also called the *Poiseuille coefficient*

*ent*, as considered in rarefied gas dynamics (RGD) [2] are used to determine the pressure distribution ( $p_z$ ) along the piston-cylinder gap of PCAs and to calculate their effective area ( $A_0$ ). The theoretical results based on the Bhatnagar-Gross-Krook (BGK) model of the Boltzmann equation are compared with the Dadson theory and with the experimental results.

## 2. Poiseuille coefficient and pressure distribution calculation

For PCAs with a sufficiently small ratio of the gap width ( $h$ ) to the piston radius ( $r$ ),  $h/r \leq 10^{-4}$ , the gas flow through the annular gap is considered as a flow between two infinite parallel plates, and the corresponding solutions of the BGK model covering the viscous, transition and molecular flow regimes are applied. However, this model stays adequate only as long as the molecular mean free path is smaller than the PCA radius. In the free-molecular regime, when this condition is violated, the influence of the annular shape of the piston-cylinder gap is taken into account solving the kinetic equation for molecular flow through the annular gap. When the pressure distribution is obtained,  $A_0$  is calculated.

The Poiseuille coefficient ( $G_p$ ), which is the dimensionless flow rate, is a function of the rarefaction parameter ( $\delta$ ), the latter being inversely proportional to the Knudsen number and defined as  $\delta = hp_z \eta^{-1} (2kT/m)^{-0.5}$ , where  $\eta$  and  $m$  are gas viscosity and molecular mass,  $k$  is the Boltzmann constant and  $T$  is the gas absolute temperature. In [3-5] the kinetic Boltzmann equation was solved using the BGK model, and  $G_p$  of a plane infinite gap was calculated for the range  $\delta \geq 0.01$ . In the present work, using the BGK model, the solution of  $G_p(\delta)$  was extended to  $10^{-5} < \delta < 0.01$ . These results together with those from [3-5] are presented in Fig. 1 by the solid line. The peculiarity of this solution is that, in the limit  $\delta \rightarrow 0$ ,  $G_p$  becomes infinite because of the generated geometry. However, such a situation can never take place in PCAs because of their finite radius. To take this into account, a solution of the kinetic equation for a gas flow

<sup>1</sup> W. Sabuga, Physikalisch-Technische Bundesanstalt (PTB), Braunschweig, Germany

<sup>2</sup> F. Sharipov, Departamento de Física, Universidade Federal do Paraná, Curitiba, Brazil

<sup>3</sup> T. Priruenrom, National Institute of Metrology (Thailand) (NIMT), Pathumthani, Thailand, guest researcher at PTB

through an annular gap in the free-molecular flow ( $\delta \ll 0.01$ ) was applied, which leads to  $G_p$  depending on  $h/r$ . The  $G_p$  values for different  $h/r$  are shown in Fig. 1 by the horizontal dashed lines.

Thus,  $G_p(\delta)$  can be taken as presented in Fig. 1,  $\delta$ -dependent but, at small  $\delta$ , with an upper limit defined by the PCA  $h/r$ . Then  $p_z$  is determined by

$$p_z = p_1 - (p_1 - p_2) \int_0^z \frac{1}{h^2 G_p} dz / \int_0^l \frac{1}{h^2 G_p} dz \quad (1)$$

where  $p_1$  and  $p_2$  are the applied and the ambient pressure, respectively, and  $l$  is the piston-cylinder overlapping length. Since  $G_p$  depends on  $\delta$  and, thus, on  $p_z$ , the calculation is performed iteratively ( $G_p(z)$  and  $p_z(z)$  are calculated in turn).

### 3. Effective area calculation

The effective area of PCAs, in which  $h/r$  is of the order of  $10^{-5}$ , can be determined by

$$A_0 = (F_1 + F_2 + F_3) / (p_1 - p_2), \quad (2)$$

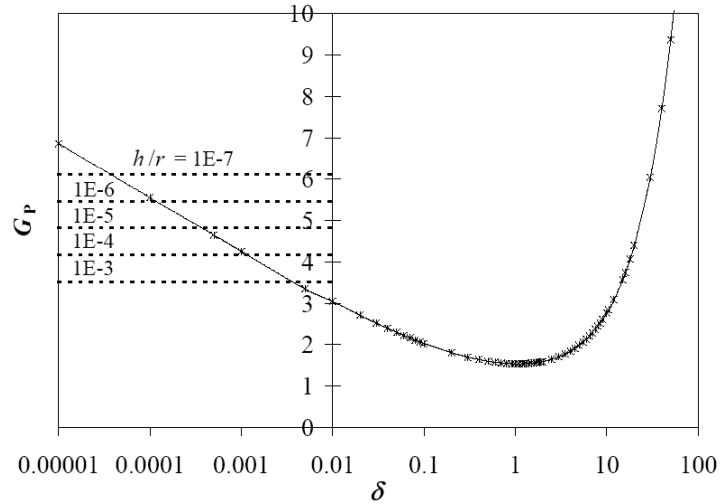
where  $F_1 = \pi r_0^2 p_1 - \pi r_1^2 p_2$ ,

$$F_2 = \pi \int_0^l r h (-dp_z / dz) dz \text{ and}$$

$$F_3 = 2\pi \int_0^l r p_z (dr / dz) dz .$$

The effective area results calculated with the Dadson and the BGK theory for different gases for the real gap profiles of a 10 cm<sup>2</sup> and a 20 cm<sup>2</sup> PCA, identified by the serial numbers DH 288 and DHI 1162, in gauge and absolute mode, are shown in Fig. 2. Here, no elastic distortion was considered.

The effective area obtained by the Dadson theory in absolute mode is independent of pressure. For PCA 288, the difference between gas species in absolute mode is much larger than in gauge mode. The difference between the Dadson and the BGK results is maximum at a pressure of 0.1 MPa and is of about 2 parts per million



For unit 1162, the effects of the operation mode and the gas species are significantly smaller than for unit 288. The maximum difference of effective areas is only about 0.4 ppm at 0.07 MPa.

### 4. Experiments

The experiment was done by pressure comparison measurements between two pressure balances. They were equipped with two nominally identical PCAs of piston-floating design and each with a nominal effective area of 10 cm<sup>2</sup>, identified by the numbers DH 288 and DH 290. One of the units, 290, was used as a reference filled with nitrogen (N<sub>2</sub>), whereas the other, 288, was a device under test operated with different gases: N<sub>2</sub>, helium (<sup>4</sup>He) and sulphur hexafluoride (SF<sub>6</sub>). To avoid a gas mixture, the two PCAs were separated by a differential pressure cell (Rosemount 3051S1CD) used to control the pressure equilibrium. The measurements were performed in gauge mode at the pressures 0.2, 0.4 and 1 MPa.

Figure 1. Poiseuille coefficient ( $G_p$ ) vs. rarefaction parameter ( $\delta$ ): solid line – solution of the BGK model for two parallel plates; dashed line – free-molecular solution for annular gap

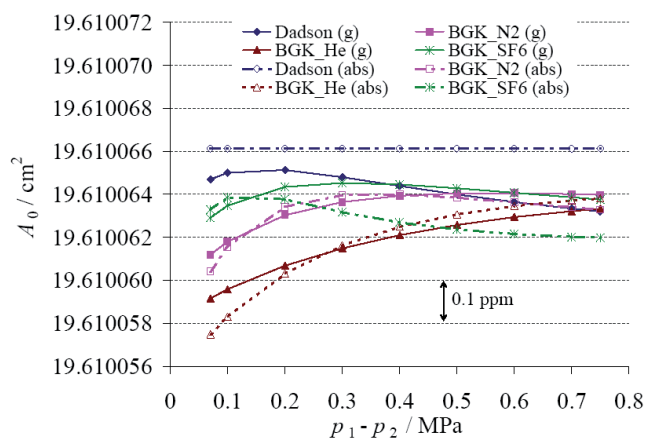
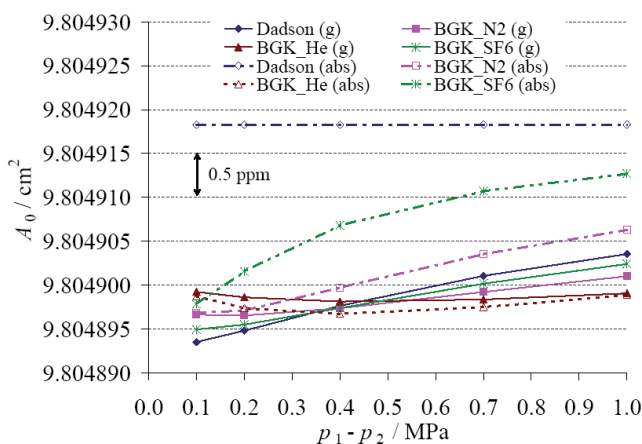


Figure 2 Effective areas of PCAs 288 (left) and 1162 (right)

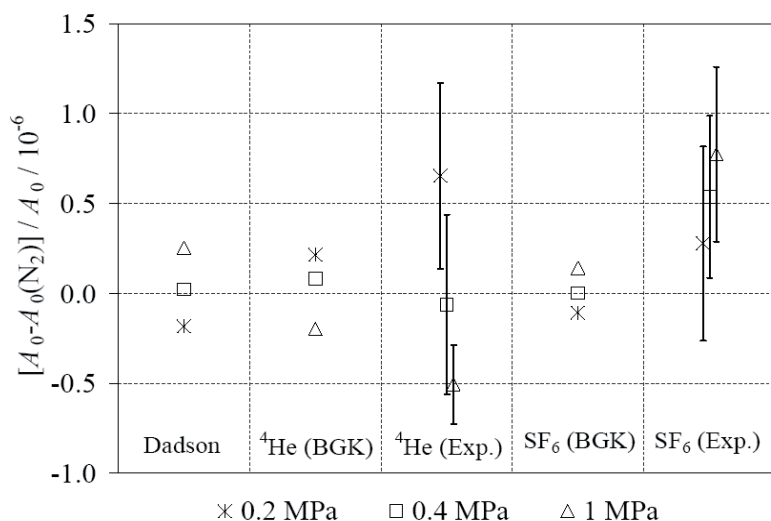


Figure 3 Relative deviations of  $A_0$  for different gases from  $A_0(N_2)$  of unit 288 in gauge mode

### 5. Results and discussion

All the results, theoretical and experimental, are shown in Fig. 3 as relative deviations from the results obtained for  $N_2$ .

The tendency of the theoretical results gained by the Dadson theory (viscous flow) is similar to that obtained by the present theory for  $SF_6$ , because  $SF_6$  has larger and heavier molecules and it is more viscous than  $N_2$  and  $^4He$ . At a low pressure, the effect of the Knudsen minimum is large, and it is reduced by increasing the pressure. The theoretical result at the pressure 1 MPa for helium is about 0.2 ppm smaller than for  $N_2$ , while for  $SF_6$  it is about 0.2 ppm larger. This is because the  $SF_6$  molecules are larger and heavier, and the helium molecules are smaller and lighter than those of nitrogen. The experimental results show the same trend as the theoretical results. However, they do not allow a quantitative check of the theory because the standard deviation of the experiment is too large compared with the observed effects. A more accurate check should be possible in the future using the special pres-

sure balances designed for the Boltzmann constant experiments and operated in absolute mode.

### 6. Conclusion

Using the new model based on the rarefied gas flow theory, the effective area of real PCAs can be calculated for a specific gas and operation mode. For the two analysed PCAs of 10 and 20 cm<sup>2</sup>, the maximum difference between the Dadson theory and the new one is about 2 and 0.4 ppm, respectively. Therefore, in most cases the Dadson theory appears to be sufficient. However, if a very small uncertainty, say 1 ppm and lower, is required, in particular in the absolute mode, then an application of the new theory will be necessary.

### Acknowledgments

Support of this research by the International Graduate School of Metrology (IGSM) Braunschweig is acknowledged.

### References

- [1] Dadson, R.S.; Lewis, S.L.; Peggs, G.N.: The Pressure Balance – Theory and Practice, London, HMSO, 1982
- [2] Sharipov, F.; Seeleznev, V.: Data on internal rarefied gas flows. J. Phys. Chem. Ref. Data **27** (1998), 657-706
- [3] Lo, S.S.; Loyalka, S.K.: An efficient computation of near-continuum rarefied gas flows. J. Applied Math. Phys. **33** (1982), 419-424
- [4] Cercignani, C.; Pagani, C.D.: Variational approach to boundary-value problems in kinetic theory. Phys. Fluids **9** (1966), 1167-1173
- [5] Loyalka, S.K.; Petrellis, N.; Storvick, T.S.: Some exact numerical results for the BGK model: Couette, Poiseuille and thermal creep flow between parallel plates. J. Applied Math. Phys. **30** (1979), 514-521

# New MSL twin pressure balance facility

Mark Fitzgerald, Chris Sutton, Darrin Jack<sup>1</sup>

## Abstract

This paper describes the design and performance of the new MSL twin gas pressure balance facility which will be used for gauge, absolute and differential gas pressure standards from 1 Pa up to 11 MPa. This new instrument uses large-area piston-cylinder units and replaces the first MSL facility that was developed in the 1980's to generate small differential pressures. Two key features of the new design are the high thermal conductivity base to minimise temperature differences between the two piston-cylinder units and increased pumping speed and flow conductance to evacuate the region above each piston-cylinder. The new twin pressure balance facility is currently being commissioned and initial results obtained from the instrument are presented including the temperature stability, base vacuum and the performance achieved when generating low differential pressures.

## Introduction

The Measurement Standards Laboratory of New Zealand (MSL) has operated gas pressure balances in the twin pressure balance configuration since the early 1980s [1]. This configuration is a versatile way to operate gas pressure balances, allowing gauge, absolute and differential pressures to be generated. For example, gauge and absolute pressures can be easily generated using only one of the pressure balances while the two pressure balances can be used for cross-float measurements or to generate small differential or absolute pressures as low as 1 Pa. Other NMIs [2, 3] have used the twin pressure balance method to generate low differential pressures and the effectiveness of the method has been shown in CCM and APMP measurement comparisons [4, 5]. The twin pressure balance technique can also be used to measure small absolute pressures that are below the pressure balance lower limit determined by the piston mass and area [6, 7].

The MSL twin pressure balance design involves mounting two piston-cylinder units into one common base that allows full operation of the pressure balances in gauge or absolute mode.

Each piston-cylinder unit is housed in a separate vacuum chamber and a manual mass loader is used to load and unload small masses onto one of the piston-cylinder units. The common base provides a thermal link to minimize the difference in temperature between each piston-cylinder unit and to reduce the drift in the generated differential pressure. For example a 0.01 °C difference between the two piston-cylinder units will change the differential pressure by 9 mPa at a line pressure of 100 kPa.

We have recently upgraded our gas pressure balances and have used this opportunity to redesign our twin pressure balance facility to house the new piston-cylinder units. This paper describes the design features of the new twin pressure balance facility and shows the results of measurements made when generating low differential pressures.

## Design

The design (Figure 1) is based around the DH Instruments PG 7601 gas pressure balance. The piston-cylinder mounting stem, electronics and mass rotation mechanism were removed from the DH Instrument bases and remounted into one large aluminium base (860 mm × 420 mm × 50 mm). The base has been machined to accept the piston-cylinder mounts, rotation mechanism and to allow all the external sensors to be fed through into the vacuum. The electronic control boards, normally mounted below each piston-cylinder unit, were moved away from the aluminium base to reduce the heat load and corresponding temperature rise of each unit when in use. Fans are used to circulate the laboratory air in the region below the base to remove heat generated by the remaining electronics and vacuum pumps.

The mounting base is designed to achieve a low vacuum pressure in the glass bell jar above each piston-cylinder unit. This pressure is governed by the gas leak rate through the piston-cylinder gap, the flow conductance between the vacuum pump and bell jar and the pumping speed. To increase the pumping speed each piston-cylinder unit is evacuated by an 80 L/s tur-

<sup>1</sup> Mark Fitzgerald, Chris Sutton, Darrin Jack, Measurement Standards Laboratory of New Zealand (MSL), Industrial Research Ltd, PO Box 31310, Lower Hutt, New Zealand. Email of corresponding author: m.fitzgerald@irl.cri.nz



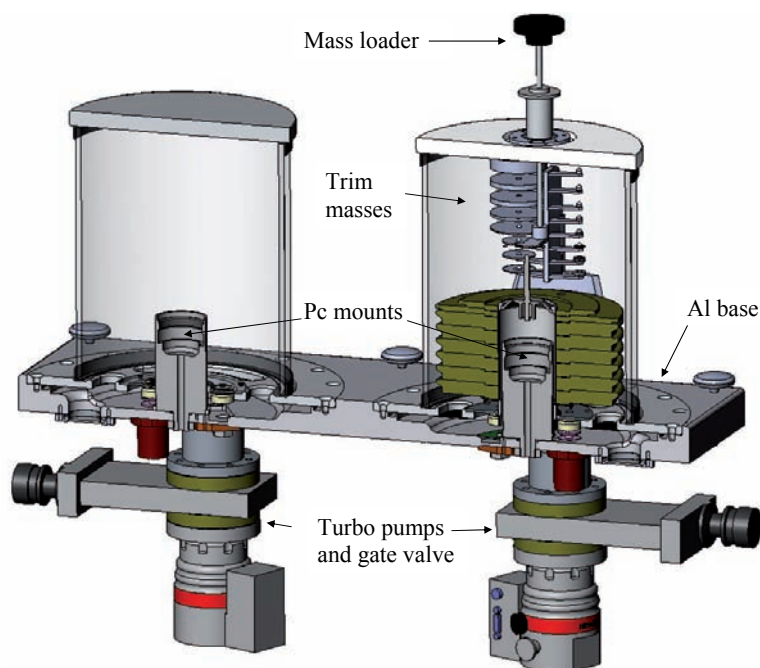


Figure 1 Schematic view of the new MSL twin pressure balance facility

bo pump (backed by an oil filled rotary pump) connected to the aluminium base through a large diameter port (DN 63). The vacuum port connects to a large volume immediately below the piston-cylinder unit and this region is connected to the bell jar above by a large area annular slot. Each piston-cylinder unit can be isolated from its turbo pump by a gate valve and there is a separate butterfly valve (not shown) to connect the two bell jars directly together.

A manual mass loader has been added to one of the bell jars so that small trim masses can be manually loaded and unloaded while the system is under vacuum (see figure 1). The 1.1 kg trim mass set consists of 13 disk shaped masses, from 0.1 g up to 500 g that can generate differential pressure from 1 Pa up to 1000 Pa when used with the 10 kPa/kg piston-cylinder unit. The loader, based on a rotary/linear vacuum feed-through, uses a slotted plate to lift each mass off a rack inside the vacuum. The loader is then rotated and lowered to place each mass onto a loading spike on the piston. This spike replaces the bolt that is normally used to retain the cap onto the piston. Each trim mass has a  $\phi 6$  mm central hole to locate it on the spike and the larger trim weights have a small step in their base to make it easier to pick them up.

### Performance

The temperature stability of the piston-cylinder units has been greatly improved by the new MSL twin pressure balance base and mounting arrangement. The cylinder temperature remains close to the ambient air temperature during absolute mode operation. Previously the piston-cylinder temperatures would increase by almost 2 °C above ambient when switched on but this

has been reduced to < 0.1 °C. The aluminium base links the temperature of the two piston-cylinder units closely together so that the two piston-cylinder units stay within 0.05 °C of each other. The drift rate in this temperature difference is small; the corresponding drift rate in the differential pressure is less than 0.5 mPa per minute.

The improvements to the vacuum system have resulted in a reduced pressure in each bell jar. A pressure of ~ 5 mPa can be reached when generating 100 kPa with the 10 kPa/kg piston-cylinder units. This reduction in bell pressure will reduce the lower limit when measuring low absolute pressures. The turbo pumps result in a fast start up with typical pump down times of 20 minutes. One problem with the vacuum system was the transmission of vibration from the rotary pumps to the piston-cylinder mounts. This vibration was reduced by locating the rotary pumps about 5 m away from the apparatus and using a flexible PVC backing hose.

### Differential Pressure Generation

The performance of the new twin pressure balance facility in generating differential pressure was assessed by determining the measurement repeatability  $u_r$  of measurements at 1 Pa, 10 Pa and 100 Pa. These measurements were made using two 10 kPa/kg piston-cylinder units, operating at a line pressure of 100 kPa, connected to a Model 398 133 Pa Baratron capacitance diaphragm gauge (CDG) and signal conditioner. The gauge output was read using a HP 3458A voltmeter. The measurement procedure for each measurement point was to repeatedly load and unload the required trim mass five times. To minimise any disturbance during the measurements the CDG was isolated from the differential pressure before changing the load and the pressure balance heights and rotation rates were not adjusted during the five load/unload cycles. After each change in load, the CDG was reconnected to the differential pressure and left for 60 s to let any transient behaviour die away. The voltage output from the CDG was then measured for ~90 s, the measurement time being an integral multiple of the natural oscillation period (1.6 s) of the pressure balance and CDG system. The resulting ten measurements recorded (5 loaded and 5 unloaded) were then analysed using a circular weighing analysis [7] to find the CDG reading, the uncertainty and to reduce the effect of drift on the measurement.

The measurements results for four 100 Pa measurements made over a period of 3 hours are shown in Figure 2. Each measurement point is calculated from five load/unload cycles and the Type A standard uncertainty is obtained from

the fit residuals. The individual measurements have a standard uncertainty component of  $\sim 0.5$  mPa for repeatability while combining all four measurements gives a reproducibility value of  $u_r \sim 1$  mPa. These reproducibility values are a combination of the twin pressure balance and CDG performance.

All the differential pressure measurements along with their  $u_r$  values are shown in Table 1. The values for  $u_r$  are generally less than 1 mPa, apart from the 1 Pa point. The small 0.1 g trim mass used to generate 1 Pa proved to be difficult to unload without bringing the spinning piston to a halt. The subsequent re-spinning of the piston disturbed the pressure balance and caused step changes in the CDG reading. We are planning to change the design of these smaller masses to make them easier to unload. The result for 0 Pa shows the performance of the system when no masses are loaded on to the piston. For these measurements the pressure balances were left running freely while the CDG voltage was measured ten times. The value of  $u_r = 0.2$  mPa represents the undisturbed performance of the pressure balance CDG combination over the usual measurement time.

Differential Pressure / Pa	$u_r$ / mPa
0	0.2
1	1.3
10	0.3
100	1

Table 1. Measurements of the differential pressure reproducibility  $u_r$  for a range of loadings.

## Conclusions

The commissioning of the new twin pressure balance is proceeding well. The large aluminium base is providing good thermal stability and limiting the temperature rise of the pressure balances to less than  $0.1$  °C above ambient. It also provides a good thermal link between the two piston-cylinder units with a typical temperature difference between the two piston-cylinder units being  $< 0.05$  °C. The drift in this temperature difference is also low resulting in differential pressure drift rates less than  $0.5$  mPa per minute. The new vacuum system and improved flow conductance have reduced the bell jar pressure to  $5$  mPa. The measurement reproducibility has been shown to be  $\leq 1.3$  mPa when generating differential pressures in the range  $1$  Pa to  $100$  Pa at a line pressure of  $100$  kPa.

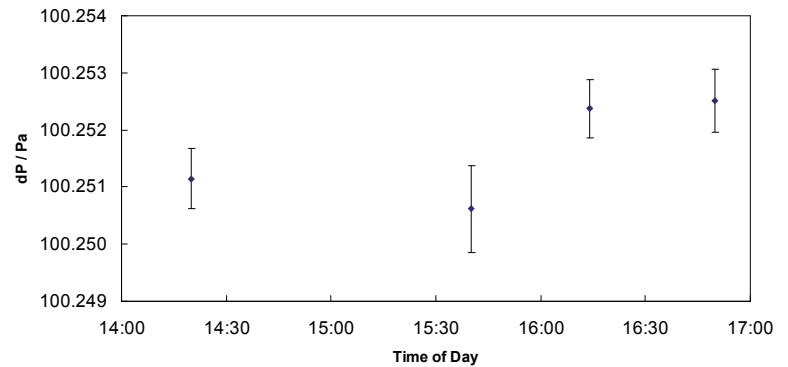


Figure 2 Repeated 100 Pa differential pressure measurements with standard uncertainties obtained from the fit residuals. Each measurement point is the result of 5 load/unload cycles.

## References

- [1] C M Sutton 1986/87 *Metrologia* **23** 187-195
- [2] M Kojima, T Kobata, K Saitou and M Hirata 2005 *Metrologia* **42** S227
- [3] S Y Woo, I M Choi, H W Song 2009 *Metrologia* **46** 125-128
- [4] A P Miiller et al 2002 *Metrologia* **39** 07002
- [5] Tokihiko Kobata et al. 2007 *Metrologia* **44**07001
- [6] C M Sutton and M P Fitzgerald 2009 *Metrologia* **46** 655
- [7] S Y Woo and I M Choi 2005 *Metrologia* **42** S193
- [8] C M Sutton and M T Clarkson 1994 *Metrologia* **30** 487

# Calculation of Effective Area for the NIM Primary Pressure Standards

Yuanchao Yang<sup>1\*</sup>, Jin Yue<sup>1</sup>

## Abstract

The primary pressure standards of the National Institute of Metrology (NIM) are a group of five oil-operated piston-cylinder assemblies of 1 cm<sup>2</sup> nominal cross-sectional area for the 10 MPa range. The five piston-cylinder assemblies were accurately dimensioned by the length division of NIM, including straightness, roundness and diameter measurements. Based on the dimensional data, the effective areas were calculated with relative standard uncertainties ranged from  $5.7 \cdot 10^{-6}$  to  $11 \cdot 10^{-6}$  using the Dadson's theory. We also carried out the cross-float measurements between each two of the piston-cylinder assemblies, and the effective area ratios were determined with relative standard uncertainties of about  $9 \cdot 10^{-6}$ . Finally, the effective areas of the five piston-cylinder assemblies were determined taking into account the results of both dimensional characterization and cross-float experiments using generalized least-squares method.

**Keywords:** primary pressure standard; piston-cylinder assembly; pressure balance; cross-float experiment; effective area

## 1. Introduction

The oil-operated primary pressure balance standard at the National Institute of Metrology (NIM) is in the 10 MPa range, of which the essential elements are five 1 cm<sup>2</sup> piston-cylinder (p-c) assemblies with maximum load of 100 kg. The five p-c units, designated as No. 650301, 650302, 650303, 66501 and 66505, were manufactured in 1960s [1]. In the past over 40 years, their effective areas were determined for three times, in 1970, 1974 and 1984 respectively. In order to study the stability of the primary standard and participate in the international key comparisons, it's important and necessary to redetermine the effective areas of the p-c assemblies. In this work, the effective areas of the five primary standards were reproduced based on the new dimensional measurements and the cross-float experiments.

The p-c assemblies are of simple form with

170 mm long pistons and 90 mm long cylinders. This feature makes the engagement length invariable and the effective area contributed by the middle part of the piston. Both pistons and cylinders were made of steel. A mixture of paraffin and transformer oil was used as the pressure-transmitting fluid in the pressure balance.

Based on the Dadson's theory [2], a formula for calculation of the effective area was derived from the force acting on the floating piston. The effective areas were calculated by numerical integration using the diameter data, and the roundness data was taken into account for the uncertainty evaluation. We also carried out the cross-float experiments between each two of the p-c assemblies to obtain the effective area ratios. The effective areas calculated from the dimensional data were adjusted by the experiment results using the generalized least-squares (GLS) estimation.

## 2. Determination of effective areas from dimensional data

Two specially designed instruments [3, 4] developed at the length division of NIM were used to measure the outer diameters of the pistons and the inner diameters of the cylinders, respectively. The measuring principle is the non-contacting comparison measurements between the piston and a gauge block of grade 1. In brief, two Michelson interferometers are applied for surface positioning, and the diameter is measured by laser interferometer combining with phase-shifting interferometry. The stated uncertainty is  $(0.05 + 0.5L) \mu\text{m}$  ( $U_{99}$ ),  $L$  is in meter. All diameters were measured near 20 °C and corrected to the reference temperature of 20 °C. For roundness and straightness measurements, a commercial equipment (Talyrond 395) was utilized.

The formulae for calculation of effective area adopted by most metrological institutes are essentially equivalent [5]. Differences arise from the geometric models constructed by the dimensional data: a simplified one or a complicated one that is close to the reality. The simplest model treats the piston and cylinder as perfectly

<sup>1</sup> Yuanchao Yang, Jin Yue, Pressure and Vacuum Group, National Institute of Metrology, Beijing 100013, China

\* Corresponding author. Tel.: +86-10-64525115; fax: +86-10-64218637. E-mail address: yangyc@nim.ac.cn

straight and round artifacts, and the averaged diameters are used. The most complex mode is to construct the cylindrical “cages” using the data on diameters, roundness and straightness [6, 7], and take into account the flow regime in the crevice [8]. Here, we used a moderate complex mode, in which piston and cylinder were perfectly round and diameters varied with height, and viscous flow solution was used. Diameters were averaged at measured latitudes and linearly interpolated between diametric datum latitudes. The roundness data was used primarily in aiding the evaluation of the overall uncertainty. The effective area  $A_p$  at gauge pressure  $p$  was calculated following the equation

$$A_p = \frac{-\pi}{p} \int_0^l rR \frac{dp_z}{dz} dz, \tag{1}$$

where  $r$  and  $R$  are piston and cylinder radii along the engagement length  $l$ ,  $p_z$  represents the gauge pressure distribution in the crevice. For oil-operated assemblies  $p_z$  was calculated as

$$p_z = p \left[ 1 - \frac{\int_0^z \frac{1}{h^3} dz}{\int_0^l \frac{1}{h^3} dz} \right], \tag{2}$$

where  $h$  is the radial clearance at the  $z$  coordinate. To lower the numerical integration errors, another equation equivalent to equation (1) was used:

$$A_p = \pi r_0^2 \left[ 1 + \frac{h_0}{r_0} + \frac{1}{r_0^2 p} \int_0^l p_z \frac{d(rR)}{dz} dz \right], \tag{3}$$

where  $r_0$  and  $h_0$  are the piston radius and radial clearance at the base. In equation (3), the result of numerical integration was a small correction item. The results of the effective area calculations for the five primary standards and the associated uncertainties are summarized in table 1. The uncertainties of piston and cylinder radius listed in column 4 and 5 of table 1 were contributed by the diameter measurements and the roundness data.

### 3. Cross-float experiments

For the five p-c assemblies, ten couples of effective area ratio were obtained from the cross-float experiments with the pressures generated in the following order (2, 4, 6, 8, 10, 10, 8, 6, 4, 2) MPa. Three cross-float cycles were measured for each couple of effective area, and totally thirty measurement cycles were implemented. The piston temperature was measured by a platinum resistance directly attached to the outer cylinder

surface, and the piston position and fall-rate was detected using an optical sensor.

The two methods used for analyzing the cross-float experiments are the so-called  $p$ -method and  $\Delta p$ -method [9, 10]. The  $p$ -method requires accurate determination of the head correction when using oil as working fluid especially at low pressures. For example, a variation of 1 mm in height difference between the reference levels can result a relative deviation of effective area to be  $8.8 \cdot 10^{-6}$  when the pressure is 1 MPa, and this would be  $0.9 \cdot 10^{-6}$  at 10 MPa. However, it's particularly difficult for us to measure the height difference with an uncertainty lower than 1 mm. Consequently, the  $\Delta p$ -method which can eliminate the effects of head correction and surface tension was used to analyze the cross-float data. The formula used to calculate the effective area ratio at pressure  $p$  and at 20 °C,  $A'_p/A_p$ , is given by

$$\text{(see bottom of page),} \tag{4}$$

where the superscript identifies the two intercompared pressure balances,  $\Delta m$  is the increased masses with the increased pressure  $\Delta p$ ,  $\rho_a$  is the density of air and  $\rho$  the density of the masses,  $t_0$  is the piston temperature at the lowest equilibrium pressure  $p_0$  and  $t$  the piston temperature at pressure  $p$ ,  $\alpha$  is the thermal expansion coefficient and  $\lambda$  is the elastic distortion coefficient. As the materials and the dimensions of the five assemblies are the same, we assume that they have a common distortion coefficient of  $3.6 \cdot 10^{-6} \text{ MPa}^{-1}$ , calculated from elastic theory [11] using an Young's modulus of  $2.1 \cdot 10^{11} \text{ Pa}$  and Poisson's ratio of 0.29. Then, the ratio of the zero-pressure effective area can be calculated using the simplified equation:

$$\frac{A'_0}{A_0} = \frac{\Delta m'}{\Delta m} \left[ 1 + \alpha(t-t') + \frac{p_0}{\Delta p} \alpha(t-t' + t'_0 - t_0) \right]. \tag{5}$$

None dependence of the effective area ratio on pressure was observed. Table 2 gives the zero-pressure effective area ratios with standard uncertainties. The relative standard deviations lie between  $0.75 \cdot 10^{-6}$  and  $1.76 \cdot 10^{-6}$ , and the uncertainties are mainly contributed by the temperature as a relatively large thermal expansion coefficient of  $2.4 \cdot 10^{-5} \text{ }^\circ\text{C}^{-1}$ . The ratios derived from experiments and the ratios calculated from dimensional data are compared, and their differences are also given in table 2. It seems that the five p-c assemblies are divided into two groups from the difference data: one group is No. 650301, 650302 and 650303, and the other is No. 66501 and 66505. The experimental ratios in the

$$\frac{A'_p}{A_p} = \frac{\Delta m' (1 - \rho_a / \rho) [1 - \alpha'(t' - 20)]}{\Delta m (1 - \rho_a / \rho) [1 - \alpha(t - 20)]} \cdot \left\{ 1 + \frac{p_0}{\Delta p} [\alpha(t - t_0) - \alpha'(t' - t'_0)] + (\lambda - \lambda') p_0 \right\} \tag{4}$$

group agree with the theoretic values within their combined standard uncertainties; however the experimental ratios between the two groups disagree with the theoretic calculations. The reason for the extraordinary discrepancy is unknown and needs further study.

#### 4. Results of adjusted effective areas and discussion

It is of great practical importance to adjust the theoretical calculations of effective area using the experimental results. As the theoretical values and experimental results have different uncertainties, it's beneficial to make the analysis using generalized least-squares (GLS) estimation, which is described in detail in [12, 13].

The improved effective areas acquired from the GLS estimation, based on the dimensional and experimental data (D+E), are given in column 2 of Table 3, and the corresponding relative standard uncertainties in column 3. The uncertainties were evaluated as

$$u_{D+E}(A_0) = \sqrt{[u_D(A_0)]^2 + \left[\frac{u_E(R)}{\sqrt{2}}\right]^2}, \quad (6)$$

where  $u_{D+E}(A_0)$  represents the uncertainty of the adjusted effective area value,  $u_D(A_0)$  is the uncertainty of the effective area calculated from dimensional data, and  $u_E(R)$  is the uncertainty of the experimental ratios. The relative differences between the improved and original values are listed in columns 4 to 8 of Table 3. It's noticeable that the differences between the ratios obtained from the improved areas and the experimental ratios are considerably reduced.

#### 5. Conclusions

In this paper, we have reproduced the effective areas of the five p-c assemblies of the NIM primary pressure balance standard. Calculations for the effective areas were carried out based on the Dadson's theory and the dimensional measurements made in the length division of NIM. Also, the effective area ratios of each two assemblies were obtained experimentally from the conventional cross-float equilibrium. To eliminate the head correction,  $\Delta p$ -method was used to analyze the experimental data. The relative standard deviations of all the ratios are found to be smaller than  $1.76 \times 10^{-6}$ . Results of calculation and experiment were combined to determine the best values of the effective areas using GLS estimation. There are some disagreements between the ratios from dimensional data and from experiments, which needs to be studied further.

#### Acknowledgements

The authors gratefully thank Weichen Wang for diameter measurements and Heng Zhang for roundness and straightness measurements. This work was financially supported by the Doctoral Fund of National Institute of Metrology (ATGQDB0903).

#### References

- [1] Sheng Yi-tang, *Acta Metrologia Sinica*, 1982, 3, 161-74.
- [2] Dadson R. S., Lewis S. L., Peggs G. N., *The Pressure Balance: Theory and Practice*, London, HMSO, 1982.
- [3] Wang Wei-chen, Zhu Xiao-ping, Cui Jing-yuan, et al., *Acta Metrologia Sinica*, 2006, 27, 77-9.
- [4] Wang W., Zhu X., et al., *Acta Metrologia Sinica*, 2010, 31, 112-5.
- [5] Molinar G., Bergoglio M., Sabuga W., et al., *Metrologia*, 2005, 42, S197-S201.
- [6] Jager J., Sabuga W., Wassmann D., *Metrologia*, 1999, 36, 541-4.
- [7] Jain K., Bowers W., Schmidt J. W., *J. Res. Natl. Inst. Stand. Technol.*, 2003, 108, 135-45.
- [8] Schmidt J. W., Jain K., Miiller A. P., et al., *Metrologia*, 2006, 43, 53-9.
- [9] Forbes A. B., Harris P. M., *Metrologia*, 1999, 36, 689-92.
- [10] Legras J. C., *Metrologia*, 1993/94, 30, 625-9.
- [11] Heydemann P. L. M., Welch B. E., *Experimental Thermodynamics Vol. II*, LeNeindre B. and Vodar B., eds., Butterworths, London, 1975, 147-201.
- [12] Sutton C. M., *Metrologia*, 2004, 41, 272-7.
- [13] Sutton C. M., Fitzgerald M. P., Giardini W., *Metrologia*, 2005, 42, S212-5.

## Tables

No.	Effective area $A_0/\text{cm}^2$	Relative standard uncertainty $u(A_0)/A_0 \times 10^6$	Standard uncertainty of piston radius $u(r)/\text{nm}$	Standard uncertainty of cylinder radius $u(R)/\text{nm}$
650301	1.0125218	6.5	32	18
650302	1.0054263	11	45	46
650303	1.0061135	7.0	34	20
66501	1.0072243	6.0	20	28
66505	1.0087441	5.7	27	18

Table 1. Effective areas calculated from dimensional data.

No.	650302		650303		66501		66505	
	Ratios	Diff. $\times 10^6$	Ratios	Diff. $\times 10^6$	Ratios	Diff. $\times 10^6$	Ratios	Diff. $\times 10^6$
650301	0.9929882 $\pm 8.2 \times 10^{-6}$	-4.1	0.9936707 $\pm 8.7 \times 10^{-6}$	-0.2	0.9947493 $\pm 8.5 \times 10^{-6}$	-18.7	0.9962511 $\pm 8.1 \times 10^{-6}$	-17.9
650302			1.0006871 $\pm 8.4 \times 10^{-6}$	3.6	1.0017737 $\pm 8.7 \times 10^{-6}$	-14.6	1.0032847 $\pm 8.0 \times 10^{-6}$	-15.2
650303					1.0010864 $\pm 8.0 \times 10^{-6}$	-17.7	1.0025940 $\pm 8.7 \times 10^{-6}$	-20.6
66501							1.0015062 $\pm 8.6 \times 10^{-6}$	-2.7

Table 2. Effective area ratios obtained from cross-float experiments with standard uncertainties and comparison with calculated values.

No.	Dimensional data + experi- mental ratios (D+E)		Rel. diff. $\times 10^6$ (D+E)-D	Rel. diff. in ratios $\times 10^6$ (D+E)-E			
	$A_0/\text{cm}^2$	$u(A_0)/A_0 \times 10^6$		650302	650303	66501	66505
650301	1.0125293	8.9	7.4	2.1	0.5	5.5	3.8
650302	1.0054317	13.0	5.4		-1.3	3.3	2.9
650303	1.0061212	9.3	7.7			4.1	6.1
66501	1.0072183	8.6	-5.9				1.8
66505	1.0087372	8.4	-6.8				

Table 3. Best values of Effective area calculated from dimensional data combined with experimental ratios (D+E) and their relative standard uncertainties. Relative difference between the best values of effective area and the values calculated from dimensional data (D). Relative difference between the ratios calculated from the best values and the experimental ratios (E).

# New Model Of Fluid Flow To Determine Pressure Balance Characteristics

P. Wongthep<sup>1,2</sup>, T. Rabault<sup>1</sup>, C. Sarraf<sup>2</sup> and R. Noguera<sup>2</sup>

## Abstract

Some projects like the Euramet Project 463 have underlined the lack of agreement between experimental measurements and calculations by finite element methods (FEM), used to determine the piston fall rate of high-pressure balance used in primary standards. Yet, piston fall rate is an essential parameter to characterize experimentally the mean gap between the piston and the cylinder and to determine the effective area ( $A_p$ ) at each pressure ( $p$ ) point. Adjusting the methods to estimate this parameter will improve the characterization of the gap, the determination of  $A_p$  and consequently the pressure distortion coefficient. One of the first possible explanations of the significant difference observed between the calculated and measured piston fall rates could be due to the determination of the fluid flow. Indeed, the former quasi 1D Stokes model assimilates the gap between piston and cylinder as formed by two parallel walls, which is an approximation. In addition, the velocity of the piston wall was neglected. In order to evaluate the influence of this model, the equations of the fluid flow are modified and are presented in this paper. Equations that were defined in a parallel planes model are defined in an annular gap model. Besides this, corrections due to the velocity of the piston wall are inserted. This research work is applied on a Desgranges et Huot DH 7594 piston-cylinder unit of PTB with a pressure up to 1 GPa, in the continuity of EURAMET Project 463 in order to quantify the influence of each correction that has been inserted in the new equations. This is carried out by using FEM. This evaluation will allow us to evaluate the improvement of our knowledge on the behavior of piston gauges and consequently to better evaluate the uncertainties due to the models.

## 1. Introduction

Pressure balances are used in many national metrology institutes (NMIs) as primary pressure standard from a few kPa up to approximately 1 GPa. The pressure balance consists of a loaded piston inserted into a closely fitted cylinder. The

effective area ( $A_p$ ) of the piston-cylinder unit (PCU) is commonly defined as a function of the effective area at zero pressure ( $A_0$ ), the pressure applied ( $p$ ) and the pressure distortion coefficient ( $\lambda$ ):

$$A_p = A_0(1 + \lambda \times p) \quad (1)$$

For pressure above 10 MPa,  $\lambda$  contributes greatly to the final uncertainty. That is why its evaluation is so critical and why many studies have been carried out on this subject. EUROMET project 463 [1] was organized in 1998 to compare the agreement between laboratory calculations of the  $\lambda$  and also the piston fall rate ( $v_f$ ) by using finite element methods (FEM). The PCU of PTB (No. DH 7594) for pressure balance which operates at pressure up to 1 GPa was selected to compare the calculations. Large differences in the pressure distributions, gap profiles and particularly  $v_f$  at the maximum pressure were found [1]. The measurement of  $v_f$  is an important point to check the equilibrium condition for the comparison (cross floating method) of two pressure balances and the quality of the pressure balance and PCU. Moreover, it has to be remembered that  $v_f$  can be used to visualize the effect of the piston and cylinder distortions on the pressure balances.

## 2. Theory

The equilibrium of the PCU is a condition where fluid dynamics laws apply. Therefore the velocity profile of the fluid moving through a gap between the piston and cylinder as a function of variation in pressure at both ends of the piston-cylinder engagement length of the PCU can be determined by applying the Navier-Stokes equation [2]:

$$\frac{dv}{dt} = -\frac{1}{\rho} \text{grad } p + \nu \Delta v + \left( \frac{\xi}{\rho} + \frac{\nu}{3} \right) \text{grad } \text{div } v + F \quad (2)$$

Where  $v$  is the fluid velocity,  $\rho$  is the fluid density,  $p$  is the applied pressure,  $\nu$  is the kinematic viscosity,  $\xi$  is the second viscosity and  $F$  is the mass force of the fluid. The following realistic assumptions are made:

<sup>1</sup> Laboratoire National de métrologie et d'essais, 1 rue Gaston Boissier 75015 Paris France

<sup>2</sup> Arts et Métiers Paris Tech / DynFluide, 51 Boulevard de l'Hôpital, 75013 Paris France  
Email of corresponding author: padipat.wongthep@lne.fr

- Fluid is incompressible ( $div v = 0$ ),
- Fluid flows are stationary, isothermal and laminar ( $dv/dt = 0$ ),
- Mass force is negligible ( $F = 0$ ),
- One-dimensional flow in the  $y$  direction for the parallel planes model and in the  $z$  direction for the annular gap model.

Then the equation can be modified as:

$$\eta \Delta v = grad p \tag{3}$$

The Laplace operator  $\Delta v$  depends on the coordinate systems. In the models used until now, the gap between the piston and the cylinder was assumed to be based by parallel surfaces and the fluid velocity at each surface to be equal to zero. The calculations were made with a parallel planes model similar to the model used by Dadson [3]. In the present work, a cylindrical model more consistent with the geometry of the PCU is applied and the piston velocity is taken into account. For this paper, the following flow models are used (Figure 1):

- Model 1 is the parallel planes model in Eq. 4,
- Model 2 is the annular gap model with zero velocity imposed as boundary condition on the piston side in Eq. 5,
- Model 3 is the annular gap model with fall velocity imposed as boundary condition on the piston side in Eq. 6.

The equations of the three models are:

$$v(x) = \frac{1}{2\eta} \frac{dp}{dy} \left[ x^2 - r_p + \frac{(r_p + h)^2 - r_p^2}{h} (r_p - x) \right] \tag{4}$$

$$v(r) = \frac{1}{4\eta} \frac{dp}{dz} \left[ r^2 - (r_p + h)^2 + \left( (r_p + h)^2 - r_p^2 \right) \ln \left( \frac{r_p + h}{r} \right) \right] \ln \left( \frac{r_p + h}{r_p} \right) \tag{5}$$

$$\eta(p, t) = \eta(t) \times 10^{\alpha(t) \times p^q} \tag{7}$$

$$v(r)^* = v(r) + v_f \ln \left( \frac{r_p + h}{r} \right) \ln \left( \frac{r_p + h}{r_p} \right) \tag{6}$$

Where  $\eta$  is the dynamic viscosity,  $dp/dy$  and  $dp/dz$  are the variation of the pressure along the  $y$  direction and  $z$  direction,  $r_p$  is the piston radius and  $h$  is the gap width.

### 3. Numerical application

The numerical calculations are performed with the Structural Dynamics toolbox (SDTools) in MatLab, which allows the application of finite element methods. A common method is the separated solution of the fluid flow and structural problem. The fluid flow was analyzed in the piston-cylinder clearance, which is affected by structural distortions. Piston/cylinder distortions are determined iteratively by FEM structural analysis. The pressure distribution obtained by flow analysis is at the same time used as load condition in the structure problem. The solution of the two-coupled problems is determined by structural and fluid flow analysis performed iteratively until a convergence of the output parameters of interest is obtained. The mesh is obtained by using the gmsh software [4] to define the contour of structure of the PCU. A module is created in order to integrate the mesh within Matlab software. The calculation performed for the real profile of the undistorted gap between piston and cylinder obtained by dimensional measurements, and the elastic constants of materials are taken as initial parameters as specified in section 2 of the EUROMET project 463 [1]. To calculate the pressure distribution, the fluid density ( $\rho$ ) and dynamic viscosity ( $\eta$ ) need to be known. The di(2)-ethyl-hexyl-sebacate (DHS) is the fluid the most commonly used in the pressure balance. The experimental data on DHS density and viscosity are available in [5,6] and were evaluated in [7]. For our calculation the dynamic viscosity based on data from [5,6] was described for the temperature of 20 °C by the model equation:

where  $\eta(t)$  is the dynamic viscosity, which at  $t = 20^\circ\text{C}$  is equal to 0.028 68 Pa.s,  $\alpha(t)$  is the coefficient, which at  $t = 20^\circ\text{C}$  is equal to 0.017 29,  $p$  is the applied pressure in MPa and  $q$  is the coefficient equal to 0.8.

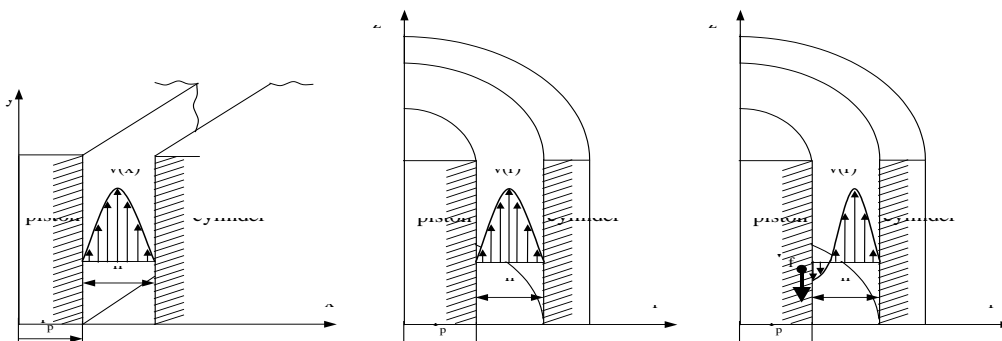


Figure 1. Calculation models: (a) parallel planes model (b) annular gap model with zero velocity imposed as boundary condition on the piston side (c) annular gap model with fall velocity imposed as boundary condition on the piston side



Model	Model 1	Model 2	Model 3
Displacement at the gap entrance in $\mu\text{m}$			
Piston	-1.080	-1.080	-1.080
Cylinder	1.832	1.831	1.831
$h$	3.584	3.583	3.583
Displacement at the gap exit in $\mu\text{m}$			
Piston	0.240	0.238	0.238
Cylinder	-0.122	-0.119	-0.119
$h$	0.023	0.028	0.028
Zero effective area in $\text{mm}^2$	49.021 39	49.021 39	49.021 39
Distortion effective area in $\text{mm}^2$	49.038 59	49.038 63	49.038 63
Piston fall rate in $\mu\text{m/s}$	0.069 54	0.067 38	0.067 38
Pressure distortion coefficient in $\times 10^{-6} \text{MPa}^{-1}$	0.390	0.391	0.388

Table 1. Comparisons of finite element method's (FEM) results for CC mode obtained with the 3 different fluid models, model 1 (parallel planes) model 2 (annular gap with zero velocity at the piston side) and model 3 (annular gap with piston fall velocity at the piston side), at pressure 900 MPa and a jacket pressure equal to  $0.1 p$

#### 4. Results

The calculations of pressure distortion coefficients and piston fall rate for the piston-cylinder unit DH 7594 were performed by FEM at pressure  $p$  in the range of 50 to 1 000 MPa in the free deformation (FD) and controlled-clearance (CC) mode. For the CC mode, the jacket pressure ( $p_j$ ) applied is equal to  $0.1p$ .

The gap profiles between the 3 calculation models under 400 MPa for FD mode and 900 MPa for CC mode are very similar to each other. The maximum difference between the calculation models of the piston and cylinder radius along the engagement length is 7 nm at the pressure 900 MPa. The maximum difference of the pressure distributions along the gap is 4 MPa at the measurement pressure 900 MPa. The maximum difference of  $A_p$  between the annular gap and parallel planes models is equal to  $4 \times 10^{-5} \text{mm}^2$  or equivalent to  $8.61 \times 10^{-7}$  and the maximum difference of  $\lambda$  is equal to  $0.002 \times 10^{-6} \text{MPa}^{-1}$  with  $p$  equal to 900 MPa (Table 1).

The maximum difference of  $v_f$  is  $-0.009 5 \mu\text{m/s}$  with  $p$  equal to 400 MPa. The displacements and  $A_0$  are similar for the three models at pressure up to 1 000 MPa. The maximum differences in  $\lambda$  and  $v_f$  between calculation and experimental methods for FD mode are  $0.012 \times 10^{-6} \text{MPa}^{-1}$  and  $-0.118 \text{mm} \cdot \text{min}^{-1}$ , respectively, at pressure 400 MPa. For CC mode, they are  $-0.045 \times 10^{-6} \text{MPa}^{-1}$  at pressure 900 MPa and  $-0.042 \text{mm} \cdot \text{min}^{-1}$  at pressure 400 MPa (Table 2).

Table 2. Pressure distortion coefficients ( $\lambda$ ) and piston fall rates ( $v_f$ ) calculated with model 1 (parallel planes) and their deviations from the experimental data obtained by PTB ( $\lambda = 0.816 \times 10^{-6} \text{MPa}^{-1}$  and  $v_f = 0.412 \text{mm} \cdot \text{min}^{-1}$  for applied pressure 400 MPa in FD mode and  $\lambda = 0.435 \times 10^{-6} \text{MPa}^{-1}$  and  $v_f = 0.108 \text{mm} \cdot \text{min}^{-1}$  for applied pressure 900 MPa in CC mode)

$p$ in MPa	$\lambda$ in $10^{-6} \text{MPa}^{-1}$	$\lambda - \lambda_{exp}$ in $10^{-6} \text{MPa}^{-1}$	$v_f$ in $\text{mm} \cdot \text{min}^{-1}$	$v_f - v_{f,exp}$ in $\text{mm} \cdot \text{min}^{-1}$
Free deformation (FD) mode				
400	0.828	0.012	0.294	-0.118
Controlled clearance (CC) mode				
400	0.425	-0.010	0.149	-0.042
900	0.390	-0.045	0.070	-0.038

#### 5. Conclusion

The pressure distortion coefficient and particularly the piston fall rate of PCU DH 7594 used for the pressure balance up to 1 GPa were determined by applying the new models of fluid flow. The experimental values given by PTB were compared with those calculated by the finite element methods. The two calculations of the pressure distortion coefficient in the Cartesian and cylindrical geometry models, performed with and without taking into account the fluid velocity at the falling piston surface, are in good agreement. They are also in good agreement with the experimental data under the uncertainty claimed for the PTB experimentation. The piston fall rates calculated for the parallel planes and annular gap models are also in good agreement, but there is still a large difference with the experimental data (Figure 2). It was shown that the fluid flow in annular gap model and the boundary condition of the fluid velocity at the piston surface have no significant effect on the pressure distortion coefficient, and the piston fall rate provided by calculation. As for the axial symmetry of the problem, it is unlikely that differences between the piston fall rate calculation and experimental results will find an answer in the two dimensional fluid flow or in the effect of the piston rotation. On another hand this difference can be explained by the dimensional properties of the cylinder at the gap inlet and outlet. To understand this difference, the authors will focus on the fluid flow in two dimensions and also on the geometry of

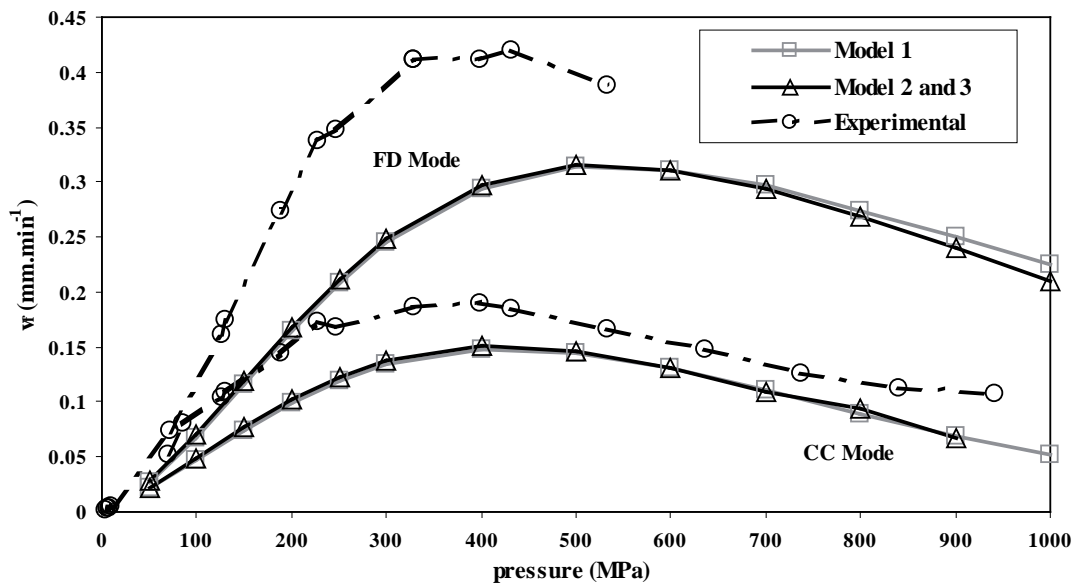


Figure 2. Piston fall rate ( $v_f$ ) in the free deformation (FD) and controlled-clearance (CC) modes measured experimentally and calculated in different models, model 1 (parallel planes), model 2 (annular gap with zero velocity at the piston side) and model 3 (annular gap with piston fall velocity at the piston side)

the piston and cylinder. This new method will be applied to LNE's PCU for the pressure balance up to 1 GPa.

## References

- [1] W. Sabuga, G. Molinar, G. Buonanno, T. Esward, J. C. Legras and L. Yagmur, Finite element method used for calculation of the distortion coefficient and associated uncertainty of a PTB 1 GPa pressure balance - EUROMET project 463, *Metrologia*, 2006, volume 43, pp. 311-325
- [2] B. Yavorski and A. Detlaf, *Aide-mémoire de physique* (Moscou, 1975)
- [3] R.S. Dadson, S.L. Lewis, G.N. Peggs, *The Pressure Balance—Theory and Practice* (London: HMSO, 1982)
- [4] G. Christophe and J. F. Remacle, *Gmsh: a three-dimensional finite element mesh generator with built-in pre- and post-processing facilities Version 2.5.0*, 2010
- [5] ASME Report, *Viscosity and density of over 40 lubricating fluids of known composition at pressures to 150,000 psi and temperatures to 425° F*, American Society of Mechanical Engineers (New York, USA, 1953)
- [6] P. Vergne, *New high-pressure viscosity measurements on di(2-ethylhexyl) sebacate and comparisons with previous data*, *High Temperatures-High Pressures*, 1990, volume 22, pp. 613-621
- [7] G. Molinar, *EUROMET Project Number 463, Density and dynamic viscosity versus pressure, up to 1 GPa, for the di(2) ethyl-hexyl-sebacate fluide at 20°C*, internal report R486 Istituto di Metrologia G. Colonnetti, 1998 (Torino Italia, December 1998)

# Multiple cross-float system for calibrating pressure balances

Tokihiko Kobata<sup>1</sup>

## Abstract

Multiple cross-float system for calibrating pressure balances has been developed. The system mainly consists of multiple pressure balances, multiple air-operated constant volume valves, a pressure controller and a precise pressure transducer. For comparing the pressures generated by the pressure balances accurately, the differential pressures between them are measured by using a comparator method. In the system, one pressure balance can be used as a reference and other test pressure balances are compared with the reference one after another by switching the valves. From the differential pressures obtained, the pressure generated by each test pressure balance is calibrated. The system can calibrate the unknown pressures generated by multiple pressure balances nearly simultaneously. In this article, the system configuration and the measuring principle are described. The typical measurement result using the system is also shown.

## 1. Introduction

A pressure balance is able to generate and measure a stable pressure and is often used as a pressure standard. A cross-float measurement using two pressure balances is widely used to calibrate a pressure balance and evaluate its characteristics [1, 2]. The unknown pressure generated by a test pressure balance can be calibrated by performing a cross-float measurement against a reference pressure balance whose pressure generated is already known. In a cross-float measurement, small fractional masses on either pressure balance are usually adjusted until the equilibrium pressure for two pressure balances is obtained. To determine whether the pressures generated by two pressure balances are equal or not, several methods have been used. A prime example is the method of observing the fall-rate, which is obtained from observing the floating position of the piston of the pressure balance with time, and the other example is the method of observing the differential pressure using a sensitive differential pressure sensor. The comparator method using a precise pressure trans-

ducer and two air-operated constant volume valves (CVVs) is also used to determine the equilibrium state between two pressure balances accurately, in which the transducer is connected first to the reference and then to the test pressure balance [3]. In this article, a multiple cross-float system for calibrating more than two pressure balances is proposed.

## 2. Multiple cross-float system using comparator method

Figure 1 shows the schematic drawing of the setup for the simple cross-float measurement using the comparator method [3]. The advantages of the method are summarized as follows: (a) by the usage of two air-operated CVVs, the pressure generated by the pressure balance can be connected and disconnected quickly to the transducer without volume change in the hydraulic circuit or heat transfer from the operator, (b) by managing the time intervals between measurements equally, the method proposed can compensate for the effect of the drift component in the successive values measured by the transducer used and (c) the short time stability of the pressure generated by each pressure balance used can be evaluated quantitatively. It was revealed that the equilibrium state could be determined accurately using the method, and the differences between this method and the conventional fall-rate method were sufficiently small [3].

Figure 2 shows the conceptual diagram of the setup for a multiple cross-float measurement using the comparator method. There are multiple pressure balances, multiple air-operated CVVs, a pressure controller and a precise pressure transducer, which are connected using pressure tubing in a circuit. Each pressure balance has a temperature sensor for measuring the temperature of piston-cylinder assembly and a position sensor for measuring the piston floating position. The function of the CVVs used is the same as described above. The CVVs can be operated remotely by changing the air pressure supplied to them. The pressure controller is used to pressurize the system pressure in the circuit and to adjust the piston position of each pressure balance

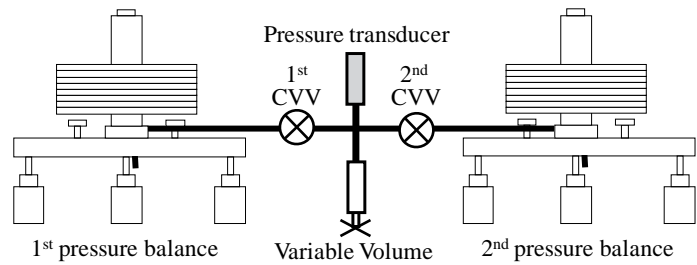
<sup>1</sup> Tokihiko Kobata, National Metrology Institute of Japan (NMIJ), National Institute of Advanced Industrial Science and Technology (AIST) AIST Tsukuba Central 3, 1-1-1 Umezono, Tsukuba, Ibaraki 305-8563, Japan  
Email of corresponding author: tokihiko.kobata@aist.go.jp

which can be operated remotely from a computer. The precise pressure transducer is used to measure the pressures generated by the pressure balances. A customized computer program written for this type of measurement is used to sample all the data which include the temperatures of the piston–cylinder assemblies, the piston floating positions, the measured pressure, and environmental data such as ambient temperature, relative humidity and atmospheric pressure.

### 3. Measurement principle

Before pressurizing the system, all the CVVs are opened. To achieve a target pressure, the approximate large mass, which is calculated using the nominal area of each piston–cylinder assembly, is applied on each pressure balance. Then, the entire system including all the pressure balances is pressurized using the pressure controller. After that, all the CVVs except 1st CVV are closed. In this state, the pressure generated by 1st pressure balance is applied to the transducer. The piston position of 1st pressure balance is adjusted by the pressure controller to the target range which is usually near the centre of the stroke, and the piston of 1st pressure balance is rotated by a motor. Thereafter, 1st CVV is closed. With this, the setting for 1st pressure balance is completed. Next, 2nd CVV is opened and the setting for 2nd pressure balance is performed and so on. After completing the setting for  $n$ -th pressure balance and waiting until the adiabatic heat had dissipated, the data collection program is started.

Table 1 shows the sequence of procedures for the valve operation and data sampling with time. First after the program started ( $t = 0$ ), the floating piston position of 1st pressure balance is readjusted by using the pressure controller. It usually takes about 15 s. 30 s after starting, the program automatically starts sampling the pressure generated by 1st pressure balance using the transducer six times every 10 s. The measurements are completed in 1 min. The average value of the six values obtained from the measurement is calculated and is indicated as  $I_{1,1}$  at 90 s after starting ( $t = \Delta t$ ). At the same time, 1st CVV is closed and 2nd CVV is opened. The time needed for the switch is less than one second at maximum. In this state, the pressure generated by 2nd pressure balance is applied to the transducer. Then, the piston position of 2nd pressure balance is readjusted by using the pressure controller. 30 s after the valve switching, the program begins to sample the pressure generated by 2nd pressure balance using the same procedure described above and the average value,  $I_{2,1}$  is obtained at  $t = 2\Delta t$ . Thereafter, the pressure generated by



each pressure balance is sequentially measured by the transducer by switching the valves in the circuit as indicated in table 1. In this method,  $I_{k,j}$  shows the  $j$ -th average value measured from  $k$ -th pressure balance obtained at  $t = t_{k,j}$  where  $t_{k,j} = [n(j-1) + k]\Delta t$ . From the data set  $(t_{k,j}, I_{k,j})$ , the best fitting straight line for  $k$ -th pressure balance is estimated as follows:

$$I_{k,t} = \alpha_k t + \beta_k, \tag{1}$$

where  $\alpha_k$  and  $\beta_k$  are the coefficients calculated by the method of least squares. The deviation of  $j$ -th value for  $k$ -th pressure balance from the straight line,  $\delta I_{k,j}$  is calculated as follows:

$$\delta I_{k,j} = I_{k,j} - \frac{1}{n} \sum_{k=1}^n (\alpha_k t_{k,j} + \beta_k). \tag{2}$$

The average deviation for  $k$ -th pressure balance,  $\delta I_{k,a}$  is calculated by the following equation.

$$\delta I_{k,a} = \frac{1}{m} \sum_{j=1}^m \delta I_{k,j}. \tag{3}$$

The difference between  $I_{k1,a}$  and  $I_{k2,a}$ ,  $\Delta I_{k1,k2}$  is calculated as follows:

$$\Delta I_{k1,k2} = \delta I_{k1,a} - \delta I_{k2,a}. \tag{4}$$

The differential pressure between two pressure balances,  $\Delta P_{k1,k2}$  is calculated as follows:

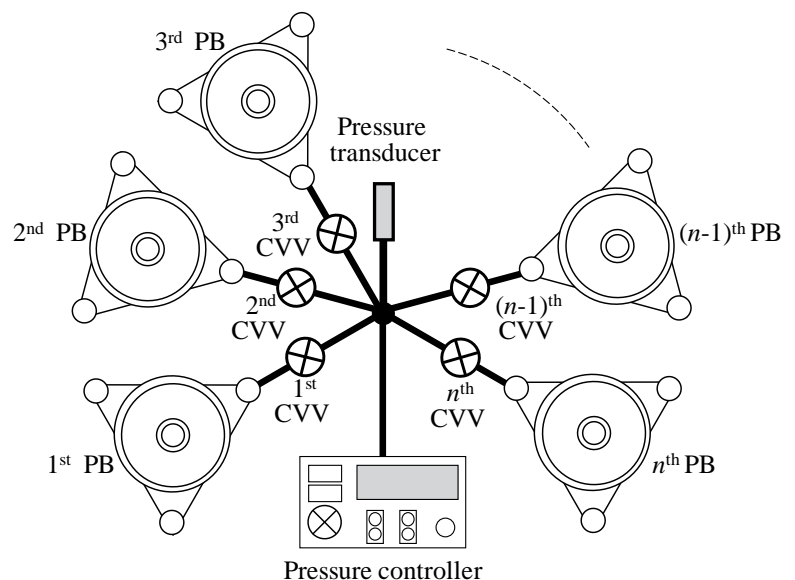


Figure 1 Schematic drawing of setup for cross-float measurement using comparator method. CVV: constant volume valve.

Figure 2 Conceptual diagram of multiple cross-float system for calibrating pressure balances. PB: pressure balance

	Interval	1 <sup>st</sup> CVV	2 <sup>nd</sup> CVV	...	(n-1) <sup>th</sup> CVV	n <sup>th</sup> CVV	I
Start	$\Delta t$	O	C	...	C	C	$I_{1\ 1}$
	$\Delta t$	C	O	...	C	C	$I_{2\ 1}$
	□	□	□	□	□	□	□
	$\Delta t$	C	C	...	O	C	$I_{(n-1)\ 1}$
	$\Delta t$	C	C	...	C	O	$I_{n\ 1}$
	$\Delta t$	O	C	...	C	C	$I_{1\ 2}$
	$\Delta t$	C	O	...	C	C	$I_{2\ 2}$
	□	□	□	□	□	□	□
	$\Delta t$	C	C	...	O	C	$I_{(n-1)\ 2}$
	$\Delta t$	C	C	...	C	O	$I_{n\ 2}$
	□	□	□	□	□	□	□
	$\Delta t$	O	C	...	C	C	$I_{1\ m}$
$\Delta t$	C	O	...	C	C	$I_{2\ m}$	
□	□	□	□	□	□	□	
$\Delta t$	C	C	...	O	C	$I_{(n-1)\ m}$	
End	$\Delta t$	C	C	...	C	O	$I_{n\ m}$

Table 1 Procedures for switching CVVs and sampling with time. O: open, C: close,  $I_{k,j}$ : j-th average value measured from k-th pressure balance.

$$\Delta P_{k_1-k_2} = f \Delta I_{k_1-k_2} \quad (5)$$

where  $f$  is the scaling factor of the transducer used and is defined by

$$P = fI + P_0 \quad (6)$$

where  $P$  is the actual pressure applied,  $I$  is the value indicated by the pressure transducer and  $P_0$  is the pressure expected at  $I = 0$ .

In the system, the multiple pressure balances can be compared one another. For example, in case that one pressure balance is used as a reference, other test pressure balances are compared with the reference one after another by switching the valves. If the pressure generated by 1<sup>st</sup> pressure balance at its reference level,  $P_r$ , is known, the pressure generated by  $k$ -th pressure balance at the reference level,  $P_k$ , is obtained as follows:

$$P_k = P_1 + \Delta P_{k-1} + (\rho_f - \rho_a)g\Delta h_{k-1} \quad (7)$$

where  $(\rho_f - \rho_a)g\Delta h_{k-1}$  is the head correction, with  $\rho_f$  the density of the working fluid,  $\rho_a$  the air density,  $g$  the local acceleration due to gravity and  $\Delta h_{k-1} = h_1 - h_k$  the vertical distance between the reference levels of 1<sup>st</sup> pressure balance and  $k$ -th pressure balance.  $\Delta P_{k-1}$  is the pressure difference between  $k$ -th pressure balance and 1<sup>st</sup> pressure balance and is obtained using equation (5).

### 4. Experiment

The multiple cross-float system was realized for three pressure balances ( $n = 3$ ). The number of iterations in the measurement described in table 1 was set to three ( $m = 3$ ). The pressure range of the three piston-cylinder assemblies was up to 100 MPa. To measure the pressures generated, an absolute pressure transducer, which uses two quartz crystal resonators, was used [4]. The measuring range of the transducer used was about 100 MPa and the resolution of the transducer could be selected by changing the integration time of data recording. In this experiment, the integration time was set to 3.425 s for one pressure measurement. The resolution in pressure measurement with this integration time was investigated from the data measured by the transducer and was found to be about  $5 \times 10^{-8}$  of the full scale (5 Pa). For evaluating the scaling factor,  $f$ , of the transducer, known reference pressure was applied to the transducer beforehand in the pressure range from 10 MPa to 100 MPa in steps of 10 MPa. Scaling factor  $f$  was calculated using a regression statistics program by fitting equation (6) to the data of the relationship between the applied pressure and the indication of the transducer. From the evaluation, the value of  $f$  was set to unity MPa/(unit of transducer) and its standard uncertainty,  $u(f)$ , was estimated at  $5 \times 10^{-4}$  MPa/(unit of transducer) in the pressure range measured. If the relative difference  $f\Delta I/P$  is less than  $10^{-4}$  with the relative uncertainty  $u(f)/f = 5 \times 10^{-4}$ , the uncertainty component  $u(f)\Delta I/P$  would be less than  $5 \times 10^{-8}$ .

Figure 3 shows an example of the indications measured by the transducer during the measurement performed according to the method shown in table 1. In figure 3(a), the vertical space between horizontal lines relatively corresponds to  $2.0 \times 10^{-6}$  of the nominal value. The scatter of the indications can be observed from the plotted points in the figure. From the measurement, nine average values measured from three pressure balances,  $I_{k,j}$  ( $k = 1, 2, 3, j = 1, 2, 3$ ), were obtained. In this example, the transducer shows a relatively large drift component with time compared with the stability of the pressure balance used. In the figure, three dotted straight lines are calculated by the method of least-squares for three pressure balances, respectively. In this example, the slope of these straight lines is almost the same. A solid straight line is the average of the three dotted lines. As shown in the figure, the drift component in the data can be evaluated quantitatively from the slope of the straight line. When the rate of the drift is almost constant during short periods, the effect of the drift component can be greatly mitigated by using the linear least-squares method described above. Figure

3(b) shows the deviations of the indications from the averaged best fitting straight line. The differential indication between pressure balances,  $\Delta I$ , is calculated by equation (4). The differential pressure,  $\Delta P$ , is obtained using equation (5) as follows:  $\Delta P_{2,1} = 0.14$  kPa,  $\Delta P_{3,1} = 0.95$  kPa. If the pressure generated by 1<sup>st</sup> pressure balance,  $P_1$ , is known, the pressures generated by 2<sup>nd</sup> and 3<sup>rd</sup> pressure balances,  $P_2$  and  $P_3$ , are calculated using equation (7).

## 5. Summary

Multiple cross-float system for calibrating multiple pressure balances is proposed. The system mainly consists of multiple pressure balances, multiple air-operated constant volume valves, a pressure controller and a precise pressure transducer. For comparing the pressures generated by multiple pressure balances accurately, the differential pressures between them are evaluated by using the comparator method. From the differential pressures obtained, the unknown pressure generated by each test pressure balance is calibrated. The system can calibrate the pressures generated by multiple pressure balances nearly simultaneously. In this article, the system configuration and the measuring principle are described and the typical measurement result using the system is presented.

## References

- [1] OIML regulation R110, edition 1994(E), Pressure Balances, (Paris, OIML: Organisation International de Metrologie Legale) (1994)
- [2] Kobata, T.: Improved methods for comparing gas and hydraulic pressure balances, Metrologia 46 (2009) pp.591-598
- [3] Kobata, T.; Olson, D. A.: Accurate determination of equilibrium state between two pressure balances using a pressure transducer, Metrologia 42 (2005) pp.S231-S234
- [4] Paroscientific, Inc. Document no. 8819-001 Revision C (2002).

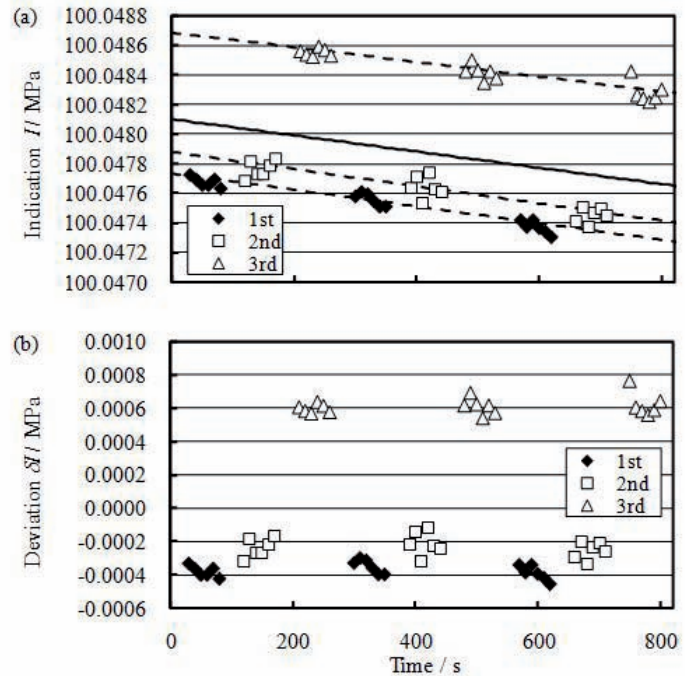


Figure 3 (a) Example of indications of the transducer during measurement, (b) deviations of indications from averaged best fitting straight line.

### Miniaturinterferometer mit Planspiegelreflektor, Serie SP

- Präzisions-Längenmesssystem, ein- oder mehrachsrig
- Messbereich:  $\leq 2$  m, Auflösung: bis 0,1 nm
- Lichtwellenleiterkopplung des Sensorkopfes



**SIOS Meßtechnik GmbH**  
 Am Vogelherd 46  
 D-98693 Ilmenau  
 Tel.: 03677/6447-0  
 E-mail: info@sios.de  
 www.sios.de



# Stability of pressure generated by controlled-clearance pressure balance up to 1 GPa

Hiroaki Kajikawa, Kazunori Ide, Tokihiko Kobata<sup>1</sup>

## Abstract

The large pressure balance equipped with a controlled-clearance piston-cylinder (CCPC) and weights of totally 1100 kg has been developed in NMIJ with the aim of improving the hydraulic pressure standard up to 1 GPa. Among several CCPCs, a newly-developed 1 MPa/kg CCPC is evaluated in terms of the stability of generated pressure and the piston fall-rate at pressures up to 1 GPa. The stability of generated pressure is similar to or better than that by top-level commercial pressure balances. The piston fall-rate is less than 0.15 mm/min under the ordinary cross-floating condition. It is confirmed that the 1 MPa/kg CCPC can generate the pressure stably during characterization experiments and calibrations.

## 1. Controlled-clearance pressure balance in NMIJ

Large pressure balances that can precisely generate pressure up to 1 GPa with the use of large weights have been realized in some national metrology institutes. Among them, for example, technical information is available from the reports [1-3] and their references. Summary of the developments using piston gauge technique for pressures up to 1 GPa or more is also found in [4].

National Metrology Institute of Japan (NMIJ) has developed a controlled-clearance pressure balance in cooperation with Nagano Keiki Co., Ltd. [5, 6]. Figure 1 shows an external appearance of the pressure balance.

The weight-loading unit is designed to handle a weight-set of totally 1100 kg. The weight-set consists of disk weights of 95 kg and 19 kg, and cylindrical weights of 2.5 kg and 0.5 kg. All weights are set in a container to keep them clean and to avoid the effects of environmental perturbations during operations. Each weight is individually supported by pneumatic actuators and lifted up or down independently. The masses of the weights are precisely and efficiently calibrated *in situ* without being brought out from the container [5]. During *in situ* mass



Figure 1  
External appearance of controlled-clearance pressure balance in NMIJ

calibration, a digital mass comparator is temporarily installed on the upper table of the pressure balance where CCPC is usually placed.

There are several CCPCs for four different pressure ranges: 0.1 MPa/kg (for pressures up to 100 MPa), 0.2 MPa/kg (200 MPa), 0.5 MPa/kg (500 MPa), and 1 MPa/kg (1 GPa). Both the piston and cylinder are made from tungsten carbide. The cylinder is encased in a housing made from steel. A sleeve is placed between the cylinder and the housing. The area of the outer surface of the cylinder covered with the sleeve is subjected to the jacket pressure  $p_j$  that comes through the side inlet of the housing. Although the housing is designed to withstand a  $p_j$  of 500 MPa,  $p_j$  is carefully applied according to the characteristics of each CCPC to avoid excess ap-

<sup>1</sup> Hiroaki Kajikawa, Kazunori Ide, Tokihiko Kobata, National Metrology Institute of Japan (NMIJ), AIST AIST Tsukuba Central 3, 1-1-1 Umezono, Tsukuba, Ibaraki 305-8563, Japan kajikawa.hiroaki@aist.go.jp

plication. The length of the sleeve is originally 35 mm against the cylinder length of 55 mm. Changing the sleeve length can alter the deformational characteristics in response to applied  $p_j$  [7]. To precisely estimate the pressure dependence of the effective area, characterization experiments based on the Heydemann-Welch model [8] have been performed for several CCPCs. Procedures and results of these experiments for a 0.2 MPa/kg CCPC and a 0.5 MPa/kg CCPC are described in [6].

In this paper, the stability of generated pressure and the piston fall-rate of a 1 MPa/kg CCPC are evaluated to confirm that the generated pressure up to 1 GPa is maintained stable for sufficient time for characterization experiments and calibrations.

## 2. Evaluation of pressure generated by 1 MPa/kg CCPC

### 2.1. Stability of generated pressure

To evaluate the stability of pressure generated by the 1 MPa/kg CCPC, the fluctuation of the pressure is calculated during the cross-float measurement, in which the 1 MPa/kg CCPC is compared with a set of free-deformational piston-cylinder (FDPC) and precise pressure multiplier (MUL) at pressures up to 1 GPa. Figure 2 shows the schematic drawing of the comparison system. A precise pressure transducer ( $PT_s$ ), a valuable volume (VV) and two shutoff valves (SV1 and SV2) are placed between CCPC and MUL. The generated pressure is measured by the same pressure transducer in series by switching the connection of the pressure line to the transducer. Before the measurement, weights loaded on CCPC or FDPC are adjusted so that the pressure applied to  $PT_s$  is almost similar.

The  $PT_s$  indications during the comparison between the 1 MPa/kg CCPC and a set of FDPC and MUL at 1000 MPa are exemplified in figure 3(a).  $p_j$  applied to CCPC is 25 % of the system pressure  $p_s$ . One measurement includes five data sets  $A_1$ - $B_1$ - $A_2$ - $B_2$ - $A_3$ ;  $A_k$  ( $k = 1,2,3$ ) denotes the pressure generated by CCPC and  $B_l$  ( $l = 1,2$ ) denotes that by a set of FDPC and MUL. Each data set consists of six  $PT_s$  indications measured at every 12 seconds. The time interval between the groups of data is 3 minutes, which includes the time for valve-switching operations and for pressure stabilization. The fluctuation of the data appears to be similar to each other.

The fluctuation of the data includes the effect of drift and resolution intrinsic to  $PT_s$  as well as the stability of pressure generated by CCPC or MUL. The drift of  $PT_s$  is observed during the comparisons at all pressures; in figure 3(a),  $PT_s$  indications slightly decrease with time. To com-

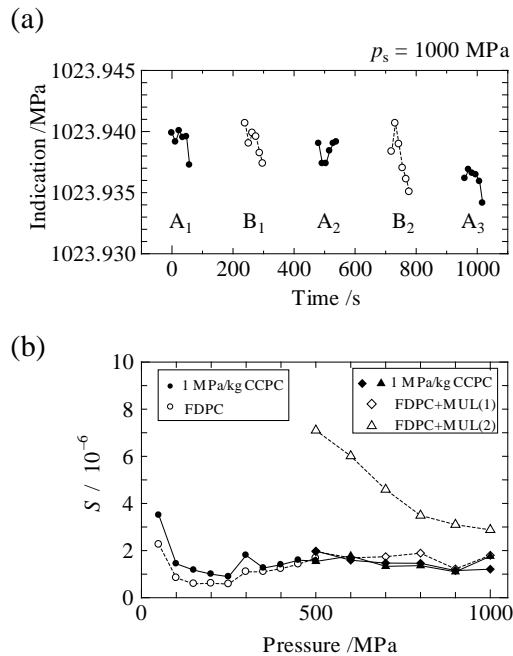
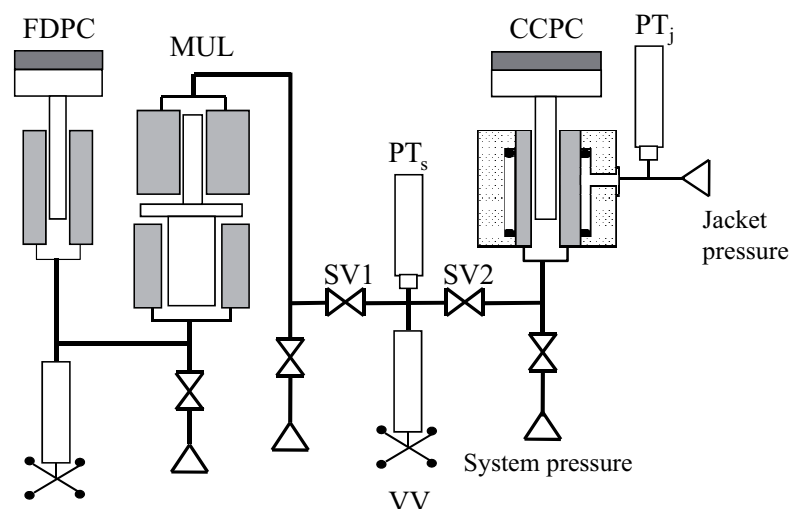


Figure 3 (a)  $PT_s$  indications during the cross-float measurement between the CCPC (solid circles) and a set of FDPC and MUL (open circles). (b) The averaged value of the relative standard deviation of  $PT_s$  indications,  $S$ , during cross-float measurement.

pensate for the effect of the drift, the linear component in the time change of  $PT_s$  indications is subtracted from the original data. Then, the standard deviation of the 6 data after drift compensation is calculated. The averaged value of the relative standard deviation during each measurement is treated as the representative value for the stability of pressure generated by either pressure balances.

The representative value of the pressure stability  $S$  was calculated at all pressures. CCPC is used under the condition of  $p_j/p_s = 0.25$ . Three pressure transducers whose applicable pressure

Figure 2 Schematic diagram of comparison system. CCPC: controlled-clearance piston-cylinder, FDPC: free-deformational piston-cylinder, MUL: precise pressure multiplier,  $PT_s$ : pressure transducer for  $p_s$ , VV: variable volume, SV: shutoff valve,  $PT_j$ : pressure transducer for  $p_j$ .





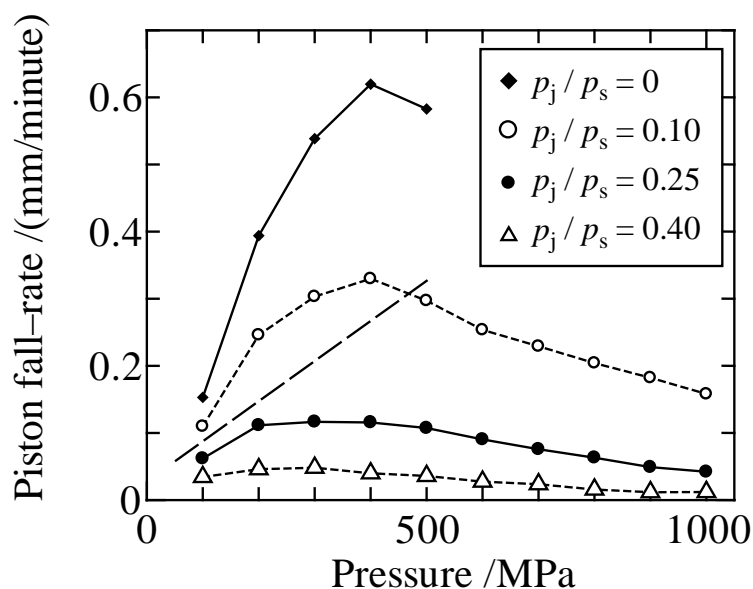


Figure 4  
Piston fall-rate of 1 MPa/kg CCPC with  $p_j/p_s = 0$  (diamonds), 0.10 (open circles), 0.25 (solid circles), and 0.40 (triangles). Dashed line denotes the typical piston fall-rate for FDPC.

ranges are 280 MPa, 500 MPa and 1000 MPa are used according to the pressure range. Pressure dependence of  $S$  during cross-float measurement is shown in figure 3(b). For pressures up to 500 MPa, CCPC is compared with a FDPC.  $S$  of CCPC is slightly larger than that of FDPC, but only less than  $2 \times 10^{-6}$  except for 50 MPa, at which the resolution of  $PT_s$  may affect the result. For pressures up to 1000 MPa, CCPC is compared with a set of FDPC and MUL. The results using different MULs, denoted by MUL(1) and MUL(2), are plotted in the figure.  $S$  of CCPC is almost similar to that of MUL(1), and much smaller than that of MUL(2). In both cases, the values of  $S$  of CCPC remain less than  $2 \times 10^{-6}$ . From these results, the stability of the pressure generated by the 1 MPa/kg CCPC is found to be comparable to or better than that of commercial FDPC and a set of FDPC and MUL.

## 2.2. Piston fall-rate

Piston fall-rate of the 1 MPa/kg CCPC with various  $p_j$  was measured at  $p_s$  up to 1 GPa. Figure 4 shows the piston fall-rate measured with  $p_j/p_s = 0, 0.10, 0.25$ , and  $0.40$ . A dashed line shows the typical piston fall-rate for FDPC used in NMIJ. Under the same  $p_j/p_s$  condition, piston fall-rate does not show monotonous increase with increasing  $p_s$ , but reaches a maximum at a few hundred MPa, and then slowly decreases with increasing  $p_s$ . Under the condition of  $p_j/p_s = 0.25$ , the piston fall-rate is less than 0.15 mm/min. It has also been confirmed that the 1 MPa/kg CCPC does not show any detectable change in the effective area with the piston floating position when operated at  $2.5 \text{ mm} \pm 1.0 \text{ mm}$  above its lowest position. Thus, the piston can generate

pressure continuously at appropriate floating position for more than 10 minutes, which is sufficient for data acquisition in characterization experiments and calibrations.

## 3. Summary

The large pressure balance equipped with controlled-clearance piston-cylinder (CCPC) and weights of totally 1100 kg has been developed in NMIJ. This paper describes the stability of generated pressure and the piston fall-rate for a newly-developed 1 MPa/kg CCPC. The stability of generated pressure is similar to or better than that by a FDPC and a set of FDPC and MUL. The piston fall-rate is less than 0.15 mm/min with  $p_j/p_s = 0.25$ . The pressure generated by the 1 MPa/kg CCPC is found to be maintained stable during characterization experiments and calibrations.

## Reference

- [1] Jager, J.; Sabuga, W.: Establishment of a primary standard for the 1 GPa range of pressure measurement, Proc. of the 2nd Intern. Pressure Metrology Workshop & Intern. Conf. on high pressure science and technology (2001) pp. 15-20
- [2] Legras, J. C.; Huot, A.; Delajoud, P.: La référence nationale de pression du BNM dans le domaine de 5 à 200 MPa, Bull. d'Information du BNM 48 (1982) pp. 9-33
- [3] Yadav, S.; Prakash, O.; Gupta, V. K.; Bandyopadhyay, A. K.: The effect of pressure-transmitting fluids in the characterization of a controlled clearance piston gauge up to 1 GPa, Metrologia 44 (2007) pp. 222-233
- [4] Molinar, G. F.: An Old Instrument in the New Technological Scenery: The Piston Gauge in Liquid Media up to 1 GPa, Metrologia 30 (1993/94) pp. 615-623
- [5] Kajikawa, H.; Kobata, T.; Ooiwa, A.: Feature of a New Controlled-clearance Pressure Balance and *In Situ* Mass Calibration of Weights, Trans. of the Society of Instrument and Control Engineers 44 (2008), pp. 219-226
- [6] Kajikawa, H.; Ide, K.; Kobata, T.: Precise determination of the pressure distortion coefficient of new controlled-clearance piston-cylinders based on the Heydemann-Welch model, Rev. Sci. Instrum. 80 (2009), 095101
- [7] Kajikawa, H.; Ide, K.; Kobata, T.: Method for altering deformational characteristics of controlled-clearance piston-cylinders, Measurement 44 (2011) pp. 359-364
- [8] Heydemann, P. L. M.; Welch, B. E.: Experimental Thermodynamics Vol. II (London: Butterworths, 1975) pp. 147-202

# Linking Hydraulic and Pneumatic Pressure Scales Using a Common Piston Gauge

Neville Owen<sup>1</sup>

NMI Australia realises a pneumatic pressure scale using a mercury manometer and a hydraulic pressure scale using a 490 mm<sup>2</sup> piston gauge (DHI01). To compare these two scales we have a very low clearance 100 mm<sup>2</sup> stainless steel piston gauge (R123) which can be operated using Di-2-Ethylhexyl Sebacate (DHS) or nitrogen as the pressure transmitting fluid. To allow effective cross floating between piston gauges with large fall rate differences required improved fall rate systems which will be briefly discussed. The cross floats conducted have provided valuable information when implementing DHI01 as a primary standard by confirming correct accounting for all forces on the piston gauge and have allowed linking these two pressure scales with greater confidence. This work has also provided a much better estimate of the real distortion coefficient operating on the pneumatic range piston gauges.

**Key words:** pressure scale; calibration; crossfloat method

## Introduction

The purpose of this work was threefold.

- i) Propagate a primary distortion coefficient into our pneumatic pressure scale.
- ii) Confirm correct accounting of forces when implementing a primary piston gauge.
- iii) Establish a robust link between our pneumatic and hydraulic pressure scales.

NMI Australia (NMI) maintains two primary realised pressure standards. A mercury interferometer manometer which operates over the absolute pressure range 1 kPa to 120 kPa [1]. A 490 mm<sup>2</sup> piston gauge (DHI01) which operates over the gauge pressure range 1.2 MPa to 10 MPa, which has been measured by our Dimensional group and subject to Finite Element Analysis (FEA) modelling [2,3] for effective area and distortion coefficient. The mercury manometer is used to define our pneumatic pressure scale and is always used in absolute pressure mode. DHI01 is used to define our hydraulic pressure scale and is always used with Di-2-Ethylhexyl Sebacate (DHS). To facilitate the comparison of these two pressure scales defined from the two primary standards, a low clearance piston gauge

(R123) which can operate using either DHS or nitrogen as the pressure transmitting fluid has been used. R123 has a nominal area of 100 mm<sup>2</sup> and both the piston and cylinder are tool steel. This required cross floats between DHI01 with R123 operating alternately on DHS or nitrogen via an oil-gas interface. This was followed by cross floats to the pneumatic pressure scale piston-cylinder set which include Ruska 2465 TL (175 kPa) and C (700 kPa) series and Ruska 2468 G (7000 kPa) series piston gauges. The TL series piston gauge was directly calibrated against the NMI interferometer manometer operating in absolute mode.

All uncertainties noted in this report are expressed as standard uncertainties ( $k = 1$ ) unless otherwise noted and are calculated in accordance with the ISO Guide [4].

## 1. Balance Point Method

The method used to detect the balance point is described by Sutton and Fitzgerald [5]. This method has been adapted to include electronic height measurement of both pistons so that two estimates of interpolated trim mass can be found. We typically achieved a balance sensitivity of  $\sim 0.3$  in  $10^6$ . This method has demonstrated similar sensitivity across the range down to 1.2 MPa. When using R123 on nitrogen, sensitivity between  $1$  in  $10^6$  and  $2$  in  $10^6$  was more common due to higher fall rates

## 2. Pneumatic Pressure Scale Distortion Coefficient

To establish a pneumatic pressure scale up to 7 MPa it is necessary to determine a reliable distortion coefficient for a piston gauge used in this range. A value can be calculated using elastic theory [6] section 5.2 but it is difficult to confidently obtain an uncertainty from that method. Alternately a calibration can be conducted based on a traceable reference distortion coefficient. Calibration of a Ruska G series (7000 kPa) piston gauge using a Ruska C series (700 kPa) piston gauge only provides an overlap of 10% of the G series piston gauge range. This does not cover enough range to provide a satisfactory estimate

<sup>1</sup> Neville Owen, National Measurement Institute, Bertie Street, Port Melbourne, Australia 3207, Neville.Owen@measurement.gov.au

of the distortion coefficient of the G series piston gauge, see Table 1.

A better method is to use a piston gauge which has a known distortion coefficient over the broadest pressure range possible. The distortion coefficient for R123 was obtained by calibration against DHI01 establishing traceability from a primary source. A set of area  $A_e$  versus pressure  $P$  data was then obtained for a cross float between the Ruska G series piston gauge and the nitrogen operation mode of R123 over the range 0.8 MPa to 7 MPa. A least squares evaluation of this data using equation (1) to find the distortion coefficient  $\lambda$  of the G series piston gauge (effective area  $A_{0,20}$  was determined but not used) provided a standard uncertainty of fitted data of  $u(A_{0,20})/A_{0,20}$  of  $2.2 \cdot 10^{-6}$ . This resulted in a much more reliable estimate than from the C series traceable path as shown in Table 1.

$$A_e = A_{0,20}(1 + \lambda P) \quad (1)$$

### 3. Accounting of Forces on DHI01

When all forces are not fully evaluate for a piston gauge, unaccounted for residual forces will result in a non linear area versus pressure characteristic [6] chapter 6. It is possible to analyse the cross float data using equation (2) where the mass load  $M$ , gravity  $g$ , density of air and weights  $\rho_a$  and  $\rho_m$ , surface tension load  $c\sigma$ , coefficient of thermal expansion  $\alpha$  and piston gauge temperature  $t$  are all known at each test pressure and effective area  $A_{0,20}$ , distortion coefficient  $\lambda$ , and effective mass  $m_e$  are the unknowns used to characterise a piston gauge [7].

$$P = \frac{M(1 - \frac{\rho_a}{\rho_m})g + c\sigma + m_e g}{A_{0,20}(1 + \lambda P)(1 + \alpha(t - 20))} \quad (2)$$

To test that we have accounted for all significant forces acting on DHI01, we are seeking to examine the hypothesis that the magnitude and sign of the effective mass of R123 evaluated in accordance with equation (2) should be zero or that any effective mass of R123, should be less than the uncertainty attributed to the effective mass.

When implementing DHI01 we determined the mass of the piston, force associated with surface tension and mass of oil that accumulates on the piston surfaces. For this cross float aimed at accounting forces we determined the mass of R123 and for the DHS case, force associated with

surface tension and mass of oil that accumulates on the piston surfaces.

We conducted an analysis of cross float data using equation (2) for the application of DHI01 as a reference piston gauge with R123 operating alternately using DHS then nitrogen (via an oil-gas interface) as the pressure transmitting fluid to find the values of  $m_e$  for R123 in both operating modes. We repeated the analysis in both operating modes while ignoring the estimated oil contribution on DHI01 to test if this oil contribution was a valid estimate.

From Table 2 we can see that the effective mass of R123 for DHS operation is well within the expanded uncertainty and becomes smaller when we ignore the estimated oil contribution on DHI01. Conversely the effective mass of R123 for nitrogen operation becomes larger when we ignore the estimated oil contribution on DHI01 and exceeds the expanded uncertainty by a larger amount.

We had expected the nitrogen operation mode to give a clearer indication of correct force accounting however operation through the oil-gas interface resulted in a greater test uncertainty as seen in the larger uncertainty for the effective mass for the nitrogen mode cross floats.

This test is somewhat inconclusive and demonstrates that a better oil-gas interface is required to improve confidence in correct force accounting for DHI01. What we can determine from this work is an upper limit to the estimated uncertainty for the application of DHI01.

The application of DHI01 to the calibration of R123 resulted in an expanded uncertainty ( $k = 2$ ) in effective mass of 50 mg and 78 mg respectively for the DHS and nitrogen operating modes. From these effective mass uncertainties we can calculate an uncertainty in pressure from the area of R123 as 4.9 Pa and 7.6 Pa respectively for the DHS and nitrogen operating modes. This suggests that until we can implement improvements in the oil-gas interface and our test methods, we are unlikely to be able to generate reference pressures using DHI01 with an expanded uncertainty better than 4.6 Pa for hydraulic application and 7.6 Pa for pneumatic application. This represents a minimum uncertainty to which we must add contributions from mass load, effective area, thermal effects etc. When used over the pressure range from 1.2 MPa to 10 MPa this is considered acceptable.

### 4. Linking Hydraulic and Pneumatic Pressure Scales.

To demonstrate the equivalence of the hydraulic and pneumatic pressure scales we operated R123 in a common manner using nitrogen. The flow chart of Figure 1 provides a visual representati-

Table 1. Distortion coefficient of G series (7000 kPa) pneumatic piston gauge

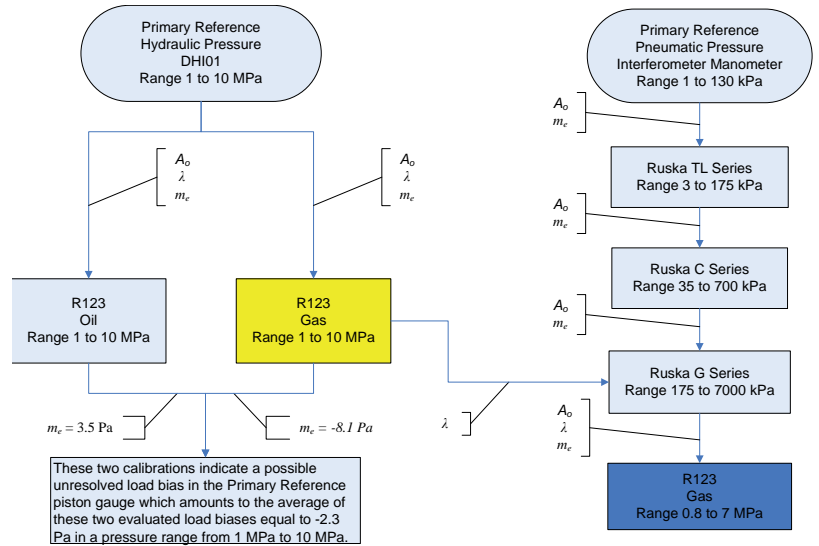
Traceable Source	Distortion Coefficient Pa <sup>-1</sup>	Standard Uncertainty Pa <sup>-1</sup>
C series piston gauge	$14 \times 10^{-12}$	$10 \times 10^{-12}$
R123 on nitrogen	$2.3 \times 10^{-12}$	$0.6 \times 10^{-12}$

Estimate of oil mass on DHI01 mg	R123 effective mass $m_e$ mg	
	DHS operation	Nitrogen operation
62	+34 ± 50	-80 ± 78
0	+21 ± 50	-92 ± 78

Table 2. Effective mass analysis of R123

on of the cross floats conducted to compare the two pressure scales. Figure 2 provides the area of R123 at each test pressure based on calibration using each of our two reference pressure scales. The error bars in Figure 2 represent the standard uncertainty estimated for each value. The data series "Hydraulic Scale" describes the calibration of R123 operating on nitrogen based on the hydraulic pressure scale derived from DHI01 over the nominal pressure range 1 MPa to 10 MPa via an oil-gas interface. The data series "Pneumatic Scale" describes the calibration of R123 operating on nitrogen based on the pneumatic scale derived from the interferometer manometer over the nominal pressure range 0.8 MPa to 7 MPa. These two calibrations differ across the pressure range on average by  $6.2 \times 10^{-6}$  and by no more than  $14 \times 10^{-6}$  at approximately 5 MPa. The normalised error,  $E_n$  varies from 0.01 to 0.61 giving acceptable results.

Figure 1. Cross Float Flow Chart.



5. Conclusion.

This project has resulted in an improved cross float method allowing us to successfully propagate a traceable distortion coefficient to our pneumatic pressure scale. We now estimate an expanded uncertainty in the pneumatic pressure scale from 700 kPa to 7000 kPa of;  $(0.0016\% + 0.0001\% \text{ MPa}^{-1})$  of reading.

By using a special purpose low clearance piston gauge we have tested our application of oil mass when estimating forces on our hydraulic scale primary piston gauge and established a best expected uncertainty for the application of DHI01.

We have compared our pneumatic and hydraulic pressure scales by calibrating a common piston gauge traceable to each pressure scale. The two scales differ on average by  $6.2 \times 10^{-6}$  and by not more than  $14 \times 10^{-6}$  across the common range from 1 MPa to 7 MPa.

6. Acknowledgments.

The author would like to thank W.Giardini (NMIA) for the original idea and design of the piston gauge R123, P.Cox (NMIA) for the dimensional measurement of piston gauges, J.Man (NMIA), G.Molinar (INRiM), G.Buonanno (UNICAS) for FEA modelling and K.Mapson (NMIA) for consultation and advice.

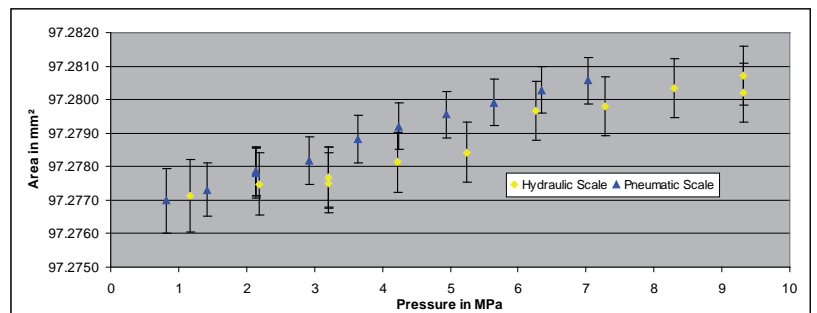


Figure 2. Area versus pressure of R123

7. References

- [1] E R Harrison, D.J. Hatt, D.B. Prowse, J. Wilburham. A New Interferometric Manometer, Metrologia, 1976, 12, P115-122.
- [2] J. Man, G. Molinar, G. Buonanno, G. Giovinco. Numerical characterisation of a 10 MPa Pressure Standard based on dimensional measurement data. Proceeding of the 7<sup>th</sup> biennial conference of the MSA.
- [3] JKL Man. Establishment of an Australian high pressure standard. Metrologia. 42 (2005) S169-S172.
- [4] ISO/IEC Guide 98-3 Uncertainty of Measurement - Part 3: Guide to the expression of uncertainty in measurement (GUM:1995).
- [5] Sutton, Fitzgerald, Giardini. A method of analysis for cross-floats between pressure balances. Metrologia. 42 (2005) S212-S215.
- [6] Dadson, Lewis, Peggs. The pressure balance: Theory and practice. London, HMSO, 1982.
- [7] Bignell N 1984 Modern Techniques in Metrology ed PL Hewitt (Singapore: World Science)

# Traceability of the pressure balance effective area at MIKES

Sari Saxholm<sup>1</sup>, Björn Hemming<sup>1</sup>, Martti Heinonen<sup>1</sup>, Pierre Otal<sup>2</sup>, Markku Rantanen<sup>1</sup>, Veli-Pekka Esala<sup>1</sup>, Antti Lassila<sup>1</sup>

## Introduction

Centre for Metrology and Accreditation (MIKES) is using pressure balances as national measurement standards for pressure. Pressure balances are used in ranges 0 to 500 MPa gauge pressure and 20 Pa to 1,8 MPa absolute pressure. MIKES has now started to determine effective areas by itself and aims to be a primary pressure laboratory.

Two of the piston cylinder units are selected to be the reference standards, one with a diameter 35 mm and the other with a diameter 50 mm. The effective area for the piston cylinder unit no. 6687 (35 mm) is determined from dimensional measurements made by MIKES and from cross-floating results made by LNE. The effective area for the piston cylinder unit no. 451 (50 mm) is determined from dimensional measurements made by MIKES and LNE and complemented with cross-floating made by LNE.

The effective areas for working standards are derived from the two dimensionally characterised piston cylinder units. There are totally 13 piston cylinder units as working standards. The cross-floating method [1] is performed for the units which overlap. The effective areas for higher pressures are calculated with help of the pressure distortion coefficients. One of the reference standards and four of the working standards has been traceable to LNE for almost 20 years. The data from this gives a strong support to the implementation of the in-house traceability and the new traceability chain of MIKES pressures.

## Determination of effective area

A measurement procedure has been developed for accurate dimensional characterisation of piston cylinder units at MIKES. Diameters are measured using 1-D measuring machine with laser interferometer as a scale. Method used is a gauge-block substitution, where a gauge block with similar dimension is used as low uncertainty reference against which the diameters of the piston and cylinder are compared by the 1-D measuring machine with the laser interferometer. For internal diameters, setting reference used

is a gauge block with short gauges wrung to both faces to form a cross.

The laser interferometer together with its temperature sensors has been calibrated against the national standards in the laser laboratory and temperature and pressure laboratories at MIKES [2]. The straightness measurements were made with a form measuring instrument on the cylinder. On the piston the straightness measurements were also made with a Fizeau interferometer. The Fizeau interferometer is intended for flatness measurements but it showed suitable also for straightness of the generatrix of the piston. Roundness measurements were done using a roundness measuring machine.

The zero pressure effective area ( $A_0$ ) of a piston-cylinder assembly is [3,4]:

$$A_0 = \pi r_0^2 \left[ \frac{1}{r_0} \frac{\int_0^l \frac{(r+R)}{(R-r)^3} dz}{\int_0^l \frac{1}{(R-r)^3} dz} - 1 \right] = \pi r_0^2 \delta A(r_0, r, R), \quad (1)$$

where:

$$\delta A(r_0, r, R) = \left[ \frac{1}{r_0} \frac{\int_0^l \frac{(r+R)}{(R-r)^3} dz}{\int_0^l \frac{1}{(R-r)^3} dz} - 1 \right]. \quad (2)$$

Here  $z$  is an axial coordinate with  $z = [0; l]$  corresponding to the piston cylinder unit effective engagement length,  $r_0$  is the piston radius at  $z = 0$ ,  $r$  and  $R$  are piston and cylinder radii along the engagement length.

The zero pressure effective area in eq. (1) is obtained from dimensional measurements. The measured profiles from the straightness measurements were fitted to the measured diameter data using least squares fitting. The results of the fitting are the piston and cylinder radii  $r$  and  $R$  along the engagement length. For the piston the discrepancy between absolute diameters and straightness data is in average about 10 nm. For the cylinder the discrepancy is below 50 nm. The roundness measurements confirmed that the roundness deviation was small within the above

<sup>1</sup> Sari Saxholm, Björn Hemming, Martti Heinonen, Markku Rantanen, Veli-Pekka Esala, Antti Lassila, Centre for Metrology and Accreditation (MIKES), Tekniikantie 1, FI-02150 Espoo, Finland

<sup>2</sup> Pierre Otal, Laboratoire National de Métrologie et d'Essais (LNE), 1 rue Gaston Boissier, FR-75015 Paris, France  
Email of corresponding author: sari.saxholm@mikes.fi

discrepancies.

**Uncertainty of effective area**

Uncertainty calculation based on eq. (1) is very complicated. When studying eq. (2), however, we can see that  $\delta A$  is actually a weighted mean of  $(r + R)$  divided by  $r_0$  and subtracted by one. Because the weights used in the weighted mean are  $(R - r)^{-3}$ , smallest radial clearances highly dominate. Using this feature, we derive an approximation for  $\delta A$  with only minor overestimation:

$$\delta A(r_0, r, R) = \left[ \frac{1}{r_0} \frac{\int_0^l \frac{(r+R)}{(R-r)^3} dz}{\int_0^l \frac{1}{(R-r)^3} dz} - 1 \right] \approx \left[ \frac{r_k + R_k}{r_0} - 1 \right] \approx \left[ \frac{r_k}{r_{k0}} + \frac{R_k}{R_{k0}} - 1 \right] \quad (3)$$

where  $r_k/r_{k0}$  and  $R_k/R_{k0}$  are the ratios of radii at the location on the z-axis where  $R - r$  is at minimum in the gap between piston and cylinder profiles. By utilizing the approximation of several factors to unity in the sensitivity coefficient calculations, we can estimate the combined uncertainty with the following equation:

$$u^2(A_0) \approx \pi^2 r_0^2 [4u^2(r_0) + u^2(r_k) + u^2(R_k)] \quad (4)$$

where

$$u^2(r_k) = u^2(r_{dk}) + u^2(\delta r_{rk}) + u^2(\delta r_{sk}) \quad \text{and} \quad (5)$$

$$u^2(R_k) = u^2(R_{dk}) + u^2(\delta R_{rk}) + u^2(\delta R_{sk}) \quad (6)$$

Here, subscript k refers to the location  $z_k$  and subscripts d, r and s to diameter, roundness and straightness, respectively. Taking into account the correlation between  $r_0$  and  $r_{dk}$  we finally get:

$$u^2(A_0) \approx \pi^2 r_0^2 [2u^2(r_0) + u^2(\delta r_{rk}) + u^2(\delta r_{sk}) + u^2(R_{dk}) + u^2(\delta R_{rk}) + u^2(\delta R_{sk})] \quad (7)$$

**Results for effective area**

The results for piston cylinder unit no. 6687 (35 mm) and no. 451 (50 mm) are presented in the Figures 1 – 3.

The standard uncertainties for the dimensional quantities for the piston were estimated to 53 nm for diameter, 29 nm for straightness and 30 nm for roundness. The standard uncertainties for the dimensional quantities for the cylinder were estimated to 60 nm for diameter, 29 nm for straightness and 40 nm for roundness. The estimates include uncertainties in measurements and discrepancies when interpolating and combining measured data. The total uncertainty ( $k = 2$ ) for the effective area is 9,3 ppm for unit no. 451 and 13,1 ppm for unit no. 6687.

The effective areas for piston cylinder units are calculated using the eq. (1). However, for these type of almost identical pieces also a very simple calculation by taking an average of all the diameter results gives a quite good approximation. A biggest difference for these units was 4,0 ppm between simple and sophisticated calculation.

All the results presented in Figure 1 for unit no. 6687 agree within 3,9 ppm. The effective area for the piston cylinder unit no. 451 is determined from dimensional measurements made by MIKES and LNE. Difference between the results is 1,2 ppm. All the results presented in Figure 2 agree within 7,3 ppm.

**Discussion and conclusions**

The results presented in this paper show that MIKES is able to determine the effective area of

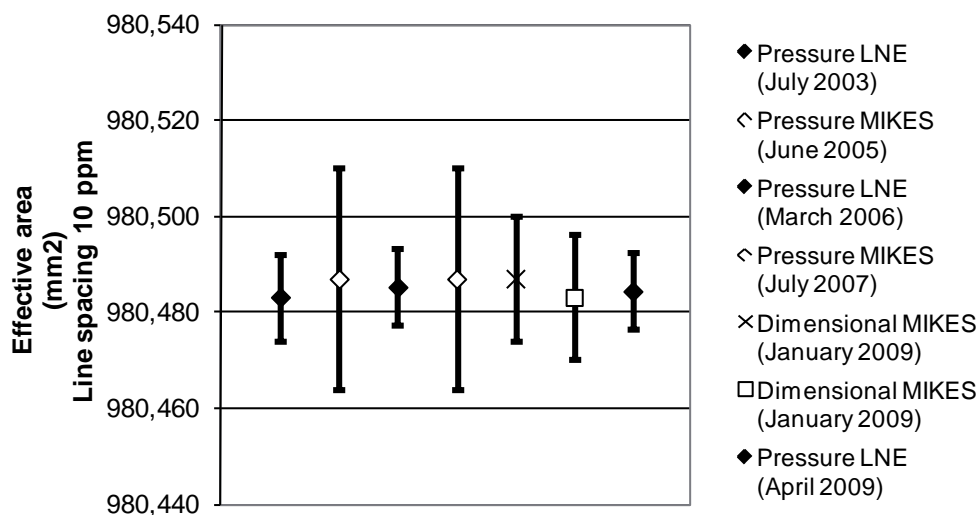


Figure 1. The effective area for the piston cylinder unit no. 6687 is determined from the dimensional measurements made by MIKES (cross, simple calculation and white square sophisticated calculation) and from the cross-floating results made by LNE (black diamonds). The cross-floating results made by MIKES (white diamonds) also agree with rest of the results. The full scale of the piston cylinder unit no. 6687 is 1 MPa gauge pressure with gas media.

Figure 2. The effective area for the piston cylinder unit no. 451 is determined from dimensional measurements made by MIKES (white square) and LNE (black square) and complemented with cross-floating made by LNE (black diamond). The cross-floating results made by MIKES (white diamonds) also agree with rest of the results. The effective area from the manufacturer is also included in the picture (black triangle). The full scale of the piston cylinder unit no. 451 is 175 kPa gauge and absolute pressure with gas media.

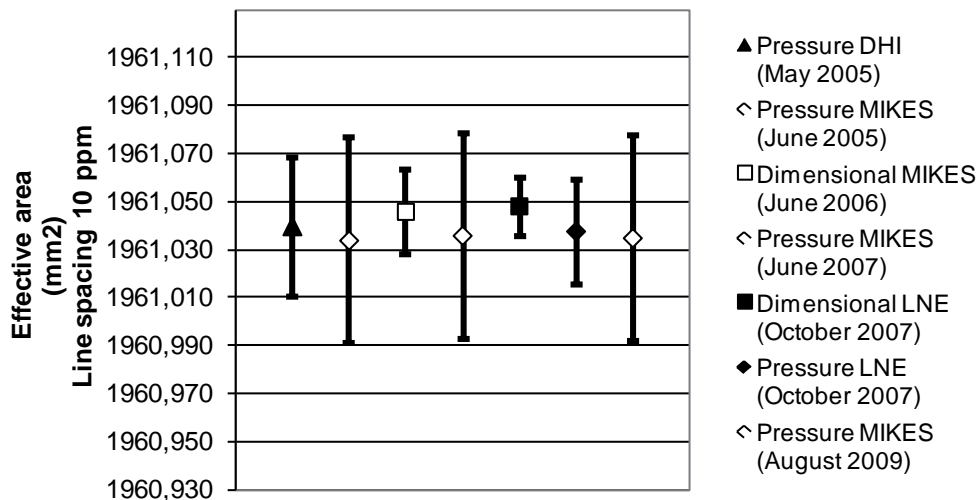
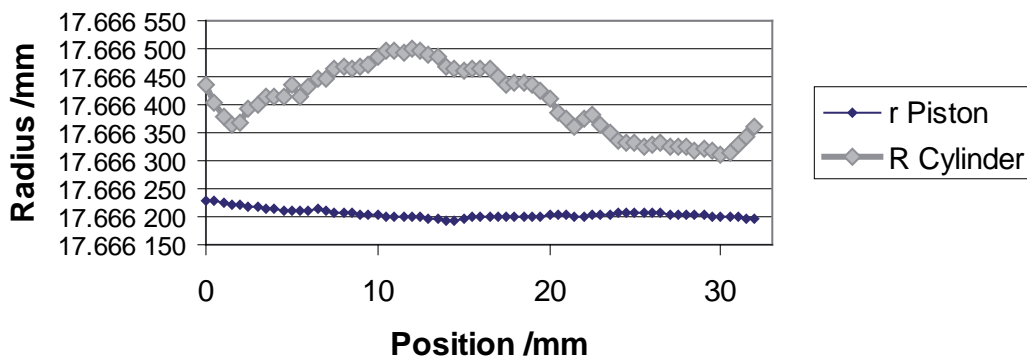


Figure 3. Gap profile for piston cylinder unit no. 6687. The profiles for the piston and the cylinder are calculated from measured diameter and straightness data.



its reference piston cylinder units. All the results presented here agree well below 10 ppm and the uncertainty level for the effective areas determined from dimensional measurements is in the level which enables to transfer the traceability over the whole pressure measurement range with a reasonable uncertainty. The results for effective areas and EURAMET.L-K4 [5] fully support MIKES decision to proceed from secondary level to primary level in pressure.

The straightness measurements made with the Fizeau interferometer were in good agreement with diameter measurements. The used approach in this paper is based on diameter and straightness measurements and naturally a full 3D reconstruction using also roundness data could be valuable.

#### Acknowledgements

The authors wish to thank Mr. Pierre Ota, Mr. Georges Vaillau, Mr. Jean Claude Legras and other colleagues at LNE for their work with pressure and dimensional measurements and the possibility to study effective area calculation

methods and uncertainty evaluation at LNE within iMERA Special Facilities project in 2007.

#### References

- [1] F. Pavese and G. Molinar, *Modern Gas-Based Temperature and Pressure Measurements*, New York and London: Plenum Press (1992) 514
- [2] A. Lassila et al., *Design and performance of an advanced metrology building for MIKES*, *Measurement* 44 (2011) 399-425
- [3] R. S. Dadson, S. L. Lewis and G. N. Peggs, *The Pressure Balance: Theory and Practice*, London: HMSO (1982) 290
- [4] G. Molinar et al., *Metrologia* 42 (2005) S197-S201
- [5] G. B. Picotto, *Final report on EUROMET.L-K4: Calibration of diameter standards, Group 1*, *Metrologia* 47 (2010) 04003

# Traceability of NIS Piston-Cylinder Assemblies up to 500 MPa

Alaaeldin A. Eltawil<sup>1</sup>, Shaker A. Gelany<sup>1</sup>, Ali H. Magrabi<sup>1</sup>

## Abstract

Measurement made using single equipment with one-to-one correspondence, without any functional relationship, is called direct measurement. This is not the case with pressure measurements where the parameter under test is functionally related to other parameters and has to be indirectly evaluated. Traceability of pressure measurements up to 1 MPa using pneumatic gauge pressure with relative uncertainty of few ppm was established from dimensional measurements of the piston cylinder assembly (PCA) in conjunction with mass measurements and adequate measurements for the acceleration of gravity.

Using a set of cross floating experiments the traceability was transferred to the pneumatic pressure up to 40 MPa and hydraulic pressure measurements up to 500 MPa in NIS pressure lab. Such traceability was validated by participating in several key comparisons with all accepted measurements within the claimed uncertainty and set of measurements using PCA that was calibrated by other recognized NMI.

## Introduction

NIS pressure lab has adopted the use of pressure balance as a primary standard with traceability to dimensional measurements. Two units of PCA, of 10 cm<sup>2</sup> nominal effective area, are the primary standard and the check standard of NIS pressure scale. Eleven PCAs are covering the NIS pressure scale range from 10 kPa up to 500 MPa with a requirement of having at least 25% range overlapping between each pair of successive PCAs. The two primary standard PCAs were measured dimensionally at PTB [1] where the piston and cylinder diameters, straightness and roundness were measured using PTB relatively up-to-date state of the art comparators.

Those two primary standards were used to calibrate the rest of the PCAs using cross floating method [2] in gas media gauge mode. In order to transfer the traceability to liquid PCAs, a liquid-to-gas separator was used to perform the calibration in low pressure liquid mode using 2 PCAs

of nominal effective area of 5 cm<sup>2</sup> and 2 cm<sup>2</sup> against the primary standards. Double check was performed between the liquid and gas PCAs as a mean of validation for the traceability.

## Establishing of the traceability

### Calculation of effective areas of the primary standards

The calculations of the effective area at zero pressure from dimensional measurements were carried out using simple averaging method [3]. Validation of these calculations was performed by solving equation (1).

$$A_0 = \pi r_0^2 \left\{ 1 + \frac{h_0}{r_0} + \frac{1}{r_0} \frac{\int_0^l \frac{(u+U)}{h^3} dz}{\int_0^l \frac{1}{h^3} dz} \right\} \quad (1)$$

### Measurements of the effective areas of the NIS PCAs

Two independent sets of measurements, traced to the two primary standards PC-NIS1 and PC-NIS2, were taken, as depicted in fig (1). Direct cross floating method was applied on all of those measurements. Nitrogen was used as a medium in gas measurements, while sebacate was used in liquid measurements.

A decisive factor in the selection of the National standard between the two primary standards was approved by comparing: i) the lowest uncertainty in the calculation of the effective area from dimensional measurements and ii) the minimum residual on the cross floating measurements.

A second decisive factor for acceptance of the generated values out of this traceability was obtained by examining the flow chart on which each pair of the obtained results for a PCA is traced to the two primary standards and investigated according to the normalized  $E_n$ . The accepted value is of  $|E_n| \leq 0.3$ . If such condition is not reached, a recalibration of the PCA is carried out traced to the two primary standards.

<sup>1</sup> Alaaeldin A. Eltawil, Shaker A. Gelany, Ali H. Magrabi, National Institute of Standards (NIS), Tersa Street, El Haram, Giza, Egypt



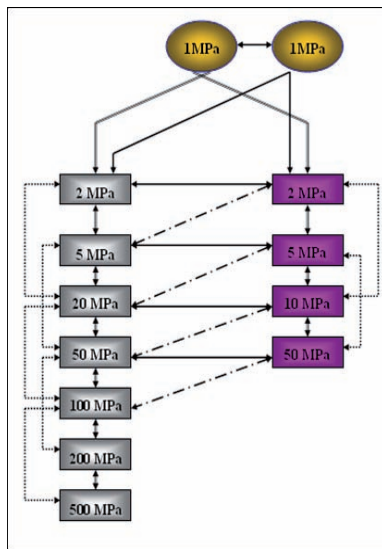


Figure 1 (left) Traceability chain for NIS PCAs

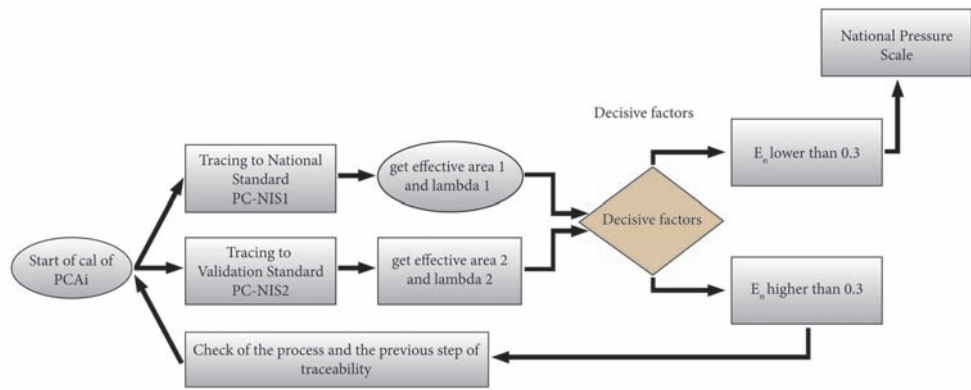


Figure 2 (right) Flow chart for the validation of the obtained value for each PCA.

**Results and Discussion**

**NIS primary standards**

PC-NIS1 and PC-NIS2 are gas primary piston gauge standards that operate from 10 kPa to 1 MPa. The assemblies are “twins” in the sense that they were made from the same casting of tungsten carbide and have the same nominal dimensions. The PCAs are changeable so they are not nominating to a fixed pressure balance base to eliminate any extra error from the base. The effective areas of primary standards were simply calculated as the average of all the dimensional data to determine the zero pressure effective area [3]. For the uncertainty calculation the standard deviations of piston and cylinder dimensions were divided by the square root of the number of points; this is taken as the uncertainty due to diameters variations. The total uncertainty is the square root of the sum of the squares of the shape deviation and uncertainty contributions of  $u(r)$  and  $u(R)$ .

The results of cross floating of the two PCAs showed that the residual of effective area calculation was lower than 2 ppm and the standard deviation of measurements was in the order of 1 ppm. However PC-NIS1 showed lower uncertainty and residual on its performance also the coherency in the calculation of its effective area was better, hence it is selected as a National Standard in the rest of measurements. The se-

cond PC-NIS2 was then used as a validation standard. Table (1) gives the calculated effective area for each PCA using the two methods, as well as the results of cross floating experiments.

The maximum disagreement between the different methods of effective area calculation was 6.6 ppm which is a good validation for the measurements.

**NIS pressure scale**

Adopting PC-NIS1 and PC-NIS2 as primary standards the system of cross floating given by fig (1) was performed using direct cross floating. The force generated by the unit under calibration is balanced with the primary standard at each generated pressure using a set of 100 kg calibrated masses and trim masses. The mass threshold was kept lower than 10 mg at all measurements under stable environmental condition of laboratory where the variation in ambient temperature was not more than  $\pm 0.2^\circ\text{C}$  during the whole cycle of measurements. In low oil pressure the system required extremely careful handling since the rotational speed affects the measurements. To avoid such effect a constant rotational speed was establishment and adopted during the whole work of this traceability chain.

In order to test the validity and coherency of the results of traceability the results were compared with the validation chain generated tracing to the PC-NIS2. The  $E_n$  ratios are calculated

Table 1 Calculated effective area of PC-NIS1 and PC-NIS2

Unit	Direct average		Integration		From cross floating (using the other primary standard as reference)	
	Value (mm <sup>2</sup> )	Relative Uncertainty (ppm)	Value (mm <sup>2</sup> )	Relative Uncertainty (ppm)	Value (mm <sup>2</sup> )	Uncertainty (ppm)
PC-NIS1	980.5428	8.9	980.5402	9.5	980.5439	11
PC-NIS2	980.4825	8.9	980.4782	9.5	980.4847	11

using a standard statistical technique, derived from the following expression, for comparing values:

$$E_n = \frac{|A_{o(PC-NIS1)} - A_{o(PC-NIS2)}|}{\sqrt{(U_{A_{o(PC-NIS1)}})^2 + (U_{A_{o(PC-NIS2)}})^2}} \quad (2)$$

where:  $A_{o(PC-NIS1)}$  and  $A_{o(PC-NIS2)}$  are the measured effective areas of a PCA tracing to PC-NIS1 and PC-NIS2 respectively, with the corresponding uncertainties  $U_{A_{o(PC-NIS1)}}$  and  $U_{A_{o(PC-NIS2)}}$  during this traceability chain values of  $|En| \leq 0.3$ .

Table (2) shows that the maximum difference between the calculated effective areas tracing to PC-NIS1 and PC-NIS2 is 2.6 ppm. It could be also noticed that En values are much lower than 1 and also confirm the decisive factor that was selected to confirm the validation processes of results.

An example for the variation of measured effective areas with applied pressure when calibrating the PC-NIS3 against PC-NIS1 and PC-NIS2 is shown in fig (3) where good coherency between results is obtained that gives a validation for the results.

### Key comparisons in pressure

Pressure laboratory of NIS started in 1998 participation in international key comparisons through APMP and EURAMET. NIS pressure laboratory has participated in 8 key comparisons, namely: APMP.M.P-K1.c, APMP.M.P-K7, APMP.M.P-K9, APMP.M.P-K13, EURAMET.M.P-K8, EURAMET.M.P-K13, APMP.M.P-K7.TRI and EURAMET.M.P-K1.c. The results of the first two are published with acceptance of all of their results. The rest comparisons are currently running except the last one which is still in the planning phase. The EURAMET.M.P- K13 report, which comprises accepted results in all pressure points, is completed [5].

Referring to the Key Comparisons APMP.M.P-K7 and CCM.P-K7 in Hydraulic Gauge Pressure range from 10 to 100 MPa, the equivalence between institutes participating in these key comparison was all accepted. However, when linking the APMP comparison with the CCM.P-K7, there noticed a shift between the results of the NIS and NIST at 10 MPa [6]. Such discrepancy led to start of the US-Egyptian Project No. (STM9-002-001)[2]. The project includes a study of the traceability of a primary standard controlled clearance pressure balance of NIST and a study of the traceability of NIS PCAs. Informal bilateral comparison of hydraulic pressure was carried out in the period from 2009 to 2010 aiming at determining the degrees of equivalence of the gauge pressures in the range up to 200 MPa. The results of the comparison were accepted.

### Conclusions

- Two separate methods were successfully implemented for the determination of  $A_0$  from dimensional data with excellent agreement; within 7 ppm. Experimental validation was also established, within 10 ppm disagreement between all results.
- Transferring the traceability to all NIS PCAs with highly accepted uncertainties ranged from 10 to 80 ppm, which is lower than the recognized CMC of NIS.
- To reduce uncertainty below the obtained limits, it is highly required to measure the primary standard PCAs dimensionally at more measuring points and to adopt several methods to calculate effective area and to estimate of uncertainty. Acquiring new PCAs to complete the calibration chain is mandatory, namely 10 MPa gas operated gas lubricated PCA, 20 MPa gas operated oil lubricated and 10 MPa oil operated will also reduce the uncertainty. Changing the primary standards

Table 2 Details of traceability results of NIS PCAs

PCA Code	Kn value of PCA	Medium	Max difference between traceability and validation (ppm)	$E_n$ of $A_0$
PC-NIS3	20 kPa/kg	Gas	-0.1	0.01
PC-NIS4	50 kPa/kg	Gas	-0.1	0.01
PC-NIS5	0.1 MPa/kg	Gas	2.5	0.11
PC-NIS6	0.5 MPa/kg	Gas	-1.5	0.06
PC-NIS7	20 kPa/kg	Oil	-1.5	0.05
PC-NIS8	50 kPa/kg	Oil	-1.5	0.05
PC-NIS9	0.2 MPa/kg	Oil	-2.6	0.10
PC-NIS10	0.5 MPa/kg	Oil	-2.6	0.11
PC-NIS11	1 MPa/kg	Oil	-2.6	0.10
PC-NIS12	2 MPa/kg	Oil	-2.6	0.08
PC-NIS13	5 MPa/kg	Oil	-2.5	0.04

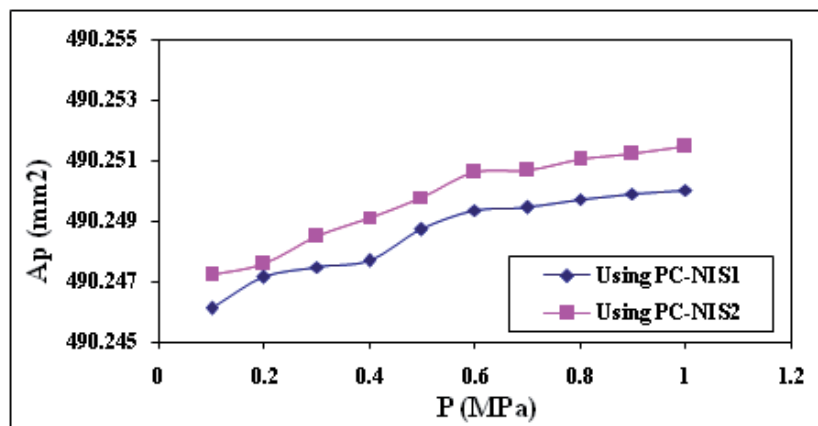


Fig (3) Variation of measured effective areas with applied pressure for PC-NIS3 using PC-NIS1 and PC-NIS2 as references.

to 20 cm<sup>2</sup> should reduce also the uncertainty.

- Validation process seems to be firm and effective to monitor the validity of results.
- Updating of NIS CMC is expected to be performed shortly.

### Acknowledgments

The authors would like to thank Prof. Dr. Ibarhim Shabaka and Prof. Dr. Ahmed Ali El Sayed for their kind revision of this work.

### References

- [1] PTB certificates Reference No. 5.31 – 05-4019764
- [2] Eltawil A. and Olson D. final report of project STM9-002-001, No. 274 “Establishment of Mutual Coherence in the Oil Primary Pressure Standards Used at NIST-US and NIS-Egypt” April, 2011.
- [3] Molinar G. et al Calculation of effective area A0 for six piston–cylinder assemblies of pressure balances. Results of the EUROMET Project 740 Metrologia 42 (2005) S197–S201
- [4] Dadson R S, Lewis S L and Peggs G N 1982 the Pressure Balance: Theory and Practice (London: HMSO) p 290
- [5] Kocas I. et al Final report on Key Comparison for 500 MPa Range of Hydraulic Gauge Pressure (EURAMET.M.P-K13) accepted for publishing in CCMP May 2–5, 2011, in Berlin-Germany.
- [6] Kobata T. et al Final Report on Key Comparison APMP.M.P-K7 in hydraulic gauge pressure from 10 MPa to 100 MPa Metrologia, 2005, 42, Tech. Suppl., 07006 .

# EURAMET Key Comparison for 500 MPa Range of Hydraulic Gauge Pressure (EURAMET.M.P-K13)

I. Kocas<sup>1</sup>, W. Sabuga<sup>2</sup>, M. Bergoglio<sup>3</sup>, A. E. Eltawil<sup>4</sup>, C. Korasie<sup>5</sup>, P. Farar<sup>6</sup>, J. Setina<sup>7</sup>, B. Waller<sup>8</sup>

The regional key comparison EURAMET.M.P-K13 for pressure measurements in liquid media from 50 MPa to 500 MPa was piloted by the TÜBİTAK UME Pressure Group Laboratories, Turkey. The transfer standard was a DH-Budenberg pressure balance with a free deformation piston-cylinder unit of 2 mm<sup>2</sup> nominal effective area. Seven laboratories from the EURAMET region, namely PTB, INRIM, NIS, SMU, IMT and NPL, and one laboratory from the APMP region, NMISA, participated in this comparison. PTB participated in this comparison as a link between this comparison, previous 500 MPa comparison EUROMET 881 and 500 MPa CCM key comparison CCM.P-K13.

All participants' results with exception of only one value at 500 MPa at were found to be consistent with each other and with the calculated reference value, within their claimed uncertainties, at all pressures. The results are therefore considered to be satisfactory.

## 1. Introduction

The objective of the comparison was to determine values of the effective area of a pressure balance  $A_p$  and their uncertainties at specified pressures.

Additionally, the zero pressure effective area,  $A_0$ , and the distortion coefficient with the associated uncertainties had to be determined.

At the EURAMET TCM Contact Persons Meeting in Bucharest in 2008 it was decided to carry out a new key comparison (KC) in the range of 500 MPa of hydraulic gauge pressure. This comparison was registered in the BIPM KCDB as a EURAMET key comparison. UME was the pilot laboratory, and PTB took a part in this comparison for a linkage between this comparison, previous comparison EUROMET 881 and 500 MPa CCM key comparison CCM.P-K13.

## 2. Details of transfer standard

The transfer standard was a piston-cylinder assembly of 2 mm<sup>2</sup> nominal effective area with serial number 6494 [1]. It was built in a pressure balance equipped with a mass carrier, all parts having been manufactured by *DH-Budenberg*,

France. Some of participants operated the TS pressure balance with their own 100 kg mass sets. Laboratories which did not have masses suitable for operation with the TS pressure balance were provided with a mass set from UME.

The TS stability was checked by the pilot laboratory comparing the results of former calibrations with those obtained at the beginning of the comparison, at the intermediate test and at the final investigation. The stability check measurements were performed at UME in May 2009, November 2009 and at the end of comparison January. The average drift of the effective area was found as 0.000016 mm<sup>2</sup>/year

## 3. Participants' standards

The standards of all laboratories were pressure balances. Almost all of them were equipped with a simple type of piston-cylinder assembly, the PTB standard was of controlled-clearance type. Table 1 gives the main specifications of these standards.

Table 1. Specifications of the laboratories' standards with their standard uncertainties

Laboratory	Effective area	Uncertainty of $A_0$	$\lambda$ coefficient
	$A_0/\text{mm}^2$	$\cdot 10^{-6}$	$\cdot 10^{-6}$
PTB	4.902256	13	0.44 ± 0.05
INRIM	1.961167	23	0.83 ± 0.05
NIS	1.96122	17	0.85 ± 0.06
NMISA	1.9615874	25	0.725 ± 0.05
SMU	1.961600	20	0.7 ± 0.07
IMT	1.960953	11	0.77 ± 0.055
NPL	1.9614694	12.3	0.96 ± 0.12
UME	1.961861	10	0.80 ± 0.05

## 4. Reference value calculation

Reference value can be calculated as a weighted mean of participants' result [2].

$$A_{p,ref} = \frac{\sum_{i=1}^8 \frac{A_{p,i}}{u^2(A_{p,i})}}{\sum_{i=1}^8 \frac{1}{u^2(A_{p,i})}}$$

The chi-squared value is formed as

$$\chi_{obs}^2 = \sum_{i=1}^8 \frac{(A_{p,i} - A_{p,ref})^2}{u^2(A_{p,i})}$$

- <sup>1</sup> UME Turkey,
- <sup>2</sup> PTB Germany,
- <sup>3</sup> INRIM Italy,
- <sup>4</sup> NIS Egypt,
- <sup>5</sup> NMISA South Africa,
- <sup>6</sup> SMU Slovakia,
- <sup>7</sup> IMT Slovenia,
- <sup>8</sup> NPL United Kingdom

And the consistency condition

$$Probability\{\chi^2(\nu) > \chi^2_{obs}\} < 0.05$$

is checked, where n is the degree of freedom,  $\nu = 7$ .

To calculate the reference  $A_p$  values median values of  $A_p$  were chosen. And uncertainty of the reference values were calculated according to

$$u(A_{p,ref.med.}) = \frac{1.858}{\sqrt{n-1}} median|A_{p,i} - A_{p,ref.med.}|$$

where  $n = 8$  is the number of participants, – their results and – the median reference values.

Table 2. Median reference values and their relative standard uncertainties

p /MPa	$A_{p,ref.med.}$ /mm <sup>2</sup>	$u(A_{p,ref.med.})/A_{p,ref.med.}$ · 10 <sup>-6</sup>
50	1.961870	10.4
100	1.961946	6.6
150	1.962034	5.2
200	1.962108	6.4
250	1.962190	10.0
300	1.962267	10.5
350	1.962342	12.9
400	1.962417	14.1
450	1.962494	16.3
500	1.962577	20.3

The deviations of participants' results from the reference values are shown graphically in Figure 1 and, with their uncertainties, in Figures 2 and 3 for 50 MPa and 500 MPa, respectively. The result of NPL at 500 MPa deviates stronger from the reference value than the uncertainty of the deviation. This is evidently caused by a difference of distortion coefficient.

The error bars in Figure 2 and Figure 3 present the expanded ( $k = 2$ ) relative uncertainties of these deviations, which were calculated by

$$U\left(\frac{\Delta A_{p,i}}{A_{p,ref.med.}}\right) = 2 \sqrt{\frac{u^2(A_{p,i}) + u^2(A_{p,ref.med.})}{A_{p,ref.med.}^2}}$$

The degrees of equivalence between the laboratories are presented in Tables 3 and 4 for 50 MPa and 500 MPa, respectively. They are given by relative differences between the participants results ( $d_{ij}$ ) and their expanded uncertainties ( $U(d_{ij})$ ) which were calculated as

$$d_{ij} = \frac{A_{p,i} - A_{p,j}}{A_{p,ref.med.}}$$

$$U(d_{ij}) = 2 \sqrt{\frac{u^2(A_{p,i}) + u^2(A_{p,j})}{A_{p,ref.med.}^2}}$$

### 5. Conclusions

The regional key comparison for pressure in liquid media covering the range from 50 MPa to 500 MPa was organized with participation of 8 NMIs. The key comparison reference value was calculated as a median. In a great majority, all results of the participants are consistent with their uncertainty claims. Linking of the key comparison reference value (KCRV) of this RMO comparison to the KCRV of comparison CCM.P-K13 will be established through PTB results.

### 6. References

[1] Kocas I. *et al*, Technical Protocol of EURAMET.M.P-K13 (500 MPa), Version 5 of 2010-1-8  
 [2] Cox M.G., The evaluation of key comparison data, *Metrologia*, 2002, **39**, 589-595

Table 3. Relative differences of participants' results ( $d_{ij}$ ) and their expanded uncertainties ( $U(d_{ij})$ ) at 50 MPa

50 MPa	Lab.		PTB		INRIM		NIS		NMISA		SMU		IMT		NPL		UME	
Lab <sub>i</sub>	$d_i$	$U(d_i)$	$d_i$	$U(d_i)$	$d_i$	$U(d_i)$	$d_i$	$U(d_i)$	$d_i$	$U(d_i)$	$d_i$	$U(d_i)$	$d_i$	$U(d_i)$	$d_i$	$U(d_i)$	$d_i$	$U(d_i)$
	· 10 <sup>-6</sup>	· 10 <sup>-6</sup>	· 10 <sup>-6</sup>	· 10 <sup>-6</sup>	· 10 <sup>-6</sup>	· 10 <sup>-6</sup>	· 10 <sup>-6</sup>	· 10 <sup>-6</sup>	· 10 <sup>-6</sup>	· 10 <sup>-6</sup>	· 10 <sup>-6</sup>	· 10 <sup>-6</sup>	· 10 <sup>-6</sup>	· 10 <sup>-6</sup>	· 10 <sup>-6</sup>	· 10 <sup>-6</sup>	· 10 <sup>-6</sup>	· 10 <sup>-6</sup>
PTB	3.8	35			-9.6	56	14.5	45	-38.3	66	-12.3	43	7.6	38	24.8	56	20.7	40
INRIM	13.4	52	9.6	56			24.1	60	-28.7	77	-2.6	58	17.2	54	34.5	68	30.3	56
NIS	-10.6	41	-14.5	45	-24.1	60			-52.8	69	-26.7	48	-6.8	44	10.4	60	6.2	46
NMISA	42.1	63	38.3	66	28.7	77	52.8	69			26.0	68	45.9	65	63.1	77	59.0	66
SMU	16.1	38	12.3	43	2.6	58	26.7	48	-26.0	68			19.9	41	37.1	58	33.0	43
IMT	-3.8	33	-7.6	38	-17.2	54	6.8	44	-45.9	65	-19.9	41			17.2	55	13.1	39
NPL	-21.0	52	-24.8	56	-34.5	68	-10.4	60	-63.1	77	-37.1	58	-17.2	55			-4.1	56
UME	-16.9	36	-20.7	40	-30.3	56	-6.2	46	-59.0	66	-33.0	43	-13.1	39	4.1	56		

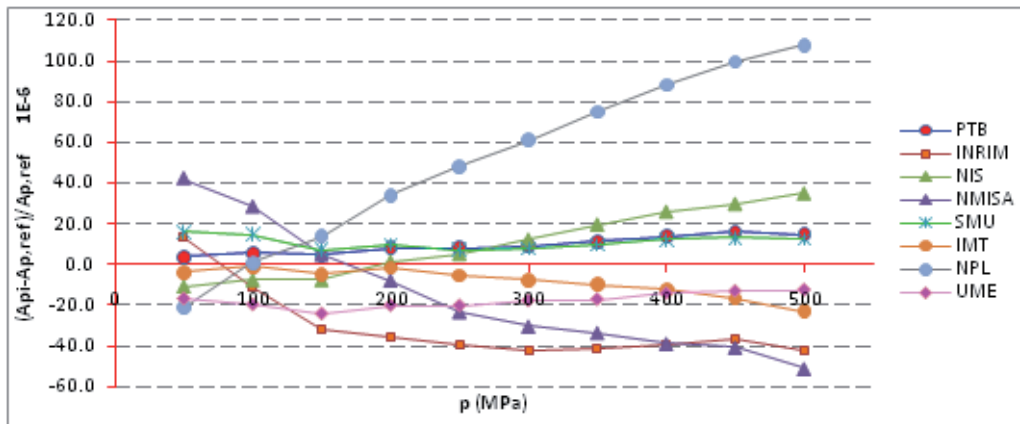


Fig. 1. Relative deviations of the participants results from the reference value

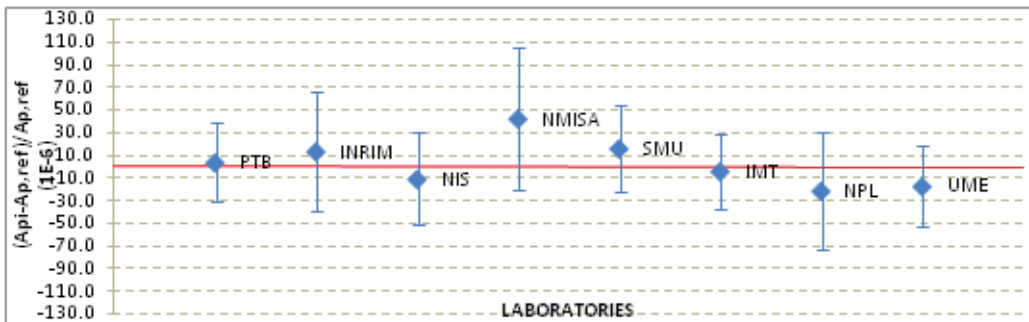


Fig. 2. Relative deviations of the participants results from the reference value and the expanded (k = 2) uncertainties of these deviations at 50 MPa

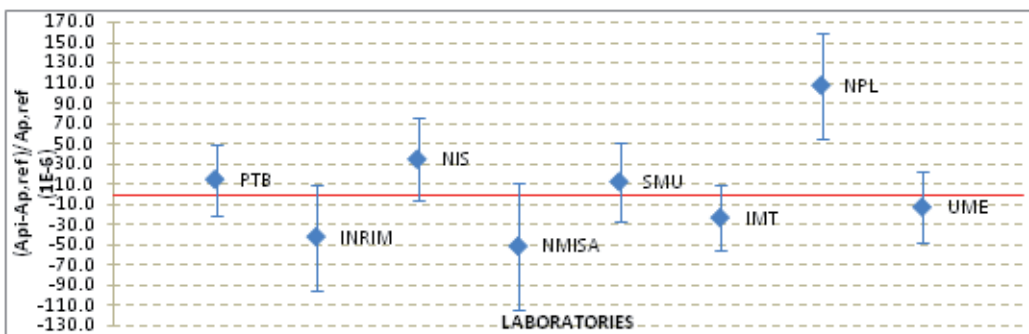


Fig 3. Relative deviations of the participants results from the reference value and the expanded (k = 2) uncertainties of these deviations at 500 MPa

Table 4. Relative differences of participants' results ( $d_{ij}$ ) and their expanded uncertainties ( $U(d_{ij})$ ) at 500 MPa

500 MPa	Lab.	PTB		INRIM		NIS		NMISA		SMU		IMT		NPL		UME			
		$d_i$	$U(d_i)$	$d_i$	$U(d_i)$	$d_i$	$U(d_i)$	$d_i$	$U(d_i)$	$d_i$	$U(d_i)$	$d_i$	$U(d_i)$	$d_i$	$U(d_i)$	$d_i$	$U(d_i)$		
Lab <sub>i</sub>		$\cdot 10^{-6}$	$\cdot 10^{-6}$	$\cdot 10^{-6}$	$\cdot 10^{-6}$	$\cdot 10^{-6}$	$\cdot 10^{-6}$	$\cdot 10^{-6}$	$\cdot 10^{-6}$	$\cdot 10^{-6}$	$\cdot 10^{-6}$	$\cdot 10^{-6}$	$\cdot 10^{-6}$	$\cdot 10^{-6}$	$\cdot 10^{-6}$	$\cdot 10^{-6}$	$\cdot 10^{-6}$		
PTB		14.9	69			56.7	88	-20.0	107	66.1	78	2.3	123	37.8	83	-93.0	88	27.4	79
INRIM		-41.9	79	-56.7	88			-76.7	114	9.3	87	-54.4	129	-18.9	92	-149.8	96	-29.3	88
NIS		34.9	100	20.0	107	76.7	114			86.1	107	22.3	143	57.9	110	-73.0	114	47.4	107
NMISA		-51.2	68	-66.1	78	-9.3	87	-86.1	107			-63.7	123	-28.2	82	-159.1	87	-38.7	79
SMU		12.5	117	-2.3	123	54.4	129	-22.3	143	63.7	123			35.5	126	-95.4	129	25.1	124
IMT		-23.0	73	-37.8	83	18.9	92	-57.9	110	28.2	82	-35.5	126			-130.9	92	-10.4	83
NPL		107.9	79	93.0	88	149.8	96	73.0	114	159.1	87	95.4	129	130.9	92			120.4	88
UME		-12.5	70	-27.4	79	29.3	88	-47.4	107	38.7	79	-25.1	124	10.4	83	-120.4	88		

# Evaluation of cross-float measurements with pressure balances – Results of EURAMET project 1125

P. Ota<sup>1</sup>, I. Morgado<sup>1</sup>, D. Steindl<sup>2</sup>, N. Medina Martín<sup>3</sup>, A. Lefkopoulos<sup>4</sup>, A. Altintas<sup>5</sup>, L. Grgec Bermanec<sup>6</sup>, S. Bursic<sup>7</sup>, J. Setina<sup>8</sup>, M. Bergoglio<sup>9</sup>, I. Spohr<sup>10</sup>, C. Wüthrich<sup>11</sup>, M. Rantanen<sup>12</sup>, C. Vámosy<sup>13</sup>, W. Sabuga<sup>14</sup>, I. Koçaş<sup>15</sup>

## Abstract

Fifteen European metrological institutes have compared their approaches to estimate the effective area parameters resulting from the calibration of pressure balances by cross-floating. The methods in estimating these parameters and the associated uncertainties are tested by applying four calibration data sets simulated numerically, two in gas (up to 10 MPa) and two in oil (up to 500 MPa). The performance of the methods is evaluated in terms of robustness and ability to estimate the uncertainties of the effective area parameters.

**Keywords:** pressure balance, effective area, cross-float, pressure distortion coefficient

## 1. Introduction

Cross-floating is the most common method used for calibrating a pressure balance. When the smallest uncertainty is required, it is recommended to determine the effective areas  $A_p$  of the piston-cylinder assembly (PCA) under test as a function of pressure. Then, the effective areas are analysed to calculate the values of the effective area at null pressure  $A_0$  and, if significant, the pressure distortion coefficient<sup>1</sup>. There exist various approaches to determine these two parameters and estimate their uncertainties, which leads to results that may differ significantly. The purpose of project Euramet 1125 was to verify numerically the performance of different methods used by NMIs by applying simulated data sets.

## 2. Data provided for the comparison

Four calibration data sets have been simulated, each calibration includes 5 cycles and 10 pressures points. First of all, arbitrary theoretical values for the effective area at null pressure  $A_{0c,th}$  and the distortion coefficient  $\lambda_{c,th}$  of the calibrated PCAs have been defined and considered as true values, with no uncertainty (table 1).

Once the effective area parameters fixed, they have then been used to generate data that satisfy exactly the pressure equation (1).

$$p = \frac{M \cdot g + \Gamma \cdot C}{A_p \cdot (1 + (\alpha_p + \alpha_c)(t - 20))} + C_h, \quad (1)$$

where  $p$  is the pressure measured at the reference level of the piston,  $A_p$  is the effective area of the PCA at 20 °C and at pressure  $p$ ,  $g$  is the local gravity acceleration,  $M$  is the applied mass corrected for air buoyancy,  $\alpha_p$  and  $\alpha_c$  are the linear thermal expansion coefficients of the piston and cylinder,  $t$  is the measured temperature of the PCA,  $\Gamma$  is the surface tension of the fluid (for gas:  $\Gamma = 0$ ),  $C$  is the circumference of the piston,  $C_h$  is the head correction. The generated data have referred to the reference pressure balance, the pressure balance under test and the environmental conditions. Then, random measurement errors and systematic errors have been added to all these data using the Analysis Toolpak (pseudo-random numbers generator from excel). All the data except the theoretical values of the effective area parameters were provided to the participants. Two types of pressure balances are considered. A gas balance in the range of 0,2 MPa –10 MPa with a nominal  $A_0$  of 49 mm<sup>2</sup>, and a oil balance in the range of 5 MPa –500 MPa with a nominal  $A_0$  of 1,9 mm<sup>2</sup>. For each pressure balance, two series of data have been generated. They have been treated as two different calibrations. The results expected from the participants were:

- The effective area  $A_p$  of the calibrated piston-cylinder assembly as a function of pressure
- The uncertainty of the effective area  $A_p$ :  $u(A_p)$ ,
- The estimate  $\hat{A}_p$  of  $A_p$ :  $\hat{A}_p = A_0 \cdot (1 + \lambda \cdot P) = A_0 + \beta \cdot P$ ,
- The standard uncertainties of the estimate:  $u(\hat{A}_p)$ .

	GAS ( 10 MPa)		OIL (500 MPa)	
	Case No1	Case No2	Case No1	Case No2
$A_{0c,th} / \text{mm}^2$	49,018900	49,019200	1,90290	1,90292
$1 / \text{Pa}^{-1}$	-2,40E-12	-2,38E-12	7,79E-13	7,80E-13

**Table 1.** Theoretical values for the effective area at null pressure and the distortion coefficient

<sup>1</sup> LNE, France,  
<sup>2</sup> BEV, Austria,  
<sup>3</sup> CEM, Spain,  
<sup>4</sup> EIM, Greece,  
<sup>5</sup> DANIAMet-FORCE, Denmark,  
<sup>6</sup> HMI-FSB, Croatia,  
<sup>7</sup> IMBiH, Bosnia-Herzegovina,  
<sup>8</sup> IMT, Slovenia,  
<sup>9</sup> INRiM, Italy,  
<sup>10</sup> IPQ, Portugal,  
<sup>11</sup> METAS, Switzerland,  
<sup>12</sup> MIKES, Finland,  
<sup>13</sup> MKEH, Hungary,  
<sup>14</sup> PTB, Germany,  
<sup>15</sup> UME, Turkey

GAS					OIL				
Nominal pressure	Case No1		Case No2		Nominal pressure	Case No1		Case No2	
	$A_p$	$u(A_p)$	$A_p$	$u(A_p)$		$A_p$	$u(A_p)$	$A_p$	$u(A_p)$
kPa	mm <sup>2</sup>	mm <sup>2</sup>	mm <sup>2</sup>	mm <sup>2</sup>	MPa	mm <sup>2</sup>	mm <sup>2</sup>	mm <sup>2</sup>	mm <sup>2</sup>
200	49,01969	0,00052	49,01997	0,00062	5,16	1,902989	0,000065	1,902826	0,000063
1 000	49,01902	0,00042	49,01931	0,00042	51,55	1,902982	0,000025	1,902982	0,000029
2 000	49,01870	0,00041	49,01892	0,00041	103,10	1,903054	0,000026	1,903070	0,000030
3 000	49,01849	0,00041	49,01877	0,00041	154,65	1,903143	0,000030	1,903150	0,000028
4 000	49,01841	0,00041	49,01868	0,00041	206,19	1,903211	0,000030	1,903216	0,000030
5 000	49,01830	0,00041	49,01857	0,00041	257,74	1,903285	0,000033	1,903299	0,000032
6 000	49,01816	0,00041	49,01843	0,00041	309,29	1,903356	0,000037	1,903377	0,000035
7 000	49,01801	0,00041	49,01826	0,00041	360,84	1,903425	0,000036	1,903451	0,000037
8 000	49,01796	0,00041	49,01819	0,00041	412,38	1,903498	0,000041	1,903531	0,000040
10 000	49,01768	0,00041	49,01797	0,00041	515,48	1,903647	0,000046	1,903684	0,000048

As the calculation methods of the NMIs are not the same, some significant deviations occurred between the calculations of the effective areas  $A_p$ . Since the most interesting results relate to the estimate  $\hat{A}_p$ , it was then decided to conduct an additional loop in which the provided data were the mean values of  $A_p$  and the associated uncertainty  $u(A_p)$  (table 2). The participants had then to calculate the estimate  $\hat{A}_p$ , the effective area at null pressure  $A_0$ , the pressure distortion coefficient  $\lambda$  and the associated uncertainties. This paper highlights the results of this second loop. Figure 1 represents the mean values of  $A_p$  and the theoretical values  $A_{thp}$  for the two 49 mm<sup>2</sup> PCAs.

### 3. Calculation methods of the participants

The methods used by the fifteen laboratories are detailed in an extensive report [1]. Four methods have been used by the laboratories in the project.

#### 3.1. OLS (BEV, CEM, EIM, FSB-LPM, IMBiH, IMT, IPQ, MIKES, MKEH, METAS)

The ordinary least squares (OLS) is the most common method used in fitting a supposed linear relation. Theoretically, it is then assumed that the errors are uncorrelated with each other and have equal variance. In some cases, and depending on the deviations in the value of the effective areas, some laboratories could not take all the data into account, especially at low pressure. The determination of the parameters by the participants is close to the method detailed in [2].

#### 3.2 WLS (DANIamet, UME)

The weighted least squares (WLS) method is adopted to take into account the fact that the effective areas have different uncertainties (heteroscedasticity). Each weight is usually equal to the reciprocal variance of the effective area.

#### 3.3 GLS (INRIM, LNE)

The generalized least squares estimation (GLS) is a method which takes the uncertainties and the correlation of the effective areas into account. This more complex approach is detailed by INRIM and LNE in the Euramet report, additional information is given in [3, 4, 5]. The results given by the method depend on the input variance-covariance matrix.

#### 3.4 A0,λ,F-model (PTB)

This method, used by PTB, assumes:

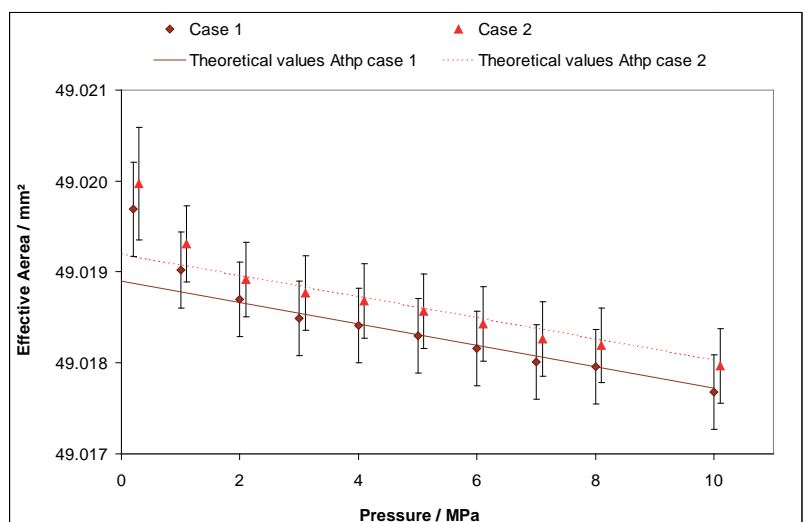
- the existence of an additional unknown force  $F$  acting on piston of the reference standard or the standard under test, which is constant in all pressure points,
- a dependence of the effective area on pressure usually dealing with unknown/incorrect pressure distortion coefficient.

The model equation describing the dependence of the effective area on pressure is then:

$$A(p) = A_0 + A_0 \lambda \cdot p + F/p \tag{2}$$

Table 2. Data provided for loop 2

Figure 1. Effective areas  $A_p$  for the two 49 mm<sup>2</sup> PCAs and theoretical values  $A_{thp}$ . The bars represent the associated standard uncertainties  $u(A_p)$ .





Parameters of the model equations are then determined by the ordinary least squares method.

#### 4. Results and analysis

The first interesting result from the study is that all the estimates of the effective areas  $\hat{A}_p$  determined by the participants agree with the reference values  $A_{thp}$  within their standard uncertainties. However, the uncertainties of the estimates of the effective areas,  $u(\hat{A}_p)$  differ by several orders of magnitude depending on the methods and the laboratories. Concerning the effective area parameters, the estimates of the effective area at null pressure  $A_0$  agree with the reference values within their standard uncertainties for all the participants. With regard to the estimate of the pressure distortion coefficient, the associated uncertainties are underestimated in fifty percent of cases involving the 49 mm<sup>2</sup> PCAs. On the other hand, this is compensated by an overestimation of the uncertainties related to the estimate of the effective areas at null pressure. For the 1,9 mm<sup>2</sup> PCAs, in just three cases out of 40, the estimate of the pressure distortion coefficients slightly disagree with the reference values. One recommendation that can be drawn from this study is that the uncertainties on the effective area parameters, especially when they are reported in calibration certificates, should be better estimated.

The second point concerns the robustness of the methods. The results obtained are presented on figure 2 as the relative deviation from the theoretical values  $A_{thp} = A_{0c_{th}} \cdot (1 + \lambda_{c_{th}} \cdot P)$ . For readability

reasons, they are grouped by method for maximum and minimum pressure points. The pairs of results are presented as Youden plot in which relative differences for case 1 are plotted as a function of case 2 [6]. For the graphical interpretation of the results, it is preferable to plot the absolute values of the differences. The points plotted in this way reflect the robustness of the method: the closer the points are to the origin the more robust the method is.

These Figures show the following points:

- The most used method, based on OLS, gives the less robust results.
- METAS gives better results by applying the same method without considering the first point.
- UME and DANIAMet give better results than the method based on OLS by applying the weighed least squares method. Indeed, data corresponding to the lowest pressure points deteriorate the determination of the fitting due to their higher uncertainties. By considering the uncertainties of the effective area, which define the weight of the values, the determination of the fitting parameters is improved. UME and DANIAMet use the same method, the results are different because the calculation of the uncertainties is different. In the case of DANIAMet, the measurements of the first pressure points have been characterized by a bigger uncertainty, it leads to better results.
- For the laboratories using the GLS method, INRIM and LNE, the results are similar and

Figure 2. Relative deviations from theoretical values, case 2 versus case 1, gas pressure balance calibrations at 200 kPa (left) and 10 MPa (right)

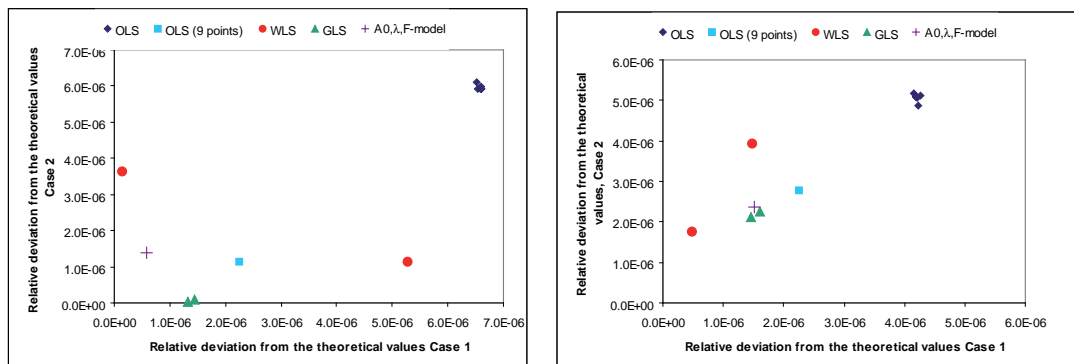
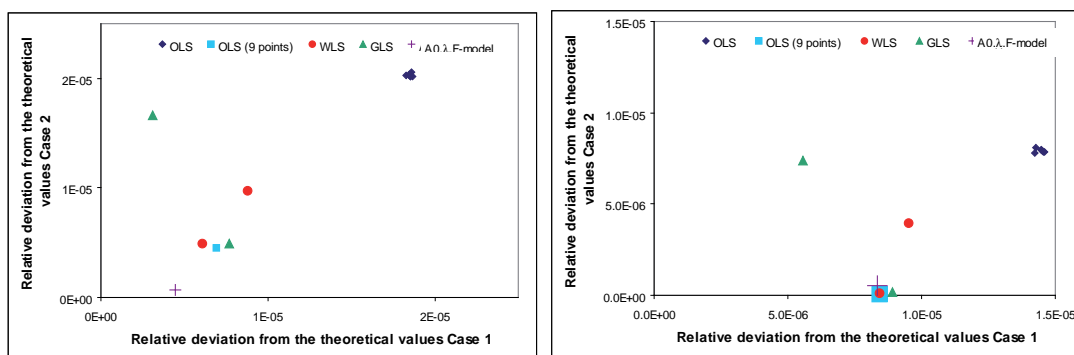


Figure 3. Relative deviations from theoretical values, case 2 versus case 1, oil pressure balance calibrations at 5 MPa (left) and 500 MPa (right)



perform typically better than OLS and WLS. However, in one case, LNE gives results close to the ones observed with the ordinary least square method. This confirms that the efficiency of the generalized least square method mainly depends on the estimation of the associated variance-covariance matrix.

- The original approach used by PTB is an interesting alternative that gives results similar to the GLS. In one case, for the high pressure piston, the method even provides more accurate estimate of the effective area parameters.

## 5. Conclusion

For the types of data provided for this project, the most used method, based on the ordinary least squares, gives the less robust results. This method can be significantly improved by not taking into account the lowest pressure points that have the highest uncertainties. The WLS method takes into account the variance of the effective areas and gives results suitable for this type of analysis. The GLS method, which takes into account the uncertainties and the correlation of the effective areas, is more complex but gives more accurate estimates of the parameters. However, attention must be paid to the associated variance-covariance matrix. An interesting and robust methodology is used by PTB. This method assumes the existence of an additional unknown force  $F$ . This approach gives in some cases the best unbiased results. This is a good alternative to the previous ones, however, it requires determining whether the additional force is intrinsic to the calibrated pressure balance or results only from the conditions of the performed calibration.

The estimates of the effective areas  $\hat{A}_p$  determined by all participants agree with the theoretical values  $A_{thp}$  within their standard uncertainties. On the other hand, there are several orders of magnitude of difference in the determination of the uncertainties of the parameters. It is necessary to analyse this point more carefully.

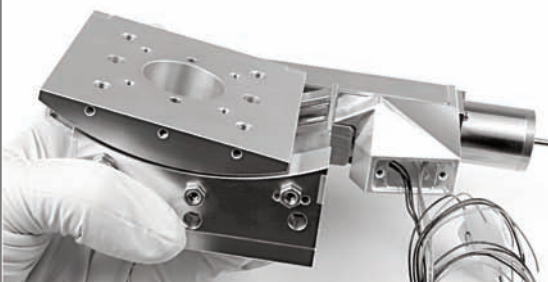


More generally, the results, although consistent with the uncertainties, show relatively large differences in terms of accuracy and uncertainty while all participants had the same input data. Considering the results of this project one wonders whether sometimes, with regards to the efforts which are required to reduce the uncertainties by improvement of hardware, it would not be worthwhile to improve the results by better calculations [7].



## References

- [1] Morgado I. et al, Evaluation of cross-float measurements with pressure balances – EURAMET project 1125
- [2] Evaluation of measurement data – Guide to the expression of uncertainty in measurement, JCGM, September 2008, 100:2008
- [3] Sutton C.M., Fitzgerald M.P. and Giardini W., Metrologia **42** (2005) S212–S215
- [4] Milton M.J.T., Harris P.M., Smith I.M., Brown A.S. and Goody B.A., Metrologia **43** (2006) S291–S298
- [5] Sutton C.M., Metrologia **41** (2004) 272–277
- [6] Youden W.J., Industrial quality control, **15** (1959) N0 11
- [7] Krystek M. and Anton M., Meas. Sci. Technol., **22** (2011) 035101

VACUUM

precision made in germany

77 K upto 100°C • Up to UHV • Custom design

Get the new **MOTION CONTROL** catalog!  
 Phone: + 49 7634 50 57 - 0 | [www.micos.ws](http://www.micos.ws)

# Comparison between GUM and Monte Carlo uncertainty frameworks in pressure field

Salustiano Ruiz<sup>1</sup>, Nieves Medina<sup>1</sup>

## Abstract

A comparison between the results of an uncertainties assessment, using different approaches, of the calibration of pressure standards (mercury column, piston cylinder assemblies and static expansion system) is made. First a classical GUM analysis is performed using the Welch-Satterthwaite formula and supposing different degrees of freedom for the uncertainties components estimated by the type B method. These results are compared with the ones obtained by Monte Carlo simulation suggested in the GUM Supplement 1. In all cases the same mathematical model is used and the same assumptions for the different uncertainty components are made. The obtained results demonstrate the equivalence of both methods for all cases except in the characterization of the static expansion system where GUM method reached different values due to the fact that the mathematical model used is significantly nonlinear.

## 1. Introduction

Traditionally the method used for the uncertainty calculation pressure has been the defined in GUM [1], but it has some limitations. That is the reason why this work uses the Monte Carlo method [2] like a validation procedure, as it provides a general

numerical approach for the probability density function. Both methods have been applied, as a part to the work of the PHD Thesis of S. Ruiz [3], in a mercury column, the calibration of two different piston-cylinder assemblies (digital and conventional) and the calibration of static expansion system.

The results are very close for the mercury column and piston-cylinder assemblies cases. As example, we only are showing the mercury column case. However the results are different in the static expansion system case.

Monte Carlo method has been put into practice by means of MS Excel software implementing random number generators developed by Alan Steele (NCR-CNRC) [4] using 100 000 samples in the evaluation. In order to obtain the 95,45 % coverage interval, the probability density function tails containing 2.275 % of the values have been eliminated.

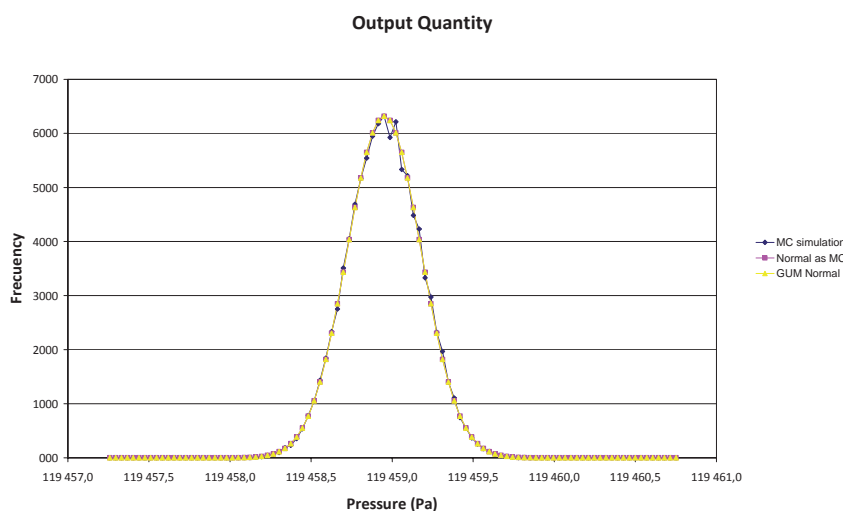
## 2. Mercury column.

The mathematical model for the pressure uncertainty calculation in the mercury column case is provided by equations (1), being the mercury

$$p_m = (\rho_{\text{Hg}} - \rho_a) \cdot (g_1 + \delta g_1) \cdot (\sum \Delta h_r + \sum \delta h_r + \sum \Delta h_m + \sum \delta h_m) + (\rho_{\text{N}_2, m} - \rho_a) \cdot g_1 \cdot \Delta H_{(\text{Hg}, m - \text{N}_2, m)} + (\rho_{\text{N}_2, r} - \rho_a) \cdot g_1 \cdot \Delta H_{(\text{Hg}, r - \text{N}_2, r)} + (p_r + \sum \delta p_r) \quad (1)$$

density calculated by (2) [5]; where  $\rho$  means density,  $g_1$  is the gravity acceleration,  $h$  is the height difference between the mercury surfaces,  $H$  is the height difference between the mercury surface and the reference level,  $t$  is the temperature of the mercury,  $A$  and  $B$  are the mercury thermal coefficients and  $\chi$  the mercury pressure coefficient. The subscripts mean "Hg" mercury, "a"

Figure 1. Probability density function for CEM mercury column.



<sup>1</sup> Salustiano Ruiz, Nieves Medina, Centro Español de Metrología (CEM), Alfar 2, 28019 Tres Cantos (Madrid), Spain, Email of corresponding author: sruiz@cem.mityc.es; mnmedina@cem.mityc.es

$$\rho_{\text{Hg}} = \frac{\rho_{\text{Hg}}(t, \bar{p}_{\text{Hg}}) + \delta\rho_{\text{Hg}}(t, \bar{p}_{\text{Hg}})}{1 + A\left((t + \sum \delta t) - 20\right) + B\left((t + \sum \delta t) - 20\right)^2} \left[ 1 - \chi\left(\frac{p_m + p_r}{2} - 101\,325\right) \right] \quad (2)$$

air, “N<sub>2</sub>” nitrogen, “l” local, “r” reference column and “m” measurement column.

In this case, the dominants input quantities are by the density, temperature and repeatability. The output function clearly follows a Gaussian distribution and Monte Carlo method and GUM uncertainty framework provide the same results. Figure 1 shows an example for 120 kPa relative pressure.

### 3. Static expansion system

For the static expansion system two methods of evaluation have been used: single expansion and gas accumulation. The expansion ratio determination in the single expansion case has been performed according to equation (3) where *f* is the expansion ratio, *v* is the volume, *p* is the pressure, *T* is the temperature, *g* deals with the fact that the gas does not perform as an ideal gas, and *o* is the outgassing. The subscripts mean *L* large volume, *s* small volume, *o* initial and *f* final.

$$f = \left( \frac{v_s}{v_s + v_L} \right) = \frac{p_{L,f} + \delta p_L \frac{T_{s,0}}{T_{L,f}} + \delta T_{p,0}}{p_{s,0} + \delta p_s \frac{T_{L,f}}{T_{L,f}} + \delta T_{L,f}} g + \delta o \quad (3)$$

Although in this case Monte Carlo method provides a distribution which is non-Gaussian (see Figure 2), the uncertainties value obtained by both methods are the same, 0.001 4 × *f*.

The Monte Carlo simulation results are shown in blue while the propagations results in yellow. The pink line represents a normal distribution function with uncertainty similar to the Monte Carlo method.

The expansion ratio determination in the gas accumulation case has been performed according to equation (4) and (5) with all the notation used previously and *n* the number of expansions.

$$f = \left[ 1 - \left( 1 + f\alpha - \frac{(p_L + \delta p_L)_n}{(p_s + \delta p_s)} \right)^{\frac{1}{n}} \right] g + \delta o \quad (4)$$

$$\alpha = \left( \frac{\Delta T}{T_0} \right)_n + \sum_{i=1}^n \frac{\Delta T_i}{(T_0)_{n-i}} (1-f)^i = a_0 + \sum_{i=1}^n a_i (1-f)^i \quad (5)$$

In this case the uncertainties values are different, 0.000 13 × *f* according to Monte Carlo method and 0.000 26 × *f* according to the GUM uncertainty framework. In addition, the Monte Carlo method provides a distribution that is very far from a Gaussian distribution as shown in Figure 3.

### 4. Result and Conclusion

In the case of CEM mercury column and pressure balance the same results are obtained by both methods.

However in the case of the static expansion system the results are different. In the single expansion method, the uncertainty takes the same value but different distribution and in gas accumulation there is a great difference both in value as in distribution. This may be due to the fact that the mathematical model used is significantly nonlinear and due to the fact that the thermal uniformity is an input quantity which contribution is clearly dominant.

Figure 2. Probability density function for the expansion ratio in the single expansion method.

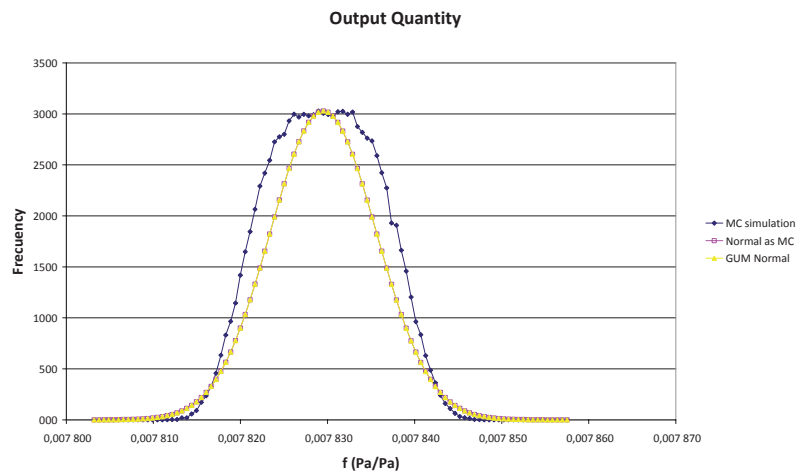
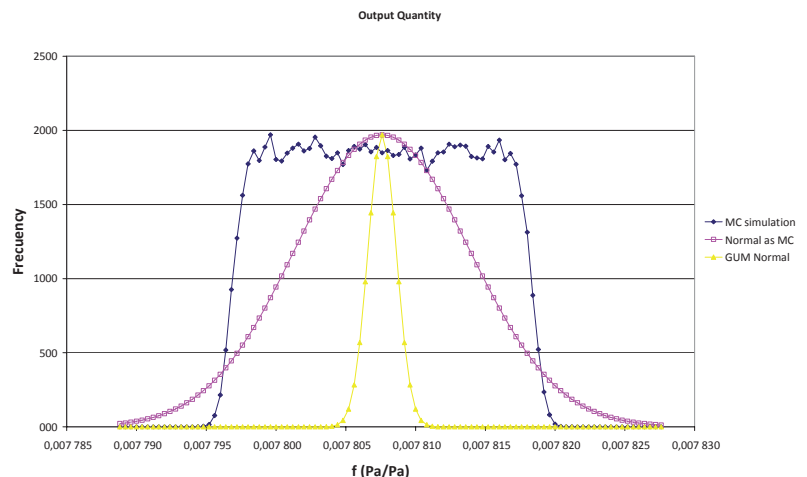


Figure 3. Probability density function for the expansion ratio in the gas accumulation method.



## 5. Reference

- [1] "Evaluation of measurement data — Guide to the expression of uncertainty in measurement". JCGM 100:2008 (GUM 1995 with minor corrections). First edition September 2008.
- [2] "Evaluation of measurement data — Supplement 1 to the "Guide to the expression of uncertainty in measurement" — Propagation of distributions using a Monte Carlo method". JCGM 101:2008. First edition 2008.
- [3] "Tesis Doctoral – Desarrollo de un nuevo patrón nacional de presión. Desde la columna de mercurio a patrones primarios de vacío". S. Ruiz. Escuela de Ingenierías Industriales – Universidad de Valladolid. 2011.
- [4] "Simplifications from Simulations". A.G. Steele and R.J. Douglas. NCSLI August 7-11, 2005.
- [5] "Supplementary information for the International Temperature Scale of 1990". Sèvres, BIPM, 1990, 117p.

# The laser interferometric oil manometer with floats

Irina Sadkovskaya<sup>1</sup>, Aleksey Eichwald<sup>1</sup>

The uncertainty of laser interferometric oil manometer (LIOM) at pressures lower than 10 Pa is determined mostly by its repeatability. The last one has been researched in the comparison of two LIOMs having similar design. It has been found to be less than the resolution of LIOM that is 1,4 mPa.

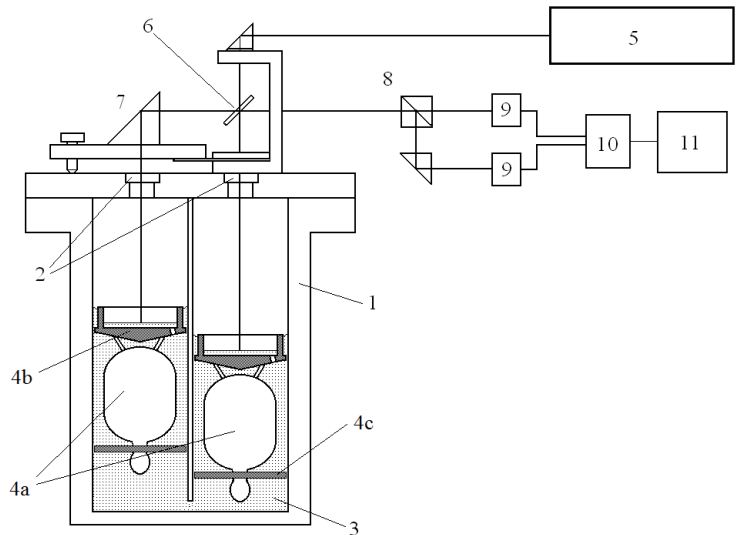
## 1 Introduction

The uncertainty of the laser interferometric oil manometer (LIOM) developed in VNIIM for primary pressure measurements in the range 1 – 1000 Pa had been declared to be  $0,01 \text{ Pa} + 10^{-4} \cdot p$  ( $k=2$ ) [1]. The recent comparison between the LIOM and the national standards of Finland (EURAMET Project № 1151) had rather good results [2] and raised two problems. The first one is the need of specification of the constant part of the total uncertainty independent of pressure. And the second problem is the lack of adequate transfer device compatible with the uncertainty of the LIOM. MKS Baratron 698A11TRA (differential type, the range 0 – 1333 Pa) used for this purpose in that comparison didn't have rather good stability.

## 2 Description of the LIOM

The LIOM design had been described earlier in [1] but its construction in modern version contains few unprincipled changes (Fig. 1). The manometer body is made now of stainless steel block with two honed channels 40,6 mm in diameter. So the device has become more secure than previous one made of glass. As in the former case the distinctive feature of the LIOM is the use of the special floats damping the waves on the oil surface. Now their glass pins touching the walls of manometer tubes have been replaced to teflon ones.

The measurement procedure is as follows. After evacuation the both limbs (measurement and comparison) of LIOM to residual pressure about  $p_0 = 10^{-4} \text{ Pa}$  the pressure change in measurement limb causes the shift of interferometric fringes and can be evaluated as



$$p - p_0 = \rho \cdot g \cdot \frac{N \cdot \lambda}{4} \quad (1)$$

where  $p$  and  $p_0$  are the gas pressure values in the measurement and comparison limbs of the manometer,  $\rho$  is the density of the oil,  $g$  is the acceleration of gravity,  $N$  is the number of counted half-fringes and  $\lambda$  is the wavelength of laser. (The similar equation (1) in [1] contained the term  $N/2$  because  $N$  was the number of whole fringes there.)

## 3 Research of the uncertainty of the LIOM

The constant part of the total uncertainty of the LIOM includes the resolution of the device (0,0014 Pa or one half fringe) that should be attributed to systematical effects. On the other hand it represents the measurement repeatability reduced by random effects. The most important of them is friction between the float pins and the walls of the tubes that leads to unstable sinking of the floats. But due to the free flow of the oil through the holes in the bottom of the float cups (Fig.1) it could show itself only through the unstable curvature of the oil surface (the capillary effect). The stability of curvature has been researched earlier in direct measurements with interferometric technics [1]. It was found that eve-

Figure 1. The construction of the LIOM  
1 – U-tube made of stainless steel; 2 – optical windows; 3 – mineral oil used in diffusion pumps; 4a – glass bulbs of floats; 4b – teflon cups; 4c – teflon pins; 5 – He-Ne laser; 6 – half mirror; 7 – prism; 8 – polarization beam splitter; 9 – photodiodes; 10 – interface scheme; 11 – computer.

<sup>1</sup> Irina Sadkovskaya, Aleksey Eichwald, D.I. Mendeleev All-Russian Institute for Metrology (VNIIM), Moskovsky pr. 19, 190005 St. Petersburg, RF, Email of corresponding author: siv@vniim.ru

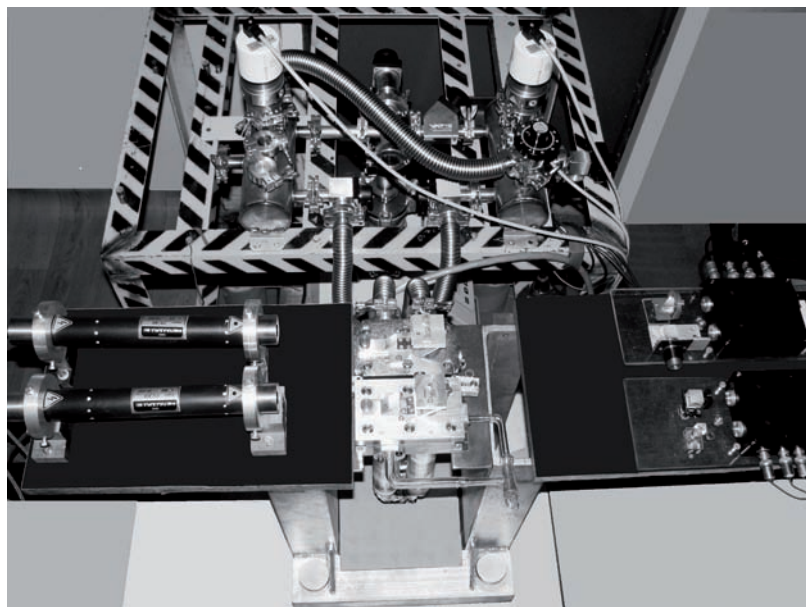


Fig. 2. Comparison between the LIOM and its copy

ry float contributed about 1,4 mPa to the uncertainty of pressure measurement (the coincident with the resolution was occasional). But that method was not sensitive enough and very laborious.

Now the alternative and more simple approach has been developed to research the repeatability more directly. For this aim the modern LIOM has been compared with its previous version and the statistics of their discrepancies has been analyzed. The idea of such comparison is as follows. If these discrepancies are measured at the certain nominal pressure many times then their standard deviation characterizes the repeatability of the worst device including all random effects (not only capillary ones). More direct manner is scarcely possible because it would demand to create absolutely the same pressure value many times.

Two LIOMs were connected tight together

(Fig.2) measuring the same pressure. The measurements were performed at low enough nominal pressure values (0,5; 1,0; 2,0 Pa) so the influence of possible temperature instability was negligible. It had been done 10 runs in increasing direction of pressure (Table 1). Every value  $\Delta N$  is the discrepancy of two LIOMs averaged over 128 readings during 5 seconds.

One can see that standard deviations of  $\Delta N$  don't exceed the resolution of the LIOM. It means that both LIOMs have rather high repeatability in spite of little difference in their device.

#### 4 Conclusion and prospects

The constant part of the LIOM's uncertainty could be reevaluated to about 0,003 Pa ( $k=1$ ) and now the task arises to improve the resolution of the LIOM reading device to 0,1 – 0,01 of fringe and to repeat the comparison of two LIOMs after that. It demands to modernize the electronic system notably (to use analog-digital (8-10 digits) conversion of the interference signal). The improvement of the LIOM resolution could lead to further decrease of the uncertainty.

The good performance of the manometer floats permits to develop the transportable version of the LIOM. There is no need to create the complex vibration protection for it and its stability would depend only upon the uncertainty of the temperature in laboratory.

#### Literature

- [1] Sadkovskaya I.V., Eichwald A.I.: A laser interferometric oil manometer as the primary standard for absolute pressure in the range 1-1000 Pa. Journal of Physics: Conference Series 100 (2008) 092006.
- [2] [http://www.mikes.fi/documents/upload/j1\\_2010.pdf](http://www.mikes.fi/documents/upload/j1_2010.pdf)

Table 1. The results of comparison between two LIOMs

Run, n	Nominal pressure, Pa					
	0,5		1,0		2,0	
	Pressure, Pa	$\Delta N$	Pressure, Pa	$\Delta N$	Pressure, Pa	$\Delta N$
1	0,50	0,1	0,99	-0,9	2,03	0,9
2	0,50	-1,0	1,00	-0,2	2,00	-0,7
3	0,50	-1,4	1,02	0,0	2,03	-0,2
4	0,51	-0,9	1,01	-0,6	2,01	-0,7
5	0,51	0,4	1,02	-0,8	2,02	-0,2
6	0,50	-0,2	1,02	0,5	2,00	0,6
7	0,51	-0,6	1,01	1,0	2,04	0,0
8	0,50	-0,8	1,01	0,1	2,02	-1,5
9	0,51	0,1	1,01	0,6	2,00	0,1
10	0,50	-0,2	1,01	0,1	2,04	-1,3
Mean value		-0,4		0,0		-0,3
Standard deviation		0,57		0,60		0,77

# The Mercury Micromanometer at PTB

J. Könemann<sup>1</sup>, S. Ehlers<sup>1</sup>, M. Jescheck<sup>1</sup>, W. Sabuga<sup>1</sup>

## Abstract

In this work, we present for the first time the mercury micromanometer experiment at PTB. Our system consists of a classical three-limb U-tube manometer for gauge pressures in the range of (-10 to 10) kPa and absolute pressures in the range between 170 mPa and 10 kPa. The length determination of the mercury columns is performed by plane mirror interferometer systems and heterodyne signal processing. As a result, we are able to demonstrate first measurements of the operation and a preliminary estimation of the combined measurement uncertainty.

**Keywords.** Low pressure, Interferometers, Units and standards, Mass and density

## 1. Introduction

According to key comparison CCM.P-K4 [1], interferometric mercury U-tube manometers are the most accurate primary standards for low absolute pressure in the range between 1 Pa and 1 kPa. Being fundamental instruments, they can be used for the low pressure verification of newly developed force-controlled non-rotating piston gauges [2,3,4], which are usually calibrated at pressures above 5 kPa but can be operated at significantly lower pressures. Usually, U-tube manometers allow both absolute and differential pressure measurements to be carried out with a minimum effort of time, and thus they have been chosen as an alternative to the diving-bell manometers [5,6] used for the measurement of small atmospheric pressure differences at PTB so far.

## 2. Experimental set-up and results

The micromanometer constructed and built at PTB has been designed as a classical U-tube manometer. In addition to the two limbs of the U-tube used for the pressure measurement, our micromanometer comprises a third tube acting as a sensor for temperature fluctuations and for calibration of the optical path length in the gas subjected to the measured pressure.

All three tubes have an utilizable length of 100 mm and an inner diameter of 60 mm and they contain floats carrying plane mirrors swim-

ming on top of the mercury surface. The manometer is filled with 0.53 l of mercury as the manometric liquid provided by NIST and calibrated by the ASMW by a method described in Ref. [7-8]. Here, the pressure is directly related to the interferometrically measured difference between the lengths of the liquid columns in the limbs of the U-tube, see Fig. 1(a) and (b).

Since the density of the mercury used and the local gravitational acceleration are known with high accuracy, measured pressure differences and absolute pressures can be calculated from this length difference tracing back the pressure unit to the base units of mass, length and time. Thus, a basic input for the pressure determination is the mercury temperature which is measured by a series of calibrated ( $\Delta T \approx 10$  mK) Pt-25 standard resistors together with an ASL inductive bridge and scanner, where six temperature sensors are attached to the manometer cells close to the liquid as well as to the N<sub>2</sub> gas phase and the instrument itself is located inside a temperature stabilized chamber ( $\Delta T \approx 0.5$  K). Although our instrument does not have active temperature control, stable conditions are provided by the external air-conditioning system and the cooling of the laser receivers, the tubes and the low standby-power servo valves inside the capsuled enclosing. Hence, a long-term standard uncertainty of  $\Delta T < 20$  mK is achieved, see Fig. 1 (c).

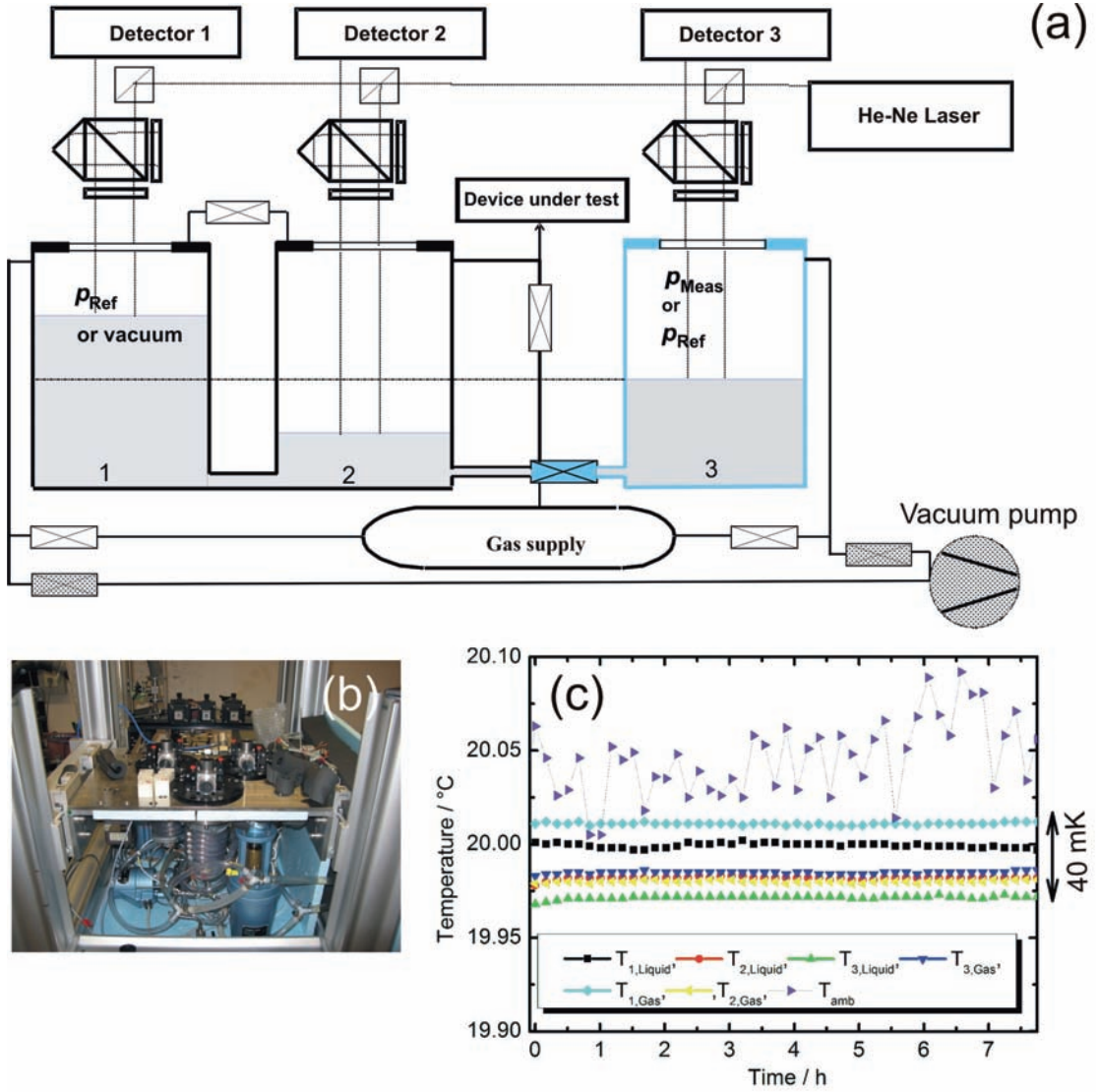
The length measurement of the mercury columns in the individual cells is performed with a commercial high-stability plane mirror interferometer HP10706B together with a laser axis board HP10897B allowing a final resolution of  $\lambda/1024$  corresponding to  $\Delta p < 1$  mPa (using a He-Ne laser with wavelength  $\lambda \approx 633$  nm) and a thermal stability of  $0.04 \mu\text{m}/^\circ\text{C}$ . Such a system with heterodyne signal processing enables robust operation, i.e. it allows pressure changes without signal outage. From the producer's datasheet the combined measurement uncertainty of the interferometer is estimated as  $u_{L,1\sigma} \sim 0.003 \mu\text{m} + 0.22 \cdot 10^{-6}L$  with the displacement length  $L$ .

In order to calculate the measured pressure  $p$ , we apply the expression

<sup>1</sup> J. Könemann, S. Ehlers, M. Jescheck, W. Sabuga, Physikalisch-Technische Bundesanstalt, Bundesallee 100, 38116 Braunschweig, Germany, E-mail: Jens.Koenemann@ptb.de



Fig. 1 (a): Block diagram of the micromanometer. (b) Photograph of the micromanometer. (c) Temperature dependence of the three cells of the micromanometer over a time period of 7.5 h.



$$p = g \cdot (\rho_{z1} \cdot h_{z1} - \rho_{z2} \cdot h_{z2} + l_{zero} \cdot \rho_0) \quad (1)$$

with  $g$  being the local acceleration of gravity and  $\rho_0$  as the mercury density at 20 °C. It also contains a contribution  $l_{zero} = 0$  with standard uncertainty  $\Delta l_{zero} = 130$  nm which is not used for the pressure calculation but instead as the zero pressure uncertainty for the estimation of the measurement uncertainty. As well the thermal expansion of the mercury in cells 1 and 2 is included, i.e.

$$\rho_{z1,2} = \rho_0 / (1 + A \cdot (T_{z1,2} - 20^\circ\text{C}) + B \cdot (T_{z1,2} - 20^\circ\text{C})^2) \quad (2)$$

where  $A$ , or resp.  $B$  denote the thermal expansion coefficients of Hg and  $T_{z1,2}$  the temperature in the two cells. The displacement of the mercury columns in the limbs is given by

$$h_{z1,2} = \lambda/2 \cdot (\Phi_{z1,2} - \Phi_{z1,2,0}) - l_{z1,2,Hg} \quad (3)$$

with  $\Phi_{z1,2}$  being the interferometer fringes of cells 1 and 2 resp. after pressurization,  $\Phi_{z1,2,0}$  being the interferometer fringes of cells 1 and 2 resp. at zero pressure and  $l_{z1,2,Hg}$  the linear thermal expansions of the mercury columns in cells 1 or 2.

For a first validation we focused on the stability and reproducibility of the zero pressure. Typical measurements are displayed in Fig. 2 (a) where both short time fluctuations and also deviations in the repetition of the zero pressure after pressure changes are visible.

These unwanted effects limit the zero-pressure resolution of the manometer, and from the histogram of a time-trace of such measurements for constant pressure we extract a standard uncertainty of  $\Delta \approx 86$  nm, cf. Fig. 2 (b). On the other hand, Fig. 2 (a) shows that the zero-point values  $\langle L_3 - L_1 \rangle$  scatter after repetitive pressure changes in a range of approx. 230 nm. Thus, after geometric summation with the half histogram width one ends up with a corresponding zero-point uncertainty  $\Delta l_{zero} \approx 130$  nm leading to a pressure uncertainty of approx. 17 mPa. This value addresses the most important contribution to the constant part of the combined measurement uncertainty, whereas another contribution is given by the residual pressure  $p_{Res}$ .

Table 1 summarizes all relevant contributions. As a result, we are able to estimate the combined standard measurement uncertainty of absolute pressure as follows:

$$u(p) = \left( 4.0 \cdot 10^{-4} + 1.3 \cdot 10^{-9} \cdot p / [\text{Pa}] + 1.2 \cdot 10^{-11} \cdot p^2 / [\text{Pa}]^2 \right)^{0.5} \text{ Pa} \quad (4)$$

This relation is displayed in Fig. 3.

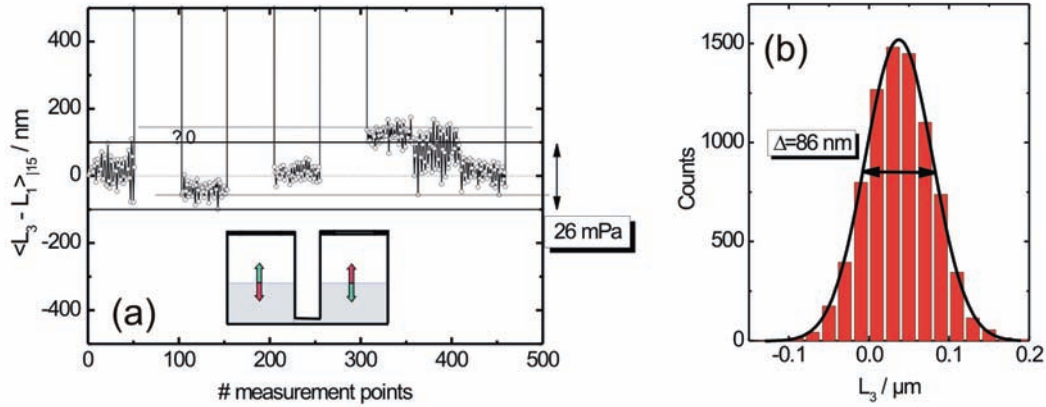


Fig. 2: (a) Difference of the column displacement of cells 3 and 1 averaged over 15 data points (of constant pressure) after pressure changes. (b) Histogram of the time-trace of a typical zero pressure measurement (no pressure changes).

Quantity	Value	Standard uncertainty
$g$	9.812533 m/s <sup>2</sup>	2.1·10 <sup>-6</sup> m/s <sup>2</sup>
$\rho_0$	13545.84 kg/m <sup>3</sup>	0.0068 kg/m <sup>3</sup>
$A$	1.812·10 <sup>-4</sup> K <sup>-1</sup>	0
$B$	8.0·10 <sup>-9</sup> K <sup>-2</sup>	0
$l_{\text{zero}}$	0 m	130 nm
$p_{\text{Res}}$	170 mPa	10 mPa
$t_{\text{Hg}}$	[19; 20] °C	20 mK
$L$	[0; 75] mm	0.003 $\mu\text{m}$ + 0.22·10 <sup>-6</sup> · $L$

Table 1: Numerical values used to calculate the combined measurement uncertainty.

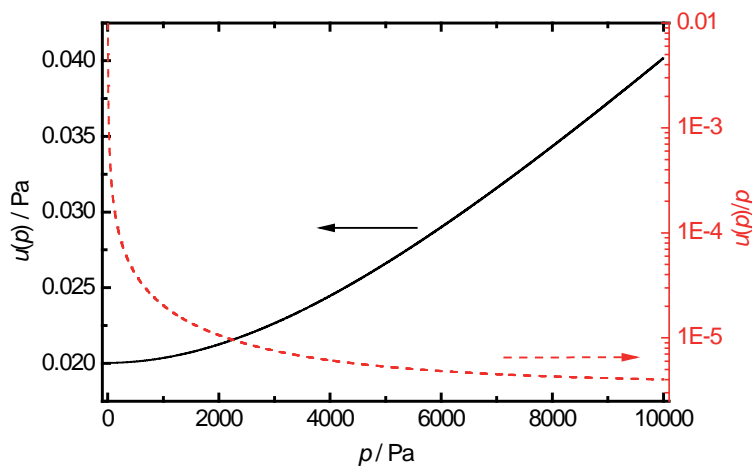


Fig. 3: Plot of the combined standard measurement uncertainty of the micromanometer.

### 3. Conclusion

In this paper, we have presented the PTB mercury micromanometer as a classical three-limb U-tube manometer for gauge pressures in the range of (-10 to 10) kPa and absolute pressures in the range between 170 mPa and 10 kPa with a column length determination by optical plane mirror interferometers with heterodyne signal processing. A first validation of the micromanometer has demonstrated its robust operation, and a preliminary estimate of the measurement uncertainty is given.

### References

- [1] *Miiller A.P., Bergoglio M., Bignell N., Fen K.M.K., Hong S.S., Jousten K., Mohan P., Redgrave F.J. and Sardi M.*: Final report on key comparison CCM.P-K4 of absolute pressure standards from 1 Pa to 1000 Pa, *Metrologia*, 39 (2002), 07001.
- [2] *Ooiwa A.*: Novel nonrotational piston gauge with weight balance mechanism for the measurement of small differential pressures, *Metrologia*, 30 (1994), 607.
- [3] *Delajoud P., Girard M.*: Piston gauge with electronic balance for calibrations of very low pressures, *Vakuum in Forschung und Praxis*, 15 (2003), 24.
- [4] *Rendle C.G., Rosenberg H.*: New absolute pressure standard in the range 1 Pa to 7 kPa, *Metrologia*, 36 (1999), 613.
- [5] *Ahrendt H.*: Vergleichsmessungen von Tauchglockenmanometern, *PTB-Mitteilungen*, 102 (1992), 463.
- [6] *Perkin M., Rendle J., Jäger J., Deken P., Eldred K., Woodhead E., Härne G., Rantanen M., Thrane M., Le Guinio J. and Sardi M.*: Comparison of European differential pressure standards in the range 3 Pa to 1000 Pa, *Metrologia*, 36 (1999), 1.
- [7] *Adametz H., Wloka M.*: Measurements of the absolute density of mercury in the ASMW, *Metrologia*, 28 (1991), 333.
- [8] *Sommer K.D., Poziemski J.*: Density, thermal expansion and compressibility of mercury, *Metrologia*, 30 (1993/94), 665.

# Static Expansion System Validation at CEM

D. Herranz<sup>1</sup>, N. Medina<sup>1</sup>, S. Ruiz<sup>1</sup>, J. Torres-Guzmán<sup>2</sup>

## Abstract

The static expansion system of CEM has been validated by a comparison with a force-balanced piston gauge and the static expansion system of CENAM by using a capacitive diaphragm gauge (CDG 133.32 Pa) and a spinning rotor gauge (SRG) as transfer standards. This paper shows the results of this validation.

## 1. Description of the system

Static expansion systems or series expansion systems are used as primary standards to generate pressures in the range of high, medium and low vacuum. Static expansion systems consist of several chambers of different volumes of capacity connected by valves and connected to a system of pressure and vacuum generation.

The static expansion system of CEM (Figure 1) consists of five chambers, two of 100 L, two of 1 L and one of 0.5 L nominally connected through a common duct with volume  $V_c$ .

There are several techniques for the accurate determination of expansion ratios. The main ones are the gravimetric technique and the expansion technique. We have used the gas expansion technique with a dead weight pressure balance, a force-balanced piston gauge (FPG8601) and a differential pressure transducer (CDG 133.32 Pa) (Figure 2). For this task different methods have been used: the gas accumulation method [1] and the single expansion method using the same configuration for both methods [2].

## 2. Validation of the system

In order to validate the system a comparison by use of a capacitive diaphragm gauge (CDG 133.32 Pa) as transfer standard has been made. The results were compared with those obtained using a digital piston cylinder force balance (FPG 8601) at different target points, such as 100 Pa, 50 Pa (Figure 3) and 10 Pa. The calibration was performed using the same CDG but with two different sets of signal conditioner (MKS Type 270D) and sensor selector (MKS Type 274) (R1 and R2 in Figure 3 and 4).

The calibration performed using a digital piston cylinder force balance (FPG 8601) as refer-

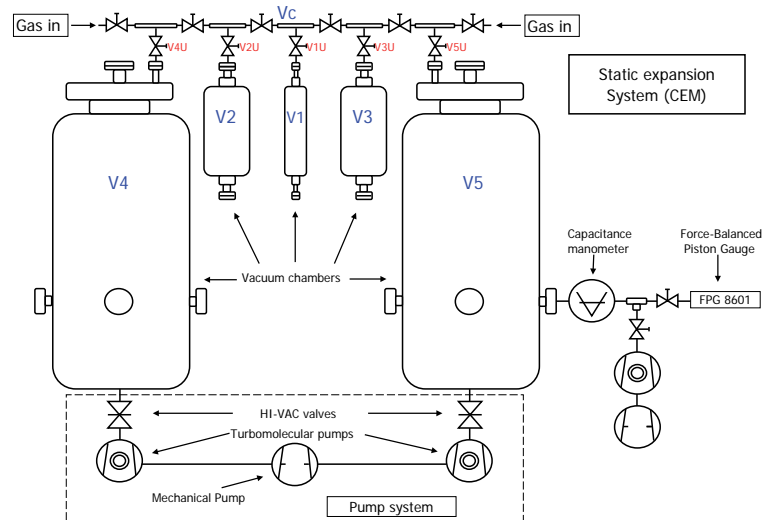


Figure 1. Scheme of static expansion system of CEM. Volumes are denoted with normal letters and numbers, central volume with  $V_c$  and valves with slanted letters and numbers.



Figure 2. Digital piston cylinder connected to the static expansion system SES by a differential pressure transducer CDG.

ence standard has also been carried out using a voltmeter connected to the signal conditioner 9D rear connection for recording the voltage output. The reason for these measurements with different set of signal conditioner and in voltage is the study of the possible influence of these devices in the calibration results. Likewise, calibrations were repeated to assess the stability over time and drift. Figure 3 shows that the effect of all these influences is negligible.

Also, an intercomparison has been performed with the system at CENAM [3] in which has been used the same capacitive diaphragm gauge (CDG), but a different set of signal conditioner

<sup>1</sup> D. Herranz, N. Medina, S. Ruiz, Centro Español de Metrología (CEM), Alfar 2, 28019 Tres Cantos (Madrid), Spain

<sup>2</sup> J. Torres-Guzmán, Centro Nacional de Metrología (CENAM), Querétaro, México  
Email of corresponding author: dherranz@cem.mityc.es; mnmedina@cem.mityc.es

Figure 3. Comparison between static expansion system SES of CEM and electronic balance FPG. The previous number identified the calibration, Rn identified read unit. The last calibration was made to evaluate the drift of the capacitive diaphragm gauge (CDG 133.32 Pa) over the validation.

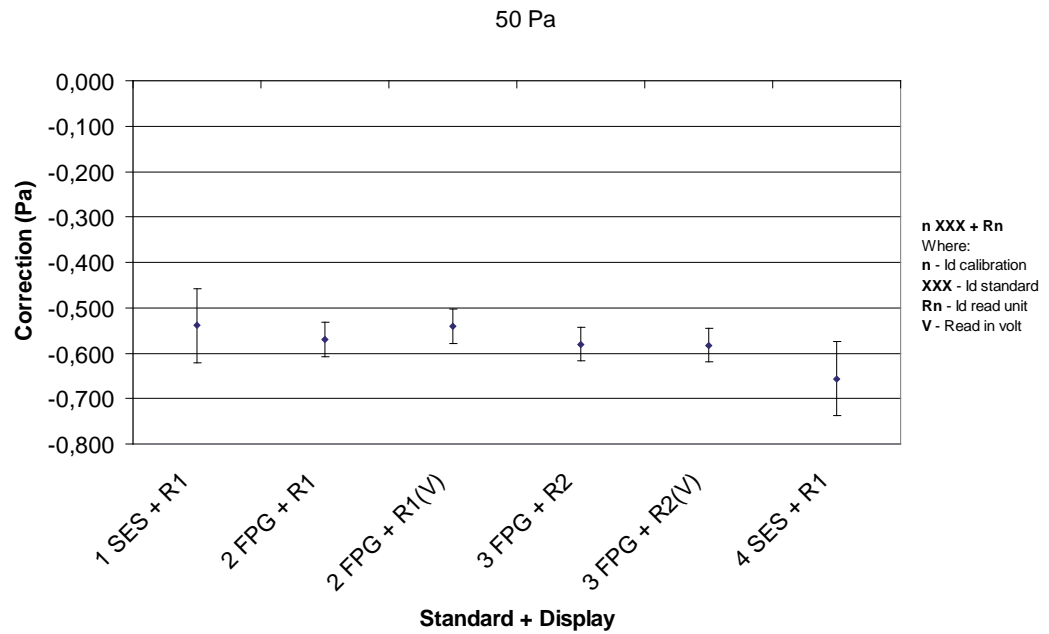


Figure 4. Comparison between CENAM and CEM in 1 Pa with CDG. The previous number identified the calibration, XXX identified the laboratory, YYY identified the standard, Rn identified read unit and V means that the reading was in volts.

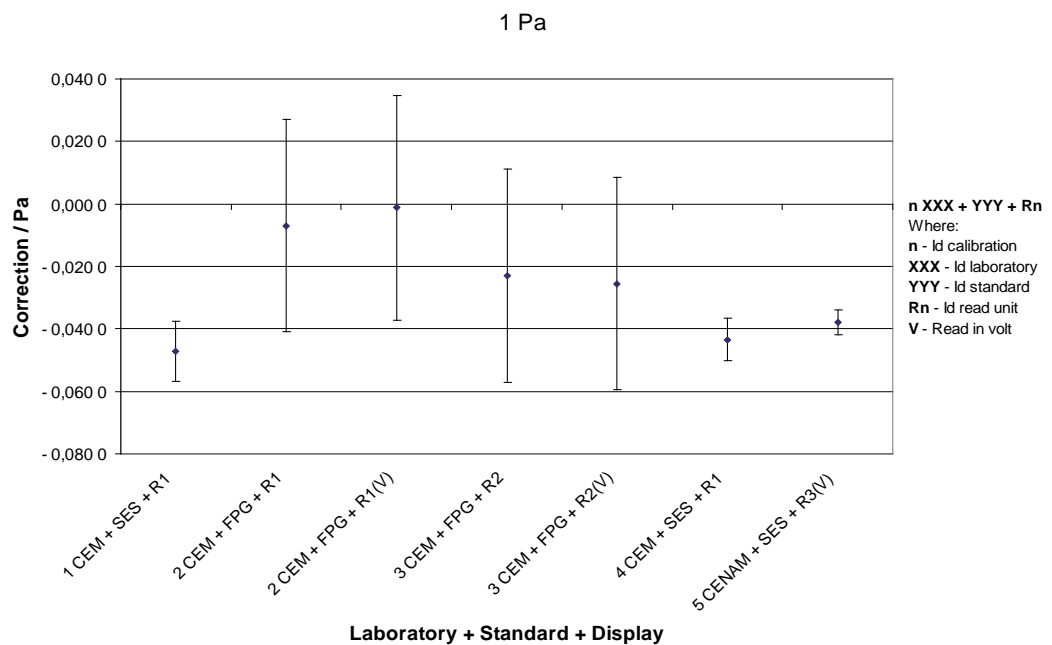
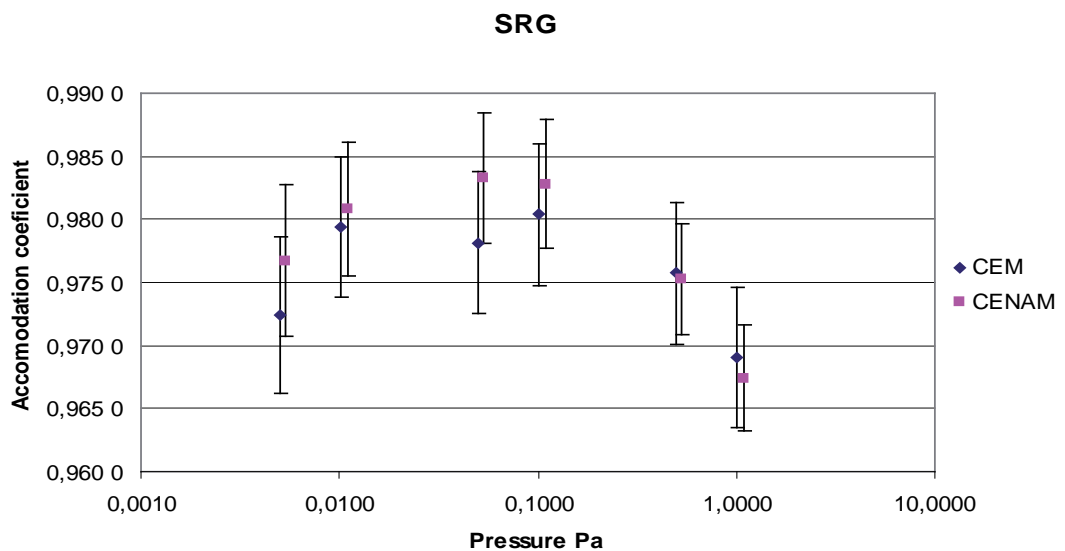


Figure 5. Comparison between CENAM and CEM with SRG



and sensor selector (R3 in Figure 4) and a spinning rotor gauge (SRG), showing the results in Figure 4 for 1 Pa for CDG and in Figure 5 for a SRG.

### 3. Conclusion

As conclusion, in view of the results obtained in the internal comparison made with the capacitive diaphragm gauge (CDG) and an electronic balance (FPG8601) and in the intercomparison carried out with the CENAM, which have used a spinning rotor gauge (SRG) and capacitive diaphragm gauge (CDG), we can consider that our static expansion system has been validated.

### References

- [1] K. Jousten, P. Röhl, V. Aranda Contreras, "Volume ratio determination in static expansion systems by means of a spinning rotor gauge", *Vacuum* 52 (1999) 491-499.
- [2] D. Herranz, S. Ruiz, N. Medina, "Volume ratio determination in static expansion systems by means of two pressure balances", XIX IMEKO World Congress 6-11. September 2009, Lisbon, Portugal, [http://www.imeko2009.it.pt/Papers/FP\\_280.pdf](http://www.imeko2009.it.pt/Papers/FP_280.pdf)
- [3] J. C. Torres Guzman, L. A. Santander, K. Jousten, "Realization of the medium and high vacuum standard in CENAM, Mexico", *Metrologia* 42 (2005) S157-160.

## Wie groß ist Ihr **Toleranzbereich?**



Wer Prozessdrücke im Vakuum zuverlässig und reproduzierbar erfassen und steuern will, muss sich auf seine Messtechnik verlassen können.

Zur Gewährleistung der Sicherheit Ihrer Prozesse empfehlen wir eine regelmäßige Überprüfung und Re-Kalibrierung Ihrer Messgeräte und Testlecks.

Wir bieten

- **Kalibrierungen nach DIN EN ISO/IEC 17025:2005** der Messgrößen Absolutdruck und Leckrate
- **Kalibrierte Testlecks**
- **Lecksuchgeräte und Kalibriersysteme für die Vakuumtechnik**

Überzeugende Details finden Sie unter

[www.oerlikon.com/leyboldvacuum](http://www.oerlikon.com/leyboldvacuum)

Oerlikon Leybold Vacuum GmbH  
Bonner Straße 498  
D-50968 Köln  
T +49 (0)221 347-0  
F +49 (0)221 347-1250  
[info.vacuum@oerlikon.com](mailto:info.vacuum@oerlikon.com)  
[www.oerlikon.com/leyboldvacuum](http://www.oerlikon.com/leyboldvacuum)

**oerlikon**  
leybold vacuum

# Characterization of the medium and high vacuum primary standard at CENAM, Mexico

A. Navarro-Nateras<sup>1</sup>, J. C. Torres-Guzman<sup>1</sup>

Figure 1. Static expansion system at CENAM.

## Abstract.

A static expansion systems (SEE-1) is the primary standard for vacuum at the Centro Nacional de Metrología, this system has four volumes, it's measurement range is from  $10^{-4}$  Pa to  $10^3$  Pa. This article describe a new characterization of the system, basically the determination of the expansion ratios by two methods: the gas accumulation method and the method with a linearized spinning rotor gauge (SRG).

## 1. Introduction

The Centro Nacional de Metrología (CENAM, Mexico), has a static expansion system with a range from  $10^{-4}$  Pa to  $10^3$  Pa [1]. Some improvements were carried out to optimize the system and obtain its best capabilities. A new characterization of the system was performed.

### 1.1 Measurement principle and system description

Gas is introduced in a previously evacuated volume  $V_0$  up to a pressure  $P_0$ , high enough to be measured with high accuracy. After measuring  $P_0$ , the gas is expanded to a previously evacuated volume  $V_f$  which is bigger than  $V_0$ . Since ideal gases behavior is not possible to obtain, the real generated pressure has to be obtained including a correction due to this effect [2]. The calibration volume pressure is determined from:

$$P_f = P_0 \cdot f \cdot \frac{T_f}{T_0} \cdot \frac{1 + B_f \cdot P_f / (R \cdot T_f)}{1 + B_0 \cdot P_0 / (R \cdot T_0)} \quad (1)$$

Where,  $T_0$  is the gas initial thermodynamic temperature,  $T_f$  the gas final thermodynamic temperature,  $R = 8\,314\,472$  Pa·L/(mol·K) and  $B_{0,f}$  the virial gas coefficients. The static expansion system (SEE-1) has 4 volumes ( $V_1=0.5$  L,  $V_2=50$  L,  $V_3=1$  L,  $V_4=100$  L). Figure 1 shows SEE-1.

In the SEE-1 the calibration chamber is  $V_4$ . Table 1 shows the different expansion paths in the SEE-1. Table 2 shows the SEE-1 pressure ranges obtainable by combining expansion paths.



Table 1. Expansion paths identification.

Identification	Expansion path
$f_A$	$V_1 \rightarrow V_1 + V_x + V_2$
$f_B$	$V_1 \rightarrow V_1 + V_x + V_2 + V_3$
$f_C$	$V_3 \rightarrow V_3 + V_4$

Table 2. Expansion paths required according to the pressure range.

Pressure range	Expansion paths
$10^{-5}$ Pa to $10^{-3}$ Pa	$f_A f_A' f_B' f_C$
$10^{-3}$ Pa to $10^{-1}$ Pa	$f_A' f_B' f_C$
$10^{-1}$ Pa to $10^1$ Pa	$f_B' f_C$
$10^1$ Pa to $10^3$ Pa	$f_C$

## 2. Expansion Ratio Determination

The SEE-1 expansion ratios were determined by 2 different methods as part of the characterization, the gas accumulation method and the SRG method.

- The gas accumulation method consists in the realization of successive expansions from  $V_0$  to  $V_f$  [1, 3]. With the system evacuated, a pressure of 100 kPa is established in  $V_0$  using nitrogen as media; then the gas is expanded into the evacuated  $V_f$ . The pressure of 100 kPa is re-established in  $V_0$  and the gas is expanded again, these expansions are repeated until the pressure in  $V_f$  can be measured with good accuracy. After  $N$  expansions under isothermal conditions the expansion ratio is:

$$f = 1 - \left( 1 - \frac{P_{fN}}{P_0} \right)^N \quad (2)$$

- SRG Method [1, 4]. For this method a SRG is used to measure the pressure, both before and after the gas expansion. Firstly, the SRG

<sup>1</sup> Navarro-Nateras, J. C. Torres-Guzman, Centro Nacional de Metrología (CENAM), Mexico. km 4.5 Carretera a Los Cues, Municipio El Marques, Queretaro, tel. +52(442)211 05 00, fax +52(442)211 05 78, anavarro@cenam.mx; jorge.torres@cenam.mx

offset is determined, the initial pressure is established in  $V_0$  then the gas is expanded into the evacuated  $V_f$ ; the deceleration rate DCR1 is measured. Then, the valve between  $V_0$  and  $V_f$  is closed,  $V_f$  is evacuated until it reaches similar values of the offset, the gas retained in  $V_0$  is again expanded and the deceleration DCR2 is measured. Under isothermal conditions and without a linearization of the deceleration rate, the expansion ratio can be determinate from:

$$f = \left( \frac{DCR1 - OFF}{DCR2 - OFF} \right)^{-1} \quad (3)$$

### 3. SEE-1 improvements performed

To optimize the system and obtain its best capabilities two improvements have been carried out:

- The SEE-1 had only one vacuum pumping system with mechanical and turbomolecular pumps in the vacuum chamber ( $V_4$ ). A new vacuum pumping system with mechanical and turbomolecular pumps has been installed to  $V_2$  to reduce evacuation time.
- Initially the SEE-1 had seven temperature sensors, these sensors were difficult to calibrate and their metrological properties were not ideal. Now, the SEE-1 has twelve Pt-100 sensors with better metrological properties and easier calibration performance.

### 4. Results of the Characterization

#### 4.1 SEE-1 outgassing.

Table 3 shows the measurements made to SEE-1 to evaluate outgassing (by means of a SRG). The maximum pressure increase is  $1.36 \times 10^{-8} \text{ Pa} \cdot \text{s}^{-1}$ , which corresponds to a specific outgassing of  $8.32 \times 10^{-11} \text{ Pa} \cdot \text{L} \cdot \text{s}^{-1} \cdot \text{cm}^{-2}$ . The lowest calibration pressure at the SEE-1 is  $10^{-4} \text{ Pa}$  and the pressure rise after 5 minutes is  $4.08 \times 10^{-6} \text{ Pa}$ , this value corresponds to the 4.08% of  $10^{-4}$ .

#### 4.2 Expansions ratios.

The three expansions ratios of the SEE-1 were determined using the gas accumulation and the SRG method. For the gas accumulation method,

2 temperature sensors were installed in  $V_0$  and 8 in  $V_f$ . In  $V_f$  a recently calibrated absolute manometer with a maximum range of 100 kPa was connected. To establish the pressure in  $V_0$  a pressure controller with a range of 200 kPa was used. Firstly,  $V_f$  was evacuated, a pressure of 100 kPa was established in  $V_0$  with the pressure controller and its temperature was recorded. Then, the nitrogen was expanded to  $V_f$  after the pressure relaxation the temperature of the sensor on  $V_f$  were read and the reading of the absolute manometer taken. The same expansion was repeated 23 times until the absolute manometer pressure indicated around 20 kPa. The expansion ratio was calculated from [1, 4]:

$$f = 1 - \left( 1 + f \cdot \alpha - \frac{P_{fN}}{P_0} \right)^N \quad (4)$$

Where  $N$  is the number of expansions to reach pressure  $P_{fN}$  with a pressure  $P_0$  of 100 kPa.  $\alpha$  is a temperature gradient correction factor between the 2 volumes and the temperatures changes over time.

$$\alpha = \sum_{i=1}^N (1-f)^{i-1} \frac{(T_f)_N - (T_0)_{1+N-i}}{(T_0)_{1+N-i}} \quad (5)$$

To solve equation (4),  $f$  was calculated without the temperature correction  $\alpha$ , and this value of  $f$  was used to calculate  $\alpha$ . With these values  $f$  was calculated by means of (4), and with this new value of  $f$  equation (5) was solved. This calculations were repeated until equation (4) was solved adequately. Equation (4) is valid for an ideal gas, the deviations were corrected with equation:

$$f_{corr} = f(1 - B \cdot \rho_m) \quad (6)$$

Where  $B$  is the nitrogen second virial coefficient and  $\rho_m$  is the gas molar density before the expansion.

$$B = -131.21 + 0.65125 \cdot T - 7.636 \cdot 10^{-4} \cdot T^2 \quad (7)$$

$$\rho_m = \frac{P}{R \cdot T} \quad (8)$$

The correction to eliminate the additional volume  $V_{ad}$  due to the test gauges and its connections to  $V_f$  used is:

Volume	$\Delta P \text{ s}^{-1}$ Pa s <sup>-1</sup>	Specific outgassing Pa·L·s <sup>-1</sup> ·cm <sup>-2</sup>	$\Delta p / 5 \text{ min}$ Pa / 5 min
V4	$1.26 \times 10^{-8}$	$1.05 \times 10^{-10}$	$3.78 \times 10^{-6}$
V4+V3	$1.31 \times 10^{-8}$	$1.06 \times 10^{-10}$	$3.93 \times 10^{-6}$
V2	$1.01 \times 10^{-8}$	$6.61 \times 10^{-11}$	$3.03 \times 10^{-6}$
V2+V1	$1.12 \times 10^{-8}$	$7.10 \times 10^{-11}$	$3.35 \times 10^{-6}$
V2+V1+V3	$1.36 \times 10^{-8}$	$8.32 \times 10^{-11}$	$4.08 \times 10^{-6}$

Table 3. Outgassing results.



$$f_{real} = \frac{1}{\frac{1}{f_{corr}} + \frac{V_{ad}}{V_s}} \tag{9}$$

To calculate the expansion ratios by the SRG method, the SRG offset was determined. For the measurements of DCR1 a pressure between 0.4 Pa and 14 Pa was established in  $V_o$  and for the measurements of DCR2 a pressure between  $4 \times 10^3$  Pa and 0.14 Pa. Equation (3) is valid under isothermal conditions, to correct temperature differences equation (10) is used.

$$f = \left[ \left( \frac{DCR1 - OFF}{DCR2 - OFF} \right) \left( \frac{T_f}{T_o} \right) \right]^{-1} \tag{10}$$

Where  $T_o$  and  $T_f$  are the temperature in  $V_o$  and  $V_f$  respectively. A second order polynomial was used to correct the no linear deceleration with pressure. Table 4 shows the results obtained.

The results obtained when the SEE-1 was established [2] are presented in the table 5. At that time, the expansion ratios were estimated using the gravimetric [1] and the SRG method [4].

Table 4. Results from the two methods. Comparison between the two methods.

Expansion ratio	Gas accumulation method	SRG method	Determined in 2010	Absolute difference	Relative difference
$f_A$	0.010 032 4 $\pm 4.1 \times 10^{-6}$	0.010 083 5 $\pm 4.4 \times 10^{-6}$	0.010 058 0 $\pm 5.1 \times 10^{-5}$	-5.1 $\times 10^{-5}$	-5.1 $\times 10^{-3}$
$f_B$	0.009 844 9 $\pm 4.1 \times 10^{-6}$	0.009 874 9 $\pm 4.6 \times 10^{-6}$	0.009 859 9 $\pm 3.1 \times 10^{-5}$	-3.0 $\times 10^{-5}$	-3.0 $\times 10^{-3}$
$f_C$	0.010 095 7 $\pm 4.1 \times 10^{-6}$	0.010 133 2 $\pm 4.0 \times 10^{-6}$	0.010 114 5 $\pm 3.8 \times 10^{-5}$	-3.7 $\times 10^{-5}$	-3.7 $\times 10^{-3}$

Table 5. Expansion ratios estimated at the time of the SEE-1 initial operation.

Expansion ratio	Gravimetric	SRG	Used at initial operations
$f_A$	0.010 046 5 $\pm 2.7 \times 10^{-6}$	0.010 092 7 $\pm 3.0 \times 10^{-6}$	0.010 069 0 $\pm 4.6 \times 10^{-5}$
$f_B$	0.009 857 6 $\pm 2.6 \times 10^{-6}$	0.009 858 1 $\pm 2.9 \times 10^{-6}$	0.009 857 8 $\pm 3.9 \times 10^{-6}$
$f_C$	0.010 098 9 $\pm 2.0 \times 10^{-6}$	0.010 094 3 $\pm 3.0 \times 10^{-6}$	0.010 096 6 $\pm 5.9 \times 10^{-6}$

Nominal pressure, Pa	Original values, Pa	Original uncertainty, Pa	New values, Pa	New uncertainty, Pa	$E_n$
$3.00 \times 10^{-4}$	$3.031 \times 10^{-4}$	$2.8 \times 10^{-6}$	$3.030 \times 10^{-4}$	$3.2 \times 10^{-6}$	0.02
$9.00 \times 10^{-4}$	$9.085 \times 10^{-4}$	$8.4 \times 10^{-6}$	$9.082 \times 10^{-4}$	$9.7 \times 10^{-6}$	0.02
$3.00 \times 10^{-3}$	$2.997 \times 10^{-3}$	$1.5 \times 10^{-5}$	$2.999 \times 10^{-3}$	$1.8 \times 10^{-5}$	-0.10
$9.00 \times 10^{-3}$	$9.008 \times 10^{-3}$	$4.3 \times 10^{-5}$	$9.015 \times 10^{-3}$	$5.5 \times 10^{-5}$	-0.11
$3.00 \times 10^{-2}$	$3.000 \times 10^{-2}$	$1.4 \times 10^{-4}$	$3.003 \times 10^{-2}$	$1.8 \times 10^{-4}$	-0.11
$9.00 \times 10^{-2}$	$9.003 \times 10^{-2}$	$4.2 \times 10^{-4}$	$9.011 \times 10^{-2}$	$5.4 \times 10^{-4}$	-0.11
$3.00 \times 10^{-1}$	$2.971 \times 10^{-1}$	$4.4 \times 10^{-4}$	$2.977 \times 10^{-1}$	$1.0 \times 10^{-3}$	-0.53
$9.00 \times 10^{-1}$	$8.935 \times 10^{-1}$	$9.3 \times 10^{-4}$	$8.953 \times 10^{-1}$	$2.9 \times 10^{-3}$	-0.58

Table 6. Comparison of the new and original values of the SEE-1.

### 5. Measurements assurance and conclusions

The results of this characterization were compared with information from a comparison carried out with the PTB's vacuum laboratory (Germany) at the time of the first operation of the SEE-1 [2]. In table 6 the last column presents the normalized error equation values ( $E_n$ ) for each applied pressure. Table 6 is a re-evaluation

of previous comparison data under the assumption that the expansion ratios did not change since then. The improvement is an indication that present expansion ratios are correct, but only another comparison can prove it for sure.

The improvements carried out at the SEE-1 and the characterization of the system probe to be adequate. The values obtained by means of the  $E_n$  on the comparison of the SEE-1 original values (used for the comparison with PTB) and the new values do not exceed 1.

### Acknowledgements.

The authors thank Yolanda C. Verdejo Guerrero, metrologist at CENAM vacuum laboratory.

### References.

- [1] J. C. Torres-Guzman, L. A. Santander and K. Jousten, Realisation of the medium and high vacuum primary standard in CENAM, Mexico. *Metrologia* 42, S157-S160, 2005.
- [2] Karl Jousten, Luis Santander, Jorge C. Torres-Guzman, Results of the Key Comparison SIM-Euromet.M.P-BK3 (bilateral comparison)

in the pressure range from  $3 \cdot 10^{-4}$  Pa to 0.9 Pa. *Metrologia* 42, 07002, 2005.

- [3] K. W. T. Elliot, P. B. Clapham, The accurate measurement of a volume ratio of vacuum vessels. NPL Report MOM 28, 1978.
- [4] K. Jousten, G. Röhl, V. Aranda, Volume Ratio Determination in Static Expansion Systems by Means of a Spinning Rotor Gauge. *Vacuum* 52, (1999) 491-499. October 1999.

# Characterization of the LNE constant pressure flowmeter for the leak flow rates measurements with reference to vacuum and atmospheric pressure

Frédéric Boineau<sup>1</sup>

## Abstract

The Laboratoire national de métrologie et d'essais (LNE) developed a constant pressure gas flowmeter to implement the continuous expansion standard. The characterization of this new standard and the associated uncertainty budget are presented in this paper. Comparisons were carried out between the constant pressure flowmeter and our other flowmeters for leak rates flowing in vacuum (constant volume flowmeter) and atmospheric pressure (infrared detection flowmeter).

Keywords: gas flow rates / gas flowmeter / leak detection

## 1 Introduction

LNE developed a constant pressure gas flowmeter in the range  $4 \cdot 10^{-12} \text{ mol} \cdot \text{s}^{-1}$  to  $4 \cdot 10^{-7} \text{ mol} \cdot \text{s}^{-1}$  to carry out the continuous expansion and calibrate leak rates with reference both to vacuum and atmospheric pressure. The volume variation is achieved by two pistons [1]. Two capillary leaks of nominal values around  $3 \cdot 10^{-10} \text{ mol} \cdot \text{s}^{-1}$  are used, first to draw up the calibration uncertainty budget of the flowmeter and second to compare it with our usual primary standard for flow rates referred to vacuum. Besides, a comparison in the field of refrigerant leak rates at atmospheric pressure is performed around  $1.3 \cdot 10^{-8} \text{ mol} \cdot \text{s}^{-1}$  with our new standard based on the infrared detection [2], using a transfer permeation leak of R-134a.

## 2 Principle of the constant pressure gas flowmeter

At a constant temperature  $T$ , the gas throughput  $Q$  is defined by equation (1) :

$$Q = \frac{d(pV)}{dt}, \quad (1)$$

where  $p$  and  $V$  are the pressure and volume of the gas respectively and  $t$  the time. During the time measurement  $\Delta t$ , the working pressure  $p_0$  is kept constant by varying the measurement volume of a quantity  $\Delta V$ :

$$Q = p_0 \frac{\Delta V}{\Delta t}. \quad (2)$$

Expression of the molar flow rate  $Q_m$  including the temperature's value is preferred. According to the perfect gas law:

$$Q_m = \frac{Q}{RT}, \quad (3)$$

where  $R$  is the molar gas constant.

The principle of the constant pressure flowmeter is illustrated figure 1: with the valve  $V_{RM}$  opened, the volumes are filled with the gas of interest at the working pressure  $p_0$ . The measurement's procedure is as follows: at the shut-off of valve  $V_{RM}$ , presence of the gas throughput makes measurement pressure  $p_M$  vary. Its variation  $\Delta p$ , measured with the differential capacitance diaphragm gauge CDG R-M (MKS, type 616, full scale 130 Pa), gives to the regulation system the difference between  $p_M$  and the reference pressure  $p_R$  in the closed reference volume, initially equal to  $p_0$ . The regulation system monitors the selected piston, moved with a worm screw assembled to a step motor, at the adequate speed  $v_0$  maintaining  $\Delta p$  to zero. Then the gas throughput  $Q(T)$  can be determined using equation (2):

$$Q(T) = p_0 \cdot S \cdot v_0, \quad (4)$$

where  $S$  is the section of the chosen piston.

The piston's speed regulation is not easy to achieve due to irregularity of screw's thread, short term stability of CDG RM output signal, etc.. Jousten and al. [3] showed advantages of a regulation method which consists of allowing  $p_M$  to have a little sawtooth variation around the mean value  $p_0$  (figure 2). During the time interval  $(t_2 - t_1)$ , the mean value of  $\Delta p$  is zero and the piston displacement is  $(x_2 - x_1)$ . According to equations (3) and (4), the molar flow rate is given by the expression:

$$Q_m = \frac{1}{RT} p_0 \cdot S \cdot \frac{x_2 - x_1}{t_2 - t_1}. \quad (5)$$

The uncertainty of  $Q_m$  includes basically gas temperature  $T$ , measured with Pt-100 sensors, working pressure  $p_0$ , the piston displacement  $(x_2 - x_1)$  measured with optical absolute transducers and time interval  $(t_2 - t_1)$ . Though, in the equation (5),

<sup>1</sup> Frédéric Boineau, Laboratoire national de métrologie et d'essais (LNE) – 1 rue Gaston Boissier, 75724 Paris Cedex 15, E-mail: frederic.boineau@lne.fr

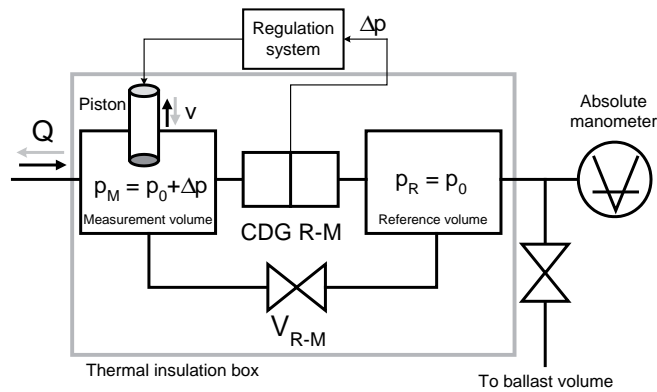


Figure 1. Principle of the constant pressure flowmeter. The output signal of the differential pressure gauge CDG R-M aims at regulating the piston's speed that keeps constant the pressure in the measurement volume.

we have considered perfect stability of the temperature which is not exactly correct. This matter is discussed in more details § 3. At stage 1, the working piston is kept still so the pressure  $\Delta p$  decreases; when the lower threshold is reached, the piston is moved at a constant speed, to produce  $\Delta p$  increase (stage 2). When the upper threshold is attained, the piston is stopped, then steps 1 and 2 are repeated until the displacement of the piston is typically higher than 5 mm.

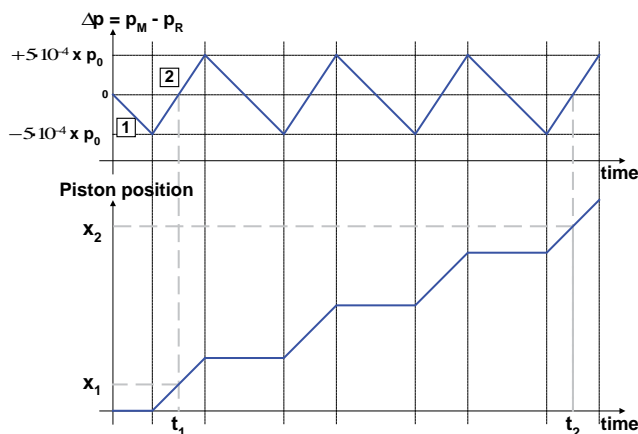


Figure 2. Sawtooth regulation of the differential pressure  $\Delta p$ .

### 3 Temperature stability

The importance of temperature stability in the flowmeter's volumes had been early anticipated thanks to previous publications [1][3][4]. In addition to a thermal insulation box (figure 1) made of polystyrene, we managed to build the measurement and reference volumes in a same stainless steel 316 L body, called "three-volumes" body, where an additional chamber for the measurement volume aims at measuring high range flow rates (figure 3). The metallic mass gives stability and homogeneity to the temperature of the gas.

As  $(pV)$  has the dimension of an energy, the throughput measurement is strongly dependent of external thermal energy transfers (air conditioning, heating equipments in the room, etc.). For a closed volume  $V$  at temperature  $T_0$  and pressure  $p_0$ , a "thermal throughput" perturba-

on  $Q_{th}$ , created by a temperature variation versus time  $dT/dt$  can be written using the perfect gas law [4]:

$$Q_{th} = V \frac{p_0}{T_0} \frac{dT}{dt} \quad (6)$$

We can notice that, other factors remaining constant, this perturbation is proportional to  $p_0$ . In the throughput measurement process, the overall  $Q_{th}$  is given by the expression:

$$Q_{th} = \frac{p_0}{T_0} \left( V_M \frac{dT_M}{dt} - V_R \frac{dT_R}{dt} \right), \quad (7)$$

where  $V_M$  and  $V_R$  are the capacities of measurement and reference volumes respectively and  $dT_M/dt$  and  $dT_R/dt$  are temperature variations versus time in each volume. In addition,  $dT/dt$  is proportional to  $dp/dt$ :

$$\frac{dp}{dt} = \frac{p_0}{T_0} \frac{dT}{dt} \quad (8)$$

Pt-100 sensors are not suitable to estimate the gas temperature stability: they are not placed in the gas, have a large response time (actually, the response time is fixed by the metal body) and pipes outside the body (towards reference manometers) are more affected by ambient temperature variations. Therefore, according to equations (7) and (8), it is useful to look closely at pressure variation in the reference volume to estimate temperature variation during each measurement.

### 4 Metrological characterization

An helium capillary leak identified CL-H150 was used to characterize the new flowmeter. The leak is supplied with pure helium at the upstream pressure of 150 kPa and its downstream pressure is vacuum. In this configuration, the nominal flow rate  $Q_m$  is about  $3.4 \cdot 10^{-12} \text{ mol} \cdot \text{s}^{-1}$  at 20 °C. When the measurements were performed, the thermal insulation box had not been yet installed. On the chart figure 4 are plotted the measured molar flow rate  $Q_{m,meas}$  and the determined pressure variation  $\Delta p_R/\Delta t$  in the reference volume, for each of the 29 measurements (the pressure variation is considered monotone and constant during the period of a measurement). It may be seen a large scattering of the measured values of the leak molar flow rate: experimental standard deviation is on the order of 1 % which is unusual for that leak. We also noticed that when  $\Delta p_R/\Delta t$  is close to zero,  $Q_{m,meas}$  seems to keep quite constant around a mean value  $\overline{Q_{m,meas}}$  of  $3.38 \cdot 10^{-10} \text{ mol} \cdot \text{s}^{-1}$ . There is a clear anti-correlation between the deviation of  $Q_{m,meas}$  from  $\overline{Q_{m,meas}}$  and  $\Delta p_R/\Delta t$  (especially measurements #15 and #20) which only can be explained by a thermal effect through  $Q_{th}$ . According to equations

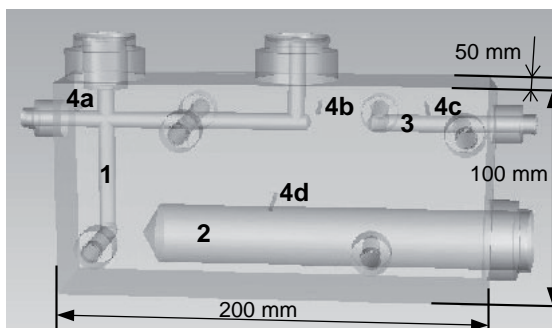


Figure 3. “Three-volumes” body, photo and scheme. (1) Measurement volume; (2) additional chamber for measurement volume; (3) reference volume; (4) Pt-100 wells. Pneumatic valves between volumes (1) and (2) and volumes (1) and (3) on the front side are not represented.

(7) and (8) and the observed anti-correlation, the thermal perturbation seems to be dominant in the reference volume (considering that  $V_R$  more or less equal to  $V_M$ ). The overall thermal flow rate  $Q_{th}$  estimated with experimental data for significant values of  $\Delta p_R/\Delta t$ , represents  $1.1\% \cdot Q_{m,meas}$  when

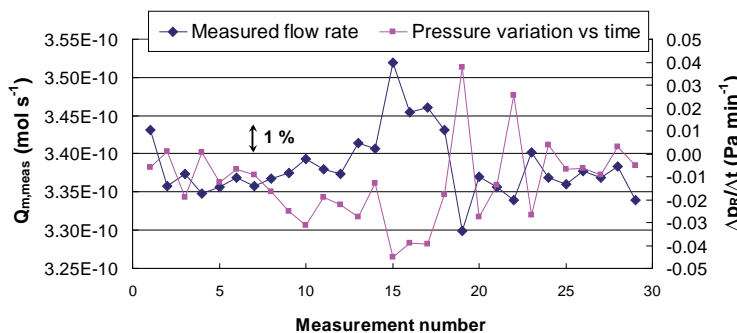


Figure 4. Measured molar flow rate with the corresponding pressure variation in the reference volume versus time for the capillary leak CL-H150.

Uncertainty source	Relative value	Contribution in the final uncertainty
Standard deviation on the mean	$1.5 \cdot 10^{-3}$	4.7 %
$p_0$	$7.9 \cdot 10^{-4}$	1.3 %
$\Delta V$	$2.0 \cdot 10^{-3}$	8.3 %
$\Delta t$	$4.6 \cdot 10^{-4}$	0.4 %
$T$	$2.3 \cdot 10^{-4}$	0.1 %
$Q_{th}$	$6.4 \cdot 10^{-3}$	85 %
Expanded uncertainty ( $k=2$ ): $U(Q_m)/Q_m = 1.4\%$		

Table 1. Uncertainty budget of the nominal molar flow rate  $Q_m = 3.4 \cdot 10^{-12} \text{ mol} \cdot \text{s}^{-1}$  at  $20^\circ\text{C}$  (capillary leak CL-H150)

$|\Delta p_R/\Delta t|$  is  $0.015 \text{ Pa} \cdot \text{min}^{-1}$ . That is the limit fixed for  $|\Delta p_R/\Delta t|$  to select measurements in the calculation of the mean leak flow rate, taken into account in the uncertainty budget Table 1.

Only the most significant standard uncertainty sources are reported. The CDG R-M drift during each measurement cycle is taken into account both in  $\Delta V$  and  $\Delta t$  (determinations of  $x_1, x_2, t_1$  and  $t_2$ ).

### 5 Comparison with other primary methods of leak rate measurements

A set f comparison was performed for leak rates referred to vacuum and atmospheric pressure with the thermal insulation box installed.

#### 5.1 Leak rates referred to vacuum

Leak rates with reference to vacuum are measured using the constant volume flowmeter: the throughput  $Q$  at the constant temperature  $T$  is deduced from equation (1) for a constant volume  $V_0$  and a pressure rise  $\Delta p/\Delta t$ :

$$Q(T) = V_0 \frac{\Delta p}{\Delta t} \quad (9)$$

Leak flow rate of a transfer helium capillary leak CL-K160 was successively measured with this method and the constant pressure flowmeter. With the thermal box, uncertainty due to thermal perturbation  $Q_{th}$  is assumed to be null. The results of this comparison are presented in the Table 2. Mentioned calibration uncertainties take into account leak’s behaviour: short term stability, temperature and downstream pressure influences. The determined deviation between the measurements methods is 0.36 %.

#### 5.2 Leak rates referred to atmospheric pressure

In recent years, LNE and Ecole des Mines de Paris designed a reference flowmeter for leak rates flowing at atmospheric pressure, for the refrigerant gas R-134a [2]. Leak flow rate of a transfer R-134a permeation leak identified P-R134-7561, with a nominal value of  $1.3 \cdot 10^{-8} \text{ mol} \cdot \text{s}^{-1}$ , was successively measured with this method and the constant pressure flowmeter within a period of six weeks. As the working pressure is high regarding the leak rate to be calibrated, the thermal perturbation  $Q_{th}$  is not negligible: corresponding relative uncertainty was

Table 2. Comparison results for the transfer capillary leak CL-K160 at 20 °C.

Method	Molar flow rate	Uncertainty ( $k = 2$ )	
	mol s <sup>-1</sup>	mol s <sup>-1</sup>	%
Constant volume flowmeter	3.683·10 <sup>-10</sup>	6.0·10 <sup>-12</sup>	1.6
Constant pressure flowmeter	3.663·10 <sup>-10</sup>	2.6·10 <sup>-12</sup>	0.71

Table 3. Comparison results for the transfer permeation leak P-R134-7561 at 20 °C and for a downstream pressure of 101325 Pa.

Method	Molar flow rate	Uncertainty ( $k = 2$ )	
	mol s <sup>-1</sup>	mol s <sup>-1</sup>	%
R-134 reference flowmeter	1.365·10 <sup>-8</sup>	4.7·10 <sup>-10</sup>	3.4
Constant pressure flowmeter	1.315·10 <sup>-8</sup>	1.6·10 <sup>-10</sup>	1.2

estimated to be at the most  $5 \cdot 10^{-3}$ . Results of this comparison are presented in the Table 3.

Calibration uncertainties take into account influence of both temperature and downstream pressure. The determined deviation between the two measurements methods is 3.9 %, not completely satisfying but compatible with the respective calibration uncertainties.

## 6 Conclusion

The matter of temperature stability is crucial in the new LNE constant pressure flowmeter as the measured quantity has the dimension of an energy. Installation of a thermal insulation box around the measurement and reference volumes of the flowmeter relevantly reduced the uncertainty due to the thermal perturbation. Comparisons have been performed with the constant volume flowmeter referred to vacuum and with the infrared detection flowmeter for R-134a leak rates at atmospheric pressure. The results are both consistent and encouraging.

## References

- [1] CALCATELLI A., RAITERI G. and RUMIANO G., "The IMGC-CNR flowmeter for automatic measurements of low-range gas flows", *Measurement*, 2003, **34**, 121-132.
- [2] MORGADO I., LEGRAS J.C. and CLODIC D. "Primary standard for the calibration of refrigerant leak flow rates", *Metrologia*, 2010, **47**, 135-145.
- [3] JOUSTEN K., MENZER H. and NIEPRASCHK R. "A new fully automated gas flowmeter at the PTB for flow rates between 10<sup>-13</sup> mol/s and 10<sup>-6</sup> mol/s", *Metrologia*, 2002, **39**, 512-529.
- [4] PEGGS G.N., "The measurement of gas throughput in range 10<sup>-4</sup> to 10<sup>-10</sup> Pa·m<sup>3</sup>·s<sup>-1</sup>", *Vacuum*, 1976, **26**, 321-328.

# International standardization for vacuum metrology and technology in recent years

K. Jousten<sup>1</sup>

## Abstract

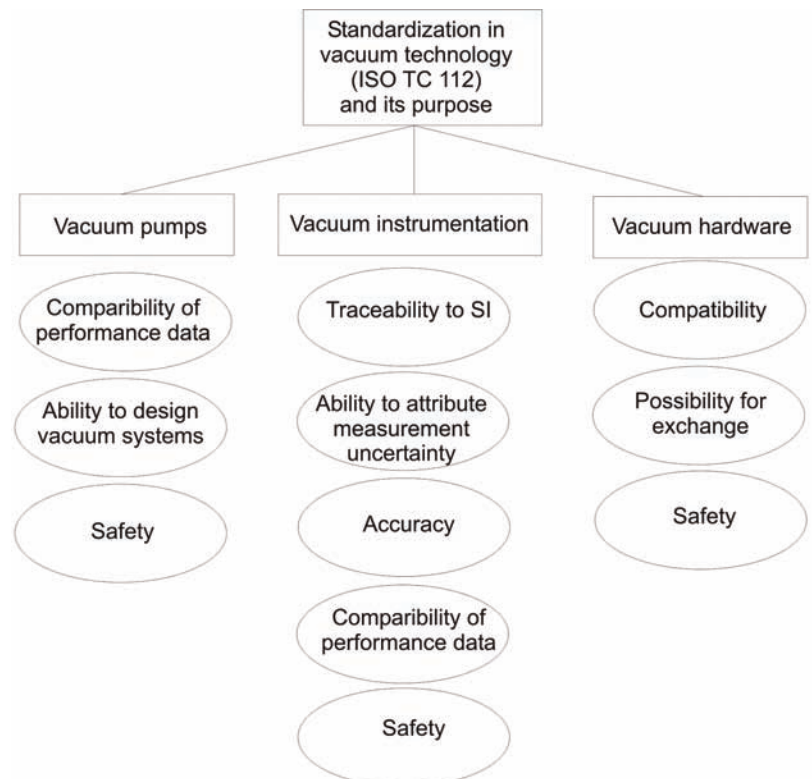
International standardization for vacuum metrology and technology has in recent years focused on laying down the basics for pressure dissemination in the vacuum range and on the characterization of vacuum pumps. Other issues were the safety of turbomolecular pumps and compatibility of vacuum hardware. Traceability to the SI and the evaluation of measurement uncertainties play an important role in the standardization for vacuum instrumentation.

KEYWORDS: Vacuum metrology, standardization, ISO, vacuum technology

## 1. Introduction

Standardization is one of the tools of industry used to increase the market by satisfying important needs of their customers such as safety, transparency, and compatibility of a product, and customer confidence in it (Fig. 1). The beginning of the industrial application of vacuum technology was evident in the lighting industry at the end of the 19<sup>th</sup> century. Later, vacuum technology became a key technology for many important fields, first for radio and radar equipment, then uranium enrichment and material processing, later for the microelectronic industry and recently for the solar and wind energy. Although it is a key technology, the vacuum-related industry was and is rather small but has acted "global" from the start and, as such, was open for international standardization.

In the 1960s and 1970s, intense standardization work within the International Organization for Standardization (ISO) was completed in order to define vacuum-related terms, to characterize the performance data of vacuum pumps, and to make fittings and flanges compatible. After more "quiet" decades where vacuum technology evolved from an experimental field into a highly developed and ripe technology, at the beginning of this century it was felt that the 20 to 30 year old standards had to be updated. In addition, new standards for vacuum gauge calibration were necessary, as the ISO 9000 series required traceability for measurement equipment [1].



Technical Committee TC 112 within ISO is responsible for standardization in vacuum technology and has developed new standards and technical specifications in recent years, which will be summarized in this article. The subjects and the order of the sections will follow the working groups (WG) organised within TC 112; these are "Vacuum Pumps" (WG 1), "Vacuum Instrumentation" (WG 2) and "Vacuum Hardware" (WG 3), where this article will lay some emphasis on vacuum instrumentation.

## 2. Standards for vacuum pumps

Each standard to characterize a special vacuum pump developed in the 1970s, and later, contained a section on how the measurement had to be performed and what the test dome should look like. After completion of these standards, it turned out that most vacuum pumps could be characterized with the same test dome and the same measurement procedure so that the vacuum standards contained almost identical sections.

Figure 1: Standardization in vacuum technology and its purpose

<sup>1</sup> K. Jousten, Physikalisch-Technische Bundesanstalt, Abbestr. 2-12, 10587 Berlin, Germany, karl.jousten@ptb.de, Tel. +49-30-3481-7262, Fax +49-30-3481-7490

For this reason, TC 112 decided to write a separate standard ISO 21360 on the measurement of standard performance data in order to relieve the standards for special vacuum pumps of these identical sections. In this context the measurement methods were also updated. The following measurement procedures for volume speed  $q_V$  (also called pumping speed  $S$ ) were established in ISO 21360:

1. Measurement by single test dome. Herein, a flowmeter is used for measuring the gas throughput  $q_{pV}$  into the pump and a calibrated vacuum gauge measures the pressure  $p$  near the inlet of the pump flange (diameter  $d$ ) at a height of  $1/2 d$ . The volume speed is given by

$$q_V = S = \frac{q_{pV}}{p}$$

2. Measurement by double test dome (known as the Fischer-Mommsen dome, Fig. 2). An orifice of conductance  $C$  between the two domes serves to generate a pressure difference  $p_d - p_e$  which is to be measured by two vacuum gauges (typically ionization gauges). The volume speed is then given by

$$q_V = S = C \left( \frac{p_d - p_{bd}}{p_e - p_{be}} - 1 \right)$$

Figure 2: The double dome, known also as the Fischer-Mommsen dome, to measure volume speed of high vacuum pumps was confirmed in ISO 21360. Reproduced by permission of DIN Deutsches Institut für Normung e.V.

where the base pressures  $p_{bd}$  and  $p_{be}$  at zero flow are subtracted both in the upper and lower chamber.

3. Measurement by pumping down a large vessel. The gas is pumped out of a large vacuum vessel with volume  $V$  for a few seconds  $\Delta t$  from value  $p_i$  to  $p_{i+1}$  with long intermissions in order to

keep the gas temperature constant in the vessel.

It is

$$q_V = \frac{V}{\Delta t} \cdot \ln \frac{p_i}{p_{i+1}}$$

Methods 1 and 2 were used also in the past, method 3 is new.

Another standard 27892 was developed for the safety of users of turbomolecular pumps. In case of a crash of the rotors, the full rotational energy is released in a very short time and there is the possibility of rupture of the casing of the turbomolecular pump. In addition, the large reaction torque might break the bolts that fix the turbomolecular pump. The standard defines the test methods for rapid shutdown torque measurement of a turbomolecular pump and molecular drag pump.

### 3. Standards for vacuum instrumentation

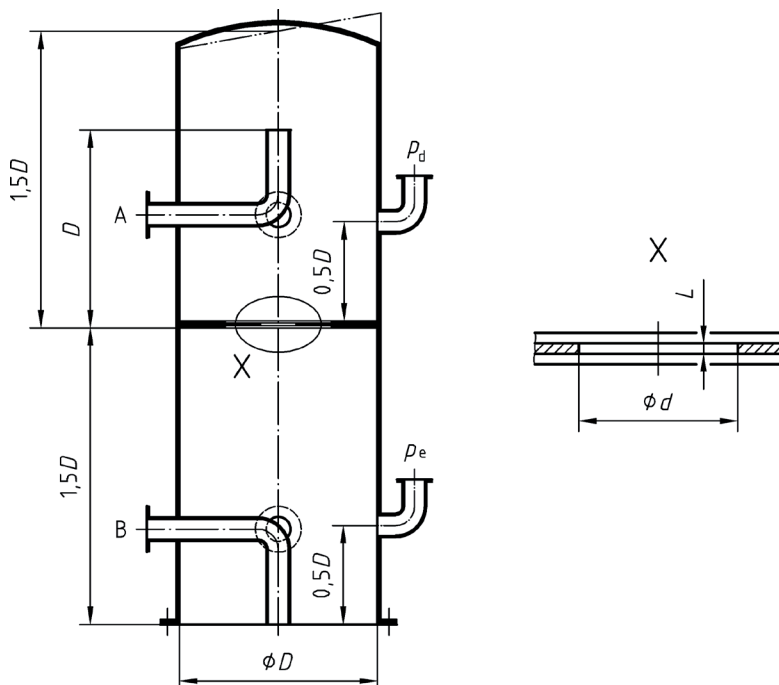
The strategic goal for the standardization of vacuum instrumentation is to put the dissemination of the pressure scale in vacuum on a firm ground (Figure 1). This shall be accomplished

- by defining the calibration system and the calibration procedure providing traceability to the SI by primary standards,
- by having the manufacturers publish all parameters of a vacuum gauge that are needed for calibration, and
- by defining the requirements during calibration for a special type of vacuum gauge, both as reference gauge and as a unit under calibration.

Accompanying this, definitions of physical quantities for vacuum metrology and guidelines to evaluate measurement uncertainties need to be given.

ISO TS 3567 defines the vacuum system and the procedure for the calibration of vacuum gauges by comparison with a calibrated reference gauge from  $10^{-6}$  Pa to 110 kPa. This reference gauge must be traceable to the SI in one or more steps. The reference gauge and the unit under calibration (UUC) must be exposed to the same density and velocity distribution of the calibration gas molecules. The same density and velocity distribution of the calibration gas molecules also means the same pressure at the two locations, but not *vice versa*. Since there are many types of vacuum gauges that do not measure pressure — but instead, for example, gas density or the impingement rate of gas molecules — the above requisite is both necessary and more stringent than only calling for equal pressures at the two entrance flanges.

The gas density (pressure) in the calibration chamber can be varied and the gauge readings of the UUC can be compared with the pressures indicated by the reference gauge.



The calibration chamber must be cylindrical symmetric to at least one axis, i.e. it can be a cylinder, a sphere, or two parts of hemispheres attached to each other. The flanges to adopt the reference gauge and UUC must be on the same equatorial plane. The calibration can be performed by isolating the chamber from the pump and letting gas in or by establishing a stationary equilibrium where the gas flow has to have cylinder symmetry as well.

ISO TS 27893 specifies how to determine and report measurement uncertainties for calibrations carried out according to ISO TS 3567. Only simple models are used, since it cannot be expected that every calibration staff has the time to learn the details of the GUM [2].

The two technical specifications, 3567 and 27893, shall be converted to standards after 2011.

ISO 27894 was the first to define the parameters of a special gauge for a calibration, in this case for an ionization vacuum gauge. Other standards will follow for capacitance diaphragm gauges, thermal conductivity gauges, spinning rotor gauges, cold cathode vacuum gauges, and vacuum gauges combining different measurement principles in one gauge. ISO 27894 will have to be extended to define the details for a calibration of an ionization gauge.

In 2010, standardization work on quadrupole mass spectrometers (QMS) began with a draft on the definitions and specifications for them. This is the first step towards an internationally agreed procedure for their calibration, but it is also very important to be able to compare units from diffe-

rent manufacturers. QMS cannot be calibrated in the sense that after calibration they can be reliably used with all their possible features. One of the reasons for this is that the sensitivity of a given gas species depends on the special gas mixture and the total pressure. Another reason is the modest stability of QMS. Instead, calibrations will be defined in order to compare different types of QMS and to be able to attribute a measurement uncertainty in some major and important applications. To define these and the conditions of calibrations, intensive research will be needed in the next years.

#### 4. Standards for vacuum hardware

The main purpose of the standardization for vacuum hardware is the compatibility between different manufacturers, e.g. some metal flanges above DN 160 were not compatible. Flanges, fittings and valve dimensions have been standardized in recent years (Table 1).

Another purpose of vacuum hardware standardization is to test its functionality and its specifications, e.g. the leak tightness of valves, for which ISO 27895 was developed.

#### 5. Conclusion

Table 1 gives an overview of the standards in vacuum technology developed since 2004. Both in the standardization for vacuum pumps and instrumentation the focus was on laying down the basics of methodology.

In the years to follow, more standards specific to the characterization of special pumps and

Table 1 Standards developed by ISO TC 112 (vacuum technology) in recent years and drafts under development. TS: technical specification.

ISO number	Status	Title	Note
TS 3567	published in 2005	Vacuum gauges – Calibration by direct comparison with a reference gauge	in conversion state to standard
TS 3669-2	published in 2007	Bakable flanges – Part 2: Dimensions of knife-edge flanges	
9803	published in 2007	Mounting dimensions of pipeline fittings Part 1: Non knife-edge flange type Part 2: Knife-edge flange type	
14291	Committee draft (CD)	Definitions and specifications for quadrupole mass spectrometers	
21358	published in 2007	Right-angle valve – Dimensions and interfaces for pneumatic actuator	
21360	published in 2007	Standard methods for measuring vacuum-pump performance – General description	
21360-2	Draft international standard (DIS)	Standard methods for measuring vacuum-pump performance – Part 2: Positive displacement vacuum pumps	
27892	published in 2010	Turbomolecular pumps – Measurement of rapid shutdown torque	
TS 27893	published in 2009	Evaluation of the uncertainties of results of calibrations by direct comparison with a reference gauge	in conversion state to standard
27894	published in 2009	Vacuum gauges – Specifications for hot cathode ionization gauges	
27895	published in 2009	Valves – Leak test	



to the calibration of special vacuum gauges have to be developed or updated in order to complete the standardization work for vacuum technology. In vacuum hardware the focus will be on the compatibility of hardware.

## 6. References

- [1] See, e.g., Section 7.6 of ISO 9001: 2000, Quality management systems – Requirements.
- [2] ISO/IEC Guide 98-3: 2008, Uncertainty of measurement – Part 3: Guide to the expression of uncertainty in measurement (GUM:1995)

## Acknowledgements

The work of all members of TC112 and their working groups is gratefully acknowledged.

# Traceability and accreditation process for vacuum and pressure laboratories in AFRIMETS

C. Korasie<sup>1</sup>, A. Eltawil<sup>2</sup>

**Abstract** – This paper will look at the process, developing NMI's in Africa go through to establish an NMI from mostly Trade and or Legal Metrology requirements. The aim is to investigate the challenges countries are faced with in obtaining traceability and eventually accreditation. A case study will be made of the roadmap followed by NMI's that has successfully entered CMC's in the BIPM database. With limited resources the tools required to maintain these newly formed NMI's and how to increase capability in various parameters will be scrutinized.

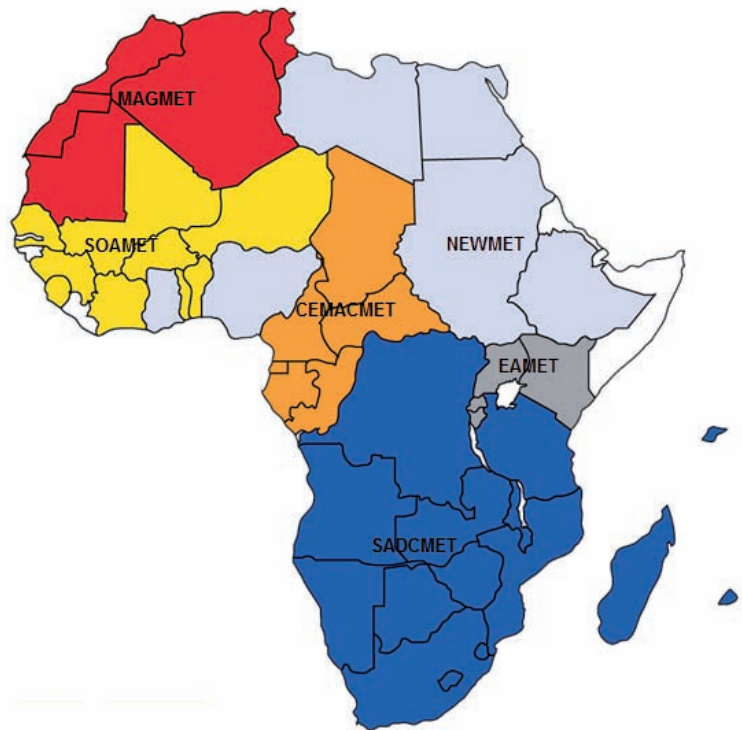
**Keywords:** accreditation, traceability, capability

## Introduction

Africa's driving force for traceability and accreditation primarily boils down to wanting a larger share in world trade. By having a quality infrastructure managed by institutions such as the African Organisation for Standardisation (ARSO), the Intra-Africa Metrology System (AFRIMETS) and the African Accreditation Cooperation (AFRAC), African countries can enjoy trade opportunities and boost its economy as well as creating sustainable growth [1]. The pillars of sustainable growth are Metrology, Standardisation, Conformity assessment and Accreditation, of which Metrology is the most basic requirement [2]. In most countries in Africa national standards bodies exist, and scientific metrology systems are being built on.

## Metrology in Africa

AFRIMETS was conceptualised in 2004/5 and came in to being in 2007. On 17 October 2008 AFRIMETS superseded SADC MET to be the regional metrology organisation (RMO) representing Africa at the Joint Committee of RMOs and the BIPM (JCRB). AFRIMETS comprise of six sub-RMOs (Fig. 1): SADC MET, EAMET, CEMAC MET, NEWMET, SOAMET and MAGMET. AFRIMETS currently have 46 member states, of which four are full members of the BIPM (South Africa, Egypt, Kenya and Cameroon) and six are associate members of the CGPM (Tunisia, Ghana, Mauritius, Zimbabwe, Zambia, Seychelles).



## Accreditation bodies in Africa

In 2010 the African Regional Accreditation Cooperation (AFRAC) was launched as a platform upon which Africa can build and develop its accreditation infrastructure. AFRAC aims to be an accreditation body for Africa in the long run, supporting countries which do not have their own accreditation systems. Currently there are three signatories to the ILAC MRA in Africa: Egyptian Accreditation Council (EGAC), South African National Accreditation System (SANAS) and Tunisian Accreditation Council (TUNAC) [1].

## The harmonisation of activities

The AFRIMETS sub-regions dealt differently with accreditation in the past, thus AFRIMETS adopted the accreditation policy of either being third party accredited or doing a self-declaration. Furthermore, pre-AFRIMETS, countries submitted their CMCs to the KCDB through other RMOs they have had associate membership of.

Figure 1: Map of the sub-regional metrological organisations in Africa.

<sup>1</sup> C. Korasie, NMISA, Pretoria, South Africa, Email: ckorasie@nmisa.org

<sup>2</sup> A. Eltawil, NIS, Cairo, Egypt

### List of Acronyms

- AFRAC (African Regional Accreditation Cooperation)
- AFRIMETS (Intra-Africa Metrology System)
- ARSO (African Organisation for Standardisation)
- CEMACMET (Communauté Economique et Monétaire de l'Afrique Centrale)
- CGPM (General Conference on Weights and Measures)
- DAkKS (Deutsche Akkreditierungsstelle)
- EAMET (East African Metrology)
- EGAC (Egyptian Accreditation Council)
- KEBS (Kenyan Bureau of Standards)
- LANEMA (Laboratoire National d'Essai de qualité, de Métrologie et d'Analyses)
- LER (laboratoire etalon regional)
- MAGMET (Maghreb, 'Western' in Arabic Metrology)
- NEWMET (North East and West African Metrology)
- SADCNET (Southern African Development Community Metrology)
- SANAS (South African National Accreditation System)
- SOAMET (Secrétariat Ouest-Africain de Métrologie)
- TUNAC (Tunisian Accreditation Council)
- UEMOA (Union économique et monétaire ouest-africaine)

Under AFRIMETS, within the next five (5) years, all member states have to submit their CMCs through the relevant AFRIMETS technical committees.

The sub-RMOs of AFRIMETS play a crucial role in capacity building in AFRICA since communication barriers often prevent effective interaction on laboratory level between Anglophone and Francophone countries. The relationships between inter-regional NMIs have developed very well over the years.

The role of the sub-RMO has thus been clearly defined:

- Organise sub-regional inter-comparisons
- Hold sub-RMO WG meetings
- Generally coordinate activities in sub-RMO
- Participate in AFRIMETS activities (annual working group meetings)

While some sub-RMOs have a number of national metrology laboratories who can participate, others lack the infrastructure. SOAMET has thus proposed a model where different NMIs in the region take responsibility for specific parameters, e.g. in Mass and related quantities, for example Cote d'Ivoire is responsible for the measurement standard for Pressure, Benin for Mass, etc.

### Capabilities in Pressure Metrology

Only South Africa and Egypt have Calibration and Measurement Capabilities (CMCs) in the BIPM key comparison database (KCDB). The National Metrology Institute of South Africa (NMISA) submitted their CMCs to the KCDB for pressure pre-AFRIMETS through APMP. The Egyptian National Institute of Standards (NIS) achieved international recognition in 2008 through peer review by EURAMET and submitted their pressure CMCs to the KCDB through EURAMET. Two case studies are presented outlined here for the different approaches to build capacity, traceability and accreditation in pressure metrology in Kenya and Cote d'Ivoire.

### Kenya

KEBS became a member state of the BIPM in 2010, and is currently preparing for accreditation so that they meet the necessary requirements to successfully submit CMCs through AFRIMETS. KEBS has for the last few years been active in the EAMET sub region. The PTB assisted with the required training, traceability and provided the bilateral in support for the initial CMC submission KEBS, due to its close affiliation with PTB, has thus aligned with the DAkKS (former DKD) accreditation system. During April 2011 the DAkKS representatives will be doing an audit of the accredited KEBS laboratories. KEBS is then scheduled for a peer review in May 2011 from the AFRIMETS representatives [3].

### Cote d'Ivoire

In August 2008 the Laboratoire National d'Essai de qualité, de Métrologie et d'Analyses (LANEMA) was selected to be the LER in pressure by UEMOA and in December of the same year LANEMA started their accreditation process. In the following six months arrangements were made for the laboratory for the training of staff. Two staff members were trained at PTB and accreditation was achieved in January 2010.

### Challenges

As mentioned there are many challenges for NMIs in Africa, these include training of staff, acquiring equipment and the general maintenance thereof. Primarily, awareness of metrology and the need for traceability is the main focus in all regions in AFRIMETS. Most regions have a Standardisation authority but seldom a Metrology Institute. While the basic skills development has been addressed by donor funded projects where specific training was provided, training in pressure metrology has not been a focus area yet. During the next cycle, pressure training will be considered as most countries rely on its realisation of pressure standards for key export sectors, mining being the major export industry.

Generic challenges include:

- The actual public status of the NMI
- Out-dated legislation or total lack of legislation
- Lack of regulation to drive legislation
- Recruitment of qualified technicians
- Calibration of the standards in other countries
- Delay in the construction of the new (suitable) laboratories
- Budgetary constraints

### Conclusion

The process for CMC submission to the KCDB in Africa is slow as most countries lack the required resources to achieve it. Currently there are Standard Bureaus which ensures that trade can continue, but the international market is limited due to international recognition. AFRIMETS has been playing a key role in ensuring that all NMIs in Africa achieve international recognition and thus develop and grow Africa's share in world trade.

### References

- [1] "An African Infrastructure for Quality", the African Union-NEPAD Approach
- [2] Metrology, standardization and conformity assessment, 2006 ISBN 92-67-10416-0
- [3] D. Moturi: "National Measurement System-Kenyan case", 5th Regional Metrology Conference (RMC 2010), 1-3 December 2010

## Neues aus der OIML

### Bericht über die 46. Sitzung des Internationalen Komitees für gesetzliches Messwesen (CIML)

Roman Schwartz<sup>1</sup>

Die 46. Sitzung des Internationalen Komitees für gesetzliches Messwesen (CIML) fand vom 11. bis 14. Oktober 2011 in Prag statt. Knapp 150 Teilnehmer aus 59 Mitgliedstaaten waren vertreten, s. Bild 1. Zur deutschen Delegation gehörten Dr. Roman Schwartz (PTB) und Dr. Heinz Waller, Leiter der deutschen Akademie für Metrologie (DAM) und stellvertretender Leiter des Bayerischen Landesamtes für Maß und Gewicht (BLMG). Weiterhin nahmen Prof. Manfred Kochsiek als Ehrenmitglied der OIML und Dr. Eberhard Seiler als „Facilitator for Developing Country Matters“ teil. Vertreten waren auch internationale und regionale Organisationen, zu denen die OIML Verbindungen unterhält, wie das Internationale Büro für Maß und Gewicht (BIPM), die europäische Zusammenarbeit im gesetzlichen Messwesen (WELMEC), die „International Electrotechnical Commission“ (IEC), die „International Laboratory Accreditation Cooperation“ (ILAC) sowie das „International Accreditation Forum“ (IAF) und der europäische Verband der Waagenhersteller (CECIP). Alle Resolutionen der 46. CIML-Sitzung finden sich unter „<http://www.oiml.org/download/>“. Die wichtigsten Entscheidungen und Entwicklungen werden nachfolgend vorgestellt.

#### 1. Zusammenarbeit der OIML mit anderen Organisationen

In Resolution Nr. 14 wird die mittlerweile sehr gute Zusammenarbeit der OIML mit dem BIPM auf allen Ebenen hervorgehoben. Es finden regelmäßige Besprechungen der beiden Präsidenten und Direktoren sowie auch der Mitarbeiter auf Arbeitsebene statt. Dennoch wird angestrebt, zusammen mit dem BIPM Möglichkeiten einer noch stärkeren Zusammenarbeit auszuloten, bis hin zu einer möglichen „collocation“, d. h. Verlegung des



Sitzes des Internationalen Büros für Gesetzliches Messwesen (BIPM) auf das Gelände des BIPM in Sèvres.

Memoranda of Understanding (MoU) der OIML bestehen bereits mit ILAC und IAF, UNIDO und BIPM sowie ISO. Bei der diesjährigen CIML-Sitzung wurde vom neuen CIML-Präsidenten, Peter Mason, sowie dem Geschäftsführer von IECCE, Pierre de Ruvo, ein weiteres MoU der OIML mit IEC unterzeichnet (Resolution Nr. 10), s. Bild 2.

Weiterhin wurden erste Kontakte zu COPOLCO, dem ISO-Komitee für Verbraucherschutz, geknüpft (Resolution Nr. 11).

In ihrem Bericht seitens CECIP hob Frau Veronika Martens, Vorsitzende der CECIP „Legal Metrology Group“, u. a. die Bedeutung von Hersteller-Prüflaboratorien sowohl für das OIML MAA als auch zur Sicherstellung bauartkonformer Serienprodukte („Conformity to type“) hervor.

Unter Vorsitz des COOMET-Sekretärs, Dr. Pavel Neyezhmakov, fand vor Beginn der

Bild 1: Teilnehmer der 46. Sitzung des Internationalen Komitees für gesetzliches Messwesen (CIML) in Prag (Tschechische Republik), Oktober 2011 (Quelle: [http://prague.oiml.org/group\\_photo.html](http://prague.oiml.org/group_photo.html))

<sup>1</sup> Dr. Roman Schwartz, Leiter der Abteilung 1 „Mechanik und Akustik“ der PTB, deutsches Mitglied und 2. Vizepräsident des CIML

CIML-Sitzung wieder ein Austausch mit Vertretern verschiedener regionaler Metrologieorganisationen (RLMOs) statt, in dem über die Aktivitäten von AFRIMETS, APLMF, COOMET, GULFMET, EAMET, MAGMET, SADCMEI, SIM und WELMEC berichtet und die Notwendigkeit einer zukünftig klareren Verteilung der Aufgaben und Verantwortung zwischen RLMOs und OIML festgestellt wurde (Resolution Nr. 13).

## 2. OIML-Empfehlungen und OIML-Dokumente

Folgende OIML-Empfehlungen (R) wurden verabschiedet (Resolution Nr. 16):

R 35-2 *Material measures of length for general use - Part 2: Test methods*

Für folgende Entwürfe von revidierten OIML-Empfehlungen (R) sind nach teilweise erforderlicher Überarbeitung im jeweiligen Technischen Komitee CIML-online-Abstimmungen vorgesehen (Resolution Nr. 17):

R 126 *Evidential breath analyzers*

R 137 (Parts 1 and 2) *Gas meters*

Folgende Revisionen von „Basic Publications“, die für die Arbeit der OIML von grundlegender Bedeutung sind, wurden ebenfalls verabschiedet (Resolutionen Nr. 15, 19 und 23):

B 3: *OIML Basic Certificate System for OIML Type Evaluation of Measuring Instruments*

B 6 (Parts 1 and 2): *Directives for OIML technical work*

B 10: *Framework for a Mutual Acceptance Arrangement on OIML Type Evaluations*

B 15 *OIML Strategy*

B 16 *Terms of reference for the Presidential Council*

So heißen herkömmliche OIML-Zertifikate aufgrund der Revision von B 3 jetzt *Basis-Zertifikate* zur Unterscheidung von *MAA-Zertifikaten* nach B 10.

Mit der Revision von B 6 sind die Würfel jetzt für eine Beibehaltung der herkömmlichen TC/SC-Struktur in der OIML und damit gegen die Einführung einer „flat structure“ (ohne TCs/SCs) gefallen (siehe Resolution Nr. 23). Zur Steigerung der Effizienz der Arbeiten in den TCs/SCs wird es allerdings eine Reihe wichtiger Änderungen geben, die viele Elemente der vorgeschlagenen „flat structure“ beinhalten, so z. B.:

- Einrichtung von temporären *Projektgruppen* (*project groups*) unterhalb der TC/SC-Ebene, die jeweils nur solange existieren, bis ein vom CIML in Auftrag gegebenes Projekt, wie z.B. die Revision einer OIML-Empfehlung, abgeschlossen ist,
- P-Mitglieder, also stimmberechtigte Mitglieder, in einem TC/SC können zu

Beginn oder im Laufe eines Projektes entscheiden, ob sie aktiv mitarbeiten wollen oder nicht. Im letzteren Fall ändert sich ihr Status und sie werden für dieses Projekt als nicht stimmberechtigte O-Mitglieder (*observer*) geführt,

- Da Abstimmungen innerhalb der TC/SCs in der Vergangenheit wegen mangelhafter Beteiligung der P-Mitglieder häufig nicht das erforderliche Quorum erreicht hatten, wurden die Abstimmungsregeln für elektronische Abstimmungen jetzt geändert; für eine erfolgreiche Abstimmung reichen jetzt 2/3 aller *abgegebenen* Stimmen,
- P-Mitglieder, die ihrer Verpflichtung zur Teilnahme an Sitzungen oder Abstimmungen wiederholt nicht nachkommen, können ihren P-Status verlieren,
- TC/SC-Sekretariate sowie die Vorsitzenden von Projektgruppen werden für jeweils 3 Jahre gewählt, mit der Möglichkeit zur Verlängerung. Für eine erfolgreiche Wahl, die vom BIML organisiert wird, sind 2/3 aller *abgegebenen* Stimmen erforderlich.
- Insgesamt ist die Rolle des BIML im Verhältnis zu den TCs/SCs erheblich gestärkt worden,
- Die Regeln von der Entwicklung bis zur Verabschiedung einer neuen oder revidierten OIML-Publikation sind insgesamt gestrafft worden, wobei das sogenannte „CIML preliminary ballot“ beibehalten wurde und Dokumente, die eine solche Abstimmung erfolgreich passiert haben, zukünftig *Final Drafts* heißen werden und vor der endgültigen CIML-Abstimmung inhaltlich nicht mehr verändert werden dürfen.

Um die Einführung der neuen *Technical Directives* zu erleichtern, wird das BIML den betroffenen TC/SC-Sekretariaten bis zum 1.12.2011 entsprechende Informationen zur Verfügung stellen, so dass mit der Umstellung ab 1.1.2012 begonnen werden kann. Die Resolution Nr. 23 sieht darüber hinaus vor, dass den TC/SC-Sekretariaten über ihre CIML-Mitglieder Gelegenheit gegeben wird, bis 31.12.2011 Vorschläge zur weiteren Verbesserung der neuen *Technical Directives* zu machen. Zum Vorsitzenden der betreffenden ad-hoc-Arbeitsgruppe wurde das deutsche CIML-Mitglied bestimmt.

Der Vollständigkeit halber sei noch erwähnt, dass das TC3-Projekt zur Revision des OIML-Dokuments D1 „Considerations for a Law on Metrology“ unter der Leitung von Prof. Manfred Kochsiek gute Fortschritte macht und der 1. Committee Draft (1CD 2011) den CIML-Mitgliedern kurz vorgestellt wurde.

### 3. Weitere technische Aktivitäten

Nach einem ersten OIML-Workshop zu dem Thema *Conformity to type* (Konformität von Serienprodukten mit einer zertifizierten Bauart) im Juni 2011 in Utrecht (NL) sowie einem zweiten OIML-Workshop unmittelbar vor der 46. CIML-Sitzung in Prag (CZ) konnten sich Australien und Neuseeland nunmehr mit ihrem Vorschlag eines neuen Subkomitees TC3/SC6 *Conformity to type* durchsetzen (siehe Resolution Nr. 22); das Sekretariat teilen sich Neuseeland und das BIML. Schwerpunkt wird zunächst die Erarbeitung eines *Guidance documents* sein, dass die bestehenden Systeme in Europa (insbesondere *MID*) und den USA (insbesondere *VCAP*) einbeziehen soll.

Das 2006 in Kraft getretene OIML-Rahmenabkommen zur gegenseitigen Anerkennung von Prüfergebnissen (*OIML MAA*) gilt nach wie vor nur für nichtselbsttätige Waagen (R76), Wägezellen (R60) und Kaltwasserzähler (R49). Die Zahl der bisher ausgestellten MAA-Zertifikate hat sich mittlerweile deutlich erhöht, wobei der Schwerpunkt nach wie vor auf Wägezellen liegt. Mit den Resolutionen Nr. 20 und 21, die beide mit einer deutlichen Mehrheit von über 80% verabschiedet wurden, konnte jetzt ein entscheidender Schritt hin zur Anerkennung von Herstellerprüfergebnissen im Rahmen des MAA gemacht werden. TC3/SC5 wurde nun die Aufgabe übertragen, die entsprechenden Bedingungen des während der CIML-Sitzung vorgestellten Konzeptes für *Hersteller-Prüflaboratorien unter kontrollierter Überwachung* in das Dokument B 10 einzuarbeiten. Ziel ist die Verabschiedung der überarbeiteten bzw. ergänzten Fassung von B 10 bei der 47. CIML-Sitzung 2012.

Dr. Philippe Richard, Vize-Direktor des METAS (Schweiz), stellte die Vorschläge des BIPM (Meterkonvention) zur *Neudefinition des Internationalen Einheitensystems (SI)* und mögliche Auswirkungen auf das gesetzliche Messwesen vor und wies auf die vom BIPM hierzu eingerichtete Webseite hin ([http://www.bipm.org/en/si/new\\_si/](http://www.bipm.org/en/si/new_si/)). Mit der Resolution Nr. 25 werden alle TC/SCs der OIML, insbesondere TC 2, TC 9, TC9/SC3 und TC 11, dazu aufgefordert, sich aktiv an der Diskussion der Vorschläge zum *New SI* zu beteiligen und bis zum 24.02.2012 mögliche Kommentare an die betreffende ad-hoc-Arbeitsgruppe der OIML (Mitglieder: Deutschland, Schweiz, Österreich, USA, Japan sowie der BIPM-Direktor) zu senden, die dann bis Mitte 2012 zu einer offiziellen Stellungnahme der OIML an das BIPM zusammengefasst werden sollen. Philippe Richard wurde auch als neue Kontaktperson der OIML im CCU, dem



beratenden Komitee des BIPM für Einheiten, als Nachfolger von Dr. Arnold Leitner (Österreich) benannt.

### 4. Personalien und Ehrungen

Peter Mason (Direktor des National Measurement Office, Großbritannien) übernahm die Amtsgeschäfte als neuer CIML-Präsident von seinem Vorgänger Alan Johnston (Kanada).

Stephen Patoray (USA) nahm nach seiner Ernennung zum 1.1.2011 erstmals als Direktor des Internationalen Büros für gesetzliches Messwesen (BIML) an einer CIML-Sitzung teil.

Der Vertrag von Willem Kool als *Assistant Director* des BIML wird ab 1.1.2012 für weitere 5 Jahre verlängert.

In Anerkennung seiner mehr als 30-jährigen Verdienste um die OIML wurde Prof. Dr. Lev Issaev mit einer OIML-Medaille ausgezeichnet und ihm die OIML-Ehrenmitgliedschaft übertragen.

Den OIML Award 2011 for Excellent Achievements in Legal Metrology in Developing Countries erhielten Juan Carlos Castillo (Bolivien) und José Dajes (Peru) für ihre gemeinsame Arbeit am Aufbau von Messeinrichtungen für die Bestimmung des Volumens und des Energiegehaltes von Erdgas.

Weitere Auszeichnungen erhielten: Mariela Saavedra (Argentinien, Letter of appreciation) und Morteza Pouyan (Iran, Letter of appreciation).

### 5. Termine

Die 47. CIML-Sitzung wird in Verbindung mit der 14. OIML-Konferenz vom 1.-5.10.2012 in Bukarest (Rumänien) stattfinden.

Nach den beiden erfolgreichen OIML-Trainingsseminaren in den Jahren 2008 und 2009 wird das BIML 2012 wieder ein mehrtägiges Seminar für TC-/SC-Sekretariate anbieten.

Bild 2: Unterzeichnung des Memorandum of Understanding (MoU) zwischen OIML und IEC durch Peter Mason, CIML-Präsident (rechts), und Pierre de Ruvo, IECEE-Generalsekretär während der 46. CIML-Sitzung in Prag, 13.10.2011

## Inhalt

---

Prüfscheine	für Module und Zusatzeinrichtungen für nichtselbsttätige Waagen	327
EG-Bauartzulassungen	• Nichtselbsttätige Waagen	328
Innerstaatliche Bauartzulassungen	• Längenmessgeräte • Messgeräte für ruhende Flüssigkeiten – Messanlagen für strömende Flüssigkeiten • Wasserzähler – Gasmessgeräte • Selbsttätige Waagen – Messgeräte für Getreide und Ölfrüchte – Messgeräte im Straßenverkehr • Messgeräte für Elektrizität • Wärmezähler • Strahlenschutzmessgeräte • Feststellungen der Gleichwertigkeit nach § 80 der Eichordnung	332 333 335 336 338 339 340 342
Konformitätsbewertung nach 2004/22/EG	• EG-Baumusterprüfbescheinigungen/ bzw. EG-Entwurfsprüfbescheinigungen • Anerkennung von Qualitätsmanagementsystemen	342 352
Prüfung explosionsgeschützter Geräte und Schutzsysteme		353

---

## Prüfscheine für Module und Zusatzeinrichtungen für nichtselbsttätige Waagen

Folgende Einrichtungen sind von der Physikalisch-Technischen Bundesanstalt gemäß der Norm DIN EN 45501, Ausgabe November 1992, als Module oder Zusatzeinrichtungen von eichfähigen Waagen geprüft worden. Diese Prüfscheine sind nicht als Bauartzulassungen im Sinne der Eichordnung anzusehen.

Prüfscheininhaber PTB-Geschäftszeichen	Prüfschein-Nr. Datum	Einrichtung, messtechnische Merkmale und Bemerkungen
<b>SGS Griep Meerwinck GmbH</b> <b>22297 Hamburg</b> <b>Deutschland</b>	<b>D09-02.01</b> 30.01.2002	<b>Software</b> WGST32.dll. Anpassung der Druckausgabe an Betriebssystem Citrix.  3. Revision vom 09.06.2011
PTB-1.12-4052603		
<b>Bitzer Wiegetechnik GmbH</b> <b>31135 Hildesheim</b> <b>Deutschland</b>	<b>D09-04.15</b> 02.06.2004	<b>Anzeige- und Bedienterminal</b> DISOVIEW E.  3. Revision vom 11.04.2011
PTB-1.12-4051720		
<b>Service4you GmbH</b> <b>81675 München</b> <b>Deutschland</b>	<b>D09-04.18</b> 06.07.2004	<b>Preisrechendes Kassensystem</b> DS4Y-Kassenterminal.  3. Revision vom 06.06.2011
PTB-1.12-4052369		
<b>Mettler-Toledo (Albstadt) GmbH</b> <b>72458 Albstadt</b> <b>Deutschland</b>	<b>D09-04.34</b> 02.11.2004	<b>Wägezelle</b> DMS-Plattformwägezelle 708, Emax = 11kg bis 200kg, Genauigkeitsklasse C3, C3 MI6, C4 Accuracy class.  3. Revision vom 08.06.2011
PTB-1.12-4052323		
<b>dennree GmbH</b> <b>95183 Töpen</b> <b>Deutschland</b>	<b>D09-07.25</b> 15.11.2007	<b>Nichtpreisrechendes Kassensystem</b> denree Kasse.  1. Revision vom 08.06.2011
PTB-1.12-4051252		
<b>datapos GmbH</b> <b>78224 Singen (Hohentwiel)</b> <b>Deutschland</b>	<b>D09-10.28</b> 02.05.2011	<b>Nichtpreisrechendes Kassensystem</b> DATAPOS-PC-KASSE zum Anschluss an preisrechende nichtselbsttätige Waagen für offene Verkaufsstellen.
PTB-1.12-4049560		
<b>Schenck Process GmbH</b> <b>64293 Darmstadt</b> <b>Deutschland</b>	<b>D09-11.04</b> 19.04.2011	<b>Auswertegerät</b> DISOMAT Tersus. Optional zur Realisierung von Mehrteilungs- oder Mehrbereichswaagen. Für Waagen der Genauigkeitsklasse III oder IIII, n ≤ 8000.
PTB-1.12-4050805		
<b>Schenck Process GmbH</b> <b>64293 Darmstadt</b> <b>Deutschland</b>	<b>D09-11.05</b> 19.04.2011	<b>Auswertegerät</b> DISOMAT Opus. Optional zur Realisierung von Mehrteilungs- oder Mehrbereichswaagen. Für Waagen der Genauigkeitsklasse III oder IIII, n ≤ 6000.
PTB-1.12-4050511		



Prüfscheininhaber PTB-Geschäftszeichen	Prüfschein-Nr. Datum	Einrichtung, messtechnische Merkmale und Bemerkungen
<b>Anyload Youngzon Transducer (Hang.) Co. Ltd. Hangzhou Economic&amp;Technol. Development Zone 310018 HangZhou China</b>	<b>D09-11.07</b> 11.04.2011	<b>Wägezelle</b> DMS-Doppelbiegebalken-Wägezelle YZ 108, Emax = 10 kg bis 100 kg, Genauigkeitsklasse C3, Accuracy class.
PTB-1.12-4040021		
<b>ReformPlus Steffen Iser 23795 Klein Rönnau Deutschland</b>	<b>D09-11.08</b> 31.05.2011	<b>Nichtpreisrechendes Kassensystem</b> ReformPlus zum Anschluss an preisrechende nichtselbsttätige Waagen für offene Verkaufsstellen.
PTB-1.12-4051078		
<b>Bizerba GmbH &amp; Co. KG 72336 Balingen Deutschland</b>	<b>D09-11.10</b> 01.06.2011	<b>Software</b> UPOS-Scale Interface.
PTB-1.12-4049650		
<b>Schenck Process GmbH 64293 Darmstadt Deutschland</b>	<b>D09-11.11</b> 27.06.2011	<b>Wägezelle</b> DMS-Druckwägezelle WDI, Emax = 15t / 25t, Genauigkeitsklasse D1, C1 Accuracy class.
PTB-1.12-4050371		
<b>Hottinger Baldwin Messtechnik GmbH 64293 Darmstadt Deutschland</b>	<b>D09-11.12</b> 29.06.2011	<b>Anzeige- und Bedienterminal</b> DWS2103.
PTB-1.12-4045795		
<b>Wincor Nixdorf International GmbH 33106 Paderborn Deutschland</b>	<b>D09-96.13</b> 18.07.1996	<b>Nichtpreisrechendes Kassensystem</b> BEETLE /... . Zum Anschluss an preisrechende Waagen für offene Verkaufsstellen.  15. Revision vom 21.04.2011
PTB-1.12-4051663		

## EG-Bauartzulassungen

### Nichtselbsttätige Waagen

Zulassungsinhaber PTB-Geschäftszeichen	Zul.-Zeichen Datum	Bauart, messtechnische Merkmale und Bemerkungen
<b>Siemens AG 76187 Karlsruhe Deutschland</b>	<b>D01-09-004</b> 05.04.2001	<b>Nichtselbsttätige elektromechanische Waage mit oder ohne Hebelwerk</b> SIWAREX A, SIWAREX M, SIWAREX AWS, ausgeführt als Brücken-, Behälter-, Wand- oder Hängebahnwaage, mit oder ohne Hebelwerk, auch als Mehrteilungs- oder Mehrbereichswaage. Max 4 kg bis 400 t, Genauigkeitsklasse III, n ≤ 6000 oder IIII, n ≤ 1000. Bauartzulassungsverlängerung bis zum 04.04.2021.  Die Bauartzulassung ist gültig bis 04.04.2021  4. Revision vom 06.06.2011
PTB-1.12-4050727		

Zulassungsinhaber PTB-Geschäftszeichen	Zul.-Zeichen Datum	Bauart, messtechnische Merkmale und Bemerkungen
<b>Bizerba GmbH &amp; Co. KG</b> <b>72336 Balingen</b> <b>Deutschland</b>  PTB-1.12-4051594	<b>D01-09-007</b>  22.06.2001	<b>Nichtselbsttätige elektromechanische Waage ohne Hebelwerk BPW... / BPWD... . Verlängerung, Neubewertung, neue Gerätevariante.</b>  Die Bauartzulassung ist gültig bis 11.05.2021  2. <i>Revision</i> vom 12.05.2011
<b>Pfister Waagen Bilanciai GmbH</b> <b>86444 Affing</b> <b>Deutschland</b>  PTB-1.12-4050744	<b>D01-09-008</b>  24.04.2001	<b>Nichtselbsttätige elektromechanische Waage mit oder ohne Hebelwerk</b> DWT 400 / DWT 410 / DWT 450 / DWT 800. Max 1 kg bis 300 t, n ≤ 10000 (Klasse III), n ≤ 1000 (Klasse IIII).  Die Bauartzulassung ist gültig bis 23.04.2021  7. <i>Revision</i> vom 07.07.2011
<b>SysTec GmbH</b> <b>50129 Bergheim</b> <b>Deutschland</b>  PTB-1.12-4048069	<b>D01-09-017</b>  12.10.2001	<b>Nichtselbsttätige elektromechanische Waage mit oder ohne Hebelwerk</b> IT3000. Option: Mehrteilungs- oder Mehrbereichswaage, Genauigkeitsklasse III oder IIII, Max 0,3 kg bis 400 kg.  Die Bauartzulassung ist gültig bis 11.10.2011  9. <i>Revision</i> vom 03.05.2011
<b>Sartorius Weighing Technology GmbH</b> <b>37075 Göttingen</b> <b>Deutschland</b>  PTB-1.12-4051156	<b>D01-09-019</b>  04.09.2001	<b>Nichtselbsttätige elektromechanische Waage mit oder ohne Hebelwerk BC</b> BL 100, BD BL 100, BD BL 200, BF BL 500, Verlängerung der Gültigkeit.  Die Bauartzulassung ist gültig bis 22.06.2021  7. <i>Revision</i> vom 23.06.2011
<b>SysTec GmbH</b> <b>50129 Bergheim</b> <b>Deutschland</b>  PTB-1.12-4048311	<b>D02-09-021</b>  24.09.2002	<b>Nichtselbsttätige elektromechanische Waage mit oder ohne Hebelwerk</b> IT8000, geänderte Sicherung, Zusatzinformationen.  Die Bauartzulassung ist gültig bis 23.09.2012  9. <i>Revision</i> vom 07.06.2011
<b>Mettler-Toledo (Albstadt) GmbH</b> <b>72458 Albstadt</b> <b>Deutschland</b>  PTB-1.12-4049715	<b>D05-09-032</b>  21.10.2005	<b>Nichtselbsttätige elektromechanische Waage mit oder ohne Hebelwerk</b> IND... Option: Mehrteilungswaage, Mehrbereichswaage, Genauigkeitsklasse II, III oder IIII, Max 3 kg bis 60 t.  Die Bauartzulassung ist gültig bis 20.10.2015  5. <i>Revision</i> vom 29.04.2011
<b>SysTec Systemtechnik und Industrieautomation GmbH</b> <b>50129 Bergheim</b> <b>Deutschland</b>  PTB-1.12-4052637	<b>D06-09-002</b>  26.01.2006	<b>Nichtselbsttätige elektromechanische fahrzeugmontierte Waage</b> SyWa 3000. Zusätzliches Anzeige- und Bedienterminal; zusätzlicher Blitzschutz.  Die Bauartzulassung ist gültig bis 25.01.2016  2. <i>Revision</i> vom 31.05.2011
<b>Bizerba GmbH &amp; Co. KG</b> <b>72336 Balingen</b> <b>Deutschland</b>  PTB-1.12-4051976	<b>D06-09-026</b>  21.12.2006	<b>Nichtselbsttätige preisrechnende Waage für offene Verkaufsstellen</b> ECII... ; Max ≤ 30 kg, Option: Mehrteilungswaage III, Option: Mult-interval instrument.  Die Bauartzulassung ist gültig bis 20.12.2016  3. <i>Revision</i> vom 06.07.2011

Zulassungsinhaber PTB-Geschäftszeichen	Zul.-Zeichen Datum	Bauart, messtechnische Merkmale und Bemerkungen
<b>Bizerba GmbH &amp; Co. KG</b> <b>72336 Balingen</b> <b>Deutschland</b>  PTB-1.12-4050995	<b>D07-09-004</b> 08.05.2007	<b>Nichtselbsttätige preisrechnende Waage für offene Verkaufsstellen</b> CE II... . Max ≤ 150 kg, n ≤ 6000 (Klasse III).  Die Bauartzulassung ist gültig bis 07.05.2017  3. <i>Revision</i> vom 04.07.2011
<b>Schenck Process GmbH</b> <b>64293 Darmstadt</b> <b>Deutschland</b>  PTB-1.12-4051367	<b>D07-09-012</b> 19.07.2007	<b>Nichtselbsttätige elektromechanische Waage mit oder ohne Hebelwerk</b> DISOMAT Tersus. Optional: Ausführung als Mehrbereichs- oder Mehrteilungswaage, Genauigkeitsklasse III oder IIII, n ≤ 8000 (III), n ≤ 1000 (IIII).  Die Bauartzulassung ist gültig bis 18.07.2017  2. <i>Revision</i> vom 20.04.2011
<b>Bizerba GmbH &amp; Co. KG</b> <b>72336 Balingen</b> <b>Deutschland</b>  PTB-1.1-4050994	<b>D08-09-021</b> 22.09.2008	<b>Nichtselbsttätige preisrechnende Waage für offene Verkaufsstellen K...</b> Max ≤ 200 kg, n ≤ 6000 (Klasse III).  Die Bauartzulassung ist gültig bis 21.09.2018  5. <i>Revision</i> vom 13.04.2011
<b>Ebinger Waagenbau GmbH</b> <b>74427 Fichtenberg</b> <b>Deutschland</b>  PTB-1.12-4049562	<b>D09-09-008</b> 31.03.2009	<b>Nichtselbsttätige elektromechanische Waage mit oder ohne Hebelwerk</b> 2790 als Plattform-, Wand-, Rohrbahn- oder Behälterwaage, mit oder ohne Hebelwerk, auch als Mehrbereichswaage. Max ≤ 100 t, Genauigkeitsklasse III, n ≤ 3200, oder IIII, n ≤ 1000. Zusätzliche Ausführung ohne E-Cal Schalter.  Die Bauartzulassung ist gültig bis 30.03.2019  1. <i>Revision</i> vom 07.04.2011
<b>Sartorius Weighing Technology</b> <b>GmbH</b> <b>37075 Göttingen</b> <b>Deutschland</b>  PTB-1.12-4052066	<b>D09-09-015</b> 19.06.2009	<b>Nichtselbsttätige elektromechanische Präzisionswaage MSX.</b> Max ≤ 12,2 kg, n ≤ 102000 (Klasse I), n ≤ 82000 (Klasse II).  Die Bauartzulassung ist gültig bis 18.06.2019  3. <i>Revision</i> vom 07.07.2011
<b>R-C-T Remote Control</b> <b>Technology</b> <b>35075 Gladenbach</b> <b>Deutschland</b>  PTB-1.12-4051127	<b>D10-09-007</b> 28.01.2010	<b>Nichtselbsttätige elektromechanische Waage ohne Hebelwerk WAER 100.</b> Geänderte Gehäuse, geänderte Frontfolie.  Die Bauartzulassung ist gültig bis 27.01.2020  3. <i>Revision</i> vom 07.04.2011
<b>R-C-T Remote Control</b> <b>Technology</b> <b>35075 Gladenbach</b> <b>Deutschland</b>  PTB-1.12-4052610	<b>D10-09-007</b> 28.01.2010	<b>Nichtselbsttätige elektromechanische Waage ohne Hebelwerk WAER 100,</b> zusätzliche Abbildungen.  Die Bauartzulassung ist gültig bis 27.01.2020  4. <i>Revision</i> vom 14.06.2011
<b>Bizerba GmbH &amp; Co. KG</b> <b>72336 Balingen</b> <b>Deutschland</b>  PTB-1.12-4051796	<b>D10-09-010</b> 27.04.2010	<b>Nichtselbsttätige preisrechnende Waage für offene Verkaufsstellen</b> SC II... . Optional: Ausführung als Mehrteilungswaage, Genauigkeitsklasse III, Max 1 kg bis 300 kg, n ≤ 7500.  Die Bauartzulassung ist gültig bis 26.04.2020  2. <i>Revision</i> vom 14.04.2011

Zulassungsinhaber PTB-Geschäftszeichen	Zul.-Zeichen Datum	Bauart, messtechnische Merkmale und Bemerkungen
<b>Voith-Werke Ing.A.Fritz Voith Ges.m.b.H.&amp; Co.KG 4050 Traun Österreich</b>  PTB-1.12-4048954	<b>D11-09-005</b> 09.06.2011	<b>Nichtselbsttätige elektromechanische Waage mit oder ohne Hebelwerk</b> SIWAREX FTA. Genauigkeitsklasse III ( $n \leq 6000$ ) oder IIII ( $n \leq 1000$ ), Max 0,1 kg bis 400 t, ausgeführt als Brücken-, Behälter-, Wand- oder Hängebahnwaage, mit oder ohne Hebelwerk, auch als Mehrteilungs- oder Mehrbereichswaage.  Die Bauartzulassung ist gültig bis 08.06.2021
<b>Bitzer Wiegetechnik GmbH 31135 Hildesheim Deutschland</b>  PTB-1.12-4050588	<b>D11-09-006</b> 12.04.2011	<b>Nichtselbsttätige elektromechanische Waage mit oder ohne Hebelwerk</b> DISOBOX plus. Optional: Ausführung als Mehrteilungs- oder Mehrbereichswaage, Genauigkeitsklasse III oder IIII, Max 1 kg bis 600 t, $n \leq 10000$ (III), $n \leq 1000$ (IIII).  Die Bauartzulassung ist gültig bis 11.04.2021
<b>Waagen-Kissling GmbH 64668 Rimbach Deutschland</b>  PTB-1.12-4051641	<b>D11-09-007</b> 30.06.2011	<b>Nichtselbsttätige elektromechanische Waage mit oder ohne Hebelwerk</b> WKN.. .  Die Bauartzulassung ist gültig bis 29.06.2021
<b>Güzey Endüstriyel Tarti Sistemleri Makina Kalibrasyon Mühendislik Sanayi ve Ticaret. Ltd.Sti Cigli/Izmir Tuerkei</b>  PTB-1.12-4049819	<b>D11-09-009</b> 21.04.2011	<b>Nichtselbsttätige elektromechanische Waage mit oder ohne Hebelwerk</b> B2. Max 0,3 kg bis 400 t, $n \leq 3000$ (Klasse III), $n \leq 1000$ (Klasse IIII).  Die Bauartzulassung ist gültig bis 20.04.2021
<b>SysTec GmbH 50129 Bergheim Deutschland</b>  PTB-1.12-4050374	<b>D11-09-012</b> 24.05.2011	<b>Nichtselbsttätige elektromechanische Waage mit oder ohne Hebelwerk</b> ITx000E. Max 0,3 kg bis 600t, $n \leq 32000$ (Klasse II), $n \leq 10000$ (Klasse IIII), $n \leq 1000$ (Klasse IIII).  Die Bauartzulassung ist gültig bis 23.05.2021
<b>Hüray Baskülleri San. ve Tic. Ltd. Sti. Ikitelli OSB Ikitelli Istanbul Tuerkei</b>  PTB-1.12-4052493	<b>D11-09-013</b> 25.05.2011	<b>Nichtselbsttätige elektromechanische Waage mit oder ohne Hebelwerk</b> B2. Max 0,3 kg bis 400 t, $n \leq 3000$ (Klasse III), $n \leq 1000$ (Klasse IIII).  Die Bauartzulassung ist gültig bis 24.05.2021
<b>Techno-Control GmbH 65719 Hofheim am Taunus Deutschland</b>  PTB-1.12-4052922	<b>D11-09-015</b> 20.06.2011	<b>Nichtselbsttätige elektromechanische Waage mit oder ohne Hebelwerk</b> ITx000E, Genauigkeitsklasse III oder III, $n \leq 6000$ .  Die Bauartzulassung ist gültig bis 19.06.2021
<b>Bizerba GmbH &amp; Co. KG 72336 Balingen Deutschland</b>  PTB-1.12-4051911	<b>D93-09-103</b> 22.12.1992	<b>Nichtselbsttätige preisrechnende Waage für offene Verkaufsstellen</b> BW-LC..... . Max 3 kg bis 150 kg, $n \leq 6000$ .  Die Bauartzulassung ist gültig bis 31.12.2002  5. Nachtrag vom 10.05.2011
<b>PESA Waagen AG Elektronische Wäge- und Sensortechnik 8330 Pfäffikon/ZH Schweiz</b>  PTB-1.12-4043450	<b>D93-09-125</b> 21.06.1993	<b>Nichtselbsttätige elektromechanische Waage mit oder ohne Hebelwerk</b> EBR 100-I, EBR 200-I, EBR 210-I, EBR 300-I, EBR 500-I und EBR 700-I. Zusätzliche Lastaufnehmer; weitere Anzeigeeinrichtung.  Die Bauartzulassung ist gültig bis 10.04.2013  2. Revision vom 24.05.2011

Zulassungsinhaber PTB-Geschäftszeichen	Zul.-Zeichen Datum	Bauart, messtechnische Merkmale und Bemerkungen
<b>Mettler-Toledo (Albstadt) GmbH 72458 Albstadt Deutschland</b>	<b>D93-09-144</b> 30.11.1993	<b>Nichtselbsttätige preisrechnende Waage für offene Verkaufsstellen L2-...</b> Genauigkeitsklasse III, n ≤ 7500, Max 1kg bis 30 kg. Optionale Ausführung auch als Mehrteilungswaage. Erhöhung der Max-Last auf 15 kg (L2-...-SCA...).
PTB-1.12-4052921		Die Bauartzulassung ist gültig bis 29.11.2013 <i>11. Revision</i> vom 23.06.2011
<b>SysTec GmbH 50129 Bergheim Deutschland</b>	<b>D95-09-030</b> 15.09.1995	<b>Nichtselbsttätige elektromechanische Waage mit oder ohne Hebelwerk</b> IT9000, geänderte Sicherung.
PTB-1.12-4048350		Die Bauartzulassung ist gültig bis 19.04.2015 <i>7. Revision</i> vom 09.06.2011
<b>ARJO Hospital Equipment AB 0 Eslöv Schweden</b>	<b>D97-09-015</b> 12.06.1997	<b>Nichtselbsttätige elektromechanische Waage ohne Hebelwerk</b> CFA 2100, eingebaut in einen Sitz- oder Liegelifter, zur Verwendung in der Heilkunde. Genauigkeitsklasse III, Max 182 kg, +10°C bis +40°C. Ausgeführt als Mehrbereichswaage mit Neigungsschalter.
PTB-1.12-4051713		Die Bauartzulassung ist gültig bis 11.06.2017 <i>3. Revision</i> vom 31.05.2011
<b>SysTec GmbH 50129 Bergheim Deutschland</b>	<b>D99-09-004</b> 09.04.1999	<b>Nichtselbsttätige elektromechanische Waage mit oder ohne Hebelwerk</b> IT6000. Änderung der Sicherung, Preisauszeichnung.
PTB-1.12-4048365		Die Bauartzulassung ist gültig bis 08.04.2019 <i>5. Revision</i> vom 08.06.2011

## Innerstaatliche Bauartzulassungen

Folgende Bauarten von Messgeräten und Zusatzeinrichtungen sind von der Physikalisch-Technischen Bundesanstalt zur innerstaatlichen Erreichung zugelassen worden.

## Längenmessgeräte und deren Kombinationen

Zulassungsinhaber PTB-Geschäftszeichen	Zul.-Zeichen Datum	Bauart, messtechnische Merkmale und Bemerkungen
<b>MiCROTEC Industriautomation GmbH 4020 Linz Österreich</b>	<b>1.4</b> <b>08.06</b> 05.06.2008	<b>Rundholzmessanlage</b> IRAS-DE. Änderung der Adresse des Zulassungsinhabers. Verwendbarkeit eines weiteren Drehimpulsgebertyps. Impulsgeber der Firma Eltra (Typ EL63D).
PTB-5.45-4052494		<i>1. Nachtrag</i> vom 20.05.2011
<b>Carometec GmbH 44534 Lünen Deutschland</b>	<b>1.5</b> <b>10.01</b> 29.04.2011	<b>Choirometer</b> AutoFom-Erkenschwick. Automatisches Choirometer zur Bestimmung des prozentualen Muskelfleischanteiles von Schweineschlachtkörpern gemäß Handelsklassenverordnung. Choirometer mit Ultraschall-Messprinzip.
PTB-5.45-4036614		
<b>Carometec GmbH 44534 Lünen Deutschland</b>	<b>1.5</b> <b>11.01</b> 16.06.2011	<b>Choirometer</b> Fat-O-Meat'er II. Halbautomatisches Handchoirometer zur Klassifizierung von Schweineschlachtkörpern, Invasive, opto-elektronische Messwerverfassung.
PTB-5.45-4028753		

Zulassungsinhaber PTB-Geschäftszeichen	Zul.-Zeichen Datum	Bauart, messtechnische Merkmale und Bemerkungen
<b>CLASSPRO GmbH</b> <b>86577 Sielenbach</b> <b>Deutschland</b>	<b>1.5</b> <b>11.03</b> 27.05.2011	<b>Choirometer</b> OptiGrade-MCP. Choirometer zur Klassifizierung von Schweineschlachtkörpern, Typ: Classpro OptiGrade MCP. Choirometer mit invasiv arbeitender optoelektronischen Einstichsonde.
PTB-5.45-4032719		

## Messgeräte für ruhende Flüssigkeiten

<b>BARTEC BENKE GmbH</b> <b>94239 Gotteszell</b> <b>Deutschland</b>	<b>4.411</b> <b>01.11</b> 31.07.2001	<b>Füllstandsmessgerät mit Schwimmer</b> VOLUTANK. Temperaturkompensations nach Verfahren 1 gemäß PTB-A 5.  <i>2. Nachtrag zur 3. Neufassung</i> vom 19.05.2011
PTB-1.5-4052518		
<b>Schrader-T+A Fahrzeugbau GmbH &amp; Co. KG</b> <b>59269 Beckum</b> <b>Deutschland</b>	<b>4.503</b> <b>02.02</b> 08.05.2002	<b>Transport-Messbehälter Lebensmittel</b> Tankgröße von 10 000 Liter bis 32 000 Liter.  <i>2. Neufassung</i> vom 21.04.2011
PTB-1.5-4052084		
<b>Nutzfahrzeuge ROHR GmbH</b> <b>94315 Straubing</b> <b>Deutschland</b>	<b>4.512</b> <b>09.27</b> 30.06.2009	<b>Zylindertank als Messbehälter mit elektronischer Peilvorrichtung</b> mit Ultraschallsonden als Volumenmesssystem TAL-51. Zusätzliche Variante des Rohrleitungs- und Pneumatikschemas.  <i>1. Nachtrag</i> vom 08.04.2011
PTB-1.5-4051952		
<b>Kurt Willig GmbH &amp; Co. KG</b> <b>94315 Straubing</b> <b>Deutschland</b>	<b>4.512</b> <b>11.30</b> 11.04.2011	<b>Zylindertank als Messbehälter mit elektronischer Peilvorrichtung</b> mit Ultraschallsonden als Volumenmesssystem 3S4205. Tanksattelanhänger mit fünf Tankkammern mit 42 000 Liter Gesamtinhalt.
PTB-1.5-4051793		
<b>Kurt Willig GmbH &amp; Co. KG</b> <b>94315 Straubing</b> <b>Deutschland</b>	<b>4.512</b> <b>11.31</b> 07.04.2011	<b>Zylindertank als Messbehälter mit elektronischer Peilvorrichtung</b> mit Ultraschallsonden als Volumenmesssystem 3S4605. Tanksattelanhänger mit fünf Tankkammern mit 46 000 Liter Gesamtinhalt.
PTB-1.5-4051795		
<b>Schrader-T+A-Fahrzeugbau GmbH &amp; Co. KG</b> <b>59269 Beckum</b> <b>Deutschland</b>	<b>4.514</b> <b>09.47</b> 07.12.2009	<b>Zylindertank als Messbehälter mit elektronischer Peilvorrichtung</b> mit Schwimmer als Volumenmesssystem Z-STA 24-44,3/4 oder Z-STA 27-44,3/4. Erweiterung um das System 3003 von Bartec Benke sowie zwei Rohrleitungsschemata.  <i>1. Neufassung</i> vom 23.05.2011
PTB-1.5-4052380		

## Messgeräte für strömende Flüssigkeiten

<b>Flüssiggas-Anlagen GmbH</b> <b>38229 Salzgitter</b> <b>Deutschland</b>	<b>5.105</b> <b>96.02</b> 09.12.1996	<b>Zapfsäule für unter Druck verflüssigte Gase</b> FAS 110, 120, 140, 210, 220, 230, 240, 250, 420, 440. Zusätzliche Ausführungsform aufgenommen.  <i>2. Nachtrag zur 2. Neufassung</i> vom 15.06.2011
PTB-1.5-4052946		

Zulassungsinhaber PTB-Geschäftszeichen	Zul.-Zeichen Datum	Bauart, messtechnische Merkmale und Bemerkungen
<b>Bohlen &amp; Doyen Bauunternehmung GmbH 26639 Wiesmoor Deutschland</b>	<b>5.181</b> <b>01.13</b> 09.10.2001	<b>Messanlage für Hochdruck-Erdgas</b> B&D Erdgaszapfstelle. Betankungsrechner T20 aufgenommen.  <i>4. Neufassung</i> vom 27.05.2011
PTB-1.5-4052570		
<b>Gilbarco GmbH &amp; Co. KG 33154 Salzkotten Deutschland</b>	<b>5.181</b> <b>10.25</b> 07.04.2010	<b>Messanlage für Hochdruck-Erdgas</b> SK700-2 CNG. Alternatives Display mit größerer Anzeige aufgenommen.  <i>1. Neufassung</i> vom 05.05.2011
PTB-1.5-4052311		
<b>Schwelm Anlagentechnik GmbH 58332 Schwelm Deutschland</b>	<b>5.181</b> <b>95.03</b> 13.12.1995	<b>Messanlage für Hochdruck-Erdgas</b> Schwelm NGV-Zapfsäule. Massezähler CNGmass eingefügt.  <i>1. Neufassung</i> vom 18.05.2011
PTB-1.5-4052381		
<b>Hermann Lümmen GmbH 53842 Troisdorf Deutschland</b>	<b>5.601</b> <b>00.13</b> 25.09.2000	<b>Elektrisches Zählwerk</b> 401/601 - 630/LO / - 630/LO/IV / - 630/LO/VI / - 630/LO/FES. Sicherung der Parameter konkretisiert.  <i>2. Nachtrag zur 2. Neufassung</i> vom 15.04.2011
PTB-1.5-4052080		
<b>Tokheim Netherlands B.V. 0 Bladel Niederlande</b>	<b>5.602</b> <b>98.11</b> 15.06.1999	<b>Elektrisches Zählwerk</b> mit Zusatzeinrichtungen World Wide Calculator (WWC). Softwareversion ergänzt.  <i>8. Neufassung</i> vom 08.04.2011
PTB-1.5-4051962		
<b>Tokheim Netherlands B.V. 0 Bladel Niederlande</b>	<b>5.602</b> <b>98.11</b> 15.06.1999	<b>Elektrisches Zählwerk</b> mit Zusatzeinrichtungen World Wide Calculator. Softwareversion ergänzt.  <i>1. Nachtrag zur 8. Neufassung</i> vom 17.05.2011
PTB-1.5-4052543		
<b>Walter Leibold e. K. 78354 Sipplingen Deutschland</b>	<b>5.631</b> <b>00.32</b> 24.02.2000	<b>Tankdatenerfassungssystem</b> BTS1 oder BTS2. Neues Platinen Layout.  <i>1. Nachtrag</i> vom 15.04.2011
PTB-1.5-4052076		
<b>Tokheim Netherlands B.V. 0 Bladel Niederlande</b>	<b>5.631</b> <b>01.36</b> 22.10.2001	<b>Tankautomat</b> OPTIMUM, OPTIMUM IQ. Softwareversion ergänzt.  <i>3. Neufassung</i> vom 06.06.2011
PTB-1.5-4052808		
<b>Hermann Lümmen GmbH 53842 Troisdorf Deutschland</b>	<b>5.631</b> <b>07.51</b> 19.11.2007	<b>Tankautomat</b> lumatic 400/600 - 401/601. Sicherung der Parameter konkretisiert.  <i>3. Nachtrag</i> vom 15.04.2011
PTB-1.5-4052078		
<b>Wincor Nixdorf International GmbH 20097 Hamburg Deutschland</b>	<b>5.631</b> <b>11.58</b> 19.05.2011	<b>Tankautomat</b> NAMOS paylane smart. Bezahlungsterminal als Teil einer Selbstbedienungseinrichtung.
PTB-1.5-4051860		

Zulassungsinhaber PTB-Geschäftszeichen	Zul.-Zeichen Datum	Bauart, messtechnische Merkmale und Bemerkungen
<b>Hermann Lümmen GmbH</b> <b>53842 Troisdorf</b> <b>Deutschland</b>	<b>5.631</b> <b>98.25</b> 15.05.1998	<b>Tankautomat</b> lumatic 400/600, 630/LO, 630/LO/IV, 630/LO/VI. Sicherung der Parameter konkretisiert.  2. <i>Nachtrag zur 1. Neufassung</i> vom 15.04.2011
PTB-1.5-4052079		
<b>Wasserzähler</b>		
<b>Sensus GmbH Hannover</b> <b>30880 Laatzen</b> <b>Deutschland</b>	<b>6.132</b> <b>96.15</b> 22.01.1997	<b>Woltmanzähler für Kaltwasser.</b> Ausführung WP mit Rücklaufsperr COSMOS WPD. Woltmanzähler für Kaltwasser der Ausfg. WP mit mech. Zählwerk und Rücklaufsperr.  3. <i>Nachtrag</i> vom 05.05.2011
PTB-1.5-4042672		
<b>Gasmessgeräte</b>		
<b>Marquis GmbH</b> <b>58454 Witten</b> <b>Deutschland</b>	<b>7.614</b> <b>10.70</b> 13.10.2010	<b>Brennwertmessgerät</b> Prozessgaschromatograph. Gasbeschaffenheitstransmitter SAM-BIO, neues Benutzerhandbuch. Änderung der Limits der Kalibrierüberwachung.  1. <i>Nachtrag</i> vom 18.04.2011
PTB-3.31-4051595		
<b>Emerson Process Management Ltd</b> <b>0 Tullibody</b> <b>United Kingdom</b>	<b>7.614</b> <b>99.39</b> 16.08.1999	<b>Brennwertmessgerät</b> Prozessgaschromatograph (PGC) DANALYZER Modell 500 mit 2350 Controller. Neues CPU-Board im Controller 2350A.  5. <i>Nachtrag</i> vom 29.06.2011
PTB-3.31-4050478		
<b>RMG Messtechnik GmbH</b> <b>35510 Butzbach</b> <b>Deutschland</b>	<b>7.732</b> <b>01.22</b> 25.07.2001	<b>Höchstbelastungs-Anzeigegerät</b> und Belastungs-Registriergerät MRG910. Neue Softwareversion, Volumenregistrierung mit Nachkommastellen.  1. <i>Nachtrag zur 3. Neufassung</i> vom 10.05.2011
PTB-1.42-4052405		
<b>Feingerätebau Tritschler GmbH</b> <b>79725 Laufenburg (Baden)</b> <b>Deutschland</b>	<b>7.732</b> <b>04.28</b> 11.11.2004	<b>Höchstbelastungs-Anzeigegerät</b> K945/MCO, neue Softwareversion.  1. <i>Nachtrag zur 1. Neufassung</i> vom 06.05.2011
PTB-1.42-4052111		
<b>Feingerätebau Tritschler GmbH</b> <b>79725 Laufenburg (Baden)</b> <b>Deutschland</b>	<b>7.732</b> <b>05.32</b> 18.04.2005	<b>Höchstbelastungs-Anzeigegerät</b> K930/TDS, neue Softwareversion.  2. <i>Nachtrag zur 1. Neufassung</i> vom 10.05.2011
PTB-1.42-4052109		
<b>RMG Messtechnik GmbH</b> <b>35510 Butzbach</b> <b>Deutschland</b>	<b>7.732</b> <b>06.34</b> 26.04.2006	<b>Höchstbelastungs-Anzeigegerät</b> und Belastungs-Registriergerät MRG 905. Neue Softwareversion, Zählwerkstände mit Nachkommastellen.  2. <i>Nachtrag zur 1. Neufassung</i> vom 10.05.2011
PTB-1.42-4052404		



Zulassungsinhaber PTB-Geschäftszeichen	Zul.-Zeichen Datum	Bauart, messtechnische Merkmale und Bemerkungen
<b>Feingerätebau Tritschler GmbH</b> 79725 Laufenburg (Baden) Deutschland	<b>7.732</b> <b>09.44</b> 21.09.2009	<b>Höchstbelastungs-Anzeigegerät</b> und Belastungs-Registriergerät G954/TC2, neue Softwareversion.  2. <i>Nachtrag</i> vom 20.05.2011

PTB-1.42-4052468

## Selbsttätige Waagen

<b>ThermoFisher Scientific Messtechnik GmbH</b> 46049 Oberhausen Deutschland	<b>10.36</b> <b>99.01</b> 15.02.1999	<b>Selbsttätige Waage zum kontinuierlichen Wägen (Förderbandwaage)</b> MT22xx, Namensänderung.  2. <i>Nachtrag</i> vom 15.06.2011
--	--	---

PTB-1.12-4052761

## Messgeräte für Getreide und Ölfrüchten

<b>Pfeuffer GmbH Mess- und Prüfgeräte</b> 97318 Kitzingen Deutschland	<b>11.26</b> <b>10.02</b> 29.06.2010	<b>Feuchtebestimmer für Getreide und Ölfrüchte</b> Granolyser. Neue SW-Version, neue Kalibrierungen für Mais und Raps.  2. <i>Nachtrag</i> vom 24.06.2011
---	--	---

PTB-3.2-4053099

## Messgeräte im Straßenverkehr

<b>HALE electronic GmbH</b> 5020 Salzburg Österreich	<b>18.01</b> <b>11.01</b> 11.04.2011	<b>Wegstreckenzähler</b> WSZ-06. Zulassung eines neuen Wegstreckenzählers des Typs WSZ-06.
--	--	--

PTB-1.31-4050200

<b>TEXA S.p.A.</b> 31050 Monastier di Treviso (TV) Italien	<b>18.09</b> <b>07.03</b> 14.08.2007	<b>Abgasmessgerät für Kompressionszündungsmotoren</b> in der Ausführung als Teilstrom-Trübungsmessgerät mit der Typbezeichnung: OPABOX Autopower mit PC. Opazimeter TEXA Opabox kann auch mit externer Batterie betrieben werden.
--	--	---

PTB-3.2-4052274

1. *Neufassung* vom 11.05.2011

<b>Robert Bosch GmbH</b> Produktbereich Diagnostics 73207 Plochingen Deutschland	<b>18.09</b> <b>96.23</b> 16.08.1996	<b>Abgasmessgerät für Kompressionszündungsmotoren</b> in der Ausführung als Teilstrom-Trübungsmessgerät mit der Typbezeichnung: RTM 430 in Verbindung mit: siehe Anlage: „Typbezeichnung“. Erweiterung durch das Modell FSA 760.
---	--	--

PTB-3.2-4052936

2. *Neufassung* vom 23.06.2011

<b>DiTEST Fahrzeugdiagnose GmbH</b> Ein AVL Unternehmen 8020 Graz Österreich	<b>18.09</b> <b>97.07</b> 26.08.2000	<b>Abgasmessgerät für Kompressionszündungsmotoren</b> in der Ausführung als Teilstrom-Trübungsmessgerät mit der Typbezeichnung: Sensor-Unit 435 in Verbindung mit "DiCom 4000". Neue Software V.4.9, 5-Gasmessgerät.
--	--	--

PTB-3.2-4052596

1. *Nachtrag zur 3. Neufassung* vom 23.05.2011

Zulassungsinhaber PTB-Geschäftszeichen	Zul.-Zeichen Datum	Bauart, messtechnische Merkmale und Bemerkungen
<b>DiTEST Fahrzeugdiagnose GmbH Ein AVL Unternehmen 8020 Graz Österreich</b>	<b>18.09</b> <b>98.05</b> 26.08.2000	<b>Abgasmessgerät für Kompressionszündungsmotoren</b> in der Ausführung als Teilstrom-Trübungsmessgerät mit der Typbezeichnung: Sensor-Unit 4000 in Verbindung mit "DiCom 4000". Neue Software V.4.9, 5-Gasmessgerät.  <i>3. Nachtrag zur 4. Neufassung vom 23.05.2011</i>
PTB-3.2-4052595		
<b>Robert Bosch GmbH Produktbereich Diagnostics 73207 Plochingen Deutschland</b>	<b>18.10</b> <b>00.23</b> 12.01.2001	<b>Abgasmessgerät für Fremdzündungsmotoren</b> der Genauigkeitsklasse 1 mit der Typbezeichnung: BEA 840/850 oder BEA 050 in Verbindung mit ESA, FSA oder MOT. Erweiterung durch das Modell FSA 760.  <i>3. Nachtrag zur 2. Neufassung vom 23.06.2011</i>
PTB-3.2-4052939		
<b>DiTEST Fahrzeugdiagnose GmbH Ein AVL Unternehmen 8020 Graz Österreich</b>	<b>18.10</b> <b>97.22</b> 23.01.1998	<b>Abgasmessgerät für Fremdzündungsmotoren</b> der Genauigkeitsklasse 1 mit der Typbezeichnung: DiGas 4000 oder "DiCom 4000". Neue Software Version 4.9, 5-Gasmessgerät.  <i>3. Nachtrag zur 5. Neufassung vom 19.05.2011</i>
PTB-3.2-4052379		
<b>DiTEST Fahrzeugdiagnose GmbH Ein AVL Unternehmen 8020 Graz Österreich</b>	<b>18.10</b> <b>98.20</b> 08.05.1998	<b>Abgasmessgerät für Fremdzündungsmotoren</b> der Genauigkeitsklasse 1 mit der Typbezeichnung: DiGas 4000 Light. Neue Software V.4.9, 5-Gasmessgerät.  <i>2. Nachtrag zur 5. Neufassung vom 23.05.2011</i>
PTB-3.2-4052591		
<b>VITRONIC Dr.-Ing. Stein Bildverarbeitungssysteme GmbH 65189 Wiesbaden Deutschland</b>	<b>18.11</b> <b>06.01</b> 23.06.2006	<b>Geschwindigkeitsüberwachungsgerät</b> PoliScan Speed. Die Falldaten des Geschwindigkeitsüberwachungsgerätes können auch mit einer neuen Version des Auswerteprogrammes ausgewertet werden.  <i>4. Neufassung vom 27.05.2011</i>
PTB-1.31-4051578		
<b>VITRONIC Dr.-Ing. Stein Bildverarbeitungssysteme GmbH 65189 Wiesbaden Deutschland</b>	<b>18.11</b> <b>07.01</b> 15.05.2007	<b>Geschwindigkeitsüberwachungsgerät</b> PoliScan Speed F1. Die Falldaten des Geschwindigkeitsüberwachungsgerätes können auch mit einer neuen Version des Auswerteprogrammes ausgewertet werden.  <i>3. Neufassung vom 27.05.2011</i>
PTB-1.31-4051579		
<b>JENOPTIK Robot GmbH 40789 Monheim am Rhein Deutschland</b>	<b>18.11</b> <b>07.02</b> 25.10.2007	<b>Geschwindigkeitsüberwachungsgerät</b> mit Drucksensoren TRAFFIPAX TraffiStar S 330, mit Anbindung an Wechselverkehrs-zeichen (WVZ). Neue Hardwareversion des IPV: IPV Kombi. Neue Softwareversion des ROBOT IPV und IPV Kombi. Neue Richtlinie zur Eichung: 4. Ausgabe vom 01.06.2011.  <i>2. Neufassung vom 07.06.2011</i>
PTB-1.31-4040249		
<b>VDS Verkehrstechnik GmbH 2708 Löbau Deutschland</b>	<b>18.11</b> <b>08.01</b> 14.08.2008	<b>Geschwindigkeitsüberwachungsgerät</b> Verkehrsüberwachungsgerät M5 Radar. Zwei Anlagen in einem Fahrzeug, neue Gebrauchsanweisung.  <i>1. Neufassung vom 09.05.2011</i>
PTB-1.31-4051336		

Zulassungsinhaber PTB-Geschäftszeichen	Zul.-Zeichen Datum	Bauart, messtechnische Merkmale und Bemerkungen
<b>LEIVTEC Verkehrstechnik GmbH</b> 35578 Wetzlar Deutschland	<b>18.11</b> <b>09.04</b> 02.07.2009	<b>Geschwindigkeitsüberwachungsgerät XV3.</b> Das Geschwindigkeitsüberwachungsgerät darf optional mit einer Monitor-Funkübertragung betrieben werden.  <i>1. Neufassung</i> vom 27.05.2011
PTB-1.31-4050937		
<b>JENOPTIK Robot GmbH</b> 40789 Monheim am Rhein Deutschland	<b>18.11</b> <b>09.09</b> 03.09.1990	<b>Geschwindigkeitsüberwachungsgerät</b> mit Drucksensoren TRAFFIPAX TraffiPhot S. Zulassung einer digitalen Kamera vom Typ SmartCamera IV.  <i>3. Neufassung</i> vom 19.04.2011
PTB-1.31-4050665		
<b>VITRONIC Dr.-Ing. Stein Bildverarbeitungssysteme GmbH</b> 65189 Wiesbaden Deutschland	<b>18.15</b> <b>10.01</b> 18.04.2011	<b>Rotlicht- und Geschwindigkeitsüberwachungsanlage</b> PoliScan F1 HP. Zulassung der stationären Rotlicht - und Geschwindigkeitsüberwachungsanlage PoliScan F1 HP.
PTB-1.31-4048211		

## Messgeräte für Elektrizität

<b>Landis+Gyr GmbH</b> 90459 Nürnberg Deutschland	<b>20.15</b> <b>03.17</b> 13.08.2003	<b>Mehrphasenzähler (elektronisches Messwerk) ZxQ...</b> Bek. Nr.: 4702 (AG-Geschz.: 2.34-07-4032536-4702)  <i>1. Neufassung</i> vom 27.05.2011
PTB-2.3-4032536		
<b>EMH metering GmbH &amp; Co. KG</b> 19243 Wittenburg Deutschland	<b>20.15</b> <b>07.07</b> 12.03.2008	<b>Mehrphasenzähler (elektronisches Messwerk) LZQJ-XC.</b> Bek. Nr. 4903  <i>4. Neufassung</i> vom 02.05.2011
PTB-2.3-4050806		
<b>Hager Electro GmbH &amp; Co. KG</b> 66440 Blieskastel Deutschland	<b>20.15</b> <b>11.02</b> 19.04.2011	<b>Einphasenzähler (elektronisches Messwerk) EHZ163xxx.</b> Bek. Nr. 4901
PTB-2.3-4050510		
<b>Itron Zähler &amp; Systemtechnik GmbH</b> 31789 Hameln Deutschland	<b>20.15</b> <b>11.06</b> 10.05.2011	<b>Einphasenzähler (elektronisches Messwerk) HZ1-A...</b> Bek. Nr. 4909
PTB-2.3-4051320		
<b>S.C. AEM S.A.</b> 300693 Timisoara Rumänien	<b>20.15</b> <b>11.07</b> 20.05.2011	<b>Mehrphasenzähler (elektronisches Messwerk) eHZ E3L-...</b> Bek. Nr. 4941
PTB-2.3-4052367		

Zulassungsinhaber PTB-Geschäftszeichen	Zul.-Zeichen Datum	Bauart, messtechnische Merkmale und Bemerkungen
<b>Ritz Instrument Transformers GmbH</b> 22041 Hamburg Deutschland	<b>20.21</b> <b>00.11</b> 25.08.2000	<b>Einzelstromwandler EKS(H)...</b> Bek. Nr. 4793 <i>1. Neufassung</i> vom 19.05.2011
PTB-2.3-4052454		
<b>MBS AG</b> 74429 Sulzbach-Laufen Deutschland	<b>20.21</b> <b>10.02</b> 29.03.2010	<b>Einzelstromwandler ASG 106.</b> Bek. Nr. 4932 <i>1. Neufassung</i> vom 11.05.2011
PTB-2.3-4052338		
<b>Ritz Instrument Transformers GmbH</b> 22041 Hamburg Deutschland	<b>20.21</b> <b>10.05</b> 07.09.2010	<b>Einzelstromwandler EKSO...; EKSS...</b> Bek. Nr. 4925 <i>1. Neufassung</i> vom 11.05.2011
PTB-2.3-4051363		
<b>Efen GmbH</b> 65344 Eltville am Rhein Deutschland	<b>20.21</b> <b>10.09</b> 12.05.2011	<b>Einzelstromwandler E<sup>3</sup>W1-3.</b> Bek. Nr. 4915
PTB-2.3-4050156		
<b>ALCE Elektrik Sanayi ve Ticaret AS</b> 34906 Pendik - Istanbul Tuerkei	<b>20.21</b> <b>11.01</b> 04.05.2011	<b>Einzelstromwandler CH.</b> Bek. Nr. 4920
PTB-2.3-4051063		
<b>ABB s.r.o. PPMV Brno 0 BRNO</b> Tschechien	<b>20.21</b> <b>11.03</b> 13.04.2011	<b>Einzelstromwandler KOKS 12A..., KOKS 17,5A...</b> Bek. Nr. 4927
PTB-2.3-4051422		
<b>Ritz Instrument Transformers GmbH</b> 22041 Hamburg Deutschland	<b>20.21</b> <b>84.52</b> 09.04.1985	<b>Einzelstromwandler EASG...; EGI...</b> Bek. Nr. 4918 <i>2. Neufassung</i> vom 04.05.2011
PTB-2.3-4050290		
<b>ELEQ Kerpen b.v.</b> 50170 Kerpen Deutschland	<b>20.25</b> <b>11.01</b> 13.04.2011	<b>Einpoliger Spannungswandler EUGE12... ; EUGE24...</b> Bek. Nr. 4499
PTB-2.3-4018204		
<b>Wärmezähler</b>		
<b>Engelmann Sensor GmbH</b> 69168 Wiesloch Deutschland	<b>22.72</b> <b>09.02</b> 19.01.2010	<b>Vollständiger Kältezähler compact Vec.</b> <i>2. Nachtrag</i> vom 21.04.2011
PTB-7.6-4051304		

Zulassungsinhaber PTB-Geschäftszeichen	Zul.-Zeichen Datum	Bauart, messtechnische Merkmale und Bemerkungen
<b>Landis + Gyr GmbH</b> <b>90459 Nürnberg</b> <b>Deutschland</b>	<b>22.72</b> <b>11.01</b> 31.05.2011	<b>Vollständiger Kältezähler T230.</b>
PTB-7.6-4049769		
<b>Endress+Hauser Wetzer GmbH+Co. KG</b> <b>87484 Nesselwang</b> <b>Deutschland</b>	<b>22.75</b> <b>11.01</b> 04.05.2011	<b>Kältezähler-Rechenwerk mit austauschbaren Temperaturfühlerpaaren</b> EngyCal® Typ RH33.
PTB-7.6-4048055		
<b>Hydrometer GmbH</b> <b>91522 Ansbach</b> <b>Deutschland</b>	<b>22.75</b> <b>11.02</b> 06.05.2011	<b>Kältezähler-Rechenwerk mit austauschbaren Temperaturfühlerpaaren</b> Typ 548.
PTB-7.6-4050826		
<b>Engelmann Sensor GmbH</b> <b>69168 Wiesloch</b> <b>Deutschland</b>	<b>22.76</b> <b>09.03</b> 26.10.2009	<b>Durchflusssensor für Kältezähler</b> SensoStar TStar.  2. <i>Nachtrag</i> vom 21.04.2011
PTB-7.6-4050851		
<b>Landis + Gyr GmbH</b> <b>90459 Nürnberg</b> <b>Deutschland</b>	<b>22.76</b> <b>11.01</b> 04.05.2011	<b>Durchflusssensor für Kältezähler 2 WR 7 bzw. T150.</b>
PTB-7.6-4050347		
<b>Landis + Gyr GmbH</b> <b>90459 Nürnberg</b> <b>Deutschland</b>	<b>22.76</b> <b>11.01</b> 04.05.2011	<b>Durchflusssensor für Kältezähler 2 WR 7 bzw. T150, neuer Mitvertreiber.</b>  1. <i>Nachtrag</i> vom 08.06.2011
PTB-7.6-4052839		

## Strahlenschutzmessgeräte

<b>RTI Electronics AB</b> <b>0 Mölndal</b> <b>Schweden</b>	<b>23.04</b> <b>07.01</b> 26.07.2007	<b>Diagnostikdosimeter</b> RTI Barracuda, neue Firmware 4.0C (MPD), 3.2N (EMM) und 4.0E (QABrowser).  2. <i>Nachtrag zur 1. Neufassung</i> vom 06.06.2011
PTB-6.25-4052234		
<b>RTI Electronics AB</b> <b>0 Mölndal</b> <b>Schweden</b>	<b>23.04</b> <b>08.01</b> 17.04.2008	<b>Diagnostikdosimeter</b> Piranha, neue Firmware Version 3.3A (cabinet), 3.2H (modul) und 4.0E (QA Browser).  1. <i>Nachtrag zur 1. Neufassung</i> vom 06.06.2011
PTB-6.25-4052233		
<b>iba Dosimetry</b> <b>90592 Schwarzenbruck</b> <b>Deutschland</b>	<b>23.04</b> <b>11.01</b> 27.05.2011	<b>Diagnostikdosimeter</b> MagicMaX kV / dose. Dosimeter zur Messung der Dosis und Dosisleistung. Dosimeter zur Messung der Dosis und Dosisleistung bei Diagnostik- und Mammographiequalitäten mit einem fest angeschlossenen Detektor sowie die Möglichkeit einen zweiten Detektor anzuschließen.
PTB-6.25-4049336		

Zulassungsinhaber PTB-Geschäftszeichen	Zul.-Zeichen Datum	Bauart, messtechnische Merkmale und Bemerkungen
<b>IBA Dosimetry GmbH</b> <b>90592 Schwarzenbruck</b> <b>Deutschland</b>	<b>23.04</b> <b>11.02</b> 27.05.2011	<b>Diagnostikdosimeter</b> MagicMaX dose. Dosimeter zur Messung der Dosis und der Dosisleistung. Dosimeter zur Messung der Dosis und Dosisleistung bei Diagnostik- und Mammographiequalitäten mit der Möglichkeit zwei Detektoren anzuschließen.
PTB-6.25-4045830		
<b>Thermo Fisher Scientific</b> <b>Messtechnik GmbH</b> <b>91056 Erlangen</b> <b>Deutschland</b>	<b>23.11</b> <b>03.03</b> 14.05.2003	<b>Radioaktive Kontrollvorrichtung</b> V1-A. Kontrollvorrichtung auch für EPD-G zugelassen, neuer Name des Zulassungsinhabers.  3. <i>Nachtrag</i> vom 13.05.2011
PTB-6.3-4052501		
<b>Thermo Fisher Scientific</b> <b>Messtechnik GmbH</b> <b>91056 Erlangen</b> <b>Deutschland</b>	<b>23.31</b> <b>05.01</b> 21.12.2005	<b>Auswerte- / Anzeigeeinrichtung</b> FHT 6020 PH, neue Firmware V1.09.  3. <i>Nachtrag</i> vom 19.04.2011
PTB-6.3-4047978		
<b>Berthold Technologies GmbH</b> <b>&amp; Co.KG</b> <b>75323 Bad Wildbad</b> <b>Deutschland</b>	<b>23.51</b> <b>10.01</b> 08.04.2011	<b>Dosimetersonde, Messgröße Umgebungs-Äquivalentdosis</b> LB 6720-H10. Neuzulassung Sonde LB 6720-H10 an Anzeigegerät LB 111.
PTB-6.3-4041116		
<b>Thermo Fisher Scientific</b> <b>Messtechnik GmbH</b> <b>91056 Erlangen</b> <b>Deutschland</b>	<b>23.52</b> <b>01.01</b> 24.04.2001	<b>Personendosimeter, Messgröße Tiefen-Personendosis</b> EPD Mk2. Eine weitere Firmwareversion V15 ist für das EPD Mk2.5 bzw. Mk2+ zugelassen.  3. <i>Nachtrag zur 1. Neufassung</i> vom 06.05.2011
PTB-6.3-4052281		
<b>Mirion Technologies (RADOS)</b> <b>GmbH</b> <b>22761 Hamburg</b> <b>Deutschland</b>	<b>23.52</b> <b>02.04</b> 16.10.2002	<b>Personendosimeter, Messgröße Tiefen-Personendosis</b> DMC 2000 S. Neues Zubehör, Teledosimetriesender iPAM-Tx.  3. <i>Neufassung</i> vom 03.05.2011
PTB-6.3-4047977		
<b>Auswertungsstelle im</b> <b>Helmholtz Zentrum München</b> <b>81739 München</b> <b>Deutschland</b>	<b>23.52</b> <b>03.04</b> 17.12.2003	<b>Personendosimeter, Messgröße Oberflächen-Personendosis</b> GSF-TL-TD 60. Geänderte Software, neue Gebrauchsanweisung.  1. <i>Neufassung</i> vom 13.05.2011
PTB-6.3-4052399		
<b>Auswertungsstelle im</b> <b>Helmholtz Zentrum München</b> <b>81739 München</b> <b>Deutschland</b>	<b>23.52</b> <b>03.05</b> 17.12.2003	<b>Personendosimeter, Messgröße Oberflächen-Personendosis</b> GSF-TL-TD 70. Geänderte Software, neue Gebrauchsanweisung.  1. <i>Neufassung</i> vom 13.05.2011
PTB-6.3-4052403		
<b>Auswertungsstelle im</b> <b>Helmholtz Zentrum München</b> <b>81739 München</b> <b>Deutschland</b>	<b>23.52</b> <b>11.01</b> 05.07.2011	<b>Personendosimeter, Messgröße Tiefen-Personendosis</b> AWST-OSL-GD01. Ganzkörper-Personendosimeter Energiebereich 16 keV bis 7 MeV, Dosisbereich 0,1 mSv bis 10 Sv.
PTB-6.3-4047738		

Zulassungsinhaber PTB-Geschäftszeichen	Zul.-Zeichen Datum	Bauart, messtechnische Merkmale und Bemerkungen
<b>Berthold Technologies GmbH &amp; Co.KG</b> 75323 Bad Wildbad Deutschland	<b>23.56</b> <b>04.01</b> 15.11.2004	<b>Ortsfestes Strahlenschutzmesssystem Messgröße Umgebungs-Äquivalentdosis</b> LB111 Micro Gamma. Erweiterung der Zulassung um Sonde 6720-H10. Erweiterung der eichtechnischen Prüfung für LED-Signallampen.  <i>1. Nachtrag</i> vom 08.04.2011
PTB-6.3-4041115		
<b>Thermo Fisher Scientific Messtechnik GmbH</b> 91056 Erlangen Deutschland	<b>23.71</b> <b>11.01</b> 19.04.2011	<b>Dosimetersonde, Messgröße Umgebungs-Äquivalentdosis</b> FHZ691-10. Dosisleistungssonde mit Szintillator und Geiger-Müller-Zählrohr für das Anzeigegerät FHT 6020 PH. Messgröße: Umgebungs-Äquivalentdosisleistung. Messbereich: 0,1 µSv/h bis 10 Sv/h, Photonenenergie: 60 keV bis 3 MeV, Winkelbereich: 0° bis +/- 45°.
PTB-6.3-4047980		

## Feststellungen der Gleichwertigkeit nach § 80 der Eichordnung

Entsprechend § 80 der Eichordnung bestätigt die PTB, dass die nachfolgend aufgeführten Messgeräte, einschließlich der Prüfungen und Kennzeichen, ein vergleichbares Niveau des Schutzes des Verbrauchers, des Wettbewerbs und anderer im öffentlichen Interesse bestehender Schutzgüter gewährleisten:

Hersteller	Bescheinigung, Datum	Bauart, messtechnische Merkmale, Bemerkungen
<b>ABB s.r.o.</b> 619 00 BRNO Tschechien	<b>PTB-Q.31-4052017</b> 15.04.2011 gültig bis: 28.02.2012	<b>Einzelstromwandler,</b> Typen TPU 4x.xx, TPU 5x.xx, TPU 6x.xx, TPU 7x.xx, KOKS12A31, KOKS12A41, KOKS17,5A31, KOKS17,5A41 <b>Einpolige Spannungswandler,</b> Typen TJC 4, 5, 6, 7, 7.1, und TJP 4.x, 5.x, 6.x, <b>Mehrpole Spannungswandler,</b> Typen TDC 4, 5, 6 PTB-Zulassungen 20.21/00.06, 20.25/00.01, 20.25/03.05 20.26/00.01, 20.21/11.03. Eichung durch das Metrologiezentrum bei ABB s.r.o. in Brno (K19), Gleichwertigkeit der Eichung  Die Bescheinigung vom 25.08.2009 wurde für Einzelstromwandler KOKS.. der PTB-Zulassung 20.21/11.03 ergänzt.

## Konformitätsbewertung nach 2004/22/EG

### EG-Baumusterprüfbescheinigungen/ bzw. EG-Entwurfsprüfbescheinigungen der europäischen Messgeräte-richtlinie 2004/22/EG

Prüfscheininhaber PTB-Geschäftszeichen	Nr. EG-Baumuster- /Entwurfsprüf- bescheinigung Datum	Einrichtung, messtechnische Merkmale und Bemerkungen
<b>ELSTER GmbH</b> 55252 Mainz-Kastel Deutschland	<b>DE-10-MI002- PTB003</b> 17.08.2010	<b>Gaszähler mit eingebauter Temperaturumwertung</b> BK-G40T, BK-G65T, BK-G100T. Optionale Ausstattung mit dem Kommunikationsmodul SCR+ .  Die Bauartzulassung ist gültig bis 16.08.2020  <i>1. Revision</i> vom 04.05.2011
PTB-1.42-4052277		

Prüfscheininhaber PTB-Geschäftszeichen	Nr. EG-Baumuster- /Entwurfsprüf- bescheinigung Datum	Einrichtung, messtechnische Merkmale und Bemerkungen
<b>RMG Messtechnik GmbH</b> <b>35510 Butzbach</b> <b>Deutschland</b>	<b>DE-11-MI002- PTB003</b> 15.04.2011	<b>Zustands-Mengenurwerter für Gas ERZ 2000</b> , p-Aufnehmer und optional auch T-Aufnehmer, extern mit Baueinheiten-Zertifikat.  Die Bauartzulassung ist gültig bis 14.04.2021
PTB-1.42-4039907		
<b>EMH metering GmbH &amp; Co. KG</b> <b>19243 Wittenburg</b> <b>Deutschland</b>	<b>DE-07-MI003- PTB009</b> 18.06.2007	<b>Elektrizitätszähler für Wirkverbrauch ITZR-...</b> Bek. Nr.: 5127.  Die Bauartzulassung ist gültig bis 17.06.2017  <i>1. Revision</i> vom 30.05.2011
PTB-2.3-4048940		
<b>Carlo Gavazzi Controls SpA</b> <b>32100 Belluno</b> <b>Italien</b>	<b>DE-07-MI003- PTB010</b> 20.08.2007	<b>Elektrizitätszähler für Wirkverbrauch EM10; EM11.</b> Bek. Nr 5052  Die Bauartzulassung ist gültig bis 20.08.2017  <i>3. Revision</i> vom 13.05.2011
PTB-2.3-4052330		
<b>EMH metering GmbH &amp; Co. KG</b> <b>19243 Wittenburg</b> <b>Deutschland</b>	<b>DE-08-MI003- PTB007</b> 08.07.2008	<b>Elektrizitätszähler für Wirkverbrauch ITZ-A.</b> Bek.-Nr. 5125  Die Bauartzulassung ist gültig bis 07.07.2018  <i>3. Revision</i> vom 07.04.2011
PTB-2.3-4048889		
<b>EMH metering GmbH &amp; Co. KG</b> <b>19243 Wittenburg</b> <b>Deutschland</b>	<b>DE-08-MI003- PTB016</b> 15.12.2008	<b>Elektrizitätszähler für Wirkverbrauch ITZ-Y.</b> Bek. Nr. 5126  Die Bauartzulassung ist gültig bis 14.12.2018  <i>1. Revision</i> vom 07.04.2011
PTB-2.3-4048937		
<b>Itron Zähler &amp; Systemtechnik GmbH</b> <b>31789 Hameln</b> <b>Deutschland</b>	<b>DE-11-MI003- PTB005</b> 13.04.2011	<b>Elektrizitätszähler für Wirkverbrauch HZ1-A...</b> Bek. Nr. 5139  Die Bauartzulassung ist gültig bis 12.04.2021
PTB-2.3-4051333		
<b>Hager Electro GmbH &amp; Co. KG</b> <b>66440 Blieskastel</b> <b>Deutschland</b>	<b>DE-11-MI003- PTB006</b> 19.04.2011	<b>Elektrizitätszähler für Wirkverbrauch EHZ163xxx.</b> Bek. Nr. 5140  Die Bauartzulassung ist gültig bis 18.04.2021
PTB-2.3-4051415		
<b>JUMO GmbH &amp; Co. KG</b> <b>36039 Fulda</b> <b>Deutschland</b>	<b>DE-06-MI004- PTB011</b> 27.02.2007	<b>Temperaturfühlerpaar</b> 902428/30, 902428/40, 902438/30, 902438/32.  Die Bauartzulassung ist gültig bis 27.02.2017  <i>2. Revision</i> vom 18.04.2011
PTB-7.6-4044174		
<b>JUMO GmbH &amp; Co. KG</b> <b>36039 Fulda</b> <b>Deutschland</b>	<b>DE-06-MI004- PTB015</b> 18.07.2008	<b>Temperaturfühlerpaar</b> 902427/10, 902427/11, 902437/10, 902437/12.  Die Bauartzulassung ist gültig bis 18.07.2018  <i>1. Revision</i> vom 18.04.2011
PTB-7.6-4044177		



Prüfscheininhaber PTB-Geschäftszeichen	Nr. EG-Baumuster- /Entwurfsprüf- bescheinigung Datum	Einrichtung, messtechnische Merkmale und Bemerkungen
<b>Engelmann Sensor GmbH</b> <b>69168 Wiesloch</b> <b>Deutschland</b>  PTB-7.6-4050774	<b>DE-08-MI004- PTB003</b> 08.04.2008	<b>Durchflusssensor</b> SensoStar Typ MSH.  Die Bauartzulassung ist gültig bis 08.04.2018  2. <i>Revision</i> vom 21.04.2011
<b>Engelmann Sensor GmbH</b> <b>69168 Wiesloch</b> <b>Deutschland</b>  PTB-7.6-4050837	<b>DE-08-MI004- PTB006</b> 29.02.2008	<b>Durchflusssensor</b> Typ WWZ... .  Die Bauartzulassung ist gültig bis 28.02.2018  2. <i>Revision</i> vom 21.04.2011
<b>Engelmann Sensor GmbH</b> <b>69168 Wiesloch</b> <b>Deutschland</b>  PTB-7.6-4050846	<b>DE-08-MI004- PTB009</b> 11.08.2008	<b>Durchflusssensor</b> MSH-QStar... .  Die Bauartzulassung ist gültig bis 11.08.2018  1. <i>Revision</i> vom 21.04.2011
<b>Engelmann Sensor GmbH</b> <b>69168 Wiesloch</b> <b>Deutschland</b>  PTB-7.6-4050866	<b>DE-09-MI004- PTB020</b> 04.09.2009	<b>Durchflusssensor</b> Typ TStar.  Die Bauartzulassung ist gültig bis 04.09.2019  2. <i>Revision</i> vom 21.04.2011
<b>Allmess GmbH</b> <b>23758 Oldenburg in Holstein</b> <b>Deutschland</b>  PTB-7.6-4051990	<b>DE-10-MI004- PTB001</b> 17.08.2010	<b>Wärmezähler</b> Integral-MK UltraMaXX.  Die Bauartzulassung ist gültig bis 17.08.2020  2. <i>Revision</i> vom 18.05.2011
<b>Endress+Hauser Wetzler</b> <b>GmbH+Co. KG</b> <b>87484 Nesselwang</b> <b>Deutschland</b>  PTB-7.6-4047657	<b>DE-10-MI004- PTB006</b> 04.05.2011	<b>Rechenwerk</b> EngyCal® Typ RH33.  Die Bauartzulassung ist gültig bis 04.05.2021
<b>Landis + Gyr GmbH</b> <b>90459 Nürnberg</b> <b>Deutschland</b>  PTB-7.6-4052731	<b>DE-11-MI004- PTB003</b> 11.02.2011	<b>Wärmezähler</b> T230.  Die Bauartzulassung ist gültig bis 11.02.2021  1. <i>Revision</i> vom 06.06.2011
<b>Landis + Gyr GmbH</b> <b>90459 Nürnberg</b> <b>Deutschland</b>  PTB-7.6-4052734	<b>DE-11-MI004- PTB004</b> 11.02.2011	<b>Wärmezähler</b> T230.  Die Bauartzulassung ist gültig bis 11.02.2021  1. <i>Revision</i> vom 06.06.2011
<b>Siemens A/S Flow Instruments</b> <b>I IA SC PI 3 SFI-DR</b> <b>6430 Nordborg</b> <b>Daenemark</b>  PTB-7.6-4050742	<b>DE-11-MI004- PTB005</b> 27.04.2011	<b>Rechenwerk</b> SITRANS FUE950.  Die Bauartzulassung ist gültig bis 27.04.2021

Prüfscheininhaber PTB-Geschäftszeichen	Nr. EG-Baumuster- /Entwurfsprüf- bescheinigung Datum	Einrichtung, messtechnische Merkmale und Bemerkungen
<b>FLOW Instruments &amp; Engineering GmbH</b> 42697 Solingen Deutschland	<b>DE-07-MI005- PTB003</b> 23.03.2007	<b>Messanlage für unter Druck verflüssigte Gase</b> Flowcom 2000 (Rev2). Messanlagenschema geändert.  Die Bauartzulassung ist gültig bis 22.03.2017  <i>10. Revision</i> vom 22.06.2011
PTB-1.5-4053047		
<b>FLOW Instruments &amp; Engineering GmbH</b> 42697 Solingen Deutschland	<b>DE-07-MI005- PTB004</b> 23.03.2007	<b>Messanlage für verflüssigtes Kohlendioxid</b> Flowcom 2000 (Rev2). Einfügen einer Spülleitung in das Messanlagenschema.  Die Bauartzulassung ist gültig bis 22.03.2017  <i>8. Revision</i> vom 18.04.2011
PTB-1.5-4052125		
<b>DEZIDATA GmbH</b> 94469 Deggendorf Deutschland	<b>DE-07-MI005- PTB010</b> 11.07.2007	<b>Messanlage für</b> die Abgabe flüssiger Chemikalien DEZICHEM-M. Geänderter Funktionsablauf bei der Abgabe von Vorwahlmengen.  Die Bauartzulassung ist gültig bis 10.07.2017  <i>3. Revision</i> vom 17.05.2011
PTB-1.5-4052542		
<b>Hectronic GmbH</b> 79848 Bonndorf Deutschland	<b>DE-08-MI005- PTB001</b> 12.02.2008	<b>Kraftstoffzapsäule</b> HECPUMP 2333. Softwareversion ergänzt.  Die Bauartzulassung ist gültig bis 11.02.2018  <i>5. Revision</i> vom 27.05.2011
PTB-1.5-4052627		
<b>Mess- und Fördertechnik Gwinner GmbH &amp; Co.</b> 21035 Hamburg Deutschland	<b>DE-08-MI005- PTB002</b> 01.04.2008	<b>Messanlage zur Be- oder Entladung von Schiffen, Kesselwagen, Tankwagen</b> Verlade-/Abfüllanlage mit MFX_4, alternative Messwert- und Dichteaufnehmer eingefügt, Software aktualisiert.  Die Bauartzulassung ist gültig bis 31.03.2018  <i>5. Revision</i> vom 14.06.2011
PTB-1.5-4052783		
<b>Nutzfahrzeuge ROHR GmbH</b> 94315 Straubing Deutschland	<b>DE-08-MI005- PTB003</b> 10.03.2008	<b>Messanlage zur Betankung von Flugzeugen</b> ARSTT. Messanlagenschema und Softwareversion ergänzt.  Die Bauartzulassung ist gültig bis 09.03.2018  <i>3. Revision</i> vom 17.05.2011
PTB-1.5-4052505		
<b>Propan &amp; Ammoniak Anlagen GmbH</b> 38229 Salzgitter Deutschland	<b>DE-08-MI005- PTB006</b> 10.03.2008	<b>Kraftstoffzapsäule für unter Druck verflüssigte Gase.</b> Variable Typbezeichnung gemäß Nr. 1.1 dieser Baumusterprüfbescheinigung, Softwareversion ergänzt.  Die Bauartzulassung ist gültig bis 09.03.2018  <i>12. Revision</i> vom 27.05.2011
PTB-1.5-4052635		
<b>Flaco Geräte GmbH</b> 33334 Gütersloh Deutschland	<b>DE-08-MI005- PTB014</b> 24.04.2008	<b>Messanlage für</b> wässrige Lösungen mit elektronischem Zählwerk FLACOJet40. Neue Softwareversion durch Anpassung der Startwerte für die Stromkontrolle.  Die Bauartzulassung ist gültig bis 23.04.2018  <i>7. Revision</i> vom 21.06.2011
PTB-1.5-4053016		

Prüfscheininhaber PTB-Geschäftszeichen	Nr. EG-Baumuster- /Entwurfsprüf- bescheinigung Datum	Einrichtung, messtechnische Merkmale und Bemerkungen
<b>Smith Meter GmbH</b> 25474 Ellerbek Deutschland  PTB-1.5-4052588	<b>DE-08-MI005- PTB022</b> 29.10.2008	<b>Messanlage zur Be- oder Entladung von Schiffen, Kesselwagen, Tankwagen LMS-...-...-...-... , alternative Messwertaufnehmer und Rechner aufgenommen.</b>  Die Bauartzulassung ist gültig bis 28.10.2018  <i>4. Revision</i> vom 14.06.2011
<b>BARTEC BENKE GmbH</b> 94239 Gotteszell Deutschland  PTB-1.5-4052280	<b>DE-08-MI005- PTB029</b> 30.10.2008	<b>Messanlage für Milch BARTEC ULTRA Impeller, Softwareversion aktualisiert.</b>  Die Bauartzulassung ist gültig bis 29.10.2018  <i>3. Revision</i> vom 05.05.2011
<b>Propan &amp; Ammoniak Anlagen GmbH</b> 38229 Salzgitter Deutschland  PTB-1.5-4052636	<b>DE-08-MI005- PTB030</b> 12.11.2008	<b>Kraftstoffzapsäule für unter Druck verflüssigte Gase.</b> Variable Typbezeichnung gemäß Nr. 1.1 dieser Baumusterprüfbescheinigung, Softwareversion ergänzt.  Die Bauartzulassung ist gültig bis 11.11.2018  <i>9. Revision</i> vom 27.05.2011
<b>BARTEC BENKE GmbH</b> 94239 Gotteszell Deutschland  PTB-1.5-4051987	<b>DE-08-MI005- PTB036</b> 28.11.2008	<b>Messanlage auf Straßentankwagen für Flüssigkeiten, Viskosität &lt;20 mPa.s TIGER 3003, Ablaufbeschreibung aktualisiert.</b>  Die Bauartzulassung ist gültig bis 27.11.2018  <i>9. Revision</i> vom 11.04.2011
<b>BARTEC BENKE GmbH</b> 94239 Gotteszell Deutschland  PTB-1.5-4052602	<b>DE-08-MI005- PTB036</b> 28.11.2008	<b>Messanlage auf Straßentankwagen für Flüssigkeiten, Viskosität &lt;20 mPa.s TIGER 3003, alternative Messstrecke eingefügt.</b>  Die Bauartzulassung ist gültig bis 27.11.2018  <i>10. Revision</i> vom 20.05.2011
<b>ISOIL Impianti S.p.A.</b> 24061 Albano S. Alessandro Italien  PTB-1.5-4052303	<b>DE-09-MI005- PTB008</b> 06.03.2009	<b>Messanlage zur Be- oder Entladung von Schiffen, Kesselwagen, Tankwagen PS..., PSM..., MSV.... . Massezähler CMF HC2 eingefügt, Softwareversionen ergänzt.</b>  Die Bauartzulassung ist gültig bis 05.03.2019  <i>4. Revision</i> vom 05.05.2011
<b>ISOIL Impianti S.p.A.</b> 24061 Albano S. Alessandro Italien  PTB-1.5-4052302	<b>DE-09-MI005- PTB009</b> 06.03.2009	<b>Messanlage in Fernleitungen PS..., PSM..., MSV.... . Massezähler CMF HC2 eingefügt, Softwareversionen ergänzt.</b>  Die Bauartzulassung ist gültig bis 05.03.2019  <i>4. Revision</i> vom 05.05.2011
<b>Endress+Hauser Messtechnik GmbH+Co. KG</b> 79576 Weil am Rhein Deutschland  PTB-1.5-4052488	<b>DE-09-MI005- PTB019</b> 02.10.2009	<b>Messanlage zur Be- oder Entladung von Schiffen, Kesselwagen, Tankwagen.</b> Messanlage in Fernleitungen PROMASS Verladeanlage kommunikationskontrollierter PCC400 als Messwertspeicher aufgenommen.  Die Bauartzulassung ist gültig bis 01.10.2019  <i>2. Revision</i> vom 13.05.2011

Prüfscheininhaber PTB-Geschäftszeichen	Nr. EG-Baumuster- /Entwurfsprüf- bescheinigung Datum	Einrichtung, messtechnische Merkmale und Bemerkungen
<b>Dr.-Ing. Ulrich Esterer GmbH &amp; Co. Fahrzeugaufbauten und Anlagen KG</b> 34298 Helsa Deutschland  PTB-1.5-4052070	<b>DE-09-MI005- PTB020</b> 29.06.2009	<b>Messanlage auf Straßentankwagen für Flüssigkeiten, Viskosität &lt;20 mPa.s EasyCount – NN, kleinste Messmenge angepasst.</b>  Die Bauartzulassung ist gültig bis 28.06.2019  <i>1. Revision</i> vom 14.04.2011
<b>Mess- und Fördertechnik Gwinner GmbH &amp; Co.</b> 21035 Hamburg Deutschland  PTB-1.5-4052784	<b>DE-09-MI005- PTB026</b> 26.08.2009	<b>Messanlage für unter Druck verflüssigte Gase.</b> Messanlage in Fernleitungen alternative Messwert- und Dichteaufnehmer eingefügt, Software aktualisiert.  Die Bauartzulassung ist gültig bis 25.08.2019  <i>2. Revision</i> vom 14.06.2011
<b>IDE GmbH</b> 33334 Gütersloh Deutschland  PTB-1.5-4052334	<b>DE-09-MI005- PTB030</b> 18.11.2009	<b>Messanlage zur Be- oder Entladung von Schiffen, Kesselwagen, Tankwagen.</b> Messanlage für Flüssigdünger, neue Softwareversion eingefügt.  Die Bauartzulassung ist gültig bis 17.11.2019  <i>2. Revision</i> vom 05.05.2011
<b>IDE GmbH</b> 33334 Gütersloh Deutschland  PTB-1.5-4053066	<b>DE-09-MI005- PTB030</b> 18.11.2009	<b>Messanlage zur Be- oder Entladung von Schiffen, Kesselwagen, Tankwagen.</b> Messanlage für Flüssigdünger, kleinste Messmenge für Optiflux herabgesetzt, Softwareversion ergänzt.  Die Bauartzulassung ist gültig bis 17.11.2019  <i>3. Revision</i> vom 23.06.2011
<b>Raiffeisen Anlagenbau GmbH</b> 32791 Lage Deutschland  PTB-1.5-4052335	<b>DE-09-MI005- PTB031</b> 18.11.2009	<b>Messanlage zur Be- oder Entladung von Schiffen, Kesselwagen, Tankwagen.</b> Messanlage für Flüssigdünger, neue Softwareversion eingefügt.  Die Bauartzulassung ist gültig bis 17.11.2019  <i>2. Revision</i> vom 05.05.2011
<b>Raiffeisen Anlagenbau GmbH</b> 32791 Lage Deutschland  PTB-1.5-4053067	<b>DE-09-MI005- PTB031</b> 18.11.2009	<b>Messanlage zur Be- oder Entladung von Schiffen, Kesselwagen, Tankwagen.</b> Messanlage für Flüssigdünger, kleinste Messmenge für Optiflux herabgesetzt, Softwareversion ergänzt.  Die Bauartzulassung ist gültig bis 17.11.2019  <i>3. Revision</i> vom 23.06.2011
<b>Mess- und Fördertechnik Gwinner GmbH &amp; Co.</b> 21035 Hamburg Deutschland  PTB-1.5-4052785	<b>DE-09-MI005- PTB033</b> 06.11.2009	<b>Messanlage zur Be- oder Entladung von Schiffen, Kesselwagen, Tankwagen</b> für Flüssigkeiten mit einer Viskosität >20 mPa.s. Messanlage mit MFX_4 für Flüssigkeiten mit einer Viskosität >20 mPa.s, alternative Messwert- und Dichteauf- nehmer eingefügt, Software aktualisiert.  Die Bauartzulassung ist gültig bis 05.11.2019  <i>3. Revision</i> vom 14.06.2011

Prüfscheininhaber PTB-Geschäftszeichen	Nr. EG-Baumuster- /Entwurfsprüf- bescheinigung Datum	Einrichtung, messtechnische Merkmale und Bemerkungen
<b>BARTEC BENKE GmbH</b> <b>94239 Gotteszell</b> <b>Deutschland</b>  PTB-1.5-4052885	<b>DE-09-MI005- PTB038</b>  24.02.2010	<b>Messanlage zur Betankung von Flugzeugen</b> PETRODAT 3002 FFB, Messwertaufnehmer MKA.. aufgenommen.  Die Bauartzulassung ist gültig bis 23.02.2020  <i>1. Revision</i> vom 14.06.2011
<b>Alfons Haar Maschinenbau GmbH &amp; Co.</b> <b>22547 Hamburg</b> <b>Deutschland</b>  PTB-1.5-4052102	<b>DE-10-MI005- PTB006</b>  12.03.2010	<b>Messanlage für unter Druck verflüssigte Gase</b> PreciGAS C ..., zusätzlicher Durchflussbereich 200 L/min bis 1000 L/min.  Die Bauartzulassung ist gültig bis 11.03.2020  <i>2. Revision</i> vom 05.05.2011
<b>Mess- und Fördertechnik Gwinner GmbH &amp; Co.</b> <b>21035 Hamburg</b> <b>Deutschland</b>  PTB-1.5-4052786	<b>DE-10-MI005- PTB020</b>  27.07.2010	<b>Messanlage in Fernleitungen.</b> Messanlage in Fernleitungen mit MFX_4, alternative Messwert- und Dichteaufnehmer eingefügt, Software aktualisiert.  Die Bauartzulassung ist gültig bis 26.07.2020  <i>3. Revision</i> vom 14.06.2011
<b>SCHWARTE JANSKY GmbH</b> <b>48282 Emsdetten</b> <b>Deutschland</b>  PTB-1.5-4052268	<b>DE-10-MI005- PTB024</b>  05.11.2010	<b>Messanlage für Milch V 6</b> , Softwaremodule ersetzt.  Die Bauartzulassung ist gültig bis 04.11.2020  <i>2. Revision</i> vom 05.05.2011
<b>SCHWARTE-MILFOR z o.o.</b> <b>10-092 Olsztyn</b> <b>Polen</b>  PTB-1.5-4052269	<b>DE-10-MI005- PTB025</b>  05.11.2010	<b>Messanlage für Milch V 6</b> , Softwaremodule ersetzt.  Die Bauartzulassung ist gültig bis 04.11.2020  <i>2. Revision</i> vom 05.05.2011
<b>Dr.-Ing. Ulrich Esterer GmbH &amp; Co. Fahrzeugaufbauten und Anlagen KG</b> <b>34298 Helsa</b> <b>Deutschland</b>  PTB-1.5-4052484	<b>DE-10-MI005- PTB029</b>  03.12.2010	<b>Messanlage auf Straßentankwagen für Flüssigkeiten, Viskosität &lt;20 mPa.s</b> ES8H- NN, Softwareversion ergänzt.  Die Bauartzulassung ist gültig bis 02.12.2020  <i>1. Revision</i> vom 13.05.2011
<b>Dr.-Ing. Ulrich Esterer GmbH &amp; Co. Fahrzeugaufbauten und Anlagen KG</b> <b>34298 Helsa</b> <b>Deutschland</b>  PTB-1.5-4052483	<b>DE-10-MI005- PTB031</b>  03.12.2010	<b>Messanlage auf Straßentankwagen für Flüssigkeiten, Viskosität &lt;20 mPa.s</b> ES10H- NN, Softwareversion ergänzt.  Die Bauartzulassung ist gültig bis 02.12.2020  <i>1. Revision</i> vom 13.05.2011
<b>IDE GmbH</b> <b>33334 Gütersloh</b> <b>Deutschland</b>  PTB-1.5-4051309	<b>DE-11-MI005- PTB005</b>  08.04.2011	<b>Messanlage zur Be- oder Entladung von Schiffen, Kesselwagen, Tankwagen.</b> Verlade-/Abfüllanlage mit CMR, Measuring System, maximaler Durchfluss 20000 L/min.  Die Bauartzulassung ist gültig bis 07.04.2021

Prüfscheininhaber PTB-Geschäftszeichen	Nr. EG-Baumuster- /Entwurfsprüf- bescheinigung Datum	Einrichtung, messtechnische Merkmale und Bemerkungen
<b>Dr.-Ing. Ulrich Esterer GmbH &amp; Co. Fahrzeugaufbauten und Anlagen KG 34298 Helsa Deutschland</b>	<b>DE-11-MI005- PTB008</b> 17.03.2011	<b>Messanlage auf Straßentankwagen für Flüssigkeiten, Viskosität &lt;20 mPa.s, EasyCount2 – NN, kleinste Messmenge angepasst.</b>  Die Bauartzulassung ist gültig bis 16.03.2021  <i>1. Revision</i> vom 14.04.2011
PTB-1.5-4052068		
<b>Dr.-Ing. Ulrich Esterer GmbH &amp; Co. Fahrzeugaufbauten und Anlagen KG 34298 Helsa Deutschland</b>	<b>DE-11-MI005- PTB008</b> 17.03.2011	<b>Messanlage auf Straßentankwagen für Flüssigkeiten, Viskosität &lt;20 mPa.s, EasyCount2- NN, Softwareversion ergänzt.</b>  Die Bauartzulassung ist gültig bis 16.03.2021  <i>2. Revision</i> vom 13.05.2011
PTB-1.5-4052482		
<b>KuS Service- u. HandelsGmbH 4632 Pichl Österreich</b>	<b>DE-11-MI005- PTB009</b> 29.03.2011	<b>Messanlage für Flüssigkeiten mit einer dynamischen Viskosität =&gt; 20 mPa.s LIQUIMASTER, alternative Gasmessverhütungs- Einheit eingefügt.</b>  Die Bauartzulassung ist gültig bis 28.03.2021  <i>1. Revision</i> vom 18.05.2011
PTB-1.5-4052568		
<b>Flüssiggas-Anlagen GmbH 38229 Salzgitter Deutschland</b>	<b>DE-11-MI005- PTB010</b> 16.05.2011	<b>Kraftstoffzapfsäule für unter Druck verflüssigte Gase FAS 120, FAS 140, FAS 220, FAS 230, FAS 240, FAS 250, Durchflussbereich 5 L/min bis 50 L/min.</b>  Die Bauartzulassung ist gültig bis 15.05.2021
PTB-1.5-4052320		
<b>Flüssiggas-Anlagen GmbH 38229 Salzgitter Deutschland</b>	<b>DE-11-MI005- PTB011</b> 16.05.2011	<b>Kraftstoffzapfsäule für unter Druck verflüssigte Gase FAS 120, FAS 140, FAS 220, FAS 230, FAS 240, FAS 250, Durchflussbereich 1,2 kg/min bis 65 kg/min.</b>  Die Bauartzulassung ist gültig bis 15.05.2021
PTB-1.5-4052321		
<b>Horn GmbH &amp; Co. KG 24937 Flensburg Deutschland</b>	<b>DE-11-MI005- PTB012</b> 31.05.2011	<b>Messanlage für Flüssigkeiten mit einer dynamischen Viskosität =&gt;20 mPa.s bei 20 °C TMS III / TKS IV, Durchfluss von 0,5 L/min bis 20 L/min im Bereich 1 zu 10 frei wählbar.</b>  Die Bauartzulassung ist gültig bis 30.05.2021
PTB-1.5-4051440		
<b>Lindner &amp; Fischer Fahrzeugbau GmbH 89129 Langenau Deutschland</b>	<b>DE-11-MI005- PTB013</b> 27.05.2011	<b>Messanlage auf Straßentankwagen für Flüssigkeiten, Viskosität &lt;20 mPa.s. Messanlage für mobile und stationäre Anwendung TTS-GMVT805-MF(M)-..., CMS-GMVT805- ML(M)-..., Durchflussbereich 40 L/min bis 800 L/min.</b>  Die Bauartzulassung ist gültig bis 26.05.2021
PTB-1.5-4052653		
<b>Lindner &amp; Fischer Fahrzeugbau GmbH 89129 Langenau Deutschland</b>	<b>DE-11-MI005- PTB014</b> 27.05.2011	<b>Messanlage auf Straßentankwagen für Flüssigkeiten, Viskosität &lt;20 mPa.s. Messanlage für mobile und stationäre Anwendung TTS-GMVZ1004-MF(M)-..., CMS-GMVZ1004- ML(M)-..., Durchflussbereich 100 L/min bis 1000 L/min.</b>  Die Bauartzulassung ist gültig bis 26.05.2021
PTB-1.5-4052655		

Prüfscheininhaber PTB-Geschäftszeichen	Nr. EG-Baumuster- /Entwurfsprüf- bescheinigung Datum	Einrichtung, messtechnische Merkmale und Bemerkungen
<b>SOMEFI S.p.A</b> <b>20125 MILANO</b> <b>Italien</b>  PTB-1.5-4052659	<b>DE-11-MI005- PTB015</b> 14.06.2011	<b>Messanlage zur Be- oder Entladung von Schiffen, Kesselwagen, Tankwagen LMS-...-...-...-... Durchflussbereich zwischen 10 L/min bis 400 L/min und 1000 L/min bis 33 000 L/min.</b>  Die Bauartzulassung ist gültig bis 13.06.2021
<b>Mettler-Toledo Garvens GmbH</b> <b>31180 Giesen</b> <b>Deutschland</b>  PTB-1.12-4051097	<b>DE-06-MI006- PTB004</b> 28.12.2006	<b>Selbsttätige Kontrollwaage</b> sowie Waage für Einzelwägungen und zur Preis- und Gewichtsauszeichnung AB C.  Die Bauartzulassung ist gültig bis 27.12.2016  <i>6. Revision</i> vom 10.07.2011
<b>Mettler-Toledo Garvens GmbH</b> <b>31180 Giesen</b> <b>Deutschland</b>  PTB-1.12-4051473	<b>DE-06-MI006- PTB005</b> 31.12.2006	<b>Selbsttätige Kontrollwaage</b> sowie Waage für Einzelwägungen und zur Preis- und Gewichtsauszeichnung ABC DMS.  Die Bauartzulassung ist gültig bis 30.12.2006  <i>8. Revision</i> vom 04.07.2011
<b>Bizerba GmbH &amp; Co. KG</b> <b>72336 Balingen</b> <b>Deutschland</b>  PTB-1.12-4052534	<b>DE-06-MI006- PTB013</b> 29.11.2006	<b>Selbsttätige Kontrollwaage</b> und Waage für Einzelwägungen sowie zur Preis- und Gewichtsauszeichnung GLM-I...  Die Bauartzulassung ist gültig bis 28.11.2016  <i>6. Revision</i> vom 22.05.2011
<b>Bizerba GmbH &amp; Co. KG</b> <b>72336 Balingen</b> <b>Deutschland</b>  PTB-1.12-4052533	<b>DE-06-MI006- PTB014</b> 28.11.2006	<b>Selbsttätige Kontrollwaage CWM...</b>  Die Bauartzulassung ist gültig bis 27.11.2016  <i>7. Revision</i> vom 19.05.2011
<b>Mettler-Toledo Garvens GmbH</b> <b>31180 Giesen</b> <b>Deutschland</b>  PTB-1.12-4051152	<b>DE-07-MI006- PTB037</b> 19.07.2007	<b>Selbsttätige Kontrollwaage</b> sowie Waage für Einzelwägungen und zur Preis- und Gewichtsauszeichnung AB C.  Die Bauartzulassung ist gültig bis 18.07.2017  <i>5. Revision</i> vom 07.07.2011
<b>WIPOTEC Wiege- und Positioniersysteme GmbH</b> <b>67657 Kaiserslautern</b> <b>Deutschland</b>  PTB-1.12-4052712	<b>DE-08-MI006- PTB028</b> 30.05.2008	<b>Selbsttätige Waage für Einzelwägungen</b> (s.a. Nr. 1.1.1.1) EC ... / HC ...  Die Bauartzulassung ist gültig bis 29.05.2018  <i>6. Revision</i> vom 10.06.2011
<b>Hottinger Baldwin Messtechnik GmbH</b> <b>64293 Darmstadt</b> <b>Deutschland</b>  PTB-1.12-4045640	<b>DE-11-MI006- PTB002</b> 20.05.2011	<b>Selbsttätige Waage für Einzelwägungen DWS 2103 SWE</b> , Genauigkeitsklasse Y(a) oder Y(b), $n \leq 6000$ .  Die Bauartzulassung ist gültig bis 19.05.2021
<b>Hottinger Baldwin Messtechnik GmbH</b> <b>64293 Darmstadt</b> <b>Deutschland</b>  PTB-1.12-4045636	<b>DE-11-MI006- PTB003</b> 19.05.2011	<b>Selbsttätige Waage zum Abwägen DWS2103 SWA</b> , Referenzgenauigkeitsklasse X(0.2), $n \leq 6000$ .  Die Bauartzulassung ist gültig bis 18.05.2021

Prüfscheininhaber PTB-Geschäftszeichen	Nr. EG-Baumuster- /Entwurfsprüf- bescheinigung Datum	Einrichtung, messtechnische Merkmale und Bemerkungen
<b>Hottinger Baldwin Messtechnik GmbH</b> <b>64293 Darmstadt</b> <b>Deutschland</b>	<b>DE-11-MI006-PTB004</b> 17.05.2011	<b>Selbsttätige Waage zum diskontinuierlichen Totalisieren</b> DWS2103 SWT, Genauigkeitsklasse 0.2.  Die Bauartzulassung ist gültig bis 16.05.2021
PTB-1.12-4045693		
<b>Waagen-Kissling GmbH</b> <b>64668 Rimbach</b> <b>Deutschland</b>	<b>DE-11-MI006-PTB008</b> 30.06.2011	<b>Selbsttätige Waage für Einzelwägungen</b> sowie selbsttätige Kontrollwaage WKS...  Die Bauartzulassung ist gültig bis 29.06.2021
PTB-1.12-4051642		
<b>Waagen-Kissling GmbH</b> <b>64668 Rimbach</b> <b>Deutschland</b>	<b>DE-11-MI006-PTB009</b> 30.06.2011	<b>Selbsttätige Waage zum Abwägen</b> WKSA...  Die Bauartzulassung ist gültig bis 29.06.2021
PTB-1.12-4051643		
<b>TEXA S.p.A.</b> <b>31050 Monastier di Treviso</b> <b>(TV)</b> <b>Italien</b>	<b>DE-07-MI010-PTB002</b> 20.11.2007	<b>Abgasanalysator Abgasanalysator der Genauigkeitsklasse 0</b> <b>Texa Gasbox Autopower mit PC Abgasanalysator TEXA</b> <b>Gasbox kann auch mit externer Batterie betrieben werden.</b>  <b>Die Bauartzulassung ist gültig bis 19.11.2017</b>
<b>PTB-3.2-4052265</b>		<b>2. Neufassung vom 16.05.2011</b>
<b>MAHA Maschinenbau Haldenwang GmbH &amp; Co KG</b> <b>87490 Haldenwang</b> <b>Deutschland</b>	<b>DE-10-MI010-PTB005</b> 26.04.2011	<b>Abgasanalysator</b> der Genauigkeitsklasse 0 MAHA "MET 6.1" mit PC Erstzulassung, Abgasanalysator Typ Maha "MET 6.1" mit PC.  Die Bauartzulassung ist gültig bis 25.04.2021
PTB-3.2-4049457		
<b>WOW! Technikzentrum</b> <b>74635 Kupferzell</b> <b>Deutschland</b>	<b>DE-10-MI010-PTB004</b> 15.04.2011	<b>Abgasanalysator der Genauigkeitsklasse 0 WGA 3</b> <b>Erstzulassung "WGA 3" nach MID; Hersteller WOW!</b> <b>Würth Online World GmbH</b>  <b>Die Bauartzulassung ist gültig bis 14.04.2021</b>
<b>PTB-3.2-4048942</b>		



## Anerkennung von Qualitätsmanagementsystemen nach Anhang D bzw. H1 der europäischen Messgeräte Richtlinie 2004/22/EG

Hersteller PTB-Geschäftszeichen	Zert.-Nr./Datum Gültigkeitsdauer	Messgerätearten	Anhang
------------------------------------	-------------------------------------	-----------------	--------

**Nordwestdeutsche Zählerrevision Ing. Aug. Knemeyer GmbH & Co. KG**, Heideweg 33, 49196 Bad Laer  
 PTB-Q.32-4048742 DE-11-AQ-PTB058MID Elektrizitätszähler für Wirkverbrauch D  
 vom 21.04.2011  
 gültig bis 20.04.2014

Standort:

**Nordwestdeutsche Zählerrevision Ing. Aug. Knemeyer GmbH & Co. KG**, 49196 Bad Laer

**Mettler-Toledo (Albstadt) GmbH**, Unter dem Malesfelsen 34, 72458 Albstadt  
 PTB-Q.32-4048213 DE-09-AQ-PTB053MID Selbsttätige Waage zum Abwägen D  
 1. Revision vom 28.04.2011 Selbsttätige Waage für Einzelwägungen  
 gültig bis 31.03.2012 Selbsttätige Gewichtsauszeichnungswaage  
 Selbsttätige Preisauszeichnungswaage

Standorte :

**Mettler Toledo (Albstadt) GmbH**, 72458 Albstadt  
**Mettler-Toledo S. A. (MT-FR)**, 78222 Viroflay Cedex (FR)  
**Mettler-Toledo GmbH (MT-AT)**, 1230 Wien (AT)  
**Mettler-Toledo B. V. (MT-NL)**, 4004 JK Tiel (NL)  
**O.F. Systems s.r.l.**, 1000 Bukarest (RO)

**Neumann & Co. Wasserzähler Glaubitz GmbH**, Industriestraße A7, 01612 Glaubitz  
 PTB-Q.32-4047941 DE-11-AQ-PTB071MID Wasserzähler D  
 vom 11.05.2011  
 gültig bis 10.05.2014

Standort :

**Neumann & Co. Wasserzähler Glaubitz GmbH**, 01612 Glaubitz

**HD Wiegetechnik & Sondermaschinen GmbH**, Charlotte-Bamberg-Str. 8, 35578 Wetzlar  
 PTB-Q.32-4044717 DE-11-AQ-PTB067MID Selbsttätige Waage zum Abwägen D  
 vom 16.05.2011  
 gültig bis 15.05.2014

Standort :

**HD Wiegetechnik & Sondermaschinen GmbH**, 35578 Wetzlar

**Scheidt & Bachmann GmbH**, Breite Straße 132, 41238 Mönchengladbach  
 PTB-Q.32-4052450 DE-09-AQ-PTB047MID Kraftstoffzapfsäule D  
 1. Revision vom 16.05.2011  
 gültig bis 14.02.2012

Standorte :

**Scheidt & Bachmann GmbH**, 41238 Mönchengladbach  
**Scheidt & Bachmann s.r.o.**, 01232 Žilina, Slowakei

**Bitzer Wiegetechnik GmbH**, Benzstraße 3, 31135 Hildesheim  
 PTB-Q.32-4051291 DE-11-AQ-PTB050MID Selbsttätige Waage für Einzelwägungen D  
 vom 25.06.2011 Selbsttätige Waage zum Abwägen  
 gültig bis 24.06.2014 Selbsttätige Waage zum diskontinuierlichen  
 Totalisieren

Standort :

**Bitzer Wiegetechnik GmbH**, 31135 Hildesheim

**c-trace GmbH**, Bielitzer Straße 42, 33699 Bielefeld  
 PTB-Q.32-4050070 DE-11-AQ-PTB073MID Selbsttätige Waage für Einzelwägungen D  
 vom 06.06.2011  
 gültig bis 05.06.2014

Standort :

**c-trace GmbH**, 33699 Bielefeld

# Prüfung explosionsgeschützter Geräte, Komponenten und Schutzsysteme

gemäß Elfter Verordnung zum Geräte- und Produktsicherheitsgesetz (Explosionsschutzverordnung - 11.GPSGV) vom 12. Dezember 1996, BGBl. I S. 1914 (als Umsetzung der Richtlinie 94/9/EG), geändert 6. Januar 2004, BGBl. I S. 2

Hersteller, Bescheinigungs-Nr. PTB	Produkt, Typbezeichnung	Kennzeichnung/Bemerkung
<b>1.1 Mess-, Steuer-, Regelgeräte</b>		
<b>EPHY-MESS GmbH, 65205 Wiesbaden-Delkenheim, Deutschland</b>		
00 ATEX 2015 U 3. Ergänzung	Nutentempersensor M-OK/AK ESH...	II 2 G Ex e II
00 ATEX 2075 U 3. Ergänzung	Messwiderstand mit Schrumpfschlauch Isolation Measuring resistor with shrinking tube insulation M-xx/DSH	II 2 G Ex eb IIC
00 ATEX 2076 U 1. Ergänzung	Starres Nutenwiderstandsthermometer NWT-ST...	II 2 G Ex eb IIC
02 ATEX 2020 X 3. Ergänzung	Thermometer EM24/38 und LT24/38 Ex i	II 2 G Ex ia IIC T6-T3 und II 2 D Ex ia IIIC Txxx °C IP67
<b>Hans Turck GmbH &amp; Co.KG, 45472 Mülheim an der Ruhr, Deutschland</b>		
10 ATEX 2024	Excom Modul DO401Ex	II (1) 2G Ex ib [ia Ga] IIC T4 Gb bzw. II (1)D [Ex ia IIIC Da]
<b>Krohne Altometer, 3313 Dordrecht, Niederlande</b>		
03 ATEX 2021 X 5. Ergänzung	Ultraschall-Durchflussmesssystem (Kompakt- Durchflussmesser) UFM 3030...-Ex	Ex de [ia/ib] IIC T6...T3
<b>KROHNE Messtechnik GmbH, 47058 Duisburg, Deutschland</b>		
11 ATEX 2012 X	Schwabekörper-Durchfluss-Messgerät + Anzeiger H250.../M40.../...../..-Ex-.. + M40.../...../..- Ex-..	II 2 G Ex ia IIC/IIB T6 Gb bzw. II 3 G Ex nA IIC/IIB T6 Gc
<b>KROHNE S.A.S, 26103 Romans cedex, Frankreich</b>		
02 ATEX 2117 X 3. Ergänzung	Vibrationsgrenzschalter OPTISWITCH 5**0 C VF1 *.C*****N*	II 1 G Ex ia IIC T6 Ga bzw. II 1/2 G Ex ia IIC T6 Ga/Gb bzw. II 2 G Ex ia IIC T6 Gb
<b>Pepperl + Fuchs GmbH, 68301 Mannheim, Deutschland</b>		
00 ATEX 2080 3. Ergänzung	Trennschaltverstärker K*D*-SR*-Ex*.W.*	II (1) G [Ex ia] IIC II (1) D [Ex ia] IIIC
00 ATEX 2081 2. Ergänzung	Trennschaltverstärker K*A*-SR*-Ex*.W.*	II (1) G [Ex ia] IIC II (2) D [Ex ia] IIIC
<b>Scheidt&amp;Bachmann GmbH, 41238 Mönchengladbach, Deutschland</b>		
07 ATEX 2058 X 2. Ergänzung	Temperatursensor CAN-BUS 05 83674	II (1) 2 G Ex ia d IIB T3
<b>VEGA Grieshaber KG, 77761 Schiltach, Deutschland</b>		
03 ATEX 2035 X 4. Ergänzung	Druckmessumformer VEGABAR BR5/6*.C*(*)****H/P/F/Z****	II 1G oder II 1/2 G oder II 2G Ex ia IIC T6 Ga, Ga/Gb, Gb
<b>Weidmüller Interface GmbH &amp; Co., 32758 Detmold, Deutschland</b>		
11 ATEX 2019	Explosionssgeschützte Energieverteilungs-, Schalt- und Steuerkombination Klippon TBe MH/QL/FS	II 1 G Ex ia IIC T6 Ga, II 2 G Ex ib IIC T6, II 3 G Ex ic IIC T6, II 2 D Ex t IIIC T120°C Db IP66/67

Hersteller, Bescheinigungs-Nr. PTB	Produkt, Typbezeichnung	Kennzeichnung/Bemerkung
<b>1.2 Elektrische Maschinen</b>		
<b>Cardo Flow Solutions AB, 201 23 Malmö, Schweden</b>		
10 ATEX 1062 X	Drehstrommotor für Tauchpumpen PE1 und PE2	II 2 G Ex d IIB T4
<b>J. Helmke &amp; Co., 30519 Hannover, Deutschland</b>		
11 ATEX 1008 X	Drehstrommotoren CDEDOR 560...-	II 2 G Ex d IIC T3 - T6 Gb, Ex d e IIC T3 - T6 Gb, Ex d ib IIC T3 - T6 Gb, Ex d e ib IIC T3 - T6 Gb
11 ATEX 3017	Drehstrommotor für Hochspannung EDOR 355...-	II 2 G Ex e IIC T1 -T4 Gb, Ex e d IIC T1 - T4 Gb, Ex e ib IIC T1 - T4 Gb, Ex e d ib IIC T1 - T4 Gb
<b>JUNG PUMPEN GmbH &amp; Co, 33803 Steinhagen, Deutschland</b>		
08 ATEX 1113 X Datenblatt 01 - 01	Drehstrommotor für Tauchpumpen D 90- 2 / 75 E bzw. D 90- 2 / 75 EK	II 2 G Ex d IIB T4
11 ATEX 1021 X	Tauchpumpenmotor . 71/2....	II 2 G Ex d IIB T4 Gb
<b>KSB Aktiengesellschaft, 06110 Halle/Saale, Deutschland</b>		
03 ATEX 1086 4. Ergänzung	Drehstrommotor für Tauchpumpen DKN 226	II 2 G Ex d IIB T3, T4 Gb
<b>Loher GmbH, 94099 Ruhstorf, Deutschland</b>		
07 ATEX 1042 X 4. Ergänzung	Drehstrommotoren D...-560...-....	II 2 G Ex d IIC T3 - T6 Gb, Ex d e IIC T3 - T6 Gb, Ex d ib IIC T3 - T6 Gb, Ex d e ib IIC T3 - T6 Gb
07 ATEX 1043 X 7. Ergänzung	Drehstrommotoren D...-560...-....	II 2 G Ex d IIB T3 - T6 Gb, Ex d e IIB T3 - T6 Gb, Ex d ib IIB T3 - T6 Gb, Ex d e ib IIB T3 - T6 Gb
07 ATEX 2038 X Datenblatt 13	Drehstrom-Asynchronmotor JHQP-710LC-04	II 2 G Ex px e ib IIC T3
07 ATEX 3006 Datenblatt 45	Drehstrom-Asynchronmotor E.G.-100LD-04	II 2 G Ex e II T1, T2, T3
07 ATEX 3007 Datenblatt 43 - 43	Drehstrom-Asynchronmotor E.G.-112MB-04	II 2 G Ex e IIT3
07 ATEX 3007 Datenblatt 44	Drehstrom-Asynchronmotor E.G.-112MB-02	II 2 G Ex e II T1, T2, T3
07 ATEX 3008 Datenblatt 99	Drehstrom-Asynchronmotor E.G.-132SB-04	II 2 G Ex e II T1, T2, T3
07 ATEX 3010 Datenblatt 118	Drehstrom-Asynchronmotor E.G.-160MB-04	II 2 G Ex e II T1, T2, T3
07 ATEX 3010 Datenblatt 119	Drehstrom-Asynchronmotor E.G.-160MD-02	II 2 G Ex e II T1, T2, T3
07 ATEX 3010 Datenblatt 121	Drehstrom-Asynchronmotor E.G.-160LB-04	II 2 G Ex e II T1, T2, T3
07 ATEX 3010 Datenblatt 123	Drehstrom-Asynchronmotor E.G.-160MB-02	II 2 G Ex e II T1, T2, T3
07 ATEX 3132 Datenblatt 53	Drehstrom-Asynchronmotor E.G.-090LX-02	II 2 G Ex e II T1, T2, T3
07 ATEX 3137 Datenblatt 70	Drehstrom-Asynchronmotor E.G.-200LG-04	II 2 G Ex e II T1, T2, T3

Hersteller, Bescheinigungs-Nr. PTB	Produkt, Typbezeichnung	Kennzeichnung/Bemerkung
09 ATEX 1009 X 4. Ergänzung	Drehstrommotor D...-710.-...	II 2 G Ex d IIB T3 - T6, Ex d e IIB T3 -T6, Ex d ib IIB T3 -T6, Ex d e ib IIB T3 - T6
11 ATEX 3004	Drehstrommotor für Niederspannung E...-250.-... und 1PS.250.-...-...	II 2 G Ex e IIC T1 - T4 Gb bzw. Ex e ib IIC T1 - T4 Gb
11 ATEX 3015 X	Drehstrommotor für Niederspannung E...-250.-... und 1PS.25.-...-...	II 2 G Ex e IIC T1 - T4 Gb bzw. Ex e ib IIC T1 - T4 Gb
11 ATEX 3019	Drehstrommotor für Niederspannung E...-280.-... und 1PS.28.-...-...	II 2 G Ex e IIC T1 - T4 Gb bzw. Ex e ib IIC T1 - T4 Gb
11 ATEX 3020 X	Drehstrommotor für Niederspannung E...-280.-... und 1PS.28.-...-...	II 2 G Ex e IIC T1 - T4 Gb bzw. Ex e ib IIC T1 - T4 Gb
<b>Rosenberg Ventilatoren GmbH, 74653 Künzelsau-Gaisbach, Deutschland</b>		
10 ATEX 3002 X	Ventilatormotoren DD 106-...	II 2 G Ex e IIC T3 Gb
10 ATEX 3002 X Datenblatt 01 - 04	Ventilatormotoren DD 106-...	II2G Ex e IIC T3 Gb
10 ATEX 3003 X	Ventilatormotoren DD 137-...	II 2 G Ex e IIC T3 Gb
10 ATEX 3003 X Datenblatt 01 - 04	Ventilatormotoren DD 137-...	II2G Ex e IIC T3 Gb
10 ATEX 3004 X	Ventilatormotoren DD 165-...	II2G Ex e IIC T3 Gb
10 ATEX 3004 X Datenblatt 01	Ventilatormotoren DD 165-...	II 2 G Ex e IIC T3 Gb
<b>Schorch Elektrische Maschinen und Antriebe GmbH, 41238 Mönchengladbach, Deutschland</b>		
07 ATEX 3036 Datenblatt 13	Drehstrommotor KE2355X-A...	II 2 G Ex e IIC T3
07 ATEX 3039 Datenblatt 07	Drehstrommotor KE2508X-A...	II 2 G Ex eib IIC T3
07 ATEX 3068 Datenblatt 01	Drehstrommotor KU6034G-EH02	II 2 G Ex eib IIC T3
11 ATEX 3016 X	Drehstrommotoren für Niederspannung der Typenreihe .E2 31.-..., .E2 35.-..., .E2 40.-..., .E2 45.-..., .E2 50.-... und .E2 56.-...	II 2 G Ex e IIC T1 - T4 Gb, Ex e d IIC T1 - T4, Ex e ib IIC T1 - T4 Gb, Ex e d ib IIC T1 - T4 Gb
11 ATEX 3018 X	Drehstrommotoren für Hochspannung der Typenreihe .E2 31.-..., .E2 35.-..., .E2 40.-..., .E2 45.-..., .E2 50.-... und .E2 56.-...	II 2 G Ex e IIC T1 - T4 Gb, Ex e d IIC T1 - T4, Ex e ib IIC T1 - T4 Gb, Ex e d ib IIC T1 - T4 Gb
<b>SEW-EURODRIVE GmbH &amp; Co KG, 76646 Bruchsal, Deutschland</b>		
04 ATEX 3033 1. Ergänzung	Drehstrommotoren eD.R 63...	II 2 G Ex e IIC T1 - T4 Gb bzw. Ex eb IIC T1 - T4, II 2 D Ex tb IIIC T 120 °C
10 ATEX 3028 Datenblatt 19 - 30	Drehstrom-Asynchronmotor für Netzbetrieb EDRE100L4	II 2 G Ex e II T1, T2, T3
10 ATEX 3032 Datenblatt 25 - 32	Drehstrom-Asynchronmotor für Netzbetrieb eDRE180L4	II 2 G Ex e II T1, T2, T3
10 ATEX 3032 Datenblatt 13 - 24	Drehstrom-Asynchronmotor für Netzbetrieb eDRE180M4	II 2 G Ex e II T1, T2, T3
10 ATEX 3033 Datenblatt 01 - 12	Drehstrom-Asynchronmotor für Netzbetrieb EDRE200L4	II 2 G Ex e IIC T3 Gb
10 ATEX 3034 Datenblatt 01 - 04	Drehstrom-Asynchronmotor für Netzbetrieb EDRE225S4	II 2 G Ex e IIC T3 Gb

Hersteller, Bescheinigungs-Nr. PTB	Produkt, Typbezeichnung	Kennzeichnung/Bemerkung
10 ATEX 3034 Datenblatt 05 - 08	Drehstrom-Asynchronmotor für Netzbetrieb EDRE225M4	II 2 G Ex e IIC T3 Gb
11 ATEX 3000 X Datenblatt 01 - 01	Asynchronmotor für Umrichterbetrieb EDRE100M4	II 2 G Ex e II T1, T2, T3
11 ATEX 3000 X Datenblatt 02	Drehstrom-Asynchronmotor für Umrichterbetrieb EDRE100LC4	II 2 G Ex e II T1, T2, T3
11 ATEX 3003 X Datenblatt 01	Drehstrom-Asynchronmotor für Umrichterbetrieb EDRS80S4	II 2 G Ex e II T1, T2, T3, T4
11 ATEX 3003 X Datenblatt 02	Drehstrom-Asynchronmotor für Umrichterbetrieb EDRS80M4	II 2 G Ex e II T1, T2, T3, T4
11 ATEX 3008 X Datenblatt 02	Drehstrom-Asynchronmotor für Umrichterbetrieb EDRE160M4	II 2 G Ex e II T1, T2, T3
11 ATEX 3009 X Datenblatt 02	Drehstrom-Asynchronmotor für Umrichterbetrieb EDRE180M4	II 2 G Ex e II T1, T2, T3
11 ATEX 3010 X	Drehstrom-Asynchronmotor für den Betrieb am Umrichter EDRE200L4	II 2 G Ex e IIC T3 Gb
11 ATEX 3011 X	Drehstrom-Asynchronmotor für den Betrieb am Umrichter EDRE225S4	II 2 G Ex e IIC T3 Gb
11 ATEX 3011 X Datenblatt 02 - 02	Drehstrom-Asynchronmotor für den Betrieb am Umrichter EDRE225M4	II 2 G Ex e IIC T3 Gb
<b>Siemens AG, 97616 Bad Neustadt, Deutschland</b>		
02 ATEX 3024 X Datenblatt 02	Asynchronmotor mit Frequenzumrichterspeisung zum Antrieb von Gasrückförpumpen 1MA7063-2	II 2 G Ex e II T3
02 ATEX 3069 Datenblatt 25	Drehstrom-Asynchronmotor 1MA6 253-2AC.	II 2 G Ex e II T1, T2
03 ATEX 2106 X Datenblatt 39	Drehstrom-Asynchronmotor 1SB4 630-6	II 2 G Ex px e IIC T3
03 ATEX 2106 X Datenblatt 37	Drehstrom-Asynchronmotor 1SB4 562-6	II 2 G Ex px e IIC T3
03 ATEX 2107 X Datenblatt 37	Drehstrom-Asynchronmotor 1SQ4 560-2	II 2 G Ex px e ib IIC T3
03 ATEX 2107 X Datenblatt 40	Drehstrom-Asynchronmotor 1SQ4 506-2	II 2 G Ex px e ib IIC T3
03 ATEX 2107 X Datenblatt 41	Drehstrom-Asynchronmotor 1SQ4 500-2	II 2 G Ex px e ib IIC T3
03 ATEX 2107 X Datenblatt 38	Drehstrom-Asynchronmotor 1SQ4 562-4	II 2 G Ex px e ib IIC T3
03 ATEX 2107 X Datenblatt 36	Drehstrom-Asynchronmotor 1SQ4 560-4	II 2 G Ex px e ib IIC T3
<b>Tyco Thermal Controls, CA 94025-1164 Menlo Park, USA</b>		
09 ATEX 1116 X	Begleitheizungssystem ..QTVR2-CT	II 2G Ex e II T4 II 2D Ex tD A21 IP66 T 130 °C
<b>VEM motors GmbH, 38855 Wernigerode, Deutschland</b>		
08 ATEX 3040 Datenblatt 16 - 19	Drehstromasynchronmotor IE2-K11R200L4	II 2 G Ex e II T1, T2, T3

Hersteller, Bescheinigungs-Nr. PTB	Produkt, Typbezeichnung	Kennzeichnung/Bemerkung
<b>1.3 Schalt- und Steuergeräte</b>		
<b>BARTEC GmbH, 97980 Bad Mergentheim, Deutschland</b>		
03 ATEX 1138 1. Ergänzung	Schalt- und Steuergerätekombination 07-42.0-.../....	II 2(1)G Ex db eb ia/ib [ia] IIA, IIB bzw. IIC T6, T5 bzw. T4 II 2G Ex db eb ia/ib [ib] IIA, IIB bzw. IIC T6, T5 bzw. T4
<b>BARTEC-VARNOST, 1414 Zagorje ob Savi, Slovenien</b>		
11 ATEX 1016 X	Abzweig- und Verbindungskästen 07-5101-****/**** und 07-5102-****/****	II 2 G Ex e ia/ib IIA, IIB, IIC T6 bzw. T5 Gb II 2 D Ex tb IIIC T80°C, T95°C Db IP66
<b>Rotech Antriebselemente GmbH, 76275 Ettlingen, Deutschland</b>		
10 ATEX 1061 X	Endschaltermodul ALB ..... AZ...	II 2 G Ex e ia IIA, IIB, IIC T6 Gb, Ex e d IIA, IIB, IIC T6 Gb, II 2 D Ex tb IIIC T80°C Db IP65 II 2 G Ex e d IIC T6 Gb / II 2 D Ex tb d IIIC T80°C Db IP65
<b>1.4 Leuchten</b>		
<b>Eltromat, 33818 Leopoldshöhe, Deutschland</b>		
11 ATEX 2013 X	Registermarkensensor RSH-PN.x und RSH-EC.x Teile-Nr.: 95781-0xxxx	II 2 G [Ex op is T4] IIB
<b>R. STAHL Schaltgeräte GmbH, 74638 Waldenburg (Württ.), Deutschland</b>		
07 ATEX 1009 2. Ergänzung	Inspektionsleuchte 6149/.....-.....	II 2 G Ex d IIC TX Gb oder Ex db IIC TX II 2 D Ex tb IIIC TXXX °C Db oder Ex tb IIIC TXXX °C
<b>1.5 Sonstige elektrische Betriebsmittel</b>		
<b>PFLITSCH GmbH &amp; Co. KG, 42499 Hückeswagen, Deutschland</b>		
11 ATEX 1007 X	Kabel- und Leitungseinführung blueglobe HT Kabelverschraubung aus Messing vernickelt und Edelstahl	II 2 G Ex e IIC Gb II 2 D Ex tb IIIC Db IP66, IP68
<b>BARTEC GmbH, 97980 Bad Mergentheim, Deutschland</b>		
11 ATEX 1011 U	Leergehäuse 07-44*1-0***/****	II 2G Ex d IIC bzw. Ex d e IIC II 2D Ex tD A21 IP66
<b>BARTEC-VARNOST, 1414 Zagorje ob Savi, Slovenien</b>		
08 ATEX 1063 U 1. Ergänzung	Aluminium-Leergehäuse 07-5180-****/****	II 2 G Ex e IIC Gb II 2 D Ex tb IIIC Db IP66
<b>BARTEC-VARNOST d.o.o., 1410 Zagorje ob Savi, Slovenien</b>		
04 ATEX 1099 U 4. Ergänzung	Leitungsdurchführung TOS*. *A. ***V	II 2 G Ex de IIC Gb bzw. I M 2 Ex de I Mb
<b>COOPER Crouse-Hinds GmbH, 69412 Eberbach, Deutschland</b>		
00 ATEX 3102 U 2. Ergänzung	Klemmenstein GHG 790 110. R....	II 2 G Ex eb IIC bzw. I M 2 Ex eb I II 2 G Ex e IIC Gb bzw. I M 2 Ex e I Mb
99 ATEX 3118 U 4. Ergänzung	Leergehäuse GHG 60. .... R....	II 2 G Ex e IIC Gb II 2 D Ex tb IIIC Db IP66
<b>FHF Funke + Huster Fernsig GmbH, 45478 Mülheim a.d. Ruhr, Deutschland</b>		
07 ATEX 2039 X 1. Ergänzung	Ex II Hupe mHP 11, mHP12, mHG11	II 2 G Ex e mb II T4, T5, T6 und II 2 D Ex tD A21 IP65 T100°C

Hersteller, Bescheinigungs-Nr. PTB	Produkt, Typbezeichnung	Kennzeichnung/Bemerkung
<b>FMC Measurement Solutions, 25474 Ellerbek, Deutschland</b>		
03 ATEX 1033 U 1. Ergänzung	Gehäuse ER...-...-...	II 2 G Exd IIC
<b>JUNG PUMPEN GmbH &amp; Co, 33803 Steinhagen, Deutschland</b>		
11 ATEX 1017 U	Leitungseinführung A4 / ..., B4 / ... und C4 / ...	II 2 G Ex d II Gb
<b>PHOENIX CONTACT GmbH &amp; Co. KG, 32825 Blomberg, Deutschland</b>		
11 ATEX 1018 U	Leergehäuse (Aluminium) EN 1 EX AL ***	II 2 G Ex e II II 2 D Ex tD A21 IP66
11 ATEX 1019 U	Leergehäuse (Edelstahl) EN 1 EX S6B ***, ENF 1 EX S6B ***, CA 1 EX S6B *** und CAF 1 EX S6B ***	II 2 G Ex e II II 2 D Ex tD A21 IP66
11 ATEX 1020 U	Leergehäuse (Polyester) EN 1 EX PE ***, EN 1 EX PE O ***, EN 1 EX PE P ***, ENF 1 EX PE *** und CA 1 EX PE ***	II 2 G Ex e II II 2 D Ex tD A21 IP66
<b>Siemens AG, 97616 Bad Neustadt, Deutschland</b>		
01 ATEX 1076 U 4. Ergänzung	Klemmenbrett und Klemmenplatte 130, 139, 230, 239, 330, 330 und 6xM6 und 6xM8	II 2 G Ex e IIC Gb
<b>Siemens AG Automation and Drives, 13629 Berlin, Deutschland</b>		
04 ATEX 3048 U 2. Ergänzung	Anschlusskasten für Hochspannung 1XD1 5**-3*A	II 2 G Ex e IIC Gb
<b>Versa products company inc., 07652 Paramus, New Jersey, USA</b>		
11 ATEX 2007	Solenoid Operator XISX6 und XISX4	II 2 G Ex ia IIC T6, T4 oder II 2 G Ex ia IIB T6, T4
<b>WISKA Hoppmann &amp; Mulow GmbH, 24568 Kaltenkirchen, Deutschland</b>		
05 ATEX 1068 X 6. Ergänzung	Kabel- und Leitungseinführung .SKE(S)(-L)-. ... (LT) (.....)	II 2 G Ex e II II 2 D Ex tD A21 IP66 bzw. IP68
<b>2. Nichtelektrische Geräte</b>		
<b>Paul Vollrath GmbH &amp; Co KG, 50354 Hürth, Deutschland</b>		
03 ATEX 5007 X Datenblatt 124 - 125	Rührwerk VRG ... nach Zeichnung 21-1264.022.00	
<b>3. Flammendurchschlagsicherung</b>		
<b>Gardner Denver Thomas GmbH, 82178 Puchheim, Deutschland</b>		
11 ATEX 4005 X	Detonationsrohrsicherung DS 21/MS bzw. DS21/VA	
<b>HANLA IMS CO.,LTD, Busan, Südkorea</b>		
11 ATEX 4007 X	Detonationssicherung HFA-15	

## Anerkennung von Qualitätssicherungssystemen

entsprechend Richtlinie 94/9/EG für Geräte oder Schutzsysteme oder Komponenten zur bestimmungsgemäßen Verwendung in explosionsgefährdeten Bereichen

Bescheinigungs-Nummer PTB	Hersteller	gültig bis	Anhang
05 ATEX Q010-2	Mess- und Fördertechnik Gwinner GmbH&Co. Weidenbaumsweg 91a 21035 Hamburg Deutschland	21.06.2014	IV
01 ATEX Q021-3	Rotronic AG Grindelstr. 6 8303 Bassersdorf Schweiz	22.12.2013	IV
04 ATEX Q002-2	GE Power Controls GmbH & Co.KG Berliner Platz 2-8 24534 Neumünster Deutschland	04.02.2013	IV
05 ATEX Q005-2	Hottinger Baldwin Measurement (Sozhou) Co., Ltd. No.106 Hengshan Road 215011 Suzhou, Jiangsu China	27.04.2014	IV
99 ATEX Q009-5	MIAG Fahrzeugbau GmbH Kocherstr. 1 38120 Braunschweig Deutschland	13.06.2014	IV
02 ATEX N012-3	OPTRO GmbH Industriestraße 75 51399 Burscheid Deutschland	28.07.2014	VI
05 ATEX N013-2	Loher GmbH Hans-Loher-Straße 32 94099 Ruhstorf Deutschland	19.06.2014	VI